585

CRANFIELD INSTITUTE OF TECHNOLOGY

SCHOOL OF INDUSTRIAL SCIENCE

PhD Thesis

Academic Year 1985-1987

D R CALLISTER

A study of fatigue crack propagation in quenched and tempered and controlled rolled HSLA steels

Supervisors: Professor J Billingham

B S Hockenhull

SEPTEMBER 1987

ABSTRACT

A range of HSLA steels reflecting the two major processing routes, quench and tempering and controlled rolling, have been tested in fatigue to assess their potential wider application in the Offshore Industry. The six steels chosen have a wide range of yield strenghts (470 to 690Nmm^{-2}), fracture toughness (31 to 260J at -40^{o}C) and carbon equivalent values (0.19 to 0.33). Fatigue testing has in general been carried out at low frequency (0.5Hz) and high load ratio (0.6) however some tests have been conducted at very low frequency (0.1Hz) and low load ratio (0.1). An in-air study was first used to assess the fatigue performance of all six parent plates. Five steels were welded by the Submerged Arc Welding process at high heat input (1.5kJmm^{-1}) to evaluate the Heat Affected Zone (HAZ) fatigue performance. A new test was devised to grow a fatigue crack through a single pass, bead on plate, HAZ whilst maintaining a constant stress intensity range. The surface crack length was continuously monitored and recorded to an accuracy of 0.01mm.

A corrosion fatigue study evaluated the performance of one controlled rolled and one quenched and tempered steel at three levels of impressed current cathodic protection.

Extensive metallographic examination was made to study the influence of microstructural features and types on fatigue crack propagation. Techniques used include optical microscopy, scanning electron microscopy, fatigue crack and surface replication and crack profile digitising. These techniques give an assessment of crack path deviation and branching, the influence of precipitates and inclusions, and an indication of the mode of fatigue crack propagation. The wide range of microalloyed HSLA steels tested have shown a significant improvement in fatigue crack propagation

resistance over structural steels conforming to BS 4360 grade 50D. Typically an improvement by a factor of two has been observed. Whilst the observed increase in fatigue life was slightly reduced by high heat input welding the slope of the Paris curves remained unaffected thus indicating a similar stress intensity range sensitivity in the HAZ to that shown by the parent plate.

The newly developed crack monitoring system coupled to a computer controlled fatigue testing machine has shown a wide variation in fatigue crack propagation rates through a heat affected zone microstructural gradient. Growth rates have increased by a factor of ten in localised coarse grained microstructural regions compared to the adjacent weld metal and outer heat affected zone.

The corrosion fatigue study has also indicated that in general HSLA steels retain their superiour fatigue resistance compared to structural steels and in particular respond more favourably to cathodic protection. Both in-air and corrosion fatigue studies have indicated that the controlled rolled steel microstructures developed mainly for line pipe application has the greatest potential for increased use offshore.

ACKNOWLEDGEMENTS

The author wishes to express his grateful thanks to the following people:

Professor John Billingham for his advice and guidance during this project.

Ray Smith for his expertise in electronics and specifically his work on the computer controlled fatigue equipment.

Fred Tribe and John Holmes for their technical assistance in the laboratories.

Dr John Nicholls for allowing the author to use the continuous crack propagation gauge developed within his group and Ken Lawson and Dennis Timpson for their assistance in producing the gauges.

CONTENTS

6.0 METALLOGRAPHY

6.1 Fatigue in Parent Plate Microstructures

6.1.1 Quenched and tempered steels

6.1.1.1 N-A-XTRA 70

6.1.1.2 RQT 501

6.1.1.3 BS4360 grade 55F

6.1.2 Controlled rolled steel

6.1.2.1 LP 6 Line-pipe

6.1.2.2 Kontroll 50 ESM

6.1.2.3 Mannesmann X80

6.1.3 Parent plate metallography summary

6.2 Multipass Submerged Arc Welded HAZ Microstructures

6.3 Corrosion Fatigue

6.3.1 Quenched and tempered steel BS4360 grade 55F

6.3.2 Controlled rolled steel, X80 Mannesmann line-pipe

6.3.3 Summary of corrosion fatigue data

6.4 Constant ΔK Fatigue Crack Propagation Through a Microstructural Gradient

List of Figures

29 Fatigue machine closed loop feedback control system.

30 Pre-fatigue, monatonic plastic zone profile.

31 Corrosion fatigue test rig.

32 Commercial crack propagation gauge with associated circuitry and typical response curve.

33 Crack propagation gauge mounted on a fatigue sample.

34 Gauge with protective coatings for corrosion fatigue monitoring.

35 Stress intensity range versus crack length profile for a threshold step down test.

36 Control system for computer controlled fatigue machine.

37 Schematic illustration of constant ΔK experimental set up.

38 Constant ΔK fatigue rig.

39 Variable resistance crack propagation gauge mounted on a fatigue sample.

40 DC sputter coater with expanded diagram of the coating chamber.

41 Resistance monitor and mask assembly.

42 Fatigue crack in gauge mounted using strain gauge adhesive.

57 Closely controlled ΔK step-down experiment showing threshold for N-A-XTRA 70.

58 Effect of load ratio on the fatigue properties of N-A-XTRA 70.

59 HAZ fatigue data for N-A-XTRA 70 illustrating effect of notch position.

60 HAZ fatigue data for Kontroll 50 ESM.

61 HAZ fatigue data for RQT 501.

62 HAZ fatigue data for BS 4360 grade 55F.

63 HAZ fatigue data for X80 line-pipe.

64 Comparison of HSLA HAZ fatigue performance with parent plate structural steel.

65 Corrosion fatigue data for the quenched and tempered steel BS 4360 grade 55F.

66 Corrosion fatigue data for the controlled rolled steel X80 line-pipe.

67 A comparison between correctly protected HSLA steels and three levels of protection for a structural steel.

68 Relative positioning of figures 69-73 to the microstructure gradient.

69 Constant ΔK, weld metal.

70 Constant ΔK, fusion boundary/coarse HAZ.

71 Constant ΔK, mid HAZ region.

72 Constant ΔK, fine HAZ region.

73 Constant ΔK, parent plate.

74 Crack profiles as a function of time for N-A-XTRA 70 tested in air at R = 0.6 with a frequency of 0.5Hz.

75 Exposed cubic precipitate revealed by the fatigue crack propagation front.

76 Intact zirconium based precipitate on the fracture surface.

77 Final failure displaying microvoid coalesence.

78 Fatigue crack fracture surface (N-A-XTRA 70).

79 RQT 501 fatigue data for three conditions of tempering.

80 Digitised and actual profile of RQT 501 (x200).

81 RQT 501 commercial plate fatigue crack profile (x400).

82 Large open type of crack branching on RQT 501 fracture surface.

83 Fatigue crack profile of BS 4360 grade 55F (X400).

84 BS 4360 grade 55F fatigue crack fracture surface.

85 Extensive delamination as seen on the fatigue fracture surface of LP-6 (x3).

86 Local microstructure associated with delamination in profile (x200).

87 Diagrammatic representation of delamination in LP-6.

88 Replication of a fatigue crack in Kontroll 50 ESM, $\Delta K = 18MPa\sqrt{m}$ (x200).

89 Crack tip replica of Kontroll 50 ESM at maximum load showing preferred direction of slip (x800).

90 Fatigue crack profile showing secondary crack occurrence in Kontroll 50 ESM (x400).

91 Shape controlled manganese sulphide inclusions exposed on Kontroll 50 ESM fatigue fracture surface.

92 Fatigue crack profile showing secondary cracking and crack path deviation in x80 line-pipe, $\Delta K = 21MPa\sqrt{m}$ (x400).

93 Fatigue fracture surface showing high occurance of secondary cracks in X80 line-pipe steel.

94 Fatigue crack profile of BS 4360 grade 55F HAZ showing reduced crack branching and deviation, $\Delta K = 20MPa\sqrt{m}$ (x200).

95 Fatigue striations and secondary cracking seen on BS 4360 grade 55F HAZ fatigue fracture surface.

96 Fatigue crack profile of Kontroll 50 ESM showing reduced secondary cracking and crack path deviation, $\Delta K = 20MPa\sqrt{m}$ (x200).

97 Fine micro cracking observed on Kontroll 50 ESM fatigue fracture surface.

98 Crack profile of free corroding BS 4360 grade 55F steel. $\Delta K = 19MPa\sqrt{m}$ (x400).

99 Crack profile of correctly protected BS 4360 grade 55F steel. $\Delta K = 20MPa\sqrt{m}$ (x400).

100 Crack profile of free corroding X80 line-pipe steel. $\Delta K = 20MPa\sqrt{m}$ (x400).

101 Crack profile of free corroding X80 line-pipe steel. $\Delta K = 18MPa\sqrt{m}$ (x400).

102 Crack profile of correctly protected X80 line-pipe steel. $\Delta K = 20MPa\sqrt{m}$ (x400).

103 Crack profile of overprotected (-1050mV) X80 line-pipe after crack arrest has occurred (x350).

104 Fatigue fracture surface in weld metal microstructure showing only faint striations.

105 Fatigue crack profile in region of sustained accelerated growth (1.53×10^{-7}m/cycle).

106 Fatigue fracture surface in region of sustained accelerated growth showing formation of fine microcracks.

107 Fatigue fracture surface in mid to fine HAZ, secondary cracks are evident but striations are indistinct.

108 Parent plate region with an abundance of striations on the fracture surface.

109 Microhardness survey accross the microstructural gradient through which the constant ΔK crack was grown.

110 Through crack in an infinite plate.

111 Theoretical strain distribution ahead of the crack tip.

112 The Bauschinger strain effect.

113 Normal loading sequence with peak overload (b).

114 Effect of the yield stress on the crack propagation rate after overload, Rpeak = 2.5.

115 Effect of the yield stress on the U ratio after an overload, Rpeak = 2.5.

116 Effect of crack closure on the plastic zone stress state.

117 Geometric upper bound data for HSLA steels for comparison with structural steel data.

118 Fatigue performance of HSLA steels and a structural steel normalised for yield strength.

119 Fatigue crack propagation data as a function of electrochemical potential in seawater (BS 4360 50D).

Tables

Notation

σ_y = Yield stress

σ_o = lattice friction stress

σ_s = solid solution hardening

σ_ε = dislocation hardening

σ_p = precipitation hardening

σ_g = grain boundary hardening

k_y = grain size coefficient

σ_i = stress constant

d = grain size

da/dN = crack extension per cycle

ΔK = stress intensity range

ΔK_{th} = threshold stress intensity range

ΔK_{eff} = effective stress intensity range

K_c = critical stress intensity

C = material constant

m = Paris exponent

ΔP = load range

Y_1 = compliance factor

B = sample thickness

W = sample width

R = loading ratio

P_{min} = minimum load in fatigue cycle

P_{max} = maximum load in fatigue cycle

K_{max} = maximum stress intensity

K_{mean} = mean stress intensity

K_{min} = minimum stress intensity

∞ = infinity

K_{op} = stress intensity at crack tip opening

a = crack length

N = elapsed fatigue cycles

fcp = fatigue crack propagation

HAZ = heat affected zone

WM = weld metal

PP = parent metal

SAW = submerged arc welding

ADC = analogue to digital converter

DAC = digital to analogue converter

VDU = visual display unit (monitor)

R = resistance

R_o = initial resistance

a_g = crack length in propagation gauge

h_v = hardness (Vickers)

σ_{ij} = stress tensor

ε_{ij} = strain tensor

E = elasticity modulus

r = polar coordinate

θ = polar coordinate

ν = Poissons ratio

s = stress

N' = 1/strain hardening experiment

$\tilde{\sigma}$ = non-dimensional stress

$\tilde{\varepsilon}$ = normalised strain

α = constant

G = constant

D = constant

x = distance in front of crack tip

ϵ = strain associated with crack tip plasticity

Z = monotonic plastic zone diameter

Equations

(1) $$y = \sigma_o + \sigma_s + \sigma_p + \sigma_g + \sigma\epsilon$$

(2) $$\sigma_y = \sigma_i + Kyd^{-\frac{1}{2}}$$

(3) $$da/dN = C\Delta K^m$$

(4) $$\Delta K = \frac{\Delta P \cdot Y1}{B \cdot \sqrt{W}} \quad (4a) \qquad R = \frac{Pmin}{Pmax}$$

(5) $$Kmax = \frac{\Delta K}{1 - R} \qquad Kmean = \frac{(Kmax - Kmin)}{2} + Kmin$$

(6) $$\frac{da}{dN} = C(Kmax)^{\alpha 1} (\Delta K)^{\alpha 2}$$

(7) $$Kmax \xrightarrow{lin} Kc; \quad \frac{da}{dN} = \infty$$

(8) $$\frac{da}{dN} = \frac{c(\Delta K)^m}{[(1 - R) Kc - \Delta K]} \beta$$

(9) $$\frac{da}{dN} = C(\Delta Keff)^m = C(U\Delta K)^m \quad \text{where } U = \frac{Kmax - Kop}{Kmax - Kmin}$$

(10) $$B_s\ (^oC) = 830 - 270\ (\%C) - 90\ (\%Mn) - 37\ (\%Ni) - 70\ (\%Cr) - 83\ (\%Mo)$$

$$(11)\qquad CEN\ (\%) = C + A(C)\left(\frac{Si}{24} + \frac{Mn}{6} + \frac{Cu}{15} + \frac{Ni}{20}\right) + \left(\frac{Cu + Mo + V + Nb}{5}\right) + 5B$$

where $A(C) = 0.75 + 0.25\tanh(20(C - 0.12))$

$$(12)\qquad \frac{da}{dN} = \frac{a(i+1) - ai}{N(i+1) - Ni}$$

$$(13)\qquad a = \sum_{i+1}^{n} \beta i\, fi\ (N)$$

$$(14)\qquad \epsilon ij = \frac{K}{\sqrt{\pi\, r\, E}}\, aij\ (\nu, \theta)$$

$$(15)\qquad \sigma ij = \frac{K}{\sqrt{\pi\, r}}\, fij\ (\theta)$$

$$(16)\qquad \tilde{\epsilon} = \tilde{\sigma} + \alpha(\tilde{\sigma})N'$$

$$(17)\qquad \tilde{\epsilon} i\ \ gij\ (\nu, \theta, N')\left(\frac{S^2 a}{\sigma_y{}^2 r}\right)\ 1/(N'+1)$$

$$+ \tilde{hij}\ (\theta, N')\ \left(\frac{S^2 a}{\sigma_y{}^2 r}\right)\ N'/(N'+1)$$

(18) $$\tilde{\sigma}_{ij} = \tilde{f}_{ij}(\theta, N') \left(\frac{S^2 a}{\sigma_y^2 r} \right)^{1/(N'+1)}$$

(19) $$\varepsilon = G - D \ln x$$

(20) $$Z = \frac{1}{2\pi} \left(\frac{K_{max}}{\sigma_y} \right)^2$$

1.0. INTRODUCTION

There are numerous existing and potential applications for High Strength Low Alloy (HSLA) steels in the context of producing weight reductions. The construction, automotive, shipbuilding and packaging industries are prime examples. However, this study has been confined to the particular problems associated with the installation of offshore structures, both fixed and buoyant, and the possible weight reduction advantages made available by the greater utilisation of higher strength steels.

In 1980 the offshore sector accounted for 22 percent of worldwide primary energy production, this figure is expected to rise to 30 percent by 1990 (1). Clearly the offshore oil industry is expanding and will continue to expand despite recent low oil prices, whilst oil remains a major energy resource.

Utilisation of higher strength steels in the offshore environment has been confined to topside facilities and equipment, specifically to regions known not to present a fatigue loading situation. Possible increase in fatigue endurance from higher strength steels is not considered in design codes, so preventing thinner material sections with associated higher local stress in a cyclic loading environment. Despite this limitation, substantial cost reductions have been achieved via greater utilisation of higher strength steels topside. Not only is a material saving made above the water line, but because of the overall reduction in topside weight, savings can be made in the overall structure.

The exploration for, and exploitation of, natural seabed resources presents stringent challenges to the steel producers and fabricators alike, particularly in the North

Sea where great water depths, severe dynamic wave forces and low temperatures place very high requirements on structures. For these reasons, structural steels have been produced with particular attention to strength and toughness behaviour coupled to good weldability. Steels conforming to BS 4360 with strengths up to grade 50D have fulfilled the requirements of the offshore industry to date. However, as exploration and recovery of oil has moved into greater depths, so the size of fixed structures has increased. Deeper waters require larger jacket structures increasing weight and cost dramatically. As the structure weight is increased, greater foundations are required adding to the overall cost increase. More recently, semi-submersible craft have been used and most recently a tethered buoyant platform, the TLP, has been developed and commissioned. Whilst this platform is presently operating 50 miles north east of the Shetland Islands in water depths of 148 metres, the TLP concept has been developed with the view to producing oil in water depths up to and beyond 900 metres (2). For a buoyant structure of this nature it is clear that weight will be a prime consideration. The weight reduction could be achieved via utilisation of these higher yield strength yet extremely tough materials in thinner sections. This will, however, with no reduction in load, create higher stresses throughout the structure. If the detected flaw size, within the heat affected zone, produced by welding remains constant for the change in material, so the stress intensity and therefore stress intensity range under cyclic loading will increase. It is therefore of paramount importance to achieve a high fatigue endurance in welded joints fabricated from this type of material if weight reductions are to be achieved in structural members exposed to a cyclic load. However, if a structure is built from a higher strength steel to similar design stresses, then any increase in fatigue endurance will increase the safe working life of the structure. Although

an offshore installation is likely to have a design life of 20 years, a change in potential climate may make it more desirable to operate at lower production rates for greater time periods. For this reason, any increase in safe working life which does not involve larger structures and increased weight is of prime importance.

It has been shown through the experience of failure due to fatigue (3) that although fatigue cracks almost invariably initiate within the heat affected zone at a welded joint, they may spend the majority of time to failure propagating within the parent plate. It is therefore essential to fully understand all the influences on fatigue crack propagation including environmental, loading variables, and most importantly microstructural, as this will also influence strength and fracture properties.

Some work has already been carried out in this area. Bhole (4) has shown favourable fracture toughness values for several HSLA steels welded by the SAW (submerged arc welding) method. Fatigue testing carried out on two HSLA steels (5,6) has also shown encouraging results. It was therefore decided to fully investigate the process of fatigue crack propagation in a range of HSLA steel microstructures whilst paying particular attention to the loading conditions presented by the North Sea environment. From this study an evaluation of the suitability of HSLA steels to offshore applications, both structural and topside, was to be made.

1.1. Fatigue Data for Design of Offshore Structures

Fatigue failure of a welded structure is almost invariably the result of a crack propagating from defects within the weld toe. Despite extensive use of Non-Destructive Testing (NDT), flaws below the resolution of the inspection technique will always be present. It is

also true to say that the stress intensity at the crack tip is far from certain. Fatigue design standards (7) are the result of data collation on different configurations of welded joints tested at various stress levels until failure occurred. From this data, cycles to failure versus stress curves (SN) are drawn from which design standards have been produced. However, several basic limitations of this type of testing procedure exist. These are as follows:-

1. Relatively small test pieces

   If welded samples are too small, tensile residual stresses will not be present to the same degree as in a welded structure. This may result in unrealistically favourable results if the cyclic stress the sample is subjected to contains a compressive component.

2. Constant amplitude tests

   Constant amplitude results are not applicable to a random loading service condition as seen by a structure operating in the North Sea. The effect of a random amplitude loading is less clear cut as it could contain an overload which may or may not arrest the crack. Alternatively, a period of sustained higher loads can result in more rapid crack propagation or initiation from a flaw previously exhibiting the thresholding phenomena.

3. High frequency tests

   For bulk data production higher frequencies are often used, the actual frequency of the North Sea being in the order of 0.15 Hertz. Again, this will result in unrealistically favourable data.

4. Laboratory welding conditions

Welding preparation and procedure control can be closely monitored and controlled in the laboratory environment. This high degree of procedure control is less easy to achieve in the field.

5. Area of weld studied

The total test data used to produce an SN curve is based on a relatively small area of weld run when compared to an actual structure. Few samples of small dimensions reduces the probability of an untypically poor result.

Due to the complexity of welded joints and the different welding processes used, similar results have been put into groups or classes in order to simplify probability of failure predictions. Each class has an SN curve as below:-

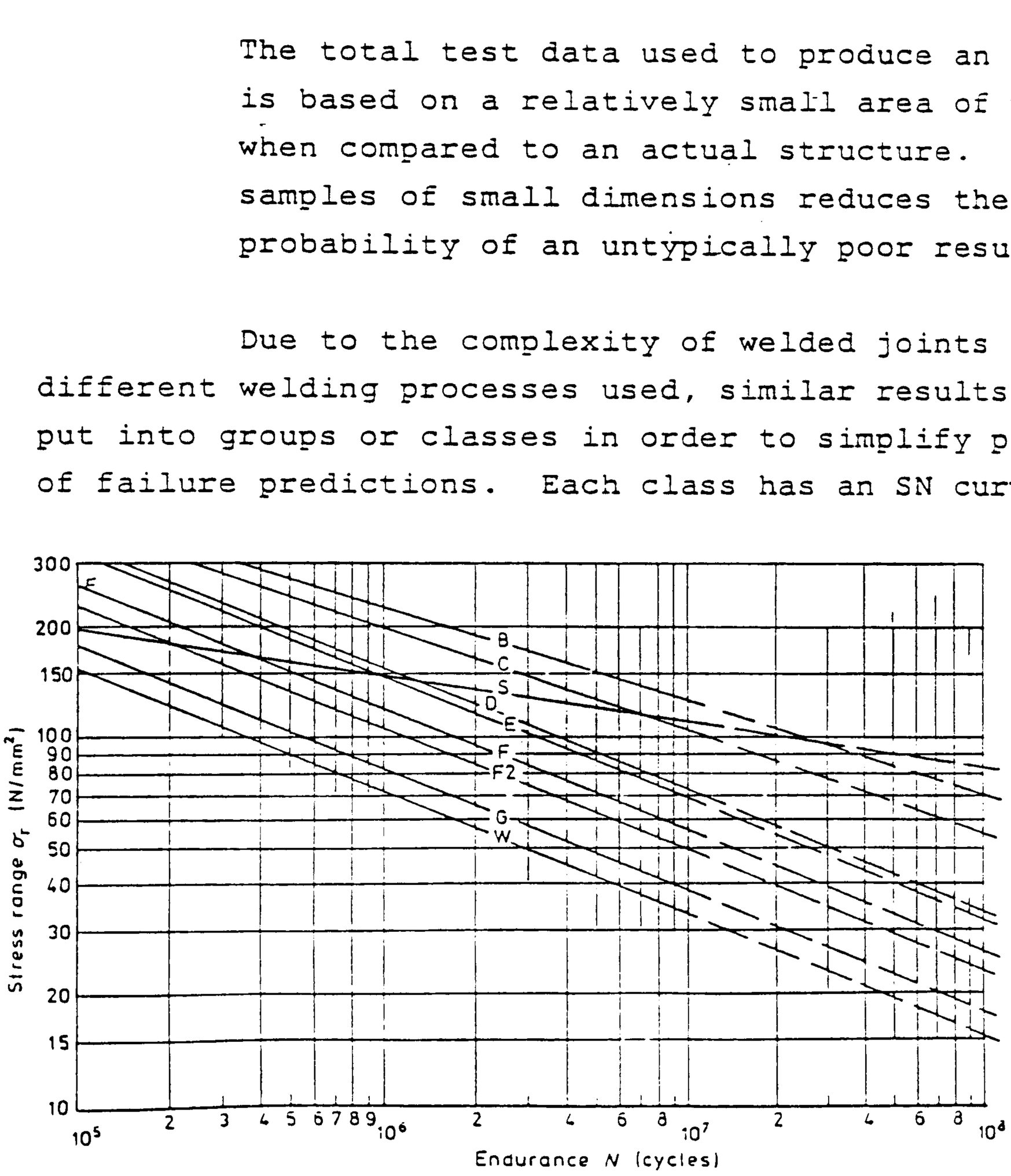

Figure 1 Cycles to failure curves for various types of welded joints.

From this, a fatigue life prediction can be made. The slope and position of the curve are very conservative to allow for shortcomings in the procedures used for data production. A "cut off" point is set at 1×10^7 cycles. If failure has not occurred after this number of cycles in a constant amplitude test, then the material is considered to be in the threshold stress intensity range below which non-propagating flaws will continue to threshold whilst the loading conditions are unchanged. However, for the purpose of this standard a safer approach is adopted and a reduced slope to allow for variable amplitude loading is used to predict failure.

A more sophisticated design approach based on SN data has been developed and termed "probabilistic fatigue". Applied to an offshore structure the main elements considered are as follows:-

Element	Notes
environment	air/seawater
load global structural response local stress	wave loading, resonance and stress concentrations
fatigue resistance	SN data
damage accumulation	Miner's rule
fracture criterion	Miner's sum to failure

The approach is as follows. Initially all random variables which may have an influence on the fatigue life are identified. Up to 25 may ultimately be considered. For each of these variables a level of uncertainty is assessed, i.e. physical, statistical or models used. This assessment may be objective but is often entirely subjective. From this information a limit state function is formulated. A safety margin is then

applied to this function to give a nominal failure probability. A decision as to whether this probability is acceptable or not is then made. This approach is clearly far more sophisticated than the simplified approach adopted by design standards such as BS 5400 mk10 (7). However, it still ultimately relies on the SN data provided by experimentation and a knowledge of stress intensities which may be occurring in stress hot spots and as a result is still widely open to criticism.

Although current fatigue design guidance is based on an average from inappropriate fatigue samples with an arbitrary safety margin, it has been used successfully for a number of years although early standards did not consider environmental effects. The SN curve design approach offers little advantage to a higher strength steel which may offer lower fatigue crack propagation rates for any given stress intensity range. Although a clear advantage may be seen when parent plate materials are compared, such dramatic losses of fatigue properties occur after welding so as to make this insignificant, the introduction of a seawater environment only adds to this problem. However, a fracture mechanics approach offers us a more detailed and realistic viewpoint. Study of fatigue crack propagation as a function of a known stress intensity range allows us to compare steel performance with similar flaws under identical loading conditions. The sensitivity of a material to a changing stress intensity range can be assessed along with more detailed examination of the thresholding phenomenon. It is likely that the majority of flaws associated with welded joints in offshore structures are predominantly in a state of threshold. If a crack were to propagate continually at a growth rate of 1×10^{-7} m/cycle, then a crack of at least a metre would be

present after ten years. A steel exhibiting a high threshold, particularly in a heat affected zone (HAZ) microstructure would clearly have great potential. The influence of cathodic protection on crack propagation rates at any given stress intensity and level of protection is readily studied by this approach. Any fatigue property benefits which may or may not be associated with HSLA steel can best be quantified by a fracture mechanic study technique.

1.2. Summary

A study into the fatigue properties of HSLA steels has been undertaken because it was felt that these higher yield strength steels may offer an advantage in terms of resistance to fatigue crack growth over the currently used structural steels. Fatigue is a yielding and fracture dominated process and therefore a material which offers higher yield strength whilst retaining good fracture toughness properties could well be expected to produce increased fatigue life. Against these predicted advantages we must also consider possible disadvantages and problems. Offshore structures are generally of a welded tubular construction which leads to a problem of high stress intensity range in the region of the weld and HAZ. Favourable fatigue and fracture properties exhibited by the parent plate must also be reflected by the HAZ. These properties must not deteriorate below acceptable levels when welding is carried out at the high heat inputs required for economic production. A second possible limitation may be imposed by the very nature of HSLA steel production processes which limits the plate section thickness which can be produced whilst retaining homogeneous through thickness properties.

In addition to the problem of unknown fatigue properties for this group of steels the current philosophy towards design standards and fatigue data do not favour higher strength steels. The improved fatigue performance shown by the parent plate in-air result may be significant. However, the introduction of a weld with its inherent flaws and its less fatigue resistant microstructure reduces the level of the S/N curves so much as to make any difference between two steels insignificant. The introduction of an aggressive environment (corrosion fatigue) reduces the properties further and therefore only adds to the problem. This is not however a very realistic approach. The design life of an offshore structure is approximately 4×10^7 cycles (20 years) and therefore when applying an S/N approach a state of thresholding must be achieved and it is on this basis that comparisons are made. However, in a real structure the loading environment is far from constant resulting in a mixture of thresholding and propagation conditions.

A fracture mechanics approach as adopted in this thesis not only allows us to compare the condition of thresholding for different steels but also the rate of crack propagation should the stress intensity range rise for a period of time (storm conditions) and the changing sensitivity to stress intensity range as a flaw increases in size.

As fatigue crack propagation is not of a continuous nature in an offshore structure but in fact consists of short periods of rapid growth followed by thresholding, a relatively small difference in crack propagation rates for two steel types may prove to be very important and is clearly worthy of further investigation.

2.0. HSLA STEELS

High strength steels began development in the early 1900's when hot rolled plates were produced to have high tensile properties. Due to the nature of early construction techniques, weldability, formability and fracture toughness were of little importance. Higher strengths were quite simply achieved via high carbon additions (0.3%). In 1934 a structural steel specification retained a high level of carbon at 0.27% but increased the manganese to 1.5% to give a steel with a yield of 350 MPa in a 3cm thick plate (8).

World War II and the introduction of welding was to change these early ideas. An alternative to high carbon content was required for successful welding of higher strength steels. Also around this time a high yield stress was found to be more important than a high tensile strength and close consideration was given to this property.

By the early 1950's the beneficial effect of ferrite grain refinement on yield stress and the ductile to brittle transition temperature had been demonstrated (9,10). Grain refining was achieved by precipitates of aluminium nitride (11). The newly developed normalised grain refined steels had yield strengths 75 to 125 MPa higher than previous structural steels together with sub-zero impact transition temperatures. Other additions such as niobium, vanadium or titanium were also found to contribute to precipitation hardening and higher yield strengths.

The need for still finer grain sizes and lower carbon additions prompted the development of controlled rolling. It was found that controlled rolling to a low finish-rolling temperature produced fine austenite and consequently fine ferrite grain size while preserving precipitation strengthening. Yield strengths had now

increased to 450 to 525 MPa with good impact transition temperatures, as low as -80^{o}C.

Accelerating the cooling of hot rolled strip products (12) produced maximum refinement of the ferrite grains by depressing the transformation temperature of the austenite.

Another approach to the development of high-strength, low alloy steels was the use of quench and tempering processes (13). These steels were first investigated about the time that controlled rolling was introduced. Quenching provides an economic means of producing high yield strengths. However, this is normally at the cost of fracture toughness. Traditional quenched steels are tempered as a means of increasing the resistance to brittle failure but subsequently suffer a reduction in yield strength. Microalloyed steels have been developed to avoid both the aforementioned limitations. Very low carbon contents produce the much tougher acicular ferrite or low carbon bainitic microstructures on quenching. Tempering does not have a detrimental effect on strength due to precipitation strengthening contributed by additions such as vanadium.

On balance steels developed along the lines of controlled rolling have been of lower yield strength than the quenched and tempered steels with lower alloying contents for excellent weldability and fracture toughness. In the offshore environment these steels have been developed for linepipe applications. Quenched and tempered steels have generally been developed for higher strength applications, however, more recently this type of steel has been produced in lower yield strengths for structural applications.

To fully understand the process of steel manufacture and development, we must consider the

individual factors contributing to the strength of a steel microstructure and any inter-relationships between them.

2.1. Strengthening Mechanisms in Steels

There are a number of different strengthening methods available for bulk steel production, these include solid-solution hardening, precipitation hardening, grain refinement, partial annealing and cold work. The technical efficiencies of the major strengthening mechanisms are considered in terms of their application in HSLA steel microstructures.

Before considering strengthening mechanisms individually we must consider all steels to be strengthened by more than one mechanism, and that these mechanisms are additive (14) in such a way that the yield strength σ_y can be described by:

$$\sigma_y = \sigma_o + \sigma_s + \sigma_p + \sigma_g + \sigma_\varepsilon \qquad \ldots (1)$$

where σ_o is the lattice friction stress and σ_s, σ_p, σ_g, and σ_ε are the respective strength increments produced by solid-solution hardening, precipitate particles, grain boundaries, and dislocations.

The relative effectiveness of these mechanisms in a modern thermomechanically treated steel is a function of composition and the details of the thermomechanical treatment to which the steel is subjected. The several strengthening contributions for steels with 0.2% carbon, 0.2% silicon, 0.15% vanadium and 0.015% nitrogen as a function of increasing manganese content are shown schematically in Figure 2 (15). As we can see, grain size makes a very substantial contribution to yield strength. However, the actual magnitude is very sensitive to the detailed thermomechanical history.

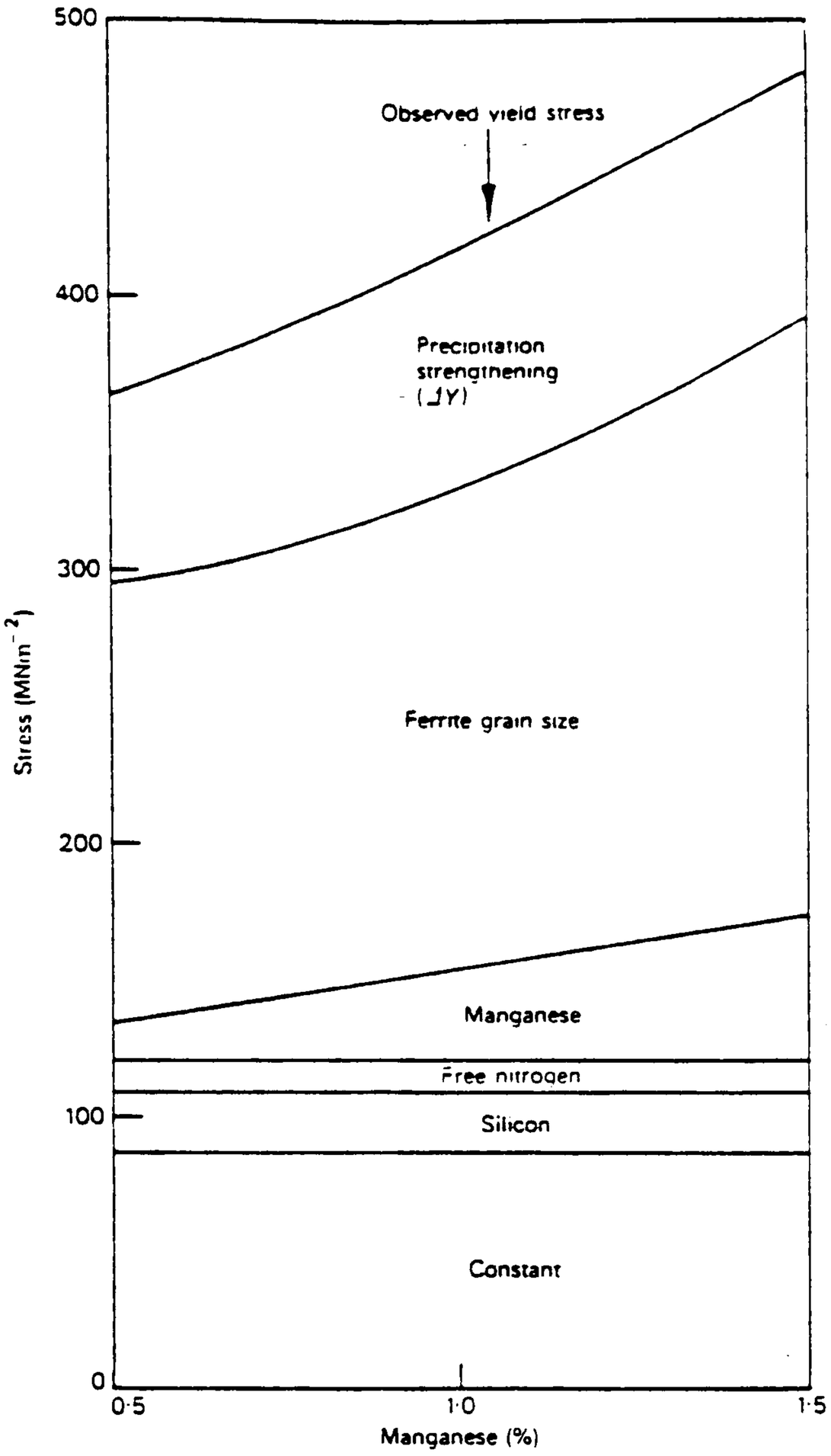

Figure 2 Strengthening contributions for carbon vanadium steels as a function of increasing manganese content.

2.1.1. Solid solution hardening

The normal result of solute atom addition is to raise the yield stress and the level of the stress strain as a whole. There are two types of solid solution. If the solute and solvent atoms are roughly similar in size, the solute atoms will occupy lattice points in the crystal lattice of the solvent atoms. This is termed "substitutional solid solution". If the solute atoms are much smaller than

the solvent atoms, they occupy interstitial positions in the solvent lattice. Carbon, nitrogen, oxygen, hydrogen and boron are the elements commonly found in steels which form interstitial solid solutions.

As solute atoms often produce a yield point discontinuity but always affect the entire stress-strain curve, we are led to conclude that solute atoms have more influence on the frictional resistance to dislocation motion than on the static locking of dislocations. Solid solution hardening is a most effective method for increasing yield strength over a pure matrix. However, the solid solubility of carbon in ferrite is less than ten parts per million (8).

2.1.2. Precipitation hardening

Traditionally, plain carbon steels have gained most of their precipitation strengthening via iron carbides in the form of pearlite. However, this is not the case with HSLA steels.

Precipitation strengthening and grain refinement cannot be considered independently due to important interactions. As a result of the combined use of controlled rolling and fine dispersions of carbo-nitrides in low alloy steels, it has been possible to obtain ferrite grain sizes between 5 and 10μm in commercial practice with extremely beneficial effects on strength.

Strengthening has been shown to depend only on the volume fraction and diameter of the precipitate providing they are non-deforming and is not influenced by their chemical composition (16,17). The variation in yield strength with particle size is schematically shown in Figure 3.

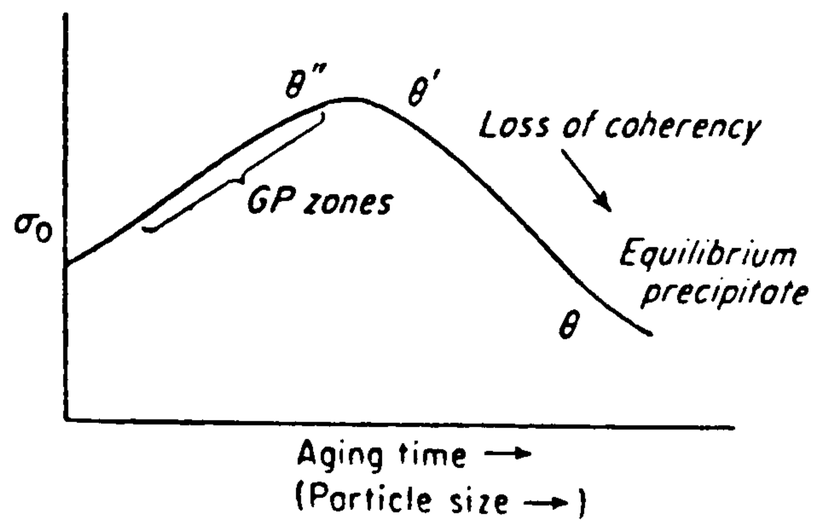

Figure 3 Variation of yield stress with aging time (schematic)

The main elements contributing to the increased strength of HSLA steels by the mechanism of precipitation hardening are titanium, niobium and vanadium. Titanium forms coarse dispersions of nitride and carbo- nitride precipitates together with a fine carbide dispersion. Niobium and vanadium form fine precipitate dispersions of carbo-nitrides.

The addition of 0.05-0.09% Nb can give a displacement of ~100 MPa between C-Mn and C-Mn-Nb steels arising from dispersion strengthening due to NbC. This is seen in the parallel curves in Figure 4 below which also show the effect of grain refinement.

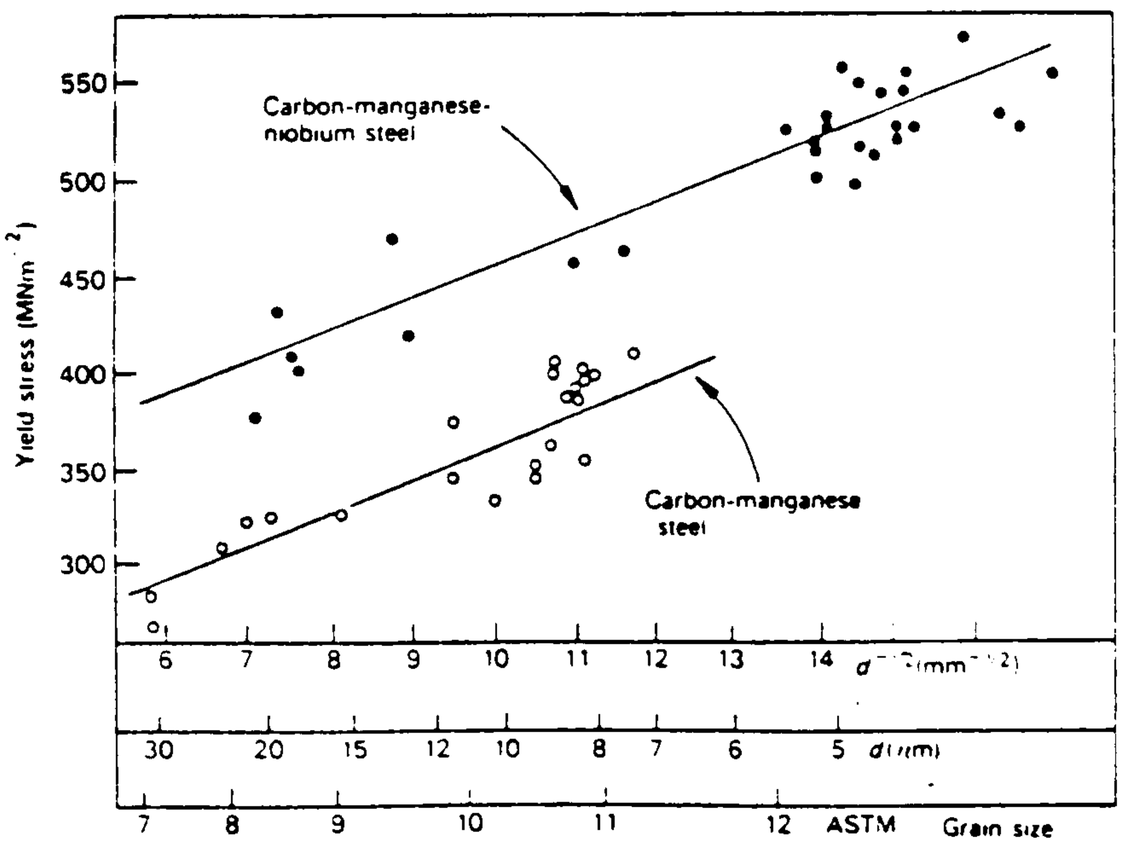

Figure 4 Effect of grain size on yield stress of a carbon-manganese-niobium steel

The effectiveness of precipitation strengthening will depend to a large extent on solubility and austenitising temperature. Shown below (15) in Figure 5 is the effect of progressively higher austenitising temperature on the yield strength of niobium containing steel.

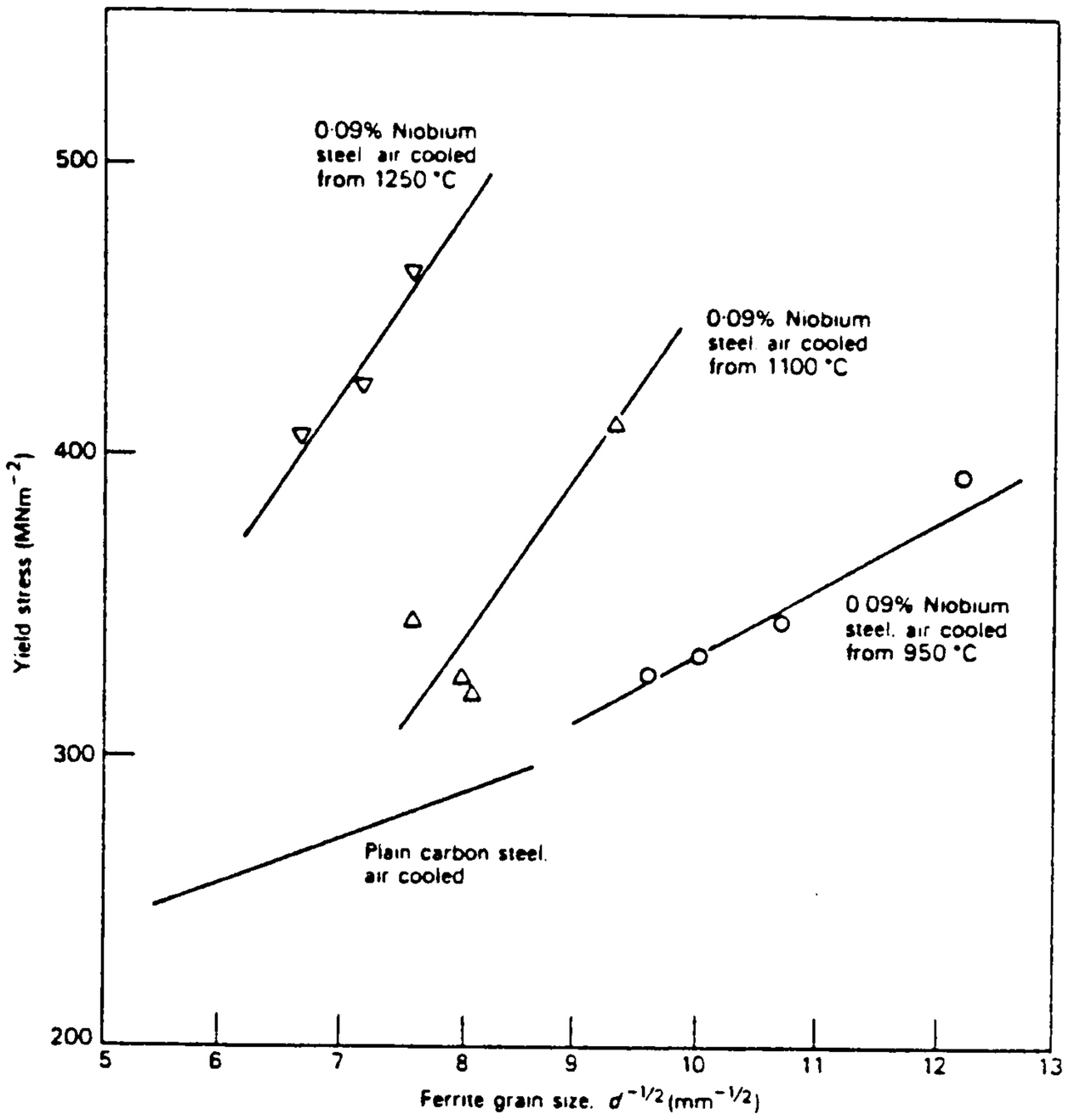

Figure 5 Effect of austenitising temperature on the yield strength of a 0.1C, 0.6Mn, 0.9Nb steel

Higher austenitising temperatures followed by air cooling results in curves with much steeper slopes, indicating a marked increase in yield strength for a particular grain size. This large increment in strength is due to the precipitation of NbC during cooling, following its solution at the higher austenitising temperatures.

Vanadium is the most soluble of the three main dispersion hardening elements and readily goes into solution in the austenite phase. This property makes it a most useful low temperature precipitate former. Vanadium preferentially

comes out of solution as $V_4 C_3$.

For quenched steels the precipitate will form as fine platelets within ferrite grains on tempering. This occurs in the temperature range 550-650^{o}C with a coarsening effect at temperatures above 700^{o}C. In a thermomechanical process, vanadium dispersions have been shown to precipitate progressively as the interphase boundaries move through the microstructure.

Similar properties are exhibited by titanium in solid solution. However, titanium is less soluble than vanadium but more soluble than niobium in the austenite phase. Overall titanium displays properties closer to those of niobium forming carbides at higher temperatures as relatively stable particles. These should remain relatively inert during commercial heat treatments involving solution temperatures no higher than 1050^{o}C.

In arriving at optimum compositions of microalloyed steels it should be borne in mind that the maximum volume fraction of precipitate which can be put into solid solution in austenite at high temperature is achieved by use of stoichiometric compositions. A combination of elements ensures formation of dispersion hardening carbides at a wide range of temperatures.

The effect of precipitates present in a matrix are twofold. Firstly, a fine dispersion of a precipitate in a material matrix will act as a barrier to dislocation movement, either acting as strong inpenetrable non-coherent particles through which dislocations can only move by sharp changes in curvature of the dislocation line, alternatively, they may act as coherent or incoherent particles through which dislocations can pass, but require an increase in stress level over that for movement through the surrounding matrix. If this increased stress level is

too great, the dislocation may be forced to bypass the second phase particles. It is therefore clear that this mechanism of strength increase is greatly dependent on particle size and dispersion.

Secondly, the consequence of precipitation may be a refinement of grain size. This has been well documented for the effect of aluminium additions to high strength steels producing a marked grain refining effect as a direct consequence of the formation of aluminium nitride particles. The size of second phase particles has an important effect on the grain size, the size of second phase particles being largely dependent upon heat treatment. The volume fraction of second phase particles is composition dependent (18).

2.1.3. Grain size

The effect of polygonal ferrite grain size, d, on the discontinuous yield stress, σ_y, has been empirically described by the Hall Petch equation (19, 10):-

$$\sigma_y = \sigma_i + k_y d^{-\frac{1}{2}} \qquad (2)$$

where σ_i = a stress constant accounting for lattice friction and solute atoms, and k_y = grain size coefficient, related to the stress concentration required to activate slip dislocation sources.

Whilst the above equation has its limitations, i.e. if extrapolated to the smallest grain size imaginable, it would predict strength levels close to the theoretical shear strength, it does however illustrate the very important effect of grain size upon yield strength. Therefore, any process or compositional variation resulting in a grain refinement will contribute greatly to the yield strength of any steel.

This relationship is shown in Figure 6 below (20) where the linear relationship between σ_y and $d^{-\frac{1}{2}}$ is clearly seen for three test temperatures.

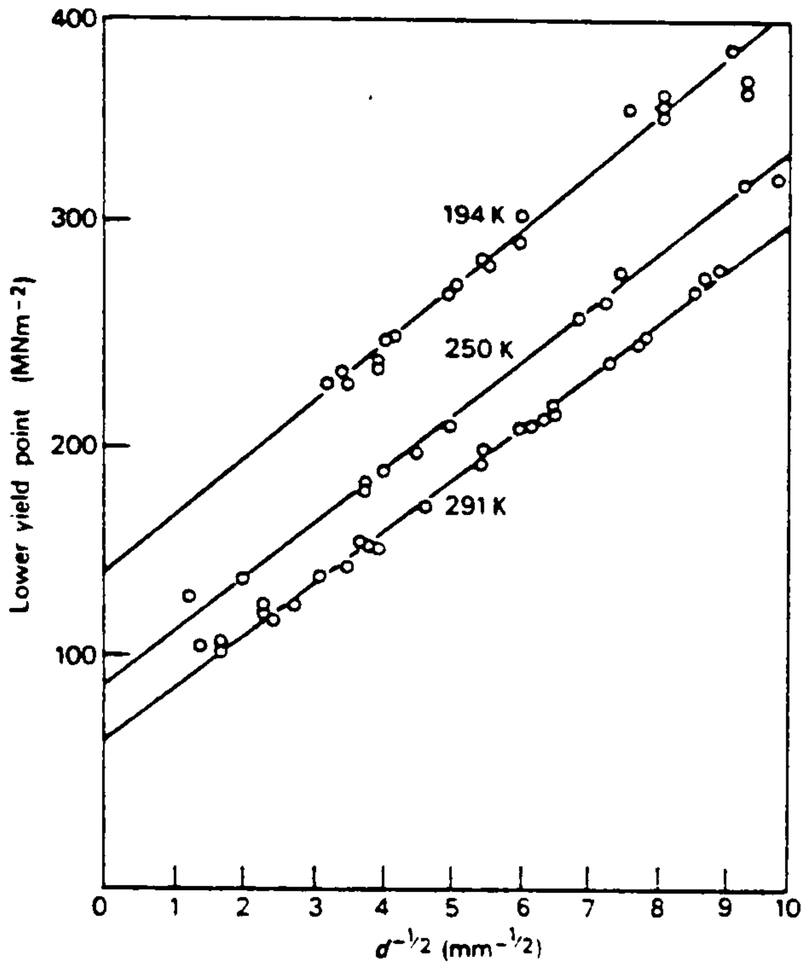

Figure 6 Dependence of the lower yield stress of mild steel on grain size

The grain size effect on yield stress can be explained by assuming that a dislocation source operates within a crystal causing dislocations to move and eventually to pile up at the grain boundary. This pile up generates stress across the boundary which activates a new source in the grain. This process is repeated and yielding occurs. The grain size therefore determines the distance over which dislocations can move before pile up and new source operation must occur. The sensitivity of yield to temperature is related to the friction stress σ_o, which is the stress required to move free dislocations along slip planes.

Grain refinement techniques cannot be separated from precipitation hardening processes as already discussed. When thermomechanical processing is allied to the aforementioned precipitation hardening, we have a most

effective means of grain refinement to produce steels of the required strength and toughness.

The most important thermomechanical process variable in determining the final grain size is the temperature at which hot working is completed or the final annealing temperature for cold worked material. In hot-working processes fine grain size is favoured by a low finishing temperature and a rapid cooling rate from the working temperature. In processing steels which undergo a structural transformation on cooling from the finishing temperature, the ferrite grain size depends on achieving a fine prior austenite grain size which is promoted by taking large reductions in the final pass which is made at the lowest possible temperature in the austenite phase field.

The formation of sub-grains in an annealed material results in a significant increase in strength and this strengthening has been shown to be additive to that produced by solid-solution hardening (18).

The formation of a substructure such as lower bainite is an alternative means of increasing yield strength but at some penalty to ductility. Bainitic plates nucleate at austenitic grain boundaries and within grains also producing secondary plate forms from primary plates away from the grain boundaries.

The cooling rates over which bainite forms may be widened by addition of ½% Mo and small concentrations of boron. The temperature at which the transformation occurs is most effectively lowered by high carbon contents, but as this is undesirable in low alloy steels, a combination of Ni, Cr and Mn is often used.

2.2. Controlled Rolling Summary

The major aim of controlled rolling is to produce a fine grained, equiaxed, polygonal microstructure. Due to the nature of thermomechanical processing, soft inclusions such as manganese sulphides must be avoided as these would become elongated and would drastically reduce fracture toughness. The primary grain refinement mechanism is the recrystallisation of austenite during hot deformation, known as dynamic recrystallisation. Large reductions per pass are favoured in this regime to promote a fine uniform recrystallised austenite. Clearly, high temperatures at this stage will be detrimental as grain growth will occur, this effect being most marked if desired reductions per pass are not achieved and interpass time delays are too great. This type of difficulty will lead to uneven grain growth resulting in a mixed grain structure and subsequent toughness loss.

These problems are to a large extent overcome by the introduction of fine particles into the austenite matrix. These particles are nitrides and carbides of aluminium, vanadium, niobium and titanium. The particles are usually found on grain boundaries because an interaction takes place between the particles and the boundary. A short length of grain boundary is replaced by the particle and the interfacial energy ensures a stable configuration. When the grain boundary attempts to migrate away from the particles, the local energy increases and thus a drag is exerted on the boundary by the particles. The degree of solubility of the stable nitrides and carbides in austenite is very important. It is essential that there is sufficient solid solubility at the highest austenitising temperatures to allow fine precipitation to occur during controlled rolling at temperatures which decrease as rolling proceeds.

The austenite phase may recrystallise several times during a controlled rolling schedule and the total effect of this will be a marked austenite grain refinement by the time the steel reaches the austenite/ferrite transformation temperature. In the later stages of austenite deformation, at lower temperatures, recrystallisation may not occur, so long flattened austenite grains may transform directly to ferrite. It has become common practice to continue rolling through the austenite/ferrite transformation to produce finer final grain sizes. However, this type of rolling imposes much higher demands on rolling mills.

The final microstructure will show exceptional grain refinement leading to high yield strength at low alloy additions coupled to excellent toughness properties. An extra degree of strengthening will occur from precipitation hardening ($\sim$ 100 MPa).

2.3. Quench and Tempering Summary

The process of quenching has been used for many years for production of higher strength steels with lower alloying levels (8). The aim of quenching is to produce a sub-grain structure and hence increased strength. However, in higher carbon steels this strengthening has been at the cost of ductility.

A high austenitising temperature is preferred to ensure good solubility of precipitation hardening particles. However, a short holding time is essential if excessive grain growth is to be avoided. A programme of controlled rolling is carried out to promote austenite recrystallisation and refinement. Close control of interpass temperatures is required so that the plate will enter the quench mill at exactly the right temperature. The temperature range at which the quench is effective can be widened by the addition of boron and ½% Mo and/or lowered by additions of

Ni, Cr and Mn. At this stage in the thermomechanical treatment a microstructure has been produced with a sub-grain structure and a small degree of precipitation strengthening. However, most of the potential particles are locked in solution by the rapid quench. At this point the steel is seen to exhibit a lower than desired yield strength with excellent toughness. On tempering, fine dispersions, often vanadium carbides, are allowed to form so increasing the strength of the steel but at some cost to ductility.

Quenched and tempered HSLA steels cover a wide range of strength levels, the higher yield strength examples often containing somewhat more carbon as well as increased alloying to obtain the necessary hardenability. The development of on-line quenching, allowing the quench to follow directly from a programme of controlled rolling, has increased strengths at lower alloying levels. However, the problem of achieving uniform temperature distribution and of the inherent low thermal diffusivity of steel limits the section size of steels produced by this process.

3.0. FATIGUE CRACK PROPAGATION

The study of fatigue crack propagation examines how a crack grows under a cyclic load whose maximum value is below the yield stress for the material. A propagating crack is normally described in terms of crack extension per cycle as a function of the stress intensity range experienced at the crack tip, the stress intensity range being calculated by means of linear elastic fracture mechanics. However, it should be noted that a propagating fatigue crack will yield average crack growth steps per cycle over a very wide range depending on the stress state, from 10^{-9} m/cycle to 10^{-6} m/cycle, indicating the presence of more than one mechanism and indeed it is generally accepted that the log da/dN versus log ΔK plot can be divided into three regions as shown in Figure 7.

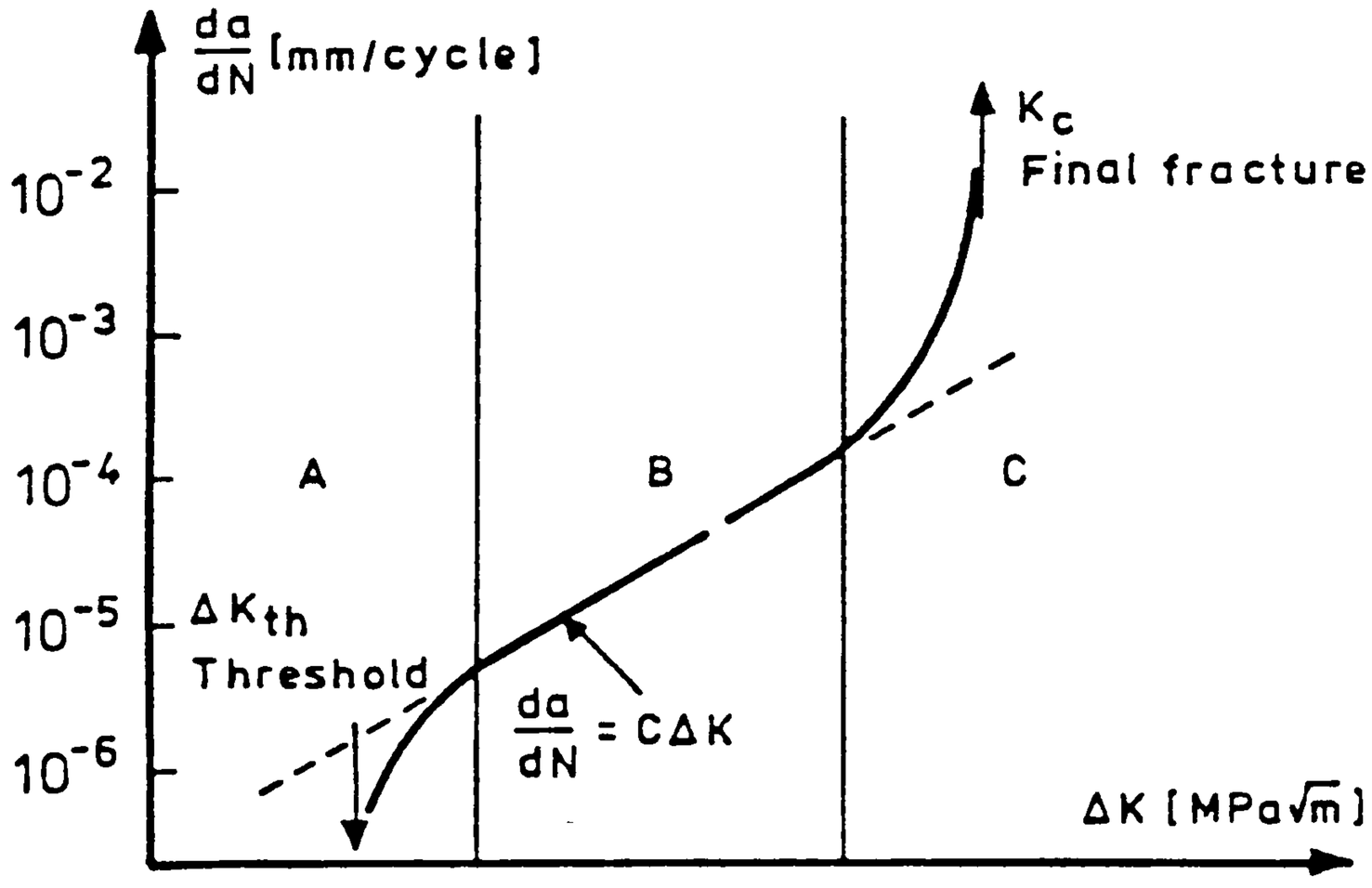

Figure 7 da/dN versus ΔK plot (schematic)

da/dN is the increase in the through specimen crack length "a" per stress cycle "N" and the parameter $\Delta K = K_{max} - K_{min}$ where K_{max} and K_{min} are the maximum and minimum stress intensity factors in the fatigue cycle. All three regions described in Figure 7 have their own characteristics and are influenced by loading parameters and environmental conditions to a greater or lesser degree depending on the microstructure of the material.

In 1963, Paris and Erdogan (21) critically reviewed the fatigue crack growth laws available at the time and concluded that the crack extension per cycle, da/dN, is related to the alternating stress intensity factor ΔK by the equation:

$$da/dN = C\ \Delta K^m \qquad (3)$$

where m has a value normally between 2 and 4, whilst C is a material constant. However, as can be seen in Figure 7, a typical log-log plot of fatigue crack growth step per cycle versus the stress intensity range, the Paris-Erdogan law is only valid for the intermediate or steady-state propagation range designated region II.

As region II is generally quoted when considering the fatigue behaviour of a material it will be considered first.

3.1. Intermediate or Stage II Crack Growth

For steels intermediate growth rates are expected to fall between 10^{-9} and 10^{-6} m/cycle, and the Paris-Erdogan law to give a good description as is generally found for region II, with the exponent m generally in the range $2 < m < 5$. This predictability and the vast accumulation of crack growth data for many engineering materials allow the defect-tolerant approach in the design against fatigue to

be applied with the greatest confidence in this intermediate growth region.

The importance of region II and the relationship for crack growth is greatly increased by this approach as the fatigue life is taken to be the number of cycles required to propagate a pre-existing defect from an initial size to the critical crack size which can initiate an unstable fast fracture. This pre-existing flaw size may be taken as that just small enough to escape detection and may be the result of fabrication processes such as welding. Clearly, a precise knowledge of the crack growth rate in a given loading environment is required together with an understanding of environmental and loading factors which may influence the steady-state propagation mechanism.

Extensive research has been conducted in an attempt to determine the laws of fatigue crack propagation which may be reliably applied to region II growth (22). Fatigue crack propagation models derived by various workers will be discussed in a separate section. It is generally accepted that within region II a linear relationship between log ΔK and log da/dN exists (21). This relationship is valid until a critical stress intensity is reached at which the propagating crack enters region III.

The crack tip stress intensity range is calculated via linear elastic fracture mechanics:-

$$\Delta K = \frac{\Delta P . Y_1}{B.\sqrt{W}} \qquad (4)$$

where ΔP = load range, B = sample thickness, W = sample width, and Y_1 = compliance factor. However, this equation does not take into consideration the loading ratio, R, where:-

$$R = \frac{P_{min}}{P_{max}} \qquad (4a)$$

the load range alone is considered. In a tensile/tensile loading cycle if the loading ratio R is increased from 0 to 1, both P_{max} and P_{min} must be increased to maintain ΔP in equation (4) and so maintain a constant stress intensity. Clearly the loading parameters are not the same despite a constant stress intensity. These parameters are K_{max} and K_{mean}.

$$K_{max} = \frac{\Delta K}{1-R} \qquad K_{mean} = \left(\frac{K_{max} - K_{min}}{2}\right) + K_{min} \qquad (5)$$

3.1.1. Effect of R

Roberts and Erdogan (23) and Forman et al (24) observed the sensitivity of crack growth rates in aluminium alloys to the mean stress intensity and subsequently modified the conventional Paris equation. From consideration of crack tip plasticity, Roberts and Erdogan proposed:-

$$\frac{da}{dN} = C(K_{max})^{\alpha 1} (\Delta K)^{\alpha 2} \qquad (6)$$

where $\alpha 1$ and $\alpha 2$ were both evaluated at 2. Forman et al considered the consequences of K_{max} exceeding the fracture toughness, K_c, of the test material and based on:-

$$K_{max} \xrightarrow{\lim} K_c \quad ; \quad \frac{da}{dN} = \infty \qquad (7)$$

they proposed:

$$\frac{da}{dN} = \frac{C\ (\Delta K)^m}{[(1-R)\ K_c - \Delta K]}\beta \qquad (8)$$

where β is unity.

Both sets of researchers attempt to account for the increase in growth increments per cycle associated with higher values of loading ratio, R, from observations and correlation with experimental data.

Another approach adopted by Elber (25,26) considers the situation at the crack tip at the minimum applied load. Elber detected crack closure in 5mm thick specimens of 2024-T3 aluminium loaded in cyclic tension/ tension. Elber suggested that the plastic zone progressing in front of the crack tip left a wake of plastic deformation on the fracture surface which would interfere with subsequent crack advancement. In this model the crack tip never closes on unloading due to the mis-match of fracture surfaces caused by the plastic deformation; thus showing an inadequacy in calculating stress intensity ranges via a simple fracture mechanics approach. This led to the introduction of a ΔK-effective to replace ΔK. However, it is clear that this phenomenon will be at its greatest at low R values. Elber has shown that the amount of closure decreases as R is increased and proposed the following modification to the Paris equation:-

$$\frac{da}{dN} = C\ (\Delta K_{eff})^m = C\ (U\ \Delta K)^m \qquad (9)$$

where $U = \dfrac{K_{max} - K_{op}}{K_{max} - K_{min}}$

K_{op} is the stress intensity at which the crack tip opens. This argument assumes that damage does not occur when the stress singularity is destroyed by closure. The work of Elber (25,26) was conducted on thin aluminium samples and there has been some controversy as to its relevance to thicker steel samples.

It is clear that a wide disagreement on the importance of different loading factors exists in the field of fatigue. One major reason for this is undoubtedly the wide range of materials studied from which general laws for fatigue crack propagation have been derived.

A summary of such expressions is given in Table I. These expressions are by and large derived from experimental data and bare no relation to a fatigue crack propagation model.

3.1.2. Effect of frequency

This already complex situation becomes more so when frequency of loading is also taken into account.

Work by Musuva and Radon (27), Figure 8, shows little effect of R ratio on 24mm thick samples tested at a frequency of 30 Hz, however, a sample of 12mm thickness in the same test showed a much stronger effect, Figure 9.

Tests conducted on similar samples at a frequency of 0.25 Hz show an increased effect of stress ratio for both thicknesses. This is shown in Figures 10 and 11. Although this type of frequency effect has been reported (27) it has not been considered in any of the crack propagation relationships encountered. Clearly, comparisons of fatigue data should be made at similar testing frequencies.

Mathematical Equation for da/dN		Author
$\alpha_1 \left(\frac{\Delta K}{\sigma_{sy}}\right)^2$	A	Liu
$\frac{\alpha_2}{l_2} \left(\frac{\Delta K}{\sigma_{sy}}\right)^4$	B	Paris
$\alpha_3 \frac{\Delta K^4}{\sigma_{sy}^2 (K_{Ic}^2 - K_{max}^2)} ; K_{max} \ll K_1, \alpha_3 \frac{\Delta K^4}{\sigma_{sy}^2 K_{Ic}^2}$	C	Raju
$\alpha_4 \frac{\Delta K^4 E}{\sigma_{sy}^3 K_{Ic}^2}$	D	Cherepanov
$\frac{\alpha_5}{l_5} \left(\frac{\Delta K}{\sigma_{sy}}\right)^4$	E	Rice
$\alpha_6 \frac{\Delta K^4}{\gamma E \sigma_{sy}^2}$	F	Weertman
$\alpha_7 \frac{\Delta K^4}{\gamma_p \mu \sigma_a^2}$	F'	Weertman Mura and Lin
$\alpha_8 \frac{\Delta K^2}{E \sigma_{sy}}$	G	Lardner
$\alpha_9 \frac{\Delta K^2}{E \sigma_{sy}}$	H	Schwalbe
$\alpha_{10} \left(\frac{\Delta K}{E}\right)^2$	I	Pook and Frost
$\frac{\pi}{8} \left(\frac{\Delta K}{\sigma_{sy}}\right)^2 \left(\frac{\Delta \sigma}{\sigma_0}\right)^{1/\beta}$	J	Tomkins
$\frac{(\Delta K - \Delta K_{TH})^2}{\sigma_{sy} E} f(\Delta K, K_{Ic}, K_{max})$	K	McEvily

Table I Summary of expressions relating crack propagation to stress intensity range

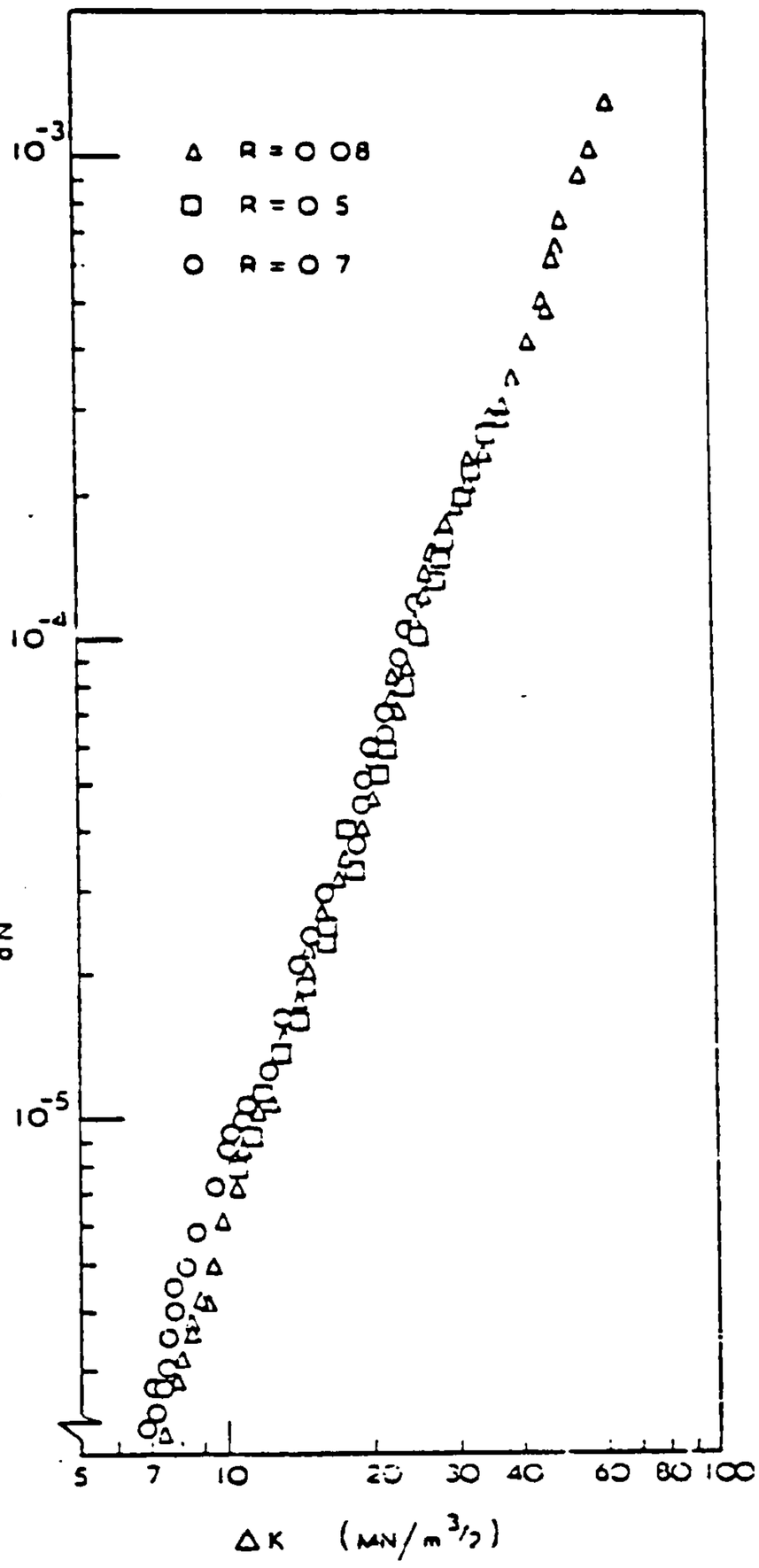

Figure 8

da/dN versus ΔK at 30 Hz,
B = 24mm

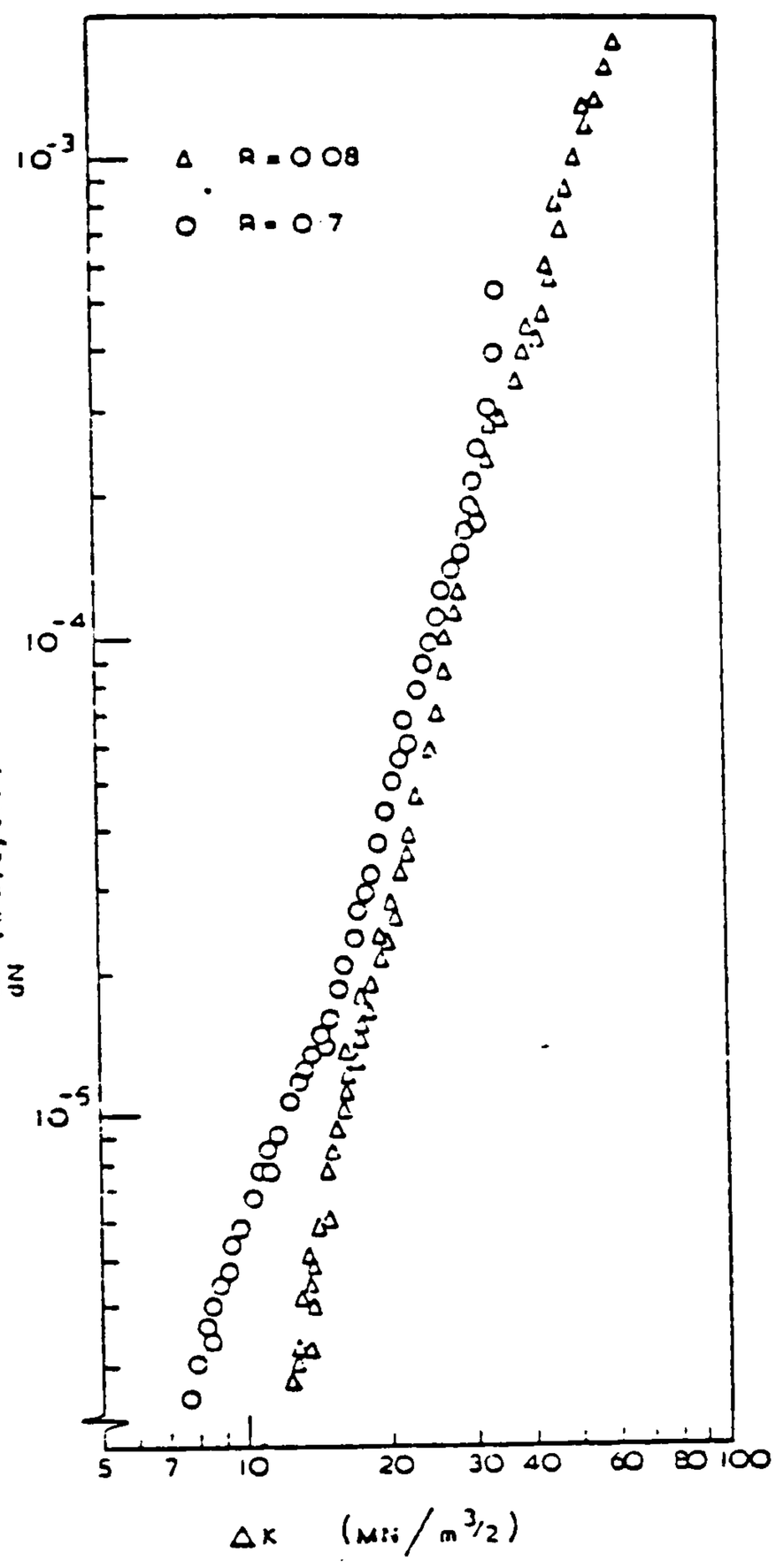

Figure 9

da/dN versus ΔK at 30 Hz,
B = 12mm

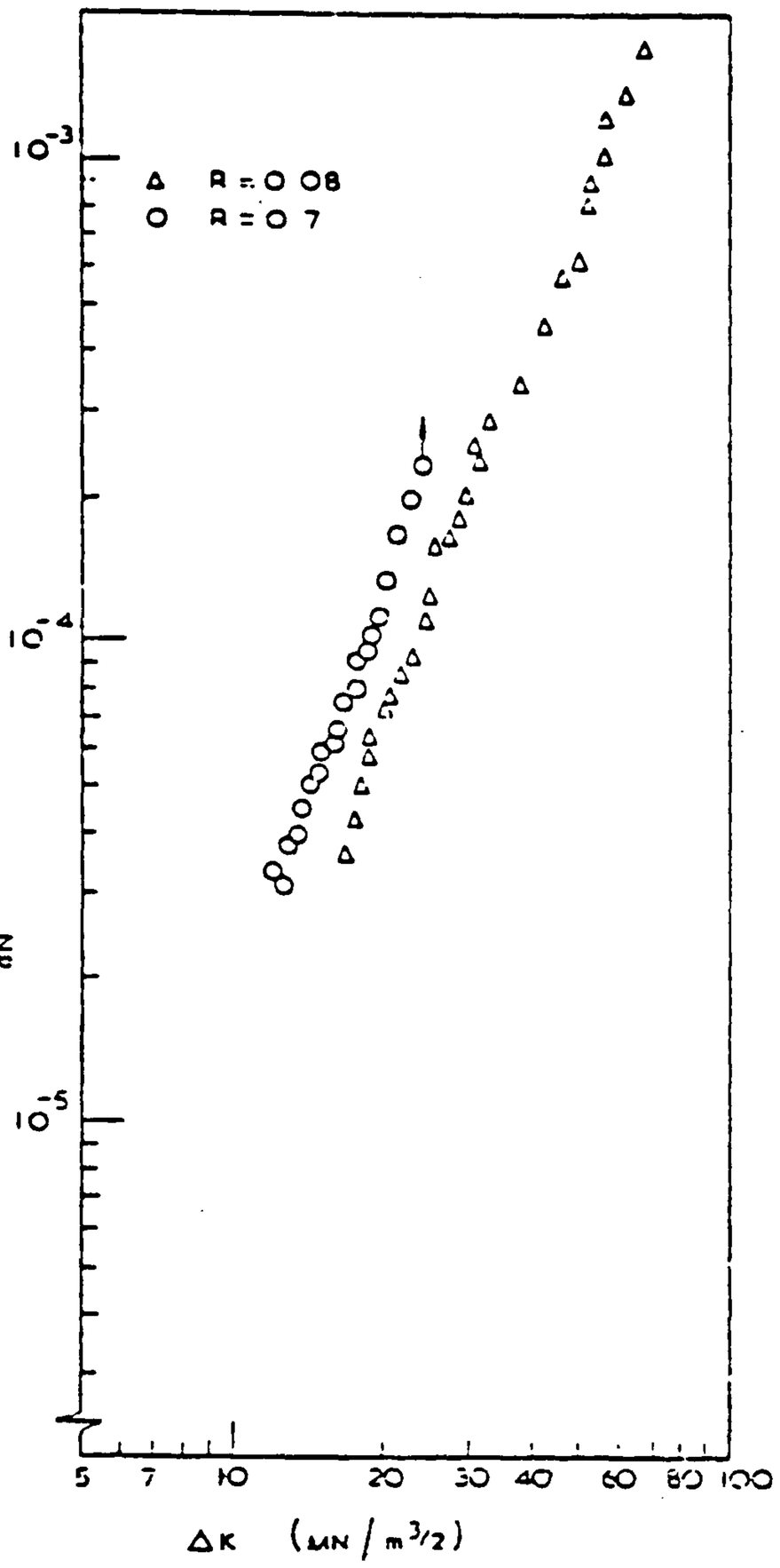

Figure 10

da/dN versus ΔK at 0.25 Hz, B = 24mm

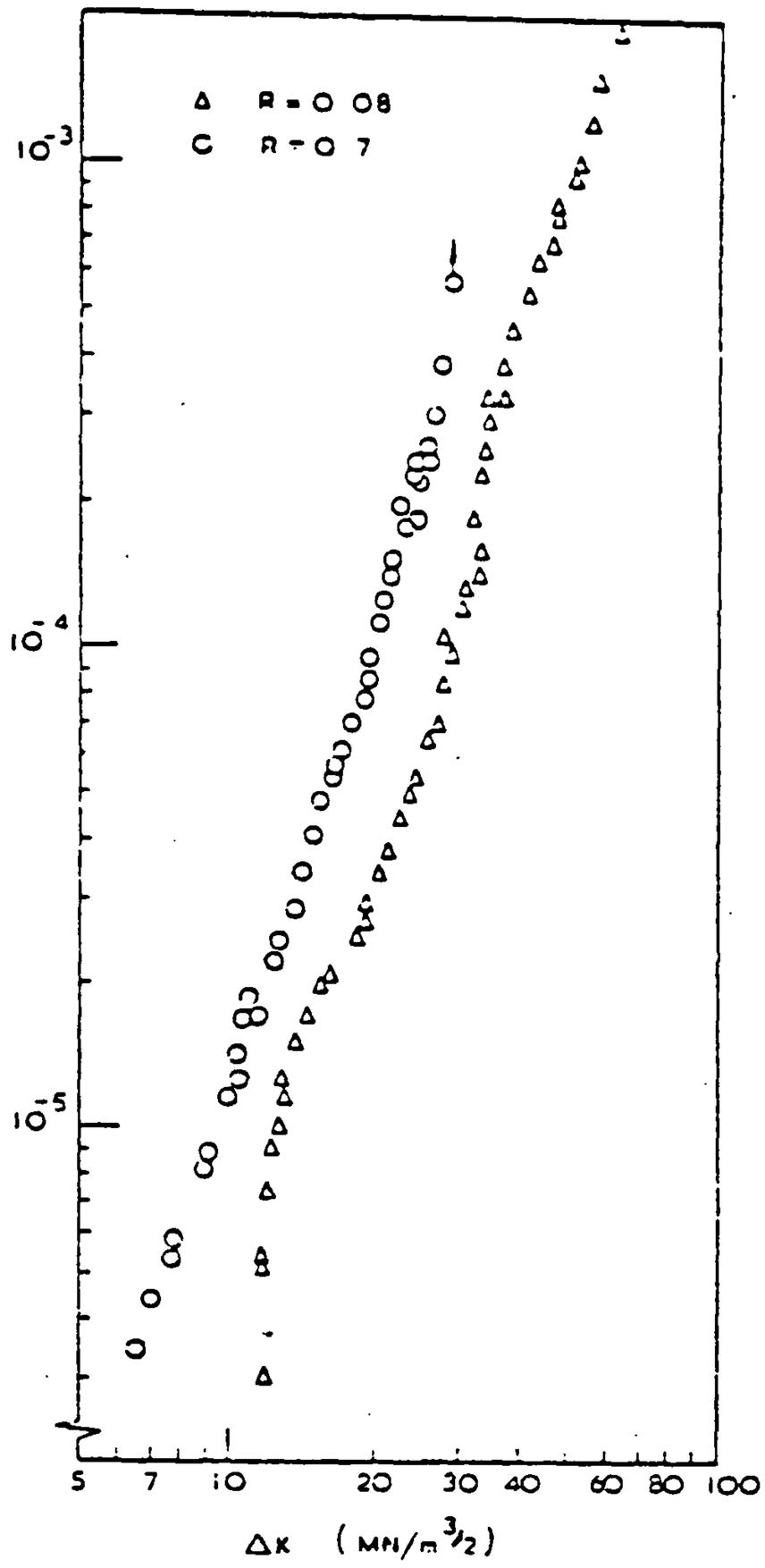

Figure 11

da/dN versus ΔK at 0.25 Hz, B = 12mm

3.1.3. Sample geometry

As stated earlier, fatigue tests have been conducted on a very wide range of sample geometries, from small scale laboratory samples up to actual structures. In laboratory testing, samples are frequently of the simple edged notched or compact tension format. This allows simple crack tip stress intensity determinations via a linear elastic fracture mechanics approach. Also direct observation of crack length and crack growth increment per cycle is greatly simplified by this approach.

However, tests are also conducted on actual nodal joints and welded samples designed to mimic in-service conditions. This complicates stress intensity determinations and creates difficulties in crack length measurements.

The main effect of sample geometry on a propagating fatigue crack is a result of the constraint offered by the material around the crack tip, so determining whether a condition of plane strain (high constraint) or plane stress exists. A crack in the centre of an infinitely thick plate will be entirely in plane strain. At the other extreme, a crack on the edge of a thin plate will be entirely in plane stress. A single edge notched sample, shown in Figure 12, exhibits a combination of the two conditions.

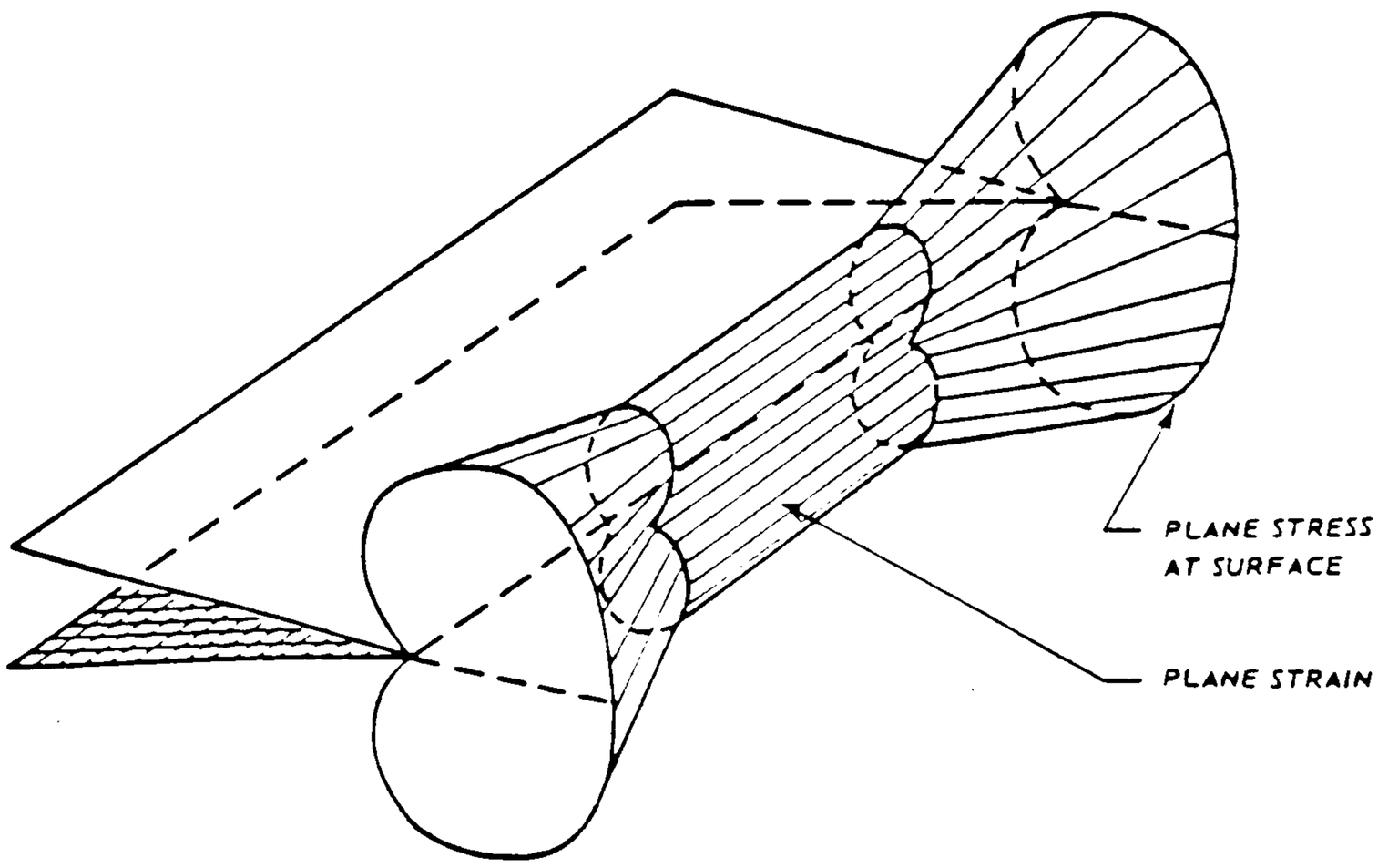

Figure 12 Plastic zone shape in single edge notched sample.

In a real structure, however, a much higher level of constraint is likely to prevail and consequently the condition of plane strain will predominate. Work by Musuva and Radom (27) has shown that a thin sample, predominantly in plane stress, will exhibit superior fatigue properties over a thicker sample when tested at low values of R (0.08). This observed effect diminishes as the R ratio is increased (0.7). At low values of R, crack closure will occur, the degree of which is influenced by the constraint offered by the sample (28). The effect of sample geometry is also emphasised by low frequency testing (frequencies below 1 Hz), (27).

3.1.4. Thresholds

The occurrence of a fatigue crack propagation threshold can be described as a region when a small reduction in stress intensity causes a vast reduction in crack growth rates and vice-versa. A wide variation between steels exists as to the stress intensity at which this change in growth mechanism occurs. Variation in fatigue crack thresholding properties cannot be rationalised only in terms of yield strength. Esaklul et al (29) has found that two HSLA steels have shown opposite trends in the threshold versus the Paris Law regime. Benson and Edmonds (30) tested a range of microstructures in ½ Cr, ½ Mo, ¼ V steel and found that the threshold decreased through the sequence of isothermally transformed ferrite, furnace-cooled ferrite, bainite, as-received ferrite, and tempered martensite. The general trend seen was a reduction in threshold as the yield stress was increased. Ritchie (31) has reported a similar trend for published threshold values in steels.

In an earlier investigation, Massunave and Bailon (32) demonstrated an effect of grain size at constant yield in a ferritic steel. They showed that while the

yield stress remained nearly constant for the coarsest grain sizes, ΔK_{th} increased as the grain size was increased by a factor of about two.

The relationship between yield strength and thresholding has been attributed by several workers (29-31) to an effect of hydrogen from the environment on a critical stress criterion for crack propagation. Ferritic, bainitic and martensite microstructures have all shown evidence of intergranular cracking at low stress intensities (30). Ritchie has stated that the occurrence of intergranular cracking in this region is due to the influence of water vapour in air environment, causing hydrogen to diffuse to and embrittle prior austenite grain boundaries. Cooke et al (33) have shown that by testing a similar steel in vacuo the intergranular fracture largely disappears.

The effect of grain size on threshold values is more widely disputed and less well understood. Massunave and Bailon (32) rationalised that the grain size effect on threshold was due to the deviation of the crack front path as it propagated through different size grains. A compatibility requirement between the propagating crack front and certain crystallographic slip systems had to be satisfied for crack growth and the probability of the necessary conditions being fulfilled increased as the grain size decreased. Priddle (34) however, concluded that crack path deviation from the plane of maximum tensile stress led to a reduction in the effective stress intensity. Additional reduction in the value of ΔK was thought to be associated with the increase in real crack surface area as compared to the observed macroscopic crack length and specimen width.

Gerberich and Moody (35) modelled the threshold stress condition by considering that a semi-cohesive zone developed due to irregularities in an equilibrium crack

front which consisted of ligaments related to the grain size. The ligaments acted as tractions to reduce the stress intensity at the crack tip. Ritchie (36) has suggested that threshold may be increased by oxide induced crack closure, especially at low R ratios. It should be remembered that yield strength and grain size are very interdependent making a true evaluation of just one effect extremely difficult.

3.1.5. Stage III fatigue crack growth

As a propagating fatigue crack enters region III the following effects are observed:

(i) an acceleration in growth per cycle,
(ii) increased values of the exponent m,
(iii) large microstructure effects,
(iv) a marked influence of load ratio.

This behaviour has been characterised in terms of the occurrence of static fracture modes (37, 38). It would follow from this that optimum fatigue cracking resistance in this region is achieved with high toughness micro-structures.

3.2. Thresholding Loading Variables and Measurement Technique

The measurement of fatigue crack growth rates, and in particular the so-called fatigue crack growth threshold (ΔK_{th}), has become increasingly important (39). Due to the low fatigue crack propagation rates which have to be measured, difficulties in achieving results in realistic time periods arise. Techniques used to determine thresholds may have a significant effect on the value obtained. Three popular techniques are described below.

(a) Pook's Method (40)

Pre-cracked samples are stress-relieved in vacuo before testing under a constant cyclic load either to failure or until some preset number of cycles (e.g. $N = 10^7$) has been achieved. This is basically an SN type experiment applied specifically to determine the threshold stress intensity.

(b) Sailon's Method (41)

Initially, pre-cracked specimens are tested from some arbitrary level of ΔK. An exponential decrease in ΔK with N is used to obtain an initial approximation to threshold. This procedure is repeated from a value of ΔK between the approximate threshold and the original starting value of ΔK. Repetition of this procedure moves the approximate ΔK to lower values until constant arrest occurs. The ΔK at which this happens is taken as the threshold.

(c) Decreasing ΔK versus Crack Length (42)

As the crack length increases the ΔK is reduced at a rate dependent upon the size of the plastic zone ahead of the crack tip. The ΔK at which the crack appears to arrest is taken to be the threshold.

Each method has its advantages. Pook's method is simple but requires large numbers of specimens. Sailon's method is probably the quickest technique for ΔK_{th} determination, however no account is given to the possible effect of a change in the $\Delta K/N$ slope on the threshold value. The decreasing ΔK with increasing crack length

technique is presently the most commonly used technique (39). However, a lack of consistency between different workers exists, in particular with regard to the magnitude of ΔK reduction per increment of crack growth and the importance placed upon plastic zone size. It may be more consistent if the same rate of reduction in ΔK with respect to the crack length was maintained, i.e. constant $d(\Delta K)/da$.

3.3. The Influence of a Seawater Environment on Fatigue Crack Propagation

It is true to say that the loading variables discussed for "in-air" fatigue testing become more important when coupled to the effects of a seawater environment. It is widely accepted that a seawater environment has a detrimental effect on fatigue crack propagation resistance when testing is conducted at low frequency (43,44,45).

Figure 13 shows the effect of seawater on a correctly protected structural steel (43). However, from corrosion fatigue studies which involved testing at higher frequencies, it has been shown that at frequencies in excess of 1.0 Hz, seawater has little if any adverse influence on fatigue crack propagation (43). There is also some evidence that saltwater environments have little effect over air on the thresholds for pre-existing sharp cracks at all frequencies (43).

The introduction of impressed current cathodic protection into this system increases the relative effects of the loading variables. Slight overprotection in sea-water causes calcareous deposits to be precipitated onto the specimen and into the fatigue crack; this may provide a physical barrier to crack tip closure on unloading, so decreasing the cyclic amplitude for a given stress cycle.

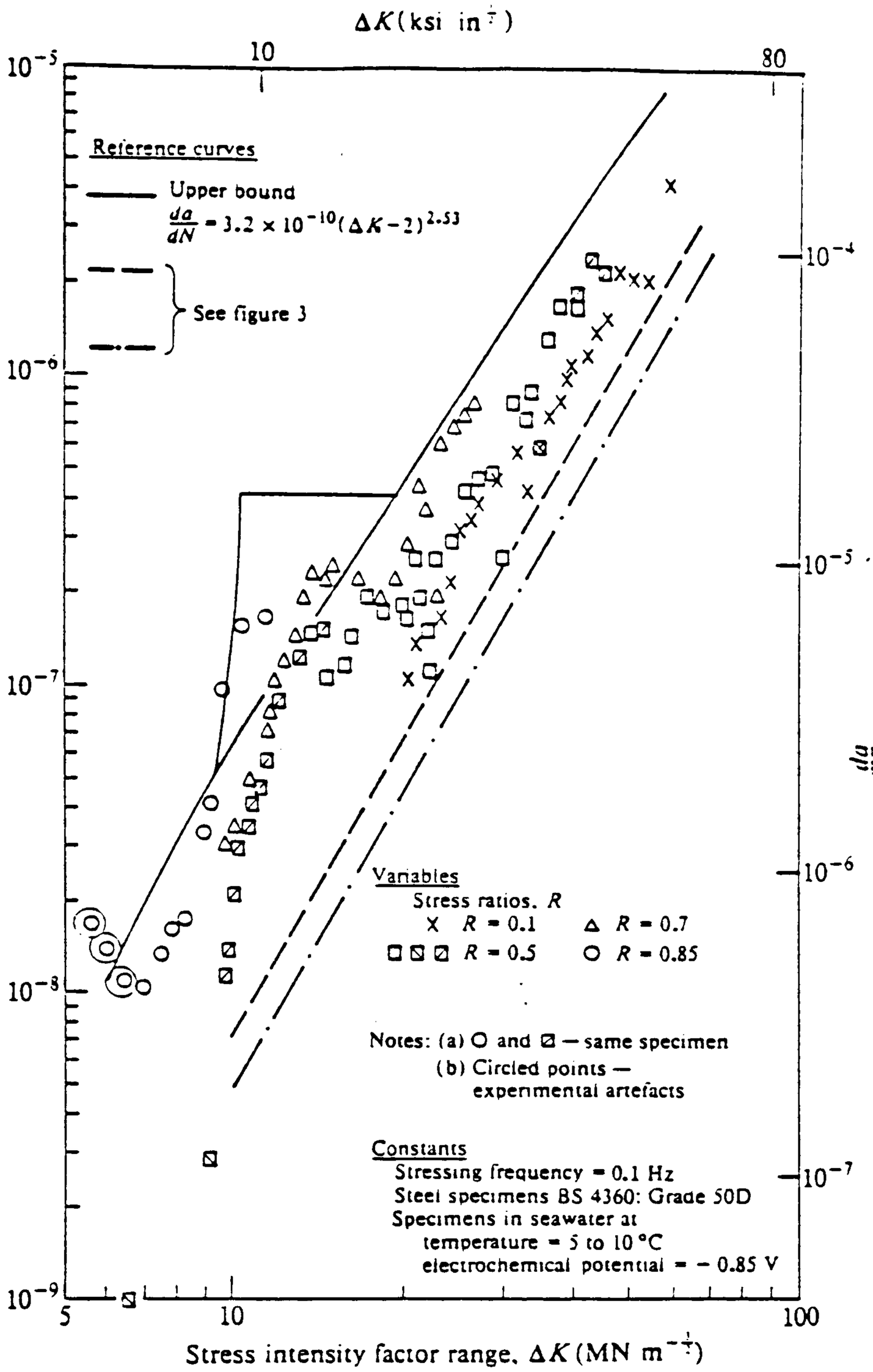

Figure 13 Crack propagation data for specimens at an electrochemical potential of -0.85 V

This effect will reduce fatigue crack propagation rates and may have its greatest influence at low stress ratios. Some earlier work in the field of corrosion fatigue was conducted in 3.5 percent sodium chloride solution and with a lack of appreciation for the considerably adverse influence of low test frequencies in a corrosive environment.(43).

It could be concluded that fatigue behaviour and its response to cathodic polarisation at frequencies of approximately 0.1 Hz in a seawater environment is a combination of corrosion and excessive cathodic polarisation and the possible beneficial effect of calcareous scale reducing crack tip closure on unloading.

3.4. Microstructural Influence on Fatigue

As previously described in Figure 2, the relationship between fatigue crack growth and ΔK for a structural alloy tested in a non-aggressive environment such as air can be divided into three regions. It is widely believed that there is a strong correlation between microstructure and thresholding properties. However, a great deal of controversy over the importance of any microstructural relationship for region II exists.
It has been stated by several researchers that microstructure is of little importance in determining the performance of a material undergoing steady state, stage II, fatigue crack propagation. This observation is generally based on the assumption that a ductile striation mechanism for fatigue crack propagation is occurring. If this was always the case then it would perhaps be fair to assume that the only influence of microstructure on fatigue crack propagation rates occur as a result of the effect of microstructure on the yielding properties of that material as defined by the yield strength and fracture toughness. If

however a significant change in microstructure was achieved whilst retaining similar yield strength and fracture toughness properties, this may result in a change in fatigue crack propagation mechanism and hence a change in crack propagation rates. This change could then be attributed directly to the effect of microstructure. Several types of departure from the ductile striation mechanism have been observed in previous research work and are discussed within this section.

3.4.1. Striation mechanism for fatigue crack propagation

Zapple and Warden (46) first observed a pattern of striations on a fatigue fracture surface. Later testing has shown a relationship between one cycle and the formation of one striation (47,48). However, every cycle may not necessarily produce a striation (29). Various researchers have produced models for a striation forming fatigue crack propagation mechanism (48,49).

Figures 14 and 15 illustrate two such models. These were proposed by Laird (49) and McMillan et al (48), respectively.

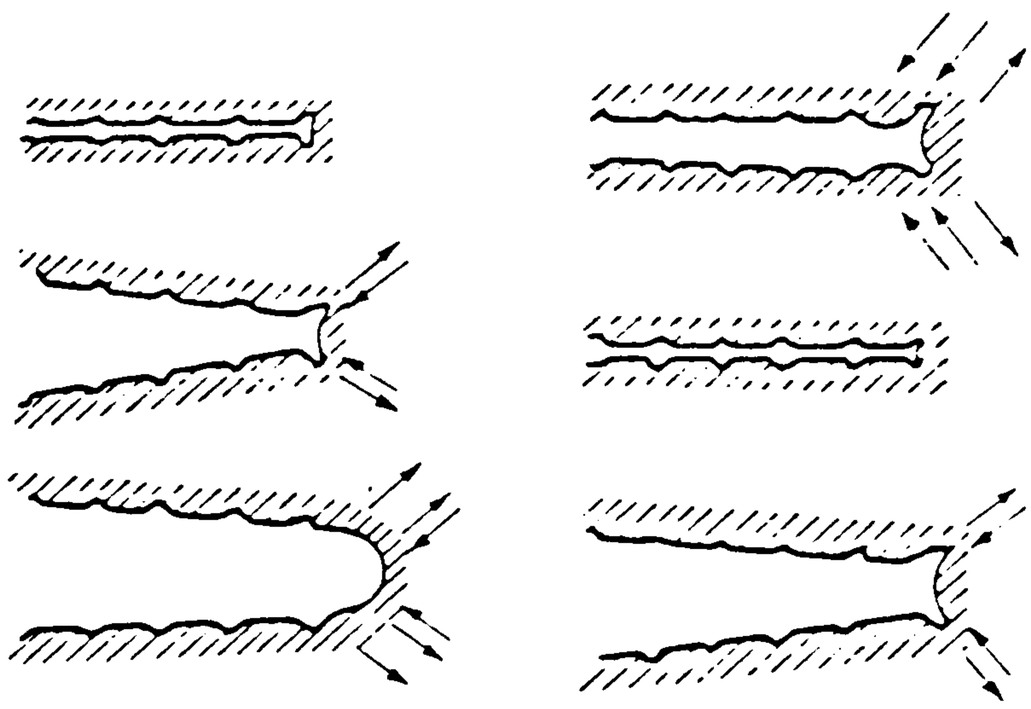

Figure 14 Diagrammatic representation of striation formation by a plastic blunting process (C Laird (49))

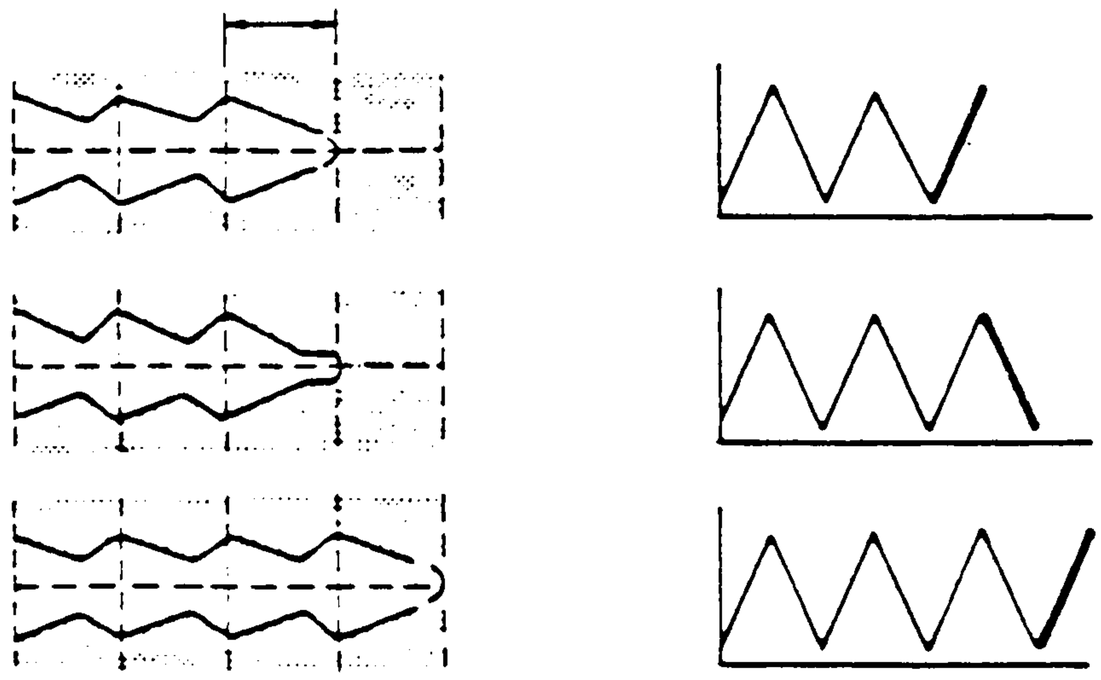

Figure 15 Diagrammatic representation of the formation of striations of "saw-tooth" profile (J C McMillan et al (48))

In both models the area of the crack tip is increased by a plastic blunting process as the load rises towards P_{max}. The crack is resharpened on unloading. However, mechanisms of crack propagation which give rise to striation formation are not seen under all loading conditions in all microstructures. Striations are less clearly visible in ferritic and bainitic structures and their presence in tempered martensite structures has not been conclusively demonstrated (50). The regularity of striations may also be distorted by the presence of large volume fractions of second phase particles as in spheroidised 1 percent carbon steel (51). Fatigue striation morphology will depend to a large extent on the available slip systems (30-33). This is demonstrated by the uniform striations formed in face centred cubic metals compared to those formed in ferritic materials (50).

3.4.2. Microcleavage

Richards (52) has observed fatigue crack propagation by combined striation formation and cleavage on (110) planes in coarse grained, 3 percent silicon iron.

Although a steady macroscopic growth rate was seen, scanning electron microscopy revealed a uniform distribution of short cleavage cracks. Complete grains in a favourable orientation to the maximum tensile force have been observed to fracture (52,53).

Microcleavage may occur during crack propagation in materials containing brittle second phase particles such as cementite in a coarse pearlite steel (51). Several other examples of microcleavage have been observed in steels (54) and high strength aluminium alloys (55-57). Fatigue crack propagation mechanisms which contain an element of microcleavage have shown enhanced crack propagation rates over a purely striation mechanism (50,57), clearly demonstrating an importance of microstructure in determining a crack propagation mechanism and therefore ultimately crack propagation rate.

3.4.3. Intergranular separation

In a sensitive microstructure, fatigue crack propagation may primarily occur along grain boundaries, this phenomena is encouraged by impurities which are known to reduce the strength of grain boundaries (58); it is favoured at low ΔK and by the presence of water vapour (50). Quenched and tempered high strength steels are prone to this mechanism (59-62), where the crack tends to follow prior austenite grain boundaries. This mechanism is less likely to predominate with increasing stress intensities (59,61).

The intergranular fatigue mechanism has also been observed in single phase, ferritic, 3 percent silicon iron and along the α-phase boundaries of high purity iron (63). The presence of this mode of fatigue crack propagation is associated with higher growth rates than a pure striation mode.

3.4.4. Void coalescence

Void or dimple formation has been extensively observed in structural metals and alloys (60, 64-71) which tend to exhibit fine microstructures and high toughness. Most observations of voids during fatigue crack growth in ferrous materials have been made on medium to high strength steels (50). Forsyth and Ryder (70) proposed a mechanism for void formation as shown in Figure 16.

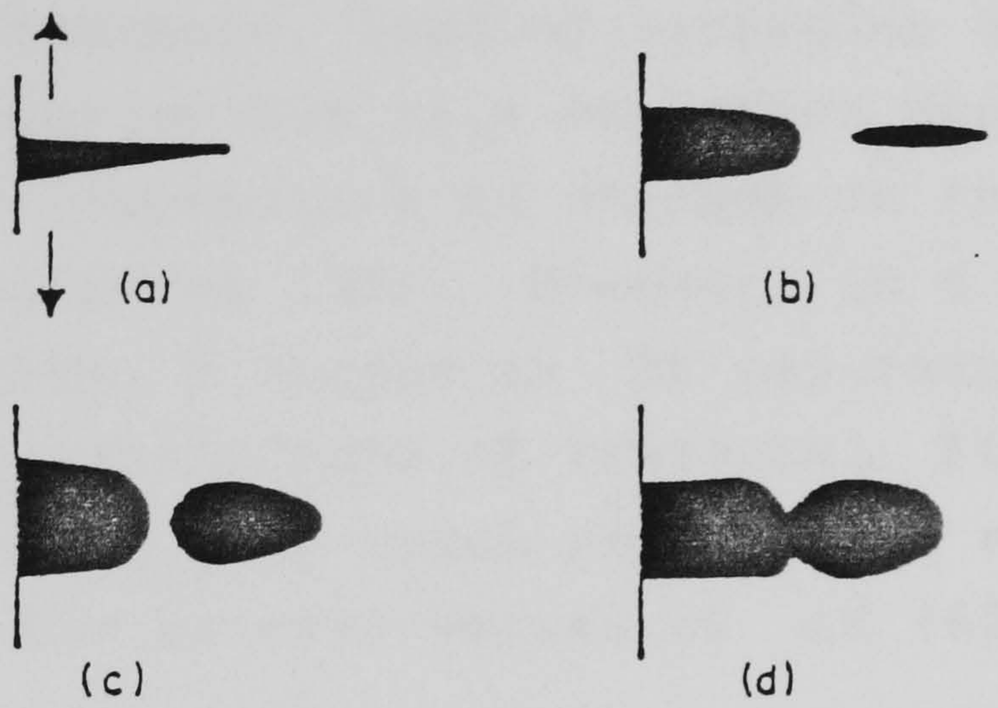

Figure 16 Fatigue crack growth during one cycle of stress:

(a) end of compressive half cycle which may have cracked inclusions ahead of crack tip

(b) tensile half cycle blunts crack tip and produces void ahead of crack in region of triaxial tension

(c) thinning of unfractured bridge under bi-axial tension

(d) final separation of separating bridge by thinning

(P J E Forsyth and D A Ryder (70))

On crack opening a void forms ahead of the crack tip. The bridging material is thinned by subsequent cyclic loading and eventually links to the main crack front. This mechanism is also favoured by Crooker et al (66). Griffiths et al (65) have demonstrated a strong influence of ΔK on both the rate and mechanism of crack propagation by void coalescence for the same K_{max} conditions and several investigations (65,66,71) have detected no difference between the appearance and size of dimples during fatigue and during final fast fracture.

3.5. Summary

It is clear from the previously reported work that fatigue crack propagation can take place by one of several mechanisms. The mechanism predominating being dependent upon microstructure, loading variables and the environment. Crack propagation due to a striation mechanism has been shown to be insensitive to changes in the mean stress and specimen thickness (50). However, in a sensitive microstructure, a change in ΔK may result in a departure from the striation mode of fracture. Figure 17 shows the influence of K_{max} on crack propagation rates in a low alloy weld metal for several values of ΔK (65).

For values of ΔK up to 40 MPa m, a horizontal line results showing no influence of K_{max} on the fatigue crack propagation rate. These samples exhibited exclusively a striation mode of fatigue crack propagation. However, similar tests conducted at ΔK values of 47 MPa$\sqrt{m}$ and above showed a strong dependence of growth per cycle to K_{max}. Samples showing this relationship were found to exhibit void coalescence as the predominating mechanism.

A material tested close to its ductile brittle transition temperature or one containing brittle second phase particles may tend to exhibit microcleavage. Both microcleavage and microvoid coalescence have been predominantly associated with low toughness microstructures, intergranular fatigue may occur in a wider range of microstructures and appears to be both ΔK and environmentally sensitive.

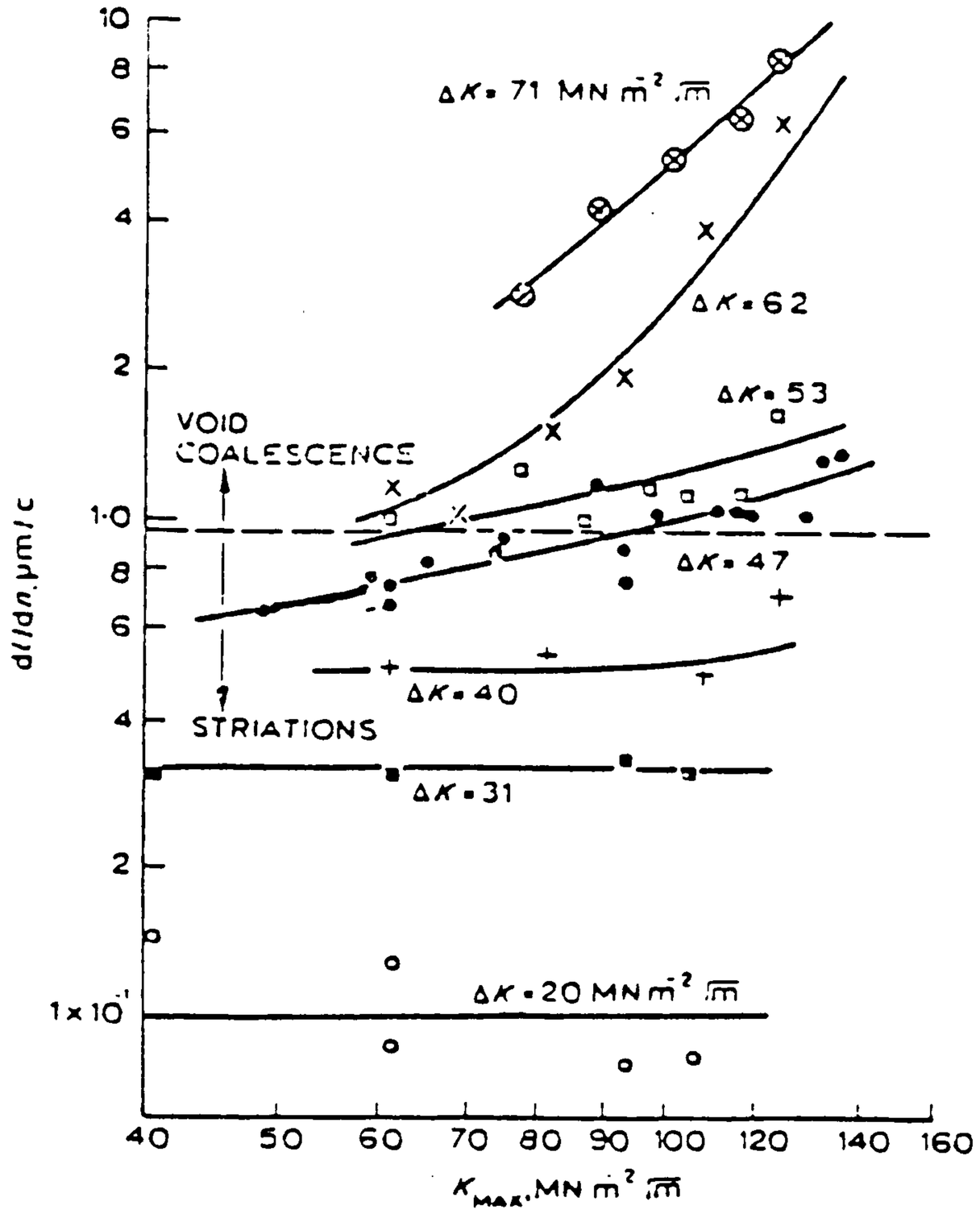

Figure 17 The effect of K_{max} on crack propagation rates for several values of ΔK in a low alloy weld metal.

From the study of previous work it appears that any departure from a purely ductile striation mechanism results in an increase in fatigue crack propagation rates. Departure from the striation mechanism is attributed directly to microstructural types or specific microstructural features for local deviations. The effect of crack path deviation both on a local scale and on a gross scale has not been studied in any detail. Local deviations such as micro-cleavage (52) do appear to be associated with increased fatigue crack propagation rates however gross deviations from the plane of maximum tensile stress may well reduce ΔK effective and so inhibit fatigue crack propagation. The multiplanar nature of a propagating crack associated with large crack path deviations and gross secondary cracking is likely to promote increased fatigue resistance as long as a departure from the ductile striation mode to a more rapid crack growth mechanism does not occur.

Z.1
EB

4.0 EXPERIMENTAL

4.1 Material

For this study a range of HSLA steels were chosen to reflect the common production routes for such products. These comprise controlled rolling (CR) or thermomechanical treatment (TMT) as it is usually referred to in Europe, and quenching and tempering (Q&T). Three controlled and three quenched and tempered steels have been tested, the microstructures of which are shown in Figures 18 to 23. The composition and mechanical properties are given in Table II.

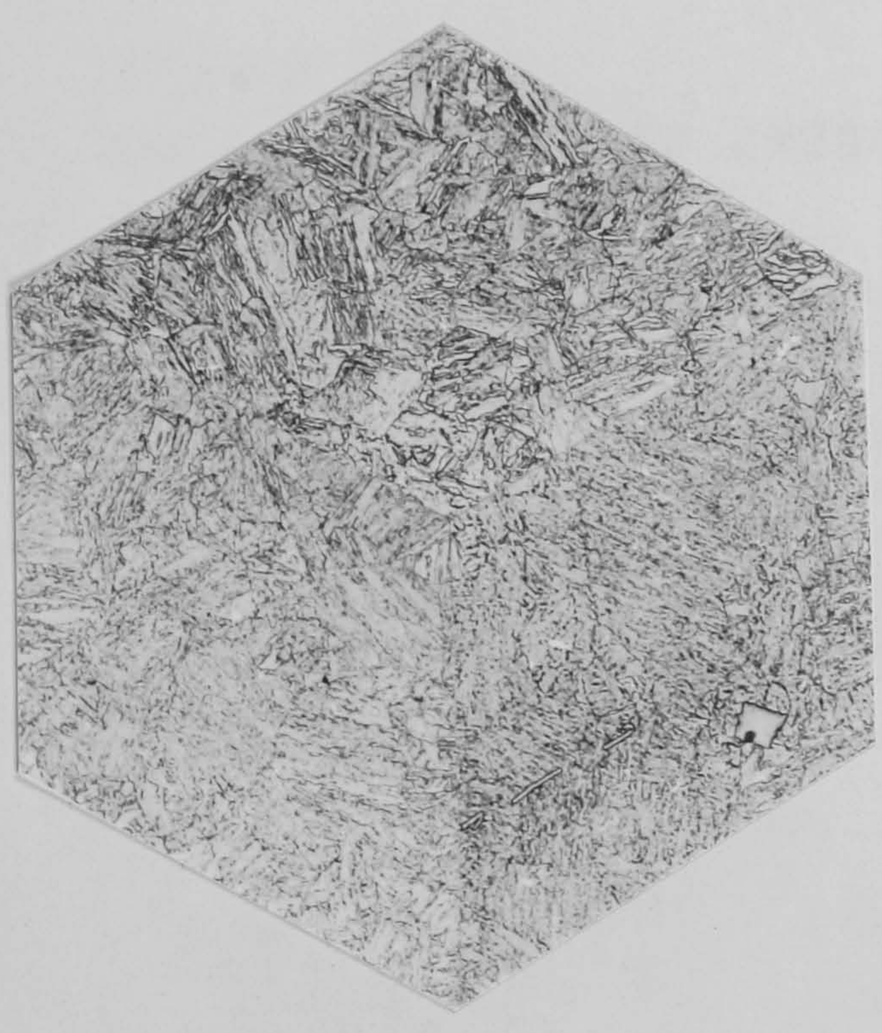

Figure 18
N-A-XTRA 70 (X200)

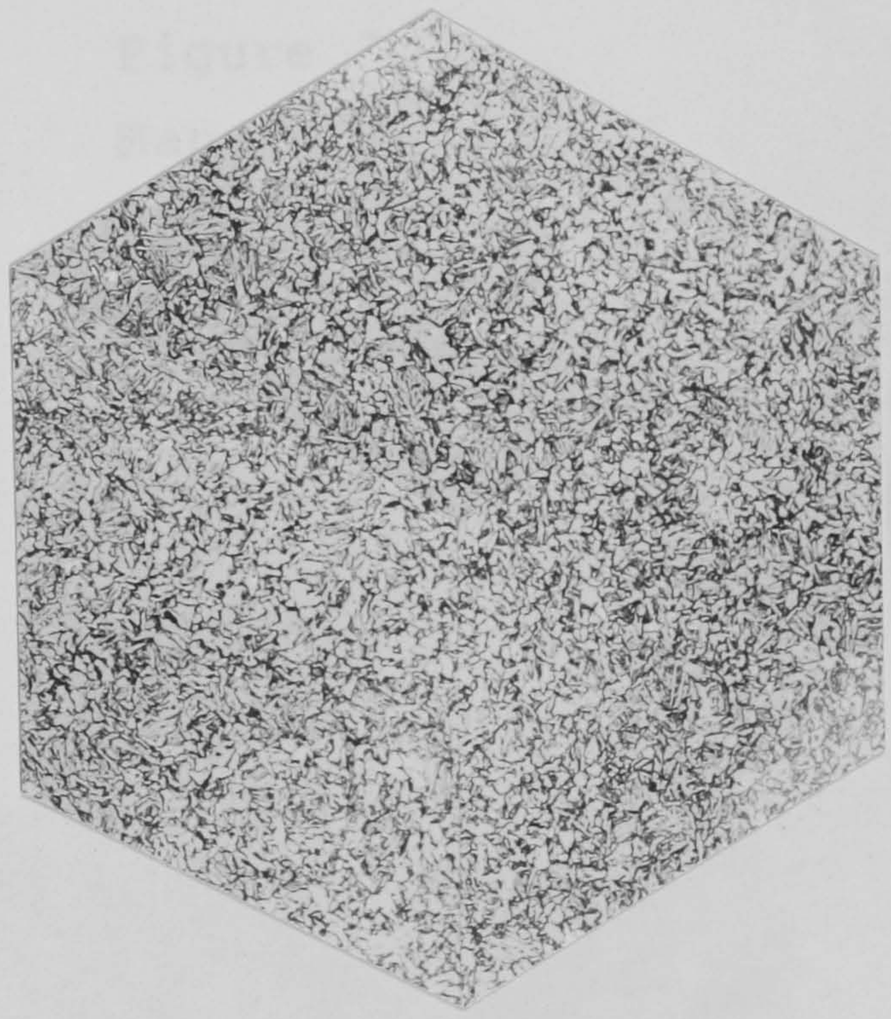

Figure 19
RQT 501 (X200)

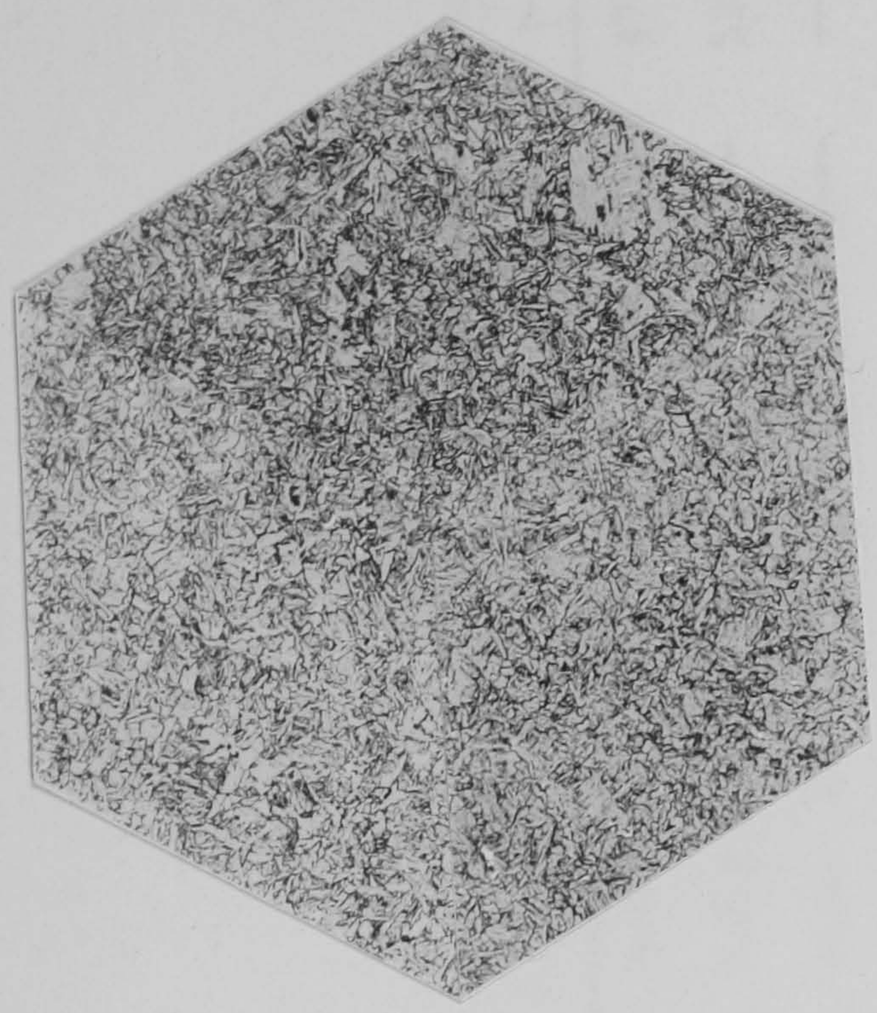

Figure 20
BS 4360 grade 55F (X200)

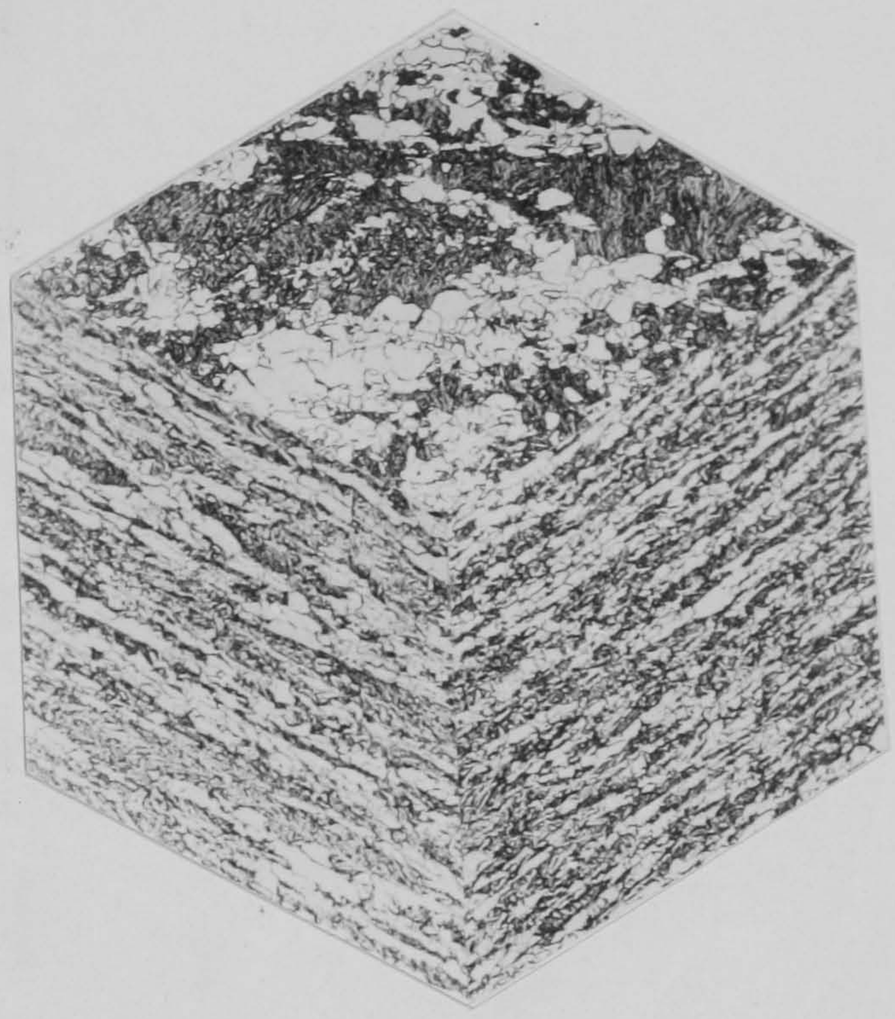

Figure 21
Mannesmann X80
line-pipe (X200)

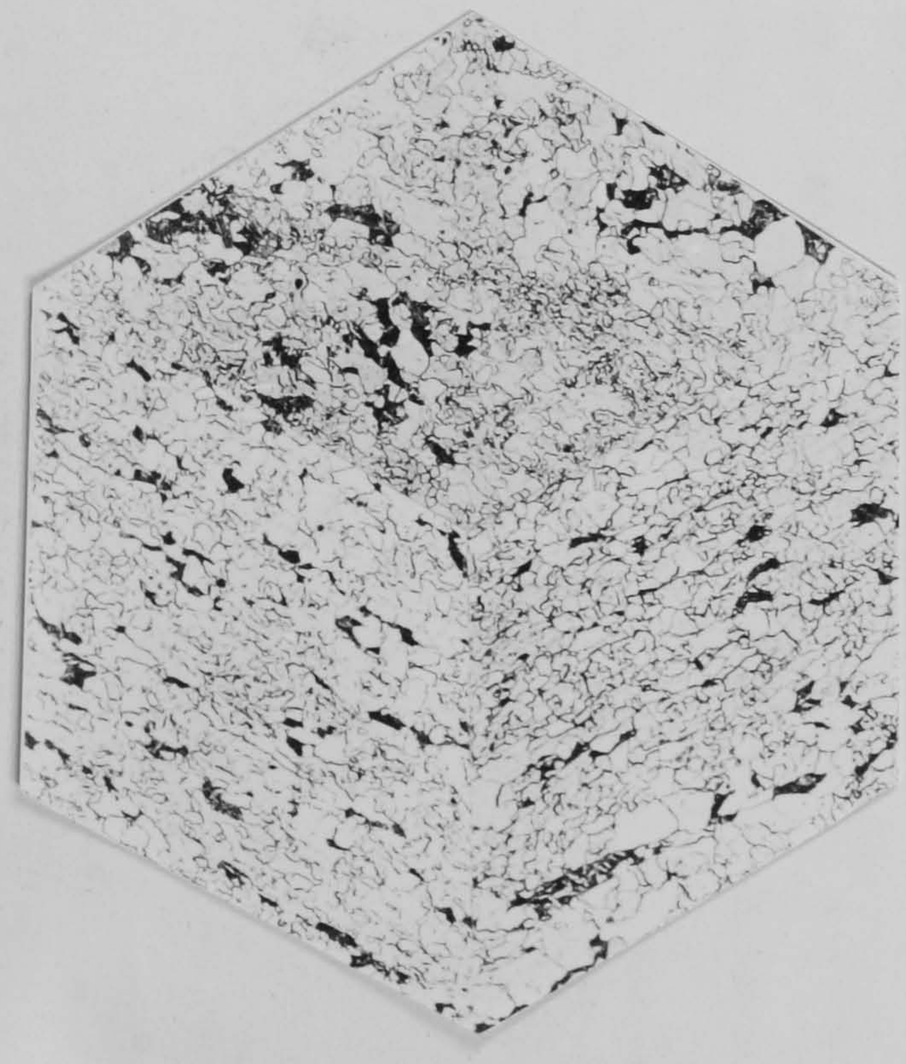

Figure 22
Kontroll 50 ESM (X200)

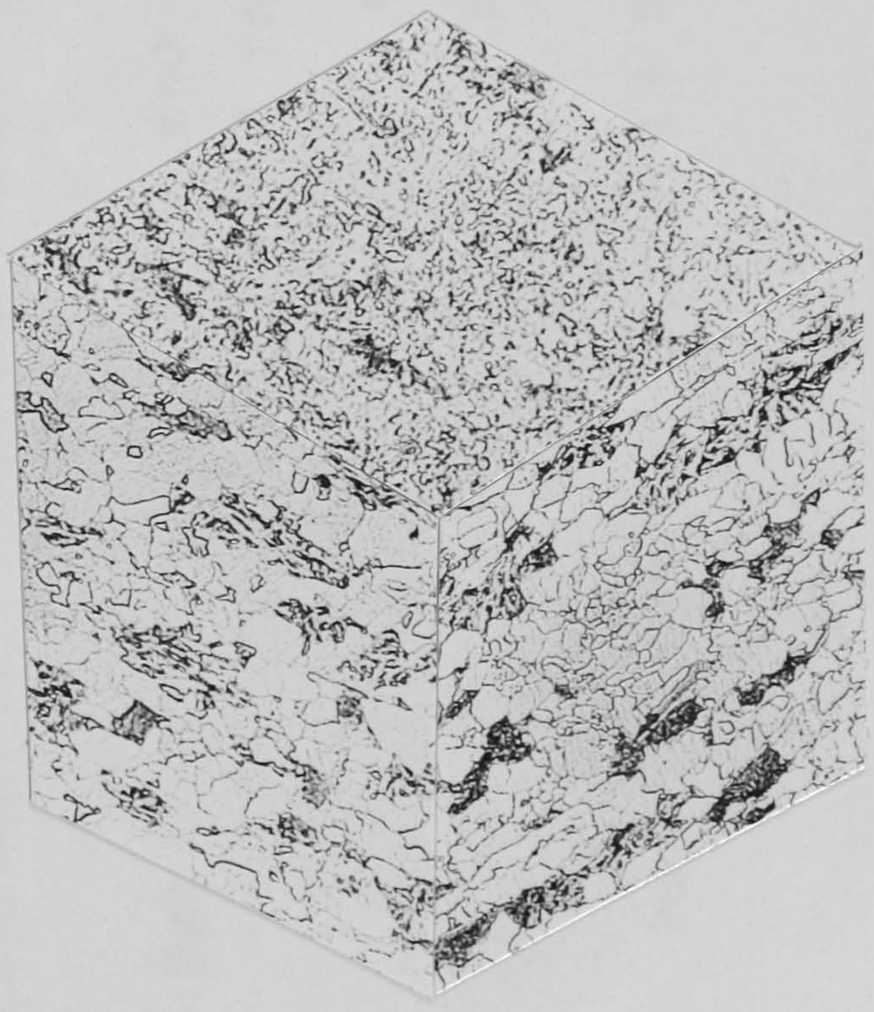

Figure 23
LP6 Line-pipe (X200)

	Element	C	S	P	Si	Mn	Ni	Nb	Cr	Mo	Ti	Cu	Al	Ca	V	Zr	Y_s MPa	C_V J	Pcm
Controlled rolled	Kontroll 50 ESM *	0.05	0.005	0.019	0.23	1.13	0.29	----	0.02	0.20	-----	0.24	0.03	----	----	----	470	260	0.19
	Manneesmann X80 #	0.08	0.003	0.017	0.43	1.70	0.04	0.04	0.05	0.04	0.012	0.06	0.05	0.30	0.02	----	550	232	0.28
	Linepipe LP-6	0.07	0.007	0.028	0.27	1.59	0.25	----	----	0.37	-----	----	0.05	----	----	----	---	---	0.27
Quenched and tempered	R.Q.T 501	0.11	0.006	0.017	0.25	1.25	0.03	----	0.02	0.11	-----	0.03	0.04	----	0.04	----	560	200	0.29
	N-A-XTRA 70 #	0.15	0.007	0.017	0.62	1.01	0.09	----	0.78	0.38	-----	0.06	0.04	----	0.01	0.05	690	31	0. 3
	BS 4360 grade 55F	0.12	0.004	0.023	0.35	1.18	0.03	----	0.02	0.14	-----	0.02	0.04	----	0.05	----	580	164	0.31

Tables II Composition and mechanical properties of the HSLA steel studied in the project

Chemical Analysis - The Welding Institute, Abington Hall, Cambridge

Pcm (carbon equivalent) - Ito & Bessyo (1968)

Table II shows a wide variation in alloy analysis reflecting the production process and influencing the properties of the final product.

All six steels reflect the modern trend towards lower carbon contents particularly the linepipe materials. This is to improve weldability particularly in the field situation where hydrogen cracking may be a problem. Lower carbon steels have the benefit of higher fracture toughness for a given strength level than those gaining most of their strength from intersitial solid solution carbon.

The need for clean steels with low sulphide inclusion counts is reflected by the low sulphur contents for all six steels again to ensure high toughness as assessed by the Charpy test. All the sulphur is not removed as it is an expensive process and some work (73) has suggested that very low sulphur levels may make the steel more susceptible to hydrogen cracking.

Phosphorus promotes ferrite formation and has a substantial solid solution hardening effect, however, the trend with low alloy steel is to reduce phosphorus levels as this element leads to segregated layers. It is a feature of HSLA steels to reduce alloying levels to a minimum, however, several elements are added for their grain refining effects. Small additions of aluminium have a strong grain refining effect when combined with nitrogen to form nitrides. This grain size reduction increases both yield strength and toughness. All six steels contain this small but very significant addition. Small additions of niobium, vanadium and titanium are also commonly found in HSLA steels. Niobium is a powerful grain growth inhibitor due to its carbide forming ability. This element is most useful in controlled rolled steel and is indeed present in the X80 linepipe material. Vanadium has similar grain growth restricting properties during controlled rolling and may also

give precipitation strengthening particularly on tempering. Small additions are seen in RQT 501 and BS 4360 grade 55F steels, both being quenched and tempered steels.

Titanium forms carbides at relatively high temperatures so inhibiting grain growth during high temperature rolling (74). In addition to this titanium is also added to restrict grain growth in the course heat affected zone formed during high heat input welding.

Manganese has been added to structural steels in the past to improve the fracture toughness of steels containing sulphur. Although this element is present in all six steels, its level must be kept down if a low carbon equivalent is to be maintained. Manganese also has a strong hardenability effect.

Other elements present in the steels to be tested include calcium, zirconium, chromium and copper. Calcium is a shape control addition (75) used to alter the morphology of manganese sulphide inclusions. Although the X80 line-pipe steel has the lowest sulphur content, an addition of calcium has been used for this purpose reflecting the need for excellent toughness at high yield strengths. Zirconium which is also used as a shape control addition is found in N-A-XTRA 70.

Both chromium and copper additions are used to offer a degree of resistance to environmental attack. Copper is found in Kontroll 50 ESM and is generally added to linepipe material for sour gas applications. Chromium is found in the quenched and tempered steel N-A-XTRA 70. Both additions also give some precipitation strengthening.

All these alloying additions will have some effect on the austenite to ferrite transformation. As shown in Figure 24, carbon and nitrogen are the strongest austenite

formers therefore delaying transformation whilst zirconium, Figure 25, is the strongest ferrite former.

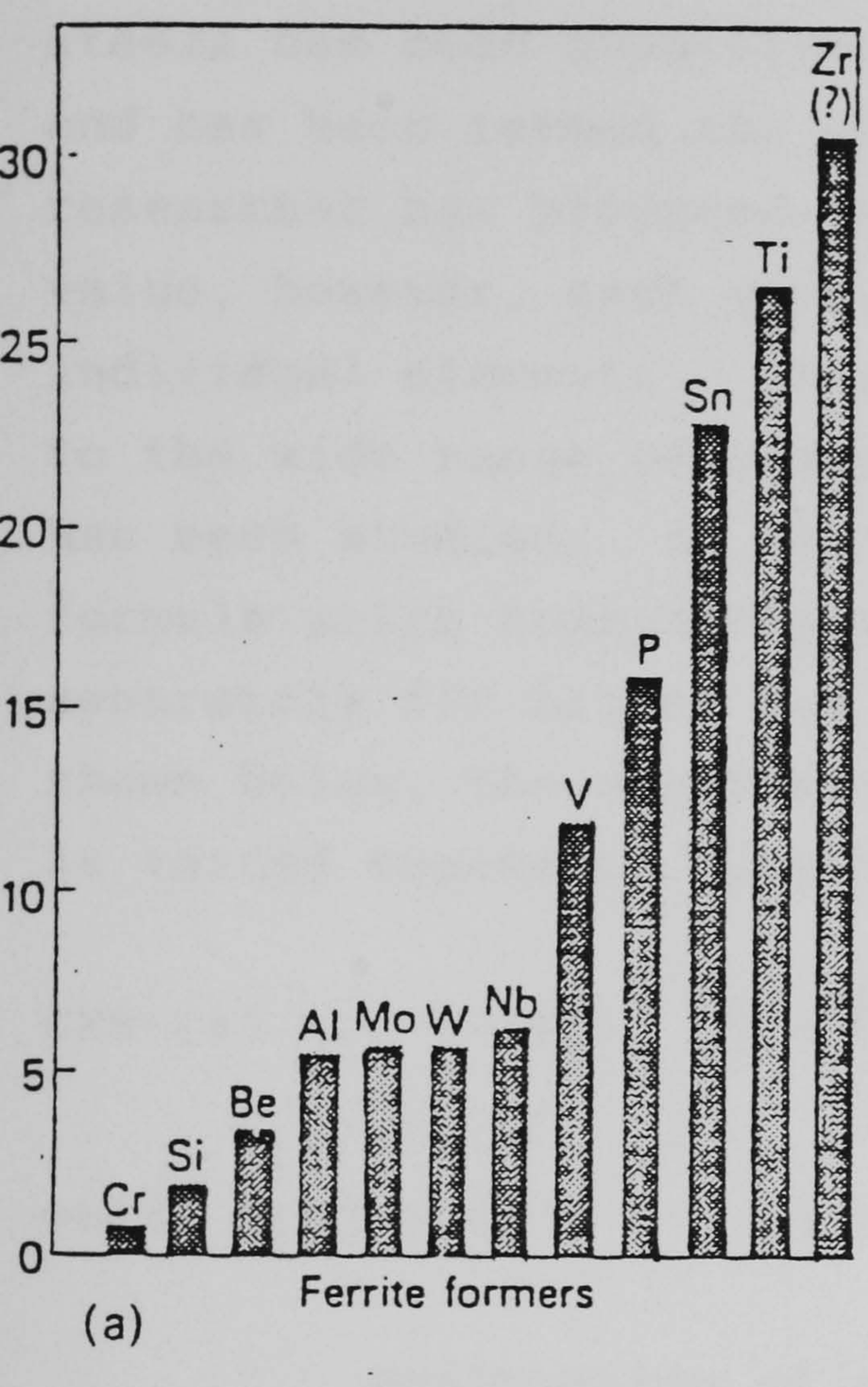

Figure 24

Ferrite promoting additions.

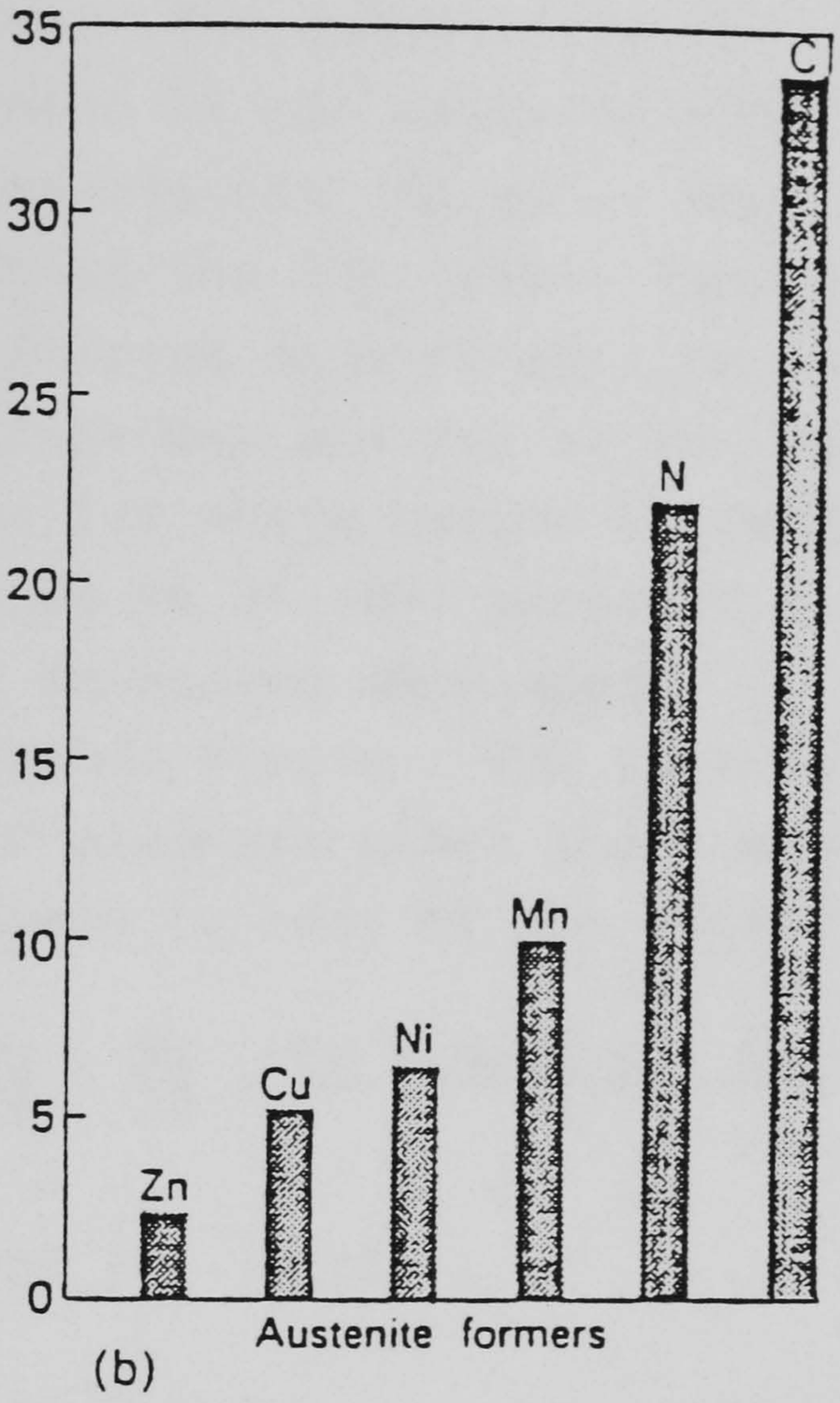

Figure 25

Austenite promoting additions.

Alloying additions may also affect the bainite formation temperature which is very important in steels to be quenched. The relationship is most strongly dependent upon carbon.

$$B_s\ (^{o}C) = 830 - 270\ (\%C) - 90\ (\%Mn) - 37\ (\%Ni) - 70\ (\%Cr) - 83\ (\%Mo) \quad (10)$$

It would appear that very low alloy steels will therefore require more efficient quenching from higher temperatures to form a bainitic microstructure. The effects of alloying elements on the austenite to ferrite or

bainite transformations must be considered when designing a steel composition and process route. However, for HSLA steels which are to be used almost exclusively in welded fabrications, a most important consideration is the effect of alloy additions on weldability. The weldability of steels has been quantified in terms of the alloying additions and has been termed the carbon equivalent (76-80). Each researcher has produced an equation for the carbon equivalent value, however, each gives a different significance to the individual elements. These differences are due in the main to the wide range of steel types for which carbon equivalence has been studied. In 1981 Yurioka et al (80) proposed a formula which combined previous equations developed separately for higher and low carbon steels. The formula is shown below, the contribution of elements other than carbon is varied depending upon the carbon content of the steel.

$$CEN\ (\%) = C + A(C)\ \left(\frac{Si}{24} + \frac{Mn}{6} + \frac{Cu}{15} + \frac{Ni}{20} + \frac{Cr + Mo + V + Nb}{5} + 5B\right) \quad (11)$$

where $A(C) = 0.75 + 0.25 \tanh (20\ (C - 0.12))$

Application of this equation to the six steels being studied reveals carbon equivalents ranging from 0.19% for Kontroll 50 ESM up to 0.3% for the quenched and tempered N-A-XTRA 70. This difference is also reflected in the yield strengths and fracture toughness values for the two steels. By comparison, a typical value of carbon equivalent for a structural steel conforming to BS 4360 grade 50D would fall in the range 0.3% to 0.4%.

4.2. Parent Plate Fatigue Testing Samples

Fatigue test samples have been machined to conform with British Standard 5762:1979, Crack Opening Displacement (COD) testing. This allowed simple calculation of crack tip stress intensity range based on a linear elastic fracture mechanics approach. Proportional dimensions and tolerances

are given in Figure 26.

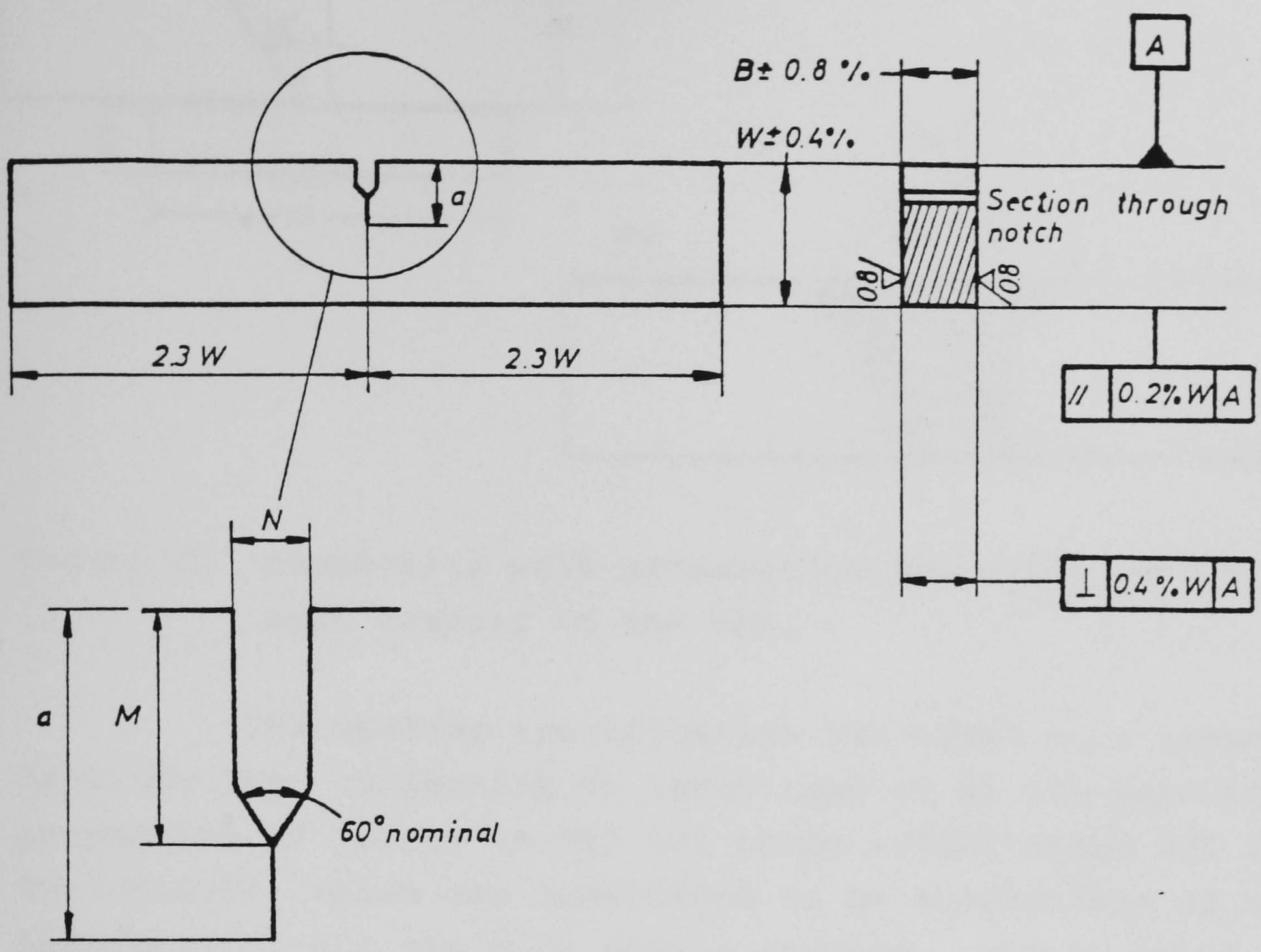

Width	= W = 26mm
Thickness	= B = 0.5 W
Half loading span L	= 2 W
Notch width N	= 0.065 W max. (if W is over 25mm) or = 1.5mm max. (if W is less than or equal to 25mm)
Effective notch length M	= 0.25 W to 0.45 W
Effective crack length a	= 0.45 W to 0.55 W

All dimensions are in millimetres

Figure 26 Proportional dimensions and tolerances for bend test pieces according to BS 5762:1979

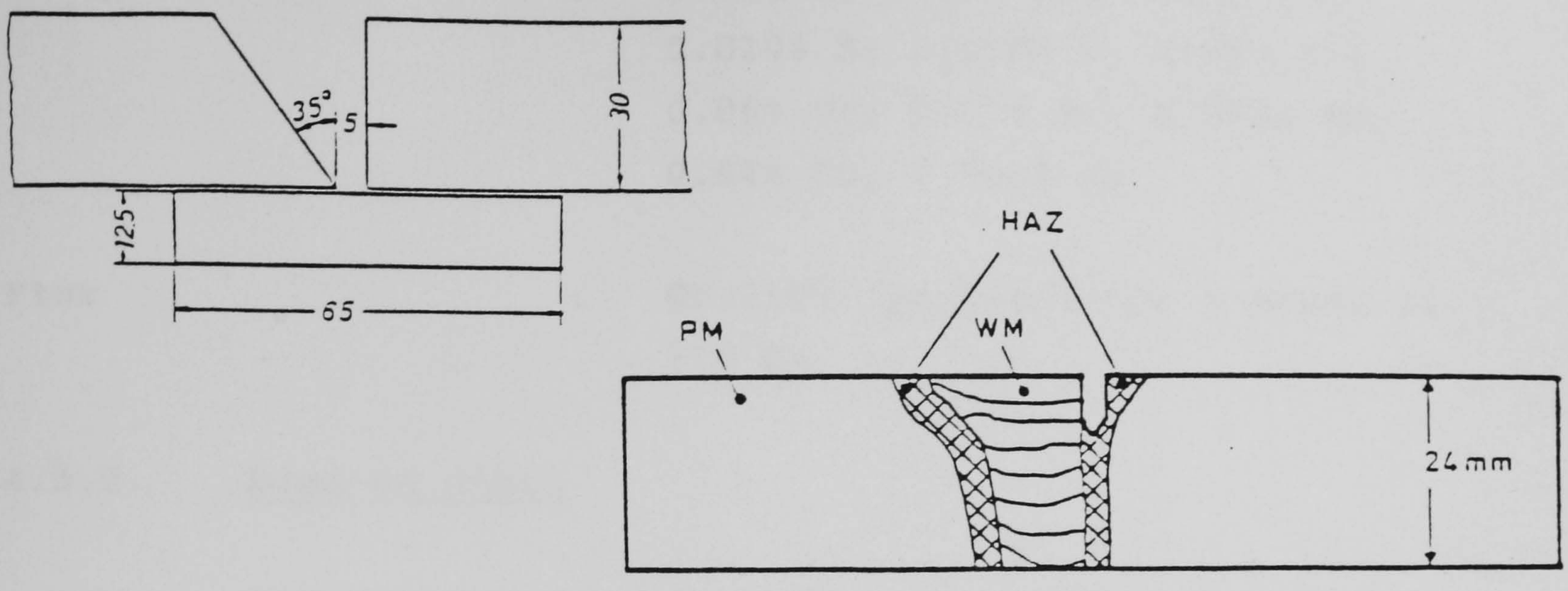

Figure 27 Asymmetric weld preparation and notch position with respect to the HAZ.

The welding specification was based on a report by Oerlikon (82) concerning an investigation of the mechanical properties of joints in RQT 501 plate welded using SD3 1Ni ½Mo/OP121TT, which was considered to be appropriate as a standard for all the HSLA steels studied. A heat input of 3.0 kJ/mm was chosen as the highest value likely to be used in fabrication and therefore the most potentially detrimental to the heat affected zone mechanical properties in terms of possible precipitation effects.

The welding specification was as follows:-

process	:	Submerged Arc Welding (SAW)
joint preparation	:	assymetrical V - 35° butt joint
preheat	:	none
interpass temperature	:	150°C
current	:	500 amps
voltage	:	30 volts
bed speed	:	5mm/s
heat input	:	3.0 kJ/mm
number of passes	:	9/10
Consumable wire	:	Oerlikon SD3 1Ni ½Mo

Analysis	:	0.09% C; 1.41% Mn; 0.29% Si; 0.010% S; 0.010% P; 0.96% Ni; 0.06% Cr; 0.27% Mo; 0.002% Nb; 0.04% Cu; 0.004% Al
Flux	:	OP121TT (prebaked for 2 hours at 300^{o}C)

4.3.2. Bead on plate

Submerged arc welding is a multipass welding process. The latter weld runs having the effect of tempering the HAZ formed by the previous weld run. For the purpose of studying a fatigue crack propagating through a microstructural gradient, this raises an additional complication. A single pass bead on plate was decided upon as the most effective means of producing a microstructural gradient from weld metal through to parent plate. A compromise had to be made between an extreme microstructural gradient, achieved by low heat input but giving a narrow HAZ which restricts the data produced, and a higher heat input with its more gradual HAZ width. The variables chosen are given below.

process	:	Submerged Arc Welding (SAW)
sample plate preparation	:	20mm x 5mm depth groove machined down centre of plate to take single bead
current	:	600 amps
voltage	:	30 volts
bed speed	:	13.85mm/s
heat input	:	1.3 kJ/mm
Consumable wire	:	Oerlikon SD3 1Ni ¼Mo
Flux	:	OP121TT (prebaked for 2 hours at 300^{o}C)

The machined groove into which the single bead was run was required to give a suitable crack length in the area of microstructural gradient to be studied and allow a standard notch size as shown in Figure 28.

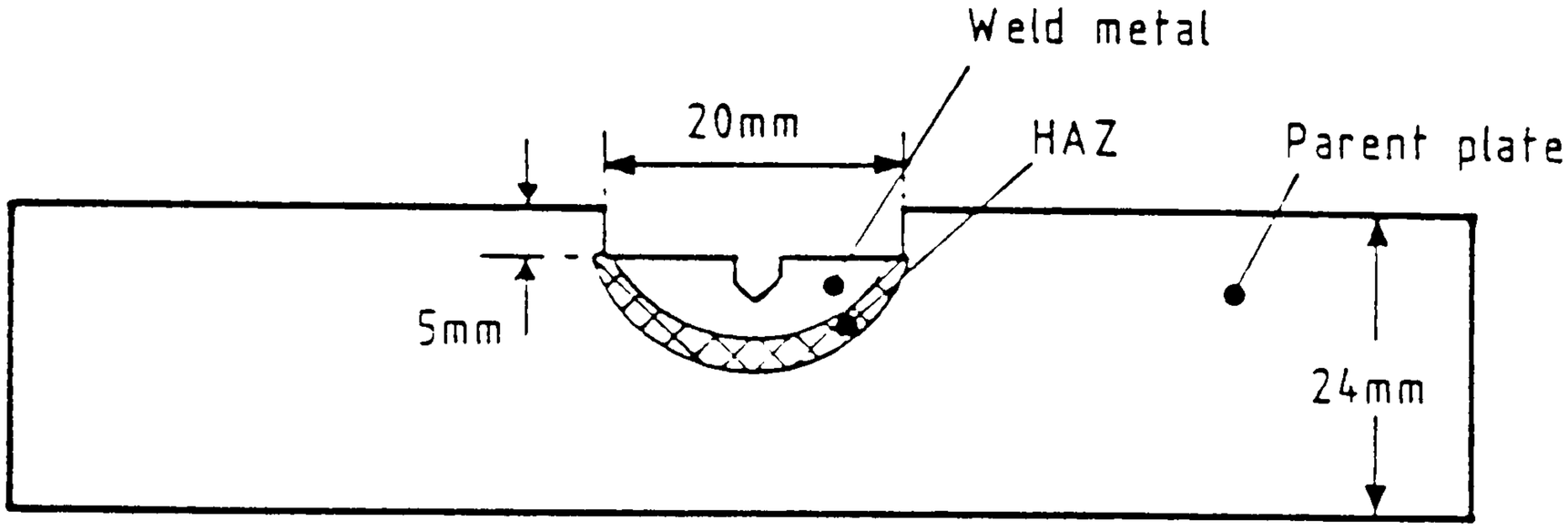

Figure 28 Single pass bead on plate sample showing notch position with respect to the HAZ.

This procedure gave a heat affected zone width of 1¼mm and a notch tip to fusion boundary distance of 3mm so that the sample required a pre-fatigue of 2mm before commencement of crack growth. In order to determine the microstructural effect more clearly, a constant stress intensity range experiment was developed.

4.4. Fatigue Crack Propagation Testing

A fatigue testing programme was designed to study crack propagation under a constant amplitude loading cycle, in laboratory air on parent plate material. This study was then extended to include samples of heat affected zone material and weld metal in the welded samples produced via multipass submerged arc welding.

A limited programme of corrosion fatigue testing considered the effect of impressed current cathodic protection on one steel selected from each of the two main production route types.

From the in-air results, a high threshold was indicated for one steel which was further investigated via a closely controlled threshold stepdown experiment.

Finally, a test was devised using a new crack length monitoring system and a computer controlled fatigue rig to study the changing nature of a fatigue crack as it propagated through a microstructural gradient under constant loading conditions.

4.4.1. Constant amplitude, rising stress intensity range testing in laboratory air environment

The bulk of crack propagation data has been derived at a loading ratio R = 0.6, but some tests have also been conducted at R = 0.1. The higher stress ratio was selected for most of the tests as it would eliminate the crack delaying effect of crack closure and hence represent the most demanding loading environment. It would also be representative of certain types of loading experienced in offshore engineering and could be compared to relevant existing published data. A loading frequency of 0.5 Hz was chosen as the lowest practicable frequency which would allow a test to be completed within a reasonable timescale of approximately one week, but would still give data representative of low frequency fatigue testing which could be most closely related to actual service experience.

Testing has been conducted on both servo-hydraulic and mechanical screw machines, the latter being favoured at low frequencies for its greater stability and reliability. Both types of machine operate in a closed loop feedback system represented in Figure 29.

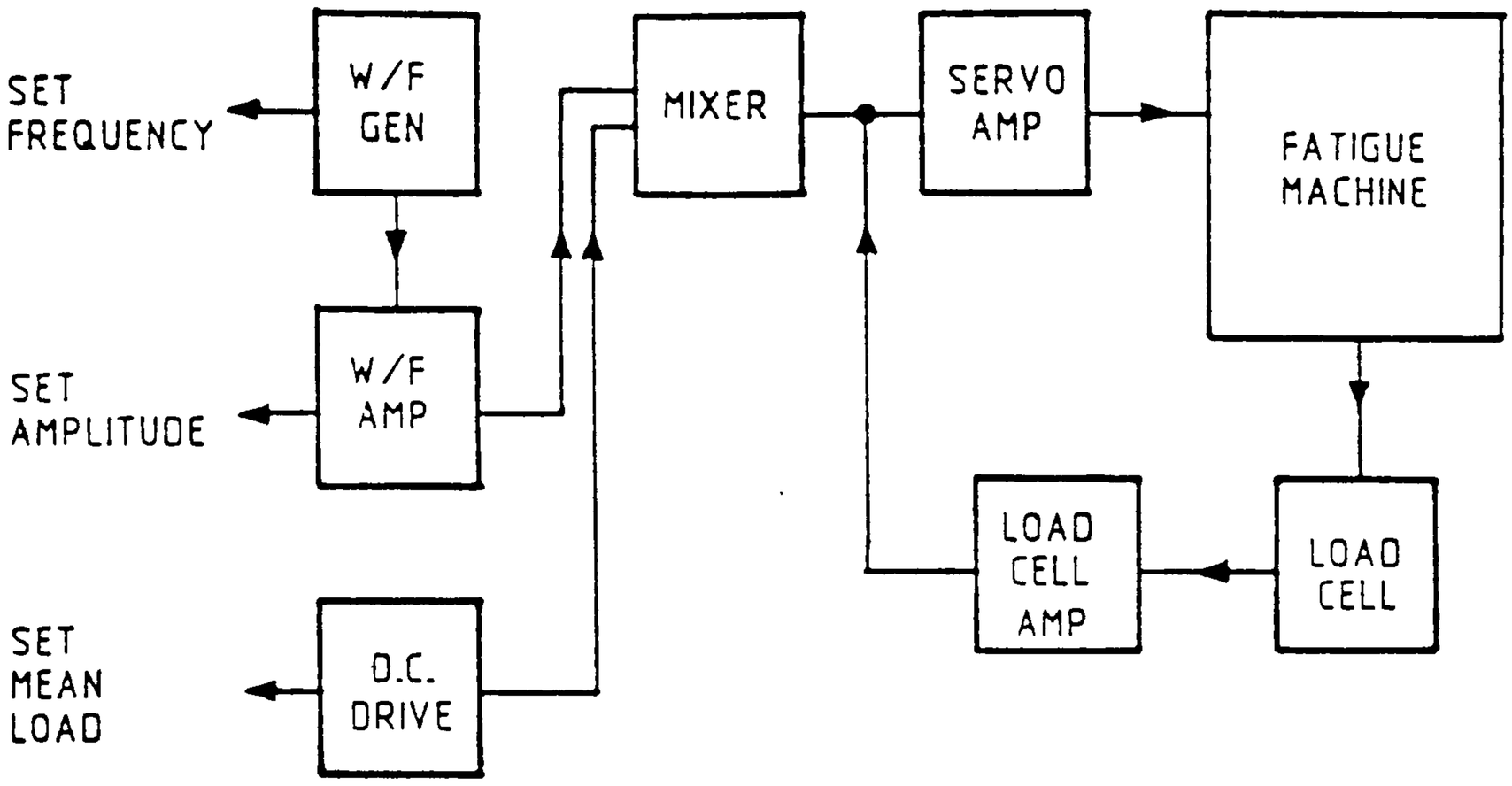

Figure 29 Fatigue machine closed loop feedback control system.

Before fatigue testing, all samples were pre-fatigued from an initial machined notch size of 8mm to a final crack length of 11.5mm via the following procedure:-

Crack Length	P_{max}	P_{min}	ΔK
8mm ⟶ 9mm	10	1.0	23.5 ⟶ 26.2
9mm ⟶ 10mm	8	0.8	17.1 ⟶ 21.4
10mm ⟶ 11mm	6	0.6	16.0 ⟶ 18.1
11mm ⟶ 11.5mm	4	0.4	12.0 ⟶ 12.8

Figure 30 shows the changing monotonic plastic zone size for a material with a yield strength of 500 MN/m^2 resulting from this step-down pre-fatigue procedure.

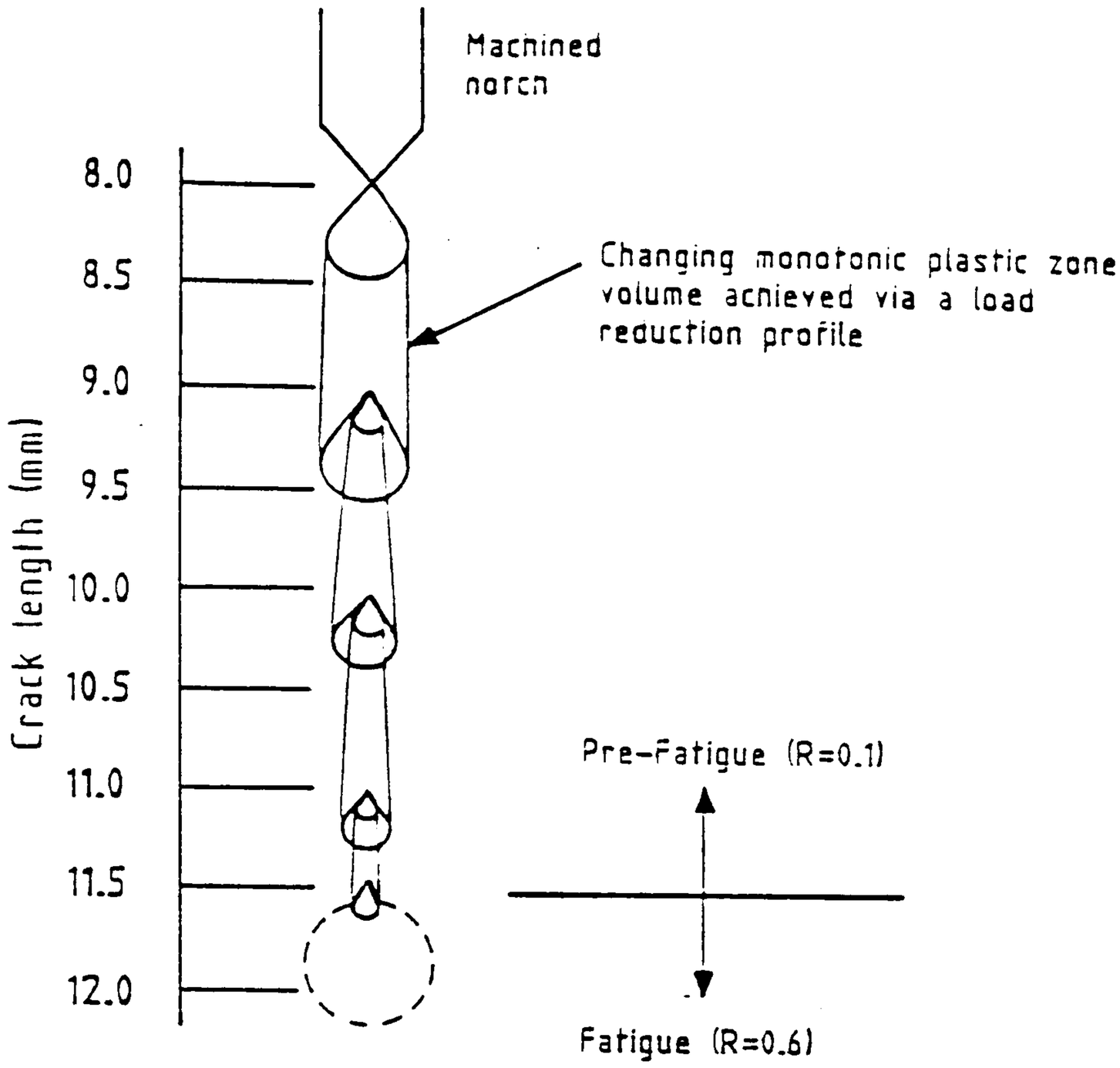

Figure 30 Pre-fatigue, monatonic plastic zone profile.

This pre-fatigue procedure was stringently applied to avoid any false thresholding effects resulting from a large pre-fatigue plastic zone. A testing frequency of 20 Hz was used for this stage of the experiments.

4.3.2. Corrosion fatigue testing

To allow direct comparison with the in-air tests a stress ratio, R = 0.6, and a frequency of 0.5 Hz were again used. For the testing programme a corrosion fatigue machine was designed and built at Cranfield. The fatigue testing machine was based on a similar design to other mechanical testing rigs previously built at Cranfield, utilising a similar load control system. An added facility of a recirculating seawater system which was thermostatically controlled and constantly aerated was designed. A means of

providing constant potential to a fatigue sample under test and up to two awaiting test was also provided. This system is diagrammatically shown in Figure 31.

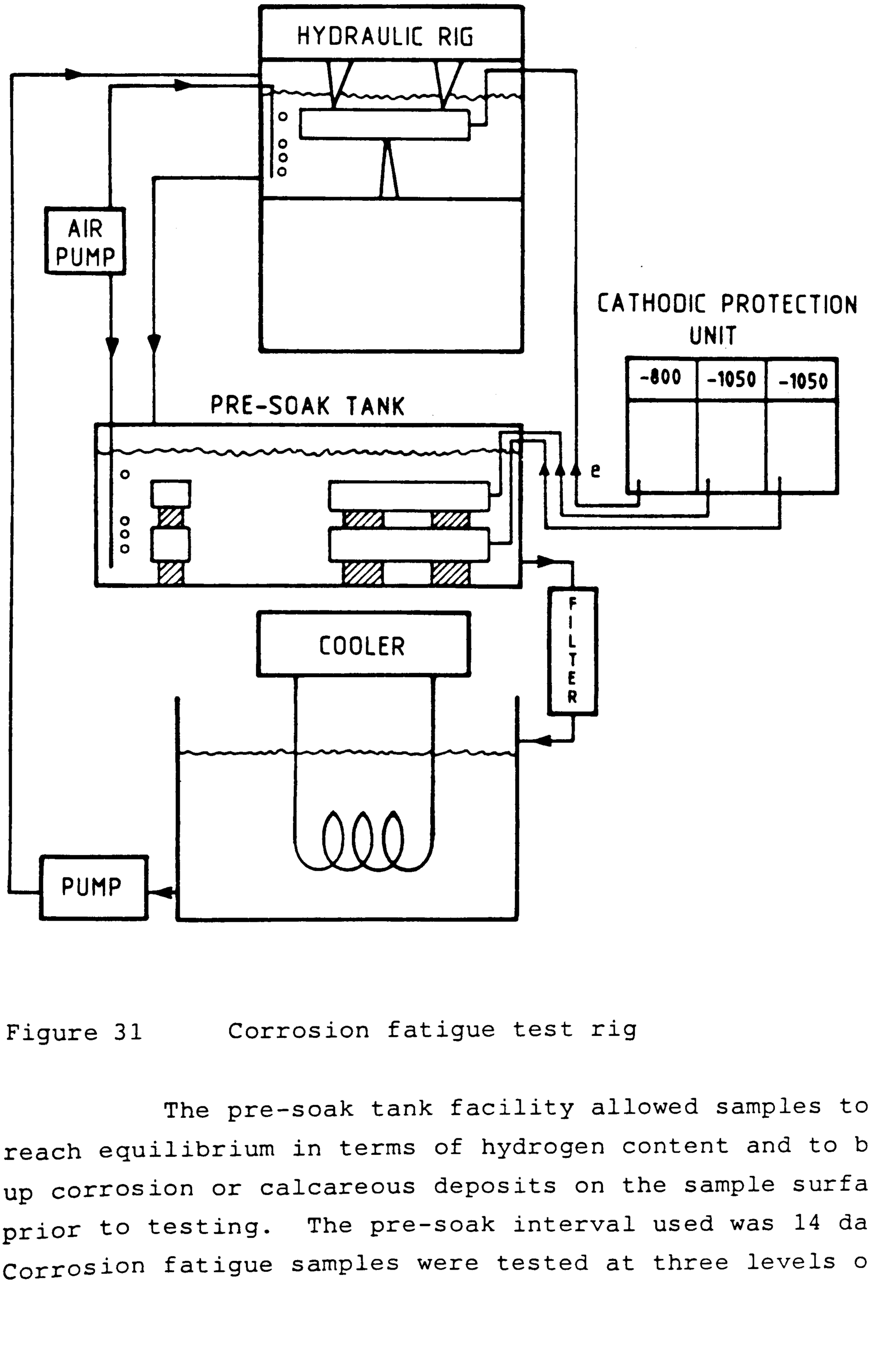

Figure 31 Corrosion fatigue test rig

The pre-soak tank facility allowed samples to reach equilibrium in terms of hydrogen content and to build up corrosion or calcareous deposits on the sample surface prior to testing. The pre-soak interval used was 14 days. Corrosion fatigue samples were tested at three levels of

impressed current cathodic protection; these being free corroding - 800mV (correctly protected) and - 1050mV (over-protected). These potentials are relative to Ag/AgCl. The natural seawater was maintained within the temperature range 4 to 8 ^{o}C.

4. .3. Crack length monitoring

Two systems of crack length measurement have been used in tandom on the majority of samples. An automated system using commercial crack propagation gauges and optical measurements using a travelling microscope. The automated system specified by the gauge manufacturer, Welwyn Strain Measurement Ltd., was used and is illustrated in Figure 32.

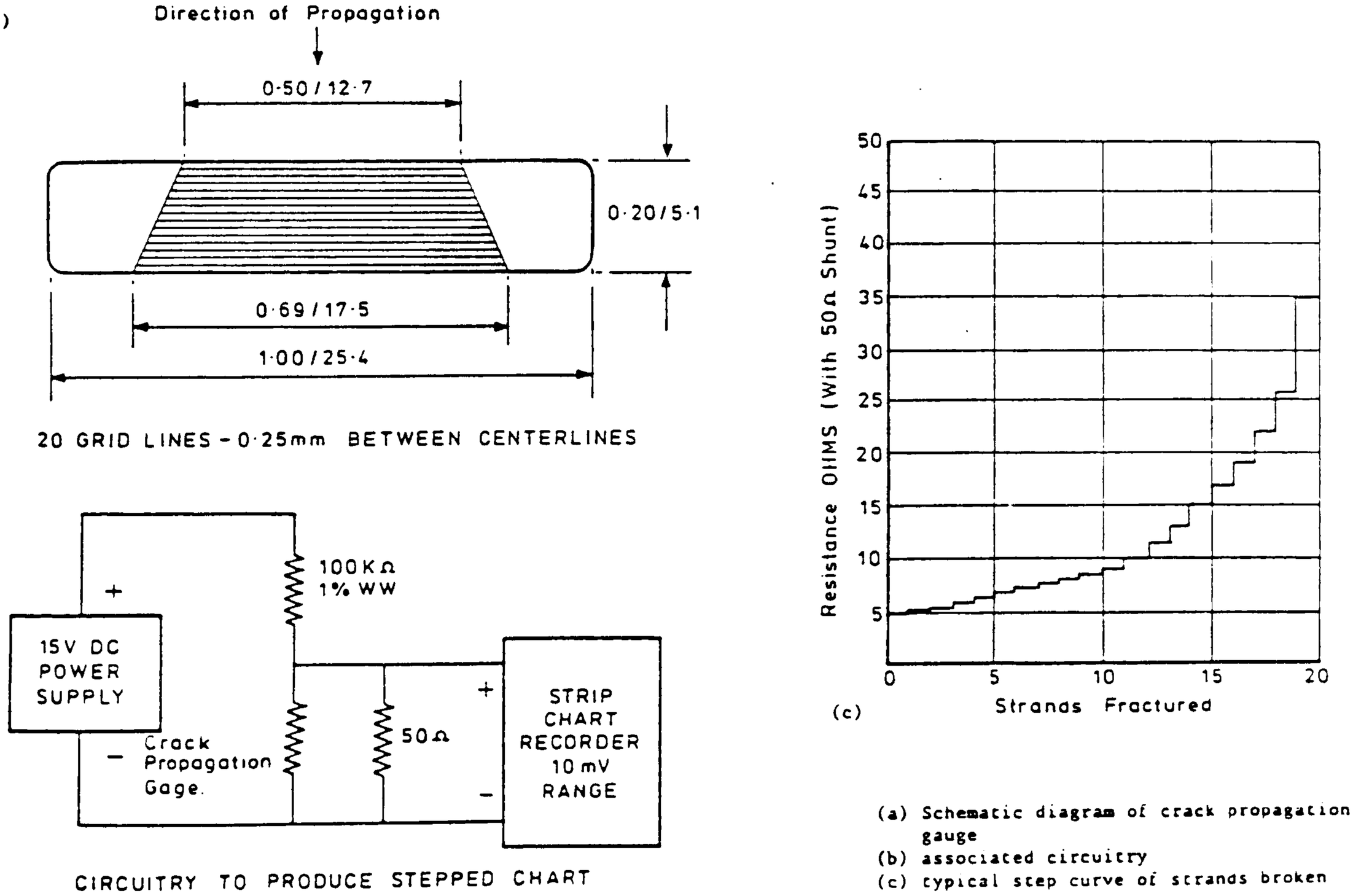

Figure 32 Commercial crack propagation gauge with associated circuitry and typical response curve.

The crack propagation gauge has twenty strands with an inter-strand spacing of 0.25mm and has a gauge span of 5mm. For this system to be of maximum benefit, the propagation gauge must be positioned very accurately to ensure maximum, automatically recorded data points. A crack within a gauge mounted on a sample has been measured under an optical microscope at 400 times magnification. The gauge has then been carefully polished until just removed and a similar measurement has been made of the crack in the actual sample.

The crack length in the gauge has been found to be within 0.01mm of the crack length in the material at stress intensity ranges corresponding to the Paris region of fatigue crack propagation, providing the gauge has been bonded to the sample using the manufacturer's specified procedure and materials.

As the crack is clearly visible whilst propagating through the gauge, it may be monitored using a travelling microscope. The automated system will yield at least 16 data points which are supplemented by about the same number of optically read points. The propagation gauge is mounted on the sample as shown in Figure 33.

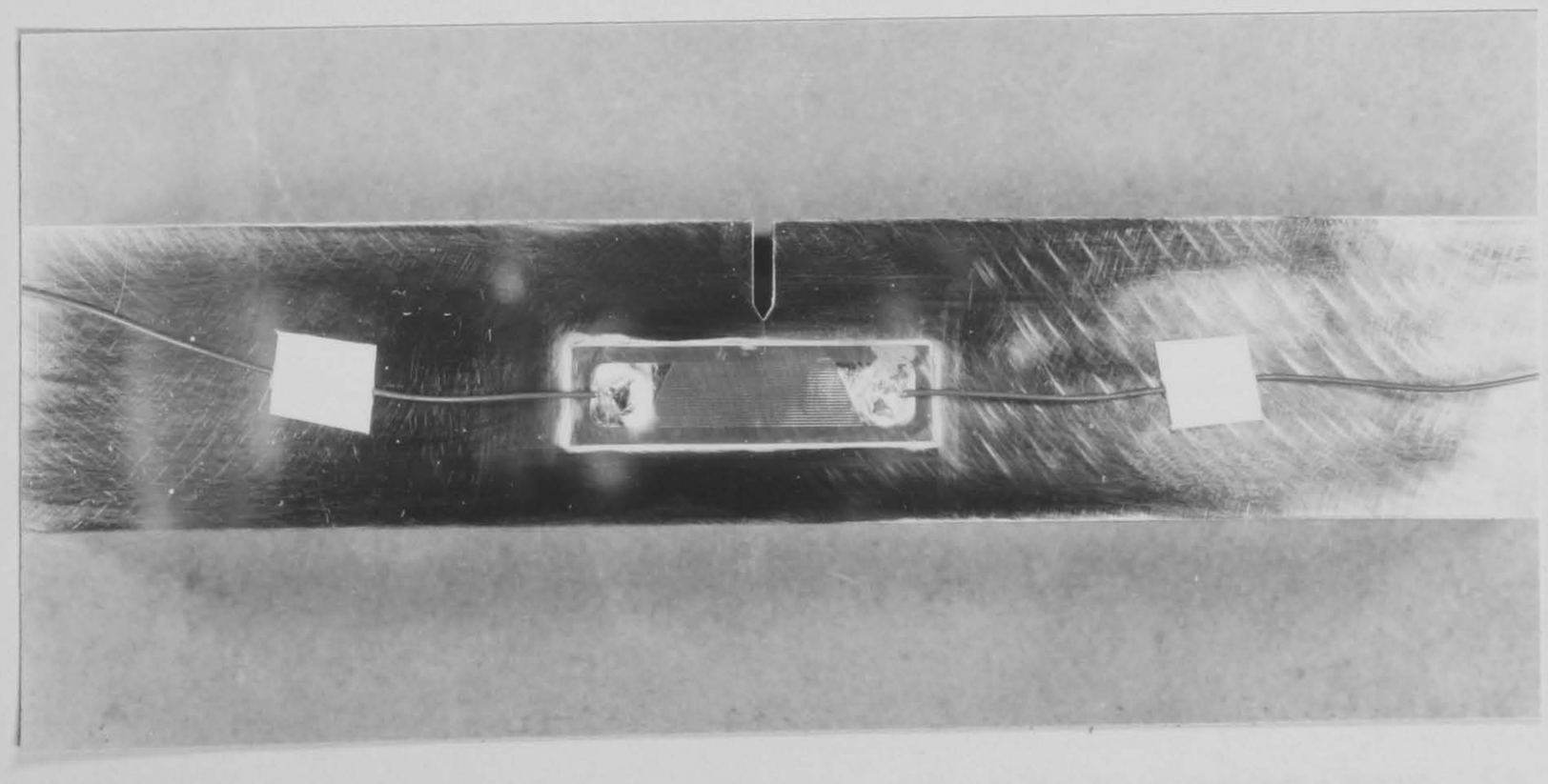

Figure 33 Crack propagation gauge mounted on a fatigue sample.

This system has also been used successfully in the seawater environment. A gauge is mounted in the normal way and the soldered connections painted with a non-porous protective plastic coating. The centre of the gauge was then coated in a very thin layer of silicone rubber onto which a piece of clear cellulose acetate was pressed. This system ensured protection for the gauge whilst still allowing direct observation with a Vernier travelling microscope. A similar piece of cellulose acetate was bonded to the opposite side of the fatigue sample to enclose both sides of the fatigue crack. This represents more closely a fatigue crack in a large plate which has not propagated through the entire thickness of that plate. The gauge and protective coatings are shown in cross-section in Figure 34.

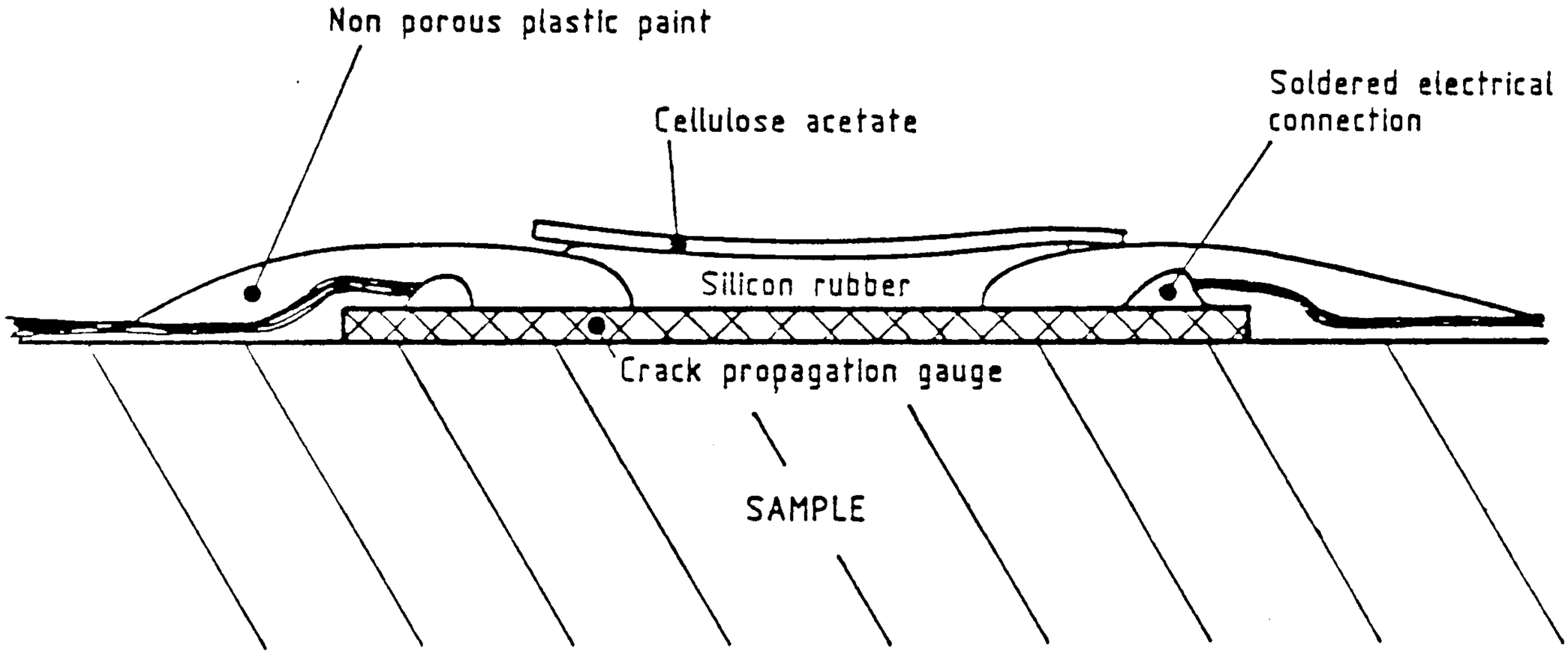

Figure 34 Gauge with protective coatings for corrosion fatigue monitoring.

Due to the nature of a stepped gauge design, there is very little error in crack length determination within the gauge length, i.e. a grid line has either failed or is intact. However, great care must be taken in measuring the distance from the samples uppermost surface to the first grid line as all the automated readings will be based on this measurement. The major limitation of this technique is the

relatively wide grid line spacing. However, this is overcome to a large extent by supplementary optical measurements. Approaches to the propagation gauge suppliers were made with the aim of obtaining a higher resolution gauge. However, no such gauge was available.

4.4.4. Threshold step down

Previous rising stress intensity range experiments had established that N-A-XTRA 70 appeared to be thresholding at a stress intensity range below 15 MPa$\sqrt{m}$. However, due to the nature of a constant amplitude experiment it was not known how far below this stress intensity range the true threshold was. A stress intensity range reduction versus crack length profile was used to investigate the threshold as shown in Figure 35, together with the load reduction profile in terms of the changing maximum and minimum loads with crack extension. A constant stress ratio of R = 0.6 was maintained throughout the experiment to allow direct comparison with earlier testing. A modified frequency of 0.2 Hz was used to allow very close control over loading parameters. Crack length measurements were made using a travelling microscope down to da/dN values of 1×10^{-8} m/cycle, below which a surface replication technique was used. This technique was preferred at very low crack extension per cycle values as it allowed extremely accurate crack extension measurements to be made at high magnification (x400). Reference lines were scribed onto the sample surface to aid crack extension measurements. At designated cycle intervals the fatigue test was suspended while a cellulose acetate replica was taken. The technique required the test to be suspended for 20 seconds but did not, however, disturb the position of the sample within the fatigue machine. The replication technique is described in more detail in the metallography section.

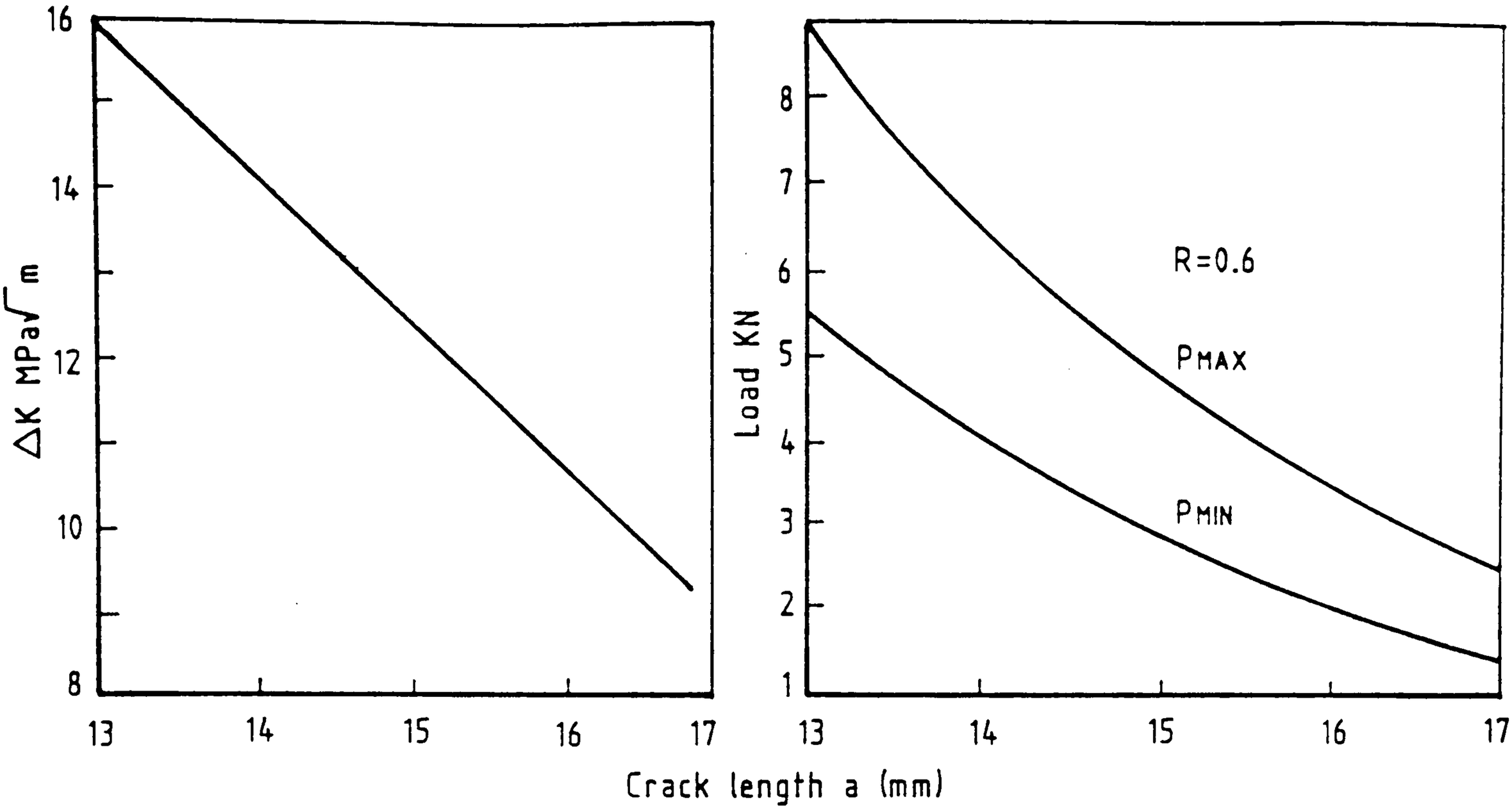

Figure 35 Stress intensity range versus crack length profile for a threshold step down test.

4.4.5. Constant stress intensity range fatigue crack propagation

An experimental technique was devised to grow a fatigue crack through a microstructural gradient whilst maintaining a constant stress intensity range and loading ratio. The microstructural gradient was produced via a single pass, bead on plate submerged arc weld as described in section 4.3.2. The constant loading parameters were stress ratio R = 0.1, frequency f = 0.1 Hz, and stress intensity range K = 19.5 MPa$\sqrt{m}$. For the stress intensity range and stress ratio to be kept constant with increasing crack length, a load reduction profile had to be maintained. The arbitary value of stress intensity range selected for the experiment was designed to produce a reasonable test duration for the experiment of two weeks. A lower value would have been preferable since it would have allowed more data to have been generated for the varying microstructure region but was not chosen because of the time restrictions of the thesis period. The material chosen was BS4360 55E.

Constant stress intensity range experiments have conventionally been achieved by manual load turn-down at fixed increments of crack extension. It was decided to design a fatigue machine control system and crack length monitoring system which would enable a fatigue test to be carried out automatically under constant stress intensity range conditions. The motivation to achieve this was to obtain more accurate control over loads and hence a truer constant stress intensity range experiment. Ideally the crack length would be measured every cycle and adjustments made accordingly to the load. For a successful automated system, an accurate means of crack length measurement was required. The commercial crack propagation gauges previously used give excellent accuracy (error = +/- 0.01mm) with very limited resolution (0.25mm), making their incorporation into an automated system only a slight improvement on a manual turn-down technique. At this time a continuous variable resistance gauge was under development elsewhere in the School of Industrial Science.

A suitable gauge for the envisaged application had been designed by Dr J R Nicholls* and Mr R Tidswell** (84). Due to the urgent requirement for the continuous gauge, production was carried out by the author and Mr Tidswell under the supervision of Mr K Lawson† and Mr D Timpson.†† The design of the gauge and production techniques are described in Section 4.5.

A Nene Instruments Ltd tensile/compression static loading machine was chosen as a base for building a computer controlled fatigue testing system. This was adapted by Mr R Smith††† for fatigue work via the installation of a function generator and load cell amplifier. The function generator was used in the normal way to produce an amplitude and offset signal required to produce the desired load sine wave. The values of the two demand signals were pre-set by the normal controls to give the maximum output required. The

* Dr J R Nicholls - Principle Research Officer, coatings technology

** R Tidswell - PhD student, coatings technology

\+ K Lawson - Research Officer, coatings technology

++ D Timpson - Senior Technician, coatings technology

+++ R Smith - Principle Electronics Technician

two function generator signals were fed to two multiplexers which were also designed and installed by Mr R Smith. The multiplexers allow a reduction in the signal they receive from the pre-set maximum value to zero depending upon the control signal received from the computer. The two signals are then combined to produce a sine wave, the amplitude and offset of which is controlled directly by the computer. This control system is illustrated schematically in Figure 36.

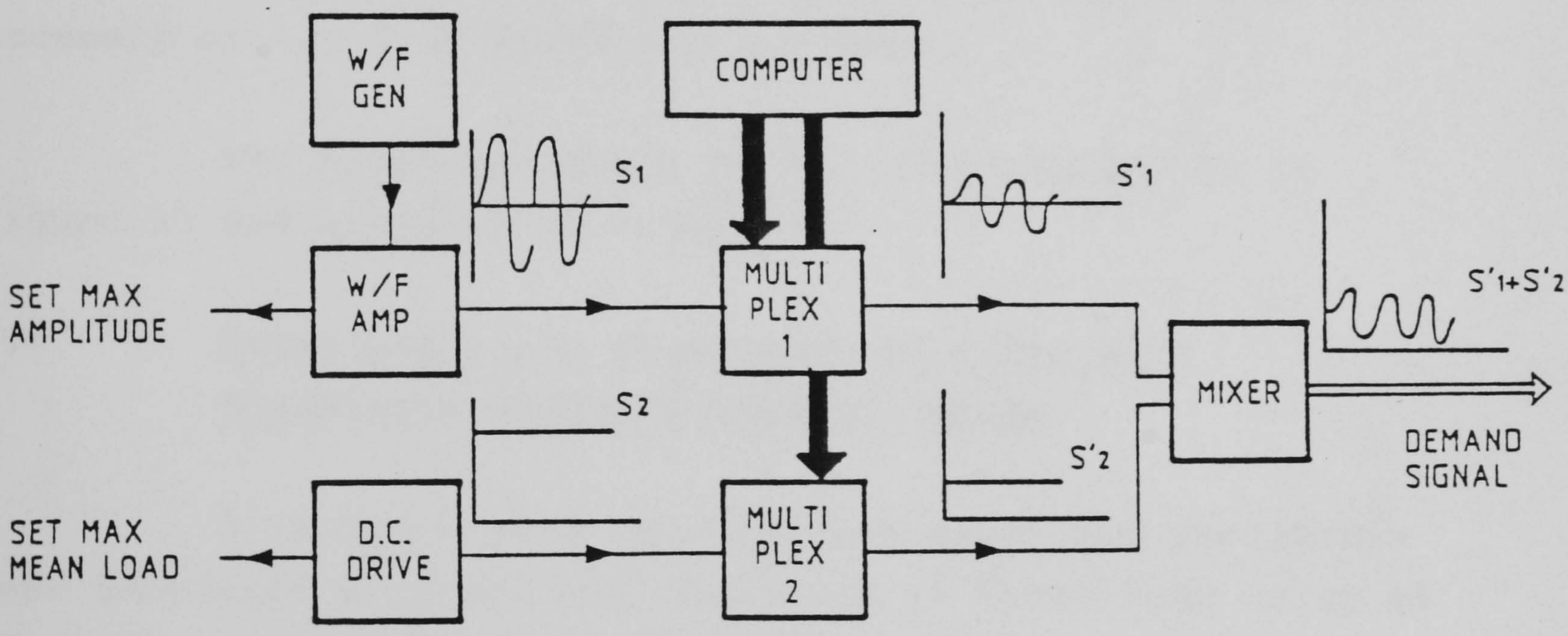

Figure 36 Control system for computer controlled fatigue machine.

The desired signal is amplified and becomes the demand signal which will be matched by the load cell output so ensuring the desired loads are applied to the specimen. Thus a system has been developed to enable direct control of a fatigue machine via computer software. The ability of the computer system to maintain a constant stress intensity range and load ratio is, to a large extent, dictated by the resolution of the analogue to digital converter (ADC) used

to convert the propagation gauge output into a number for computing, and the digital to analogue converter (DAC) used to control the multiplexers and hence control the sample loading. The ADC (crack length monitor) will convert a voltage between 0.000 and 4.096 volts to a number with a resolution of 1 millivolt. This would give a crack length measurement resolution, over 4mm of fatigue crack extension, of the order of 1/1000mm. Due to a slight strain gauge effect displayed by the gauge under load, the accuracy was reduced to 5/1000mm and to ensure a high level of confidence the data was recorded to 1/100mm. The DAC produced a voltage between 0.00 and 2.55 volts with a resolution of 0.01 volts. This degree of control would allow the stress intensity range to be maintained to within 0.1 MPa$\sqrt{m}$ over the planned 4mm crack extension. However, due to electronic drift on the control side, an actual test accuracy of +/- 0.25 MPa$\sqrt{m}$ was achieved.

The complete system is shown schematically in Figure 37 and actually in Figure 38.

4.5. Development and Production of a Variable Resistance Crack Propagation Gauge

A variable crack propagation gauge had previously been developed at Cranfield Institute of Technology using an AC sputtering coating technique (84). This gauge was capable in theory of very accurate and continuous crack length measurement.

The gauges had been coated directly onto the samples and also onto a thin plastic backing sheet. Unfortunately, due to technical difficulties, the equipment previously used was not available within the time schedule of this work. An alternative DC sputtering technique was therefore developed and used.

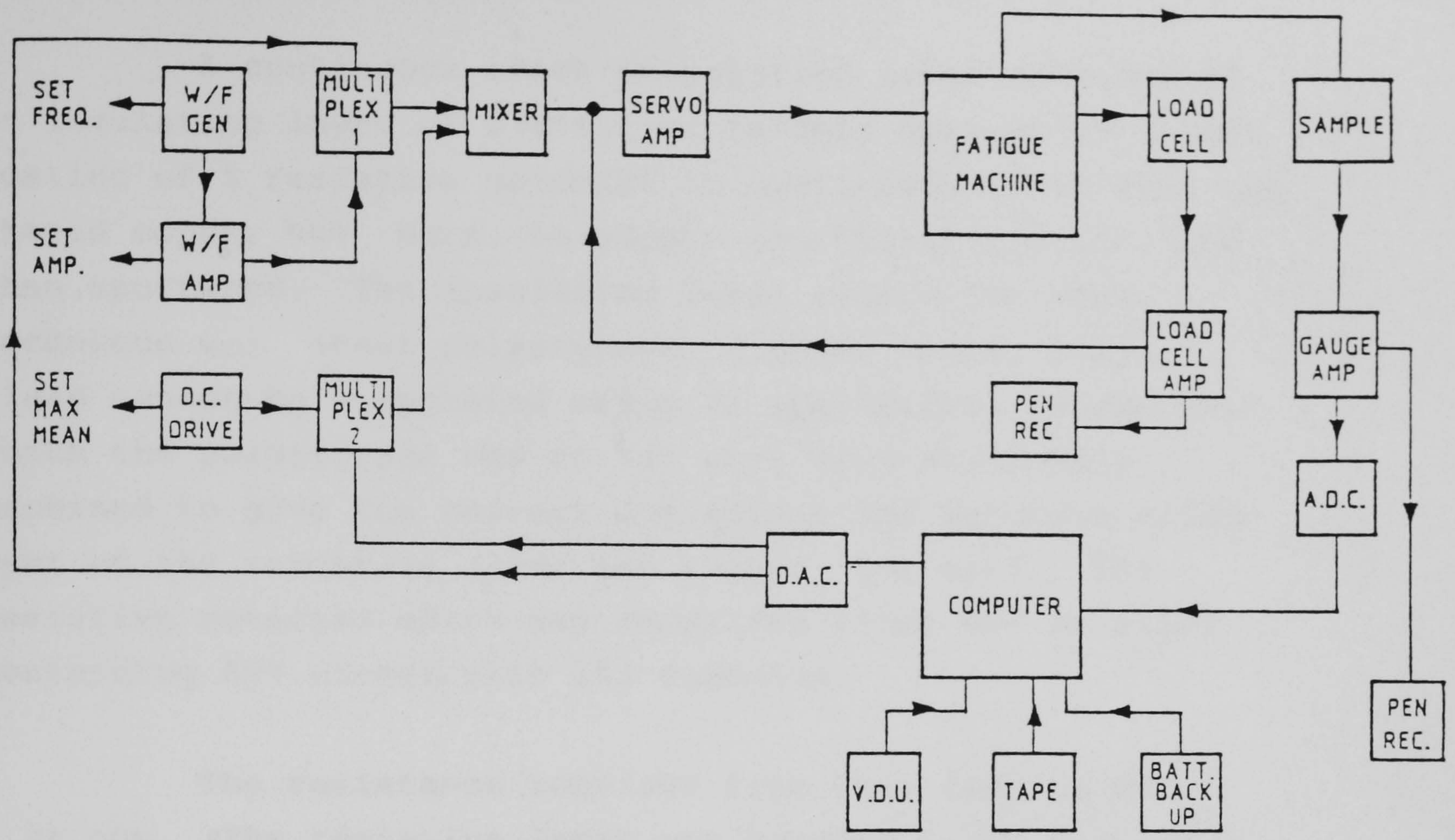

Figure 37. Schematic illustration of constant ΔK experimental set up.

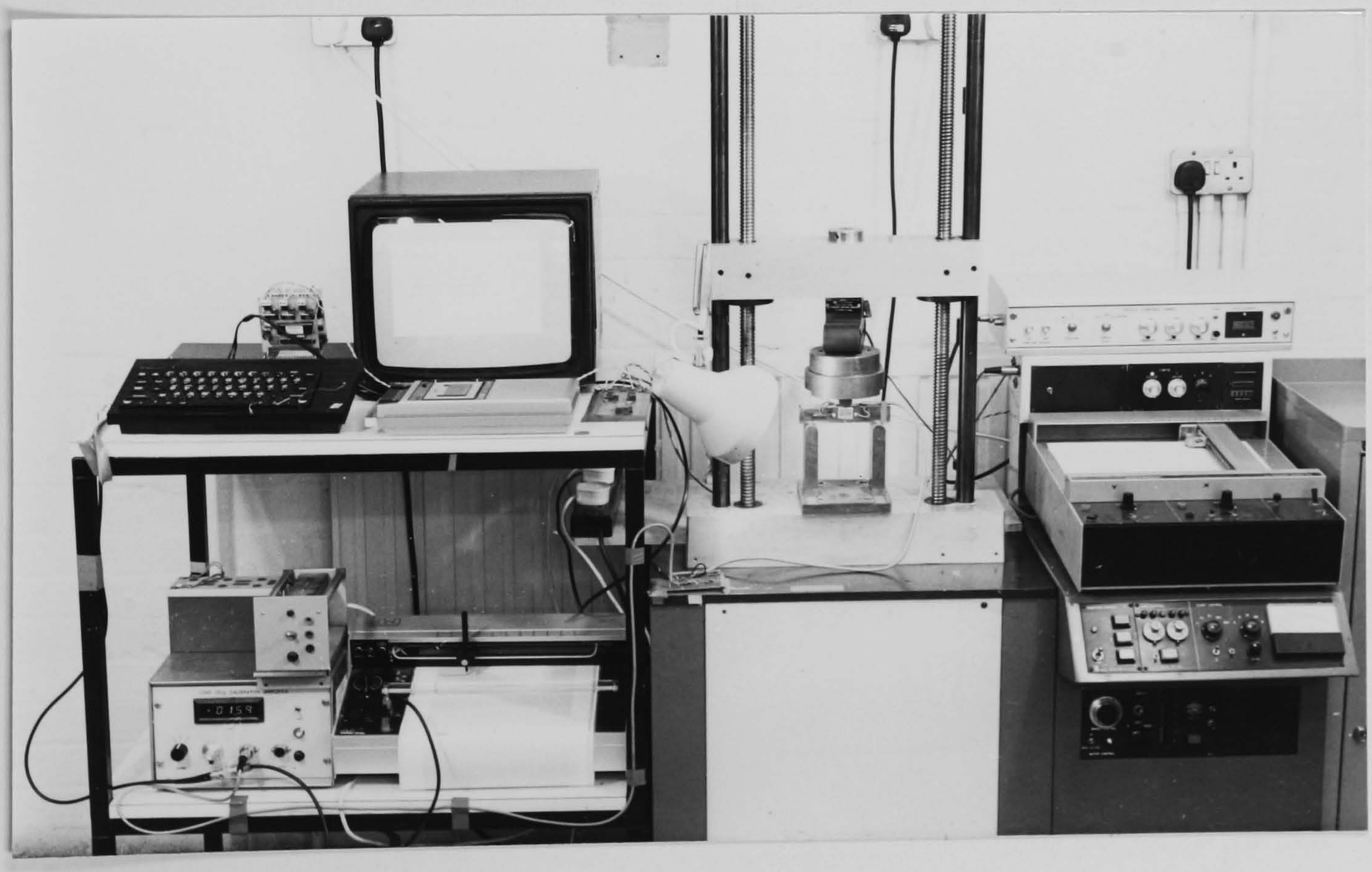

Figure 38. Constant ΔK fatigue rig.

4.5.1. Gauge construction

A continuous crack propagation gauge consists of an insulating layer of plastic or ceramic onto which a thin coating of a resistive material is sputtered. Onto this two shaped copper bus bars, to supply electrical contact, are then sputtered. The insulating layer chosen for this technique was sheet polystyrene, 0.254mm thick, since glass cannot be evaporated using DC sputtering. Masks into which the polystyrene was to fit were very accurately machined to give the correct dimensions and accurate alignment of the resistive layer and copper bus bars. The resistive material which was deposited first was an alloy containing 80% nickel with 20% chromium.

The resistance required from this coating was 1.0K ohm. The resistive layer was between 6 and 8 x 10^{-8}m thick. The copper pads were deposited as thickly as possible for physical strength and reduced the resistance of the gauge to 500 ohms. The deposit was produced in two stages of 30 seconds duration in order to avoid heat damage to the polymer. The copper deposits were 1.0 to 1.2 x 10^{-6}m thick. The gauges were cut from the sheet polymer and were mounted on the samples using a cyanoacrylate adhesive. Careful surface preparation and cleanliness ensured a good bond. A surface finish achieved with 1200 grade abrasive paper was found to be suitable. Immediately upon bonding, the gauge and sample were clamped to a pressure of approximately 10 Kg/cm^2 and were left overnight before testing. The variable resistance crack propagation gauge mounted on a sample prior to fatigue testing is shown in Figure 39.

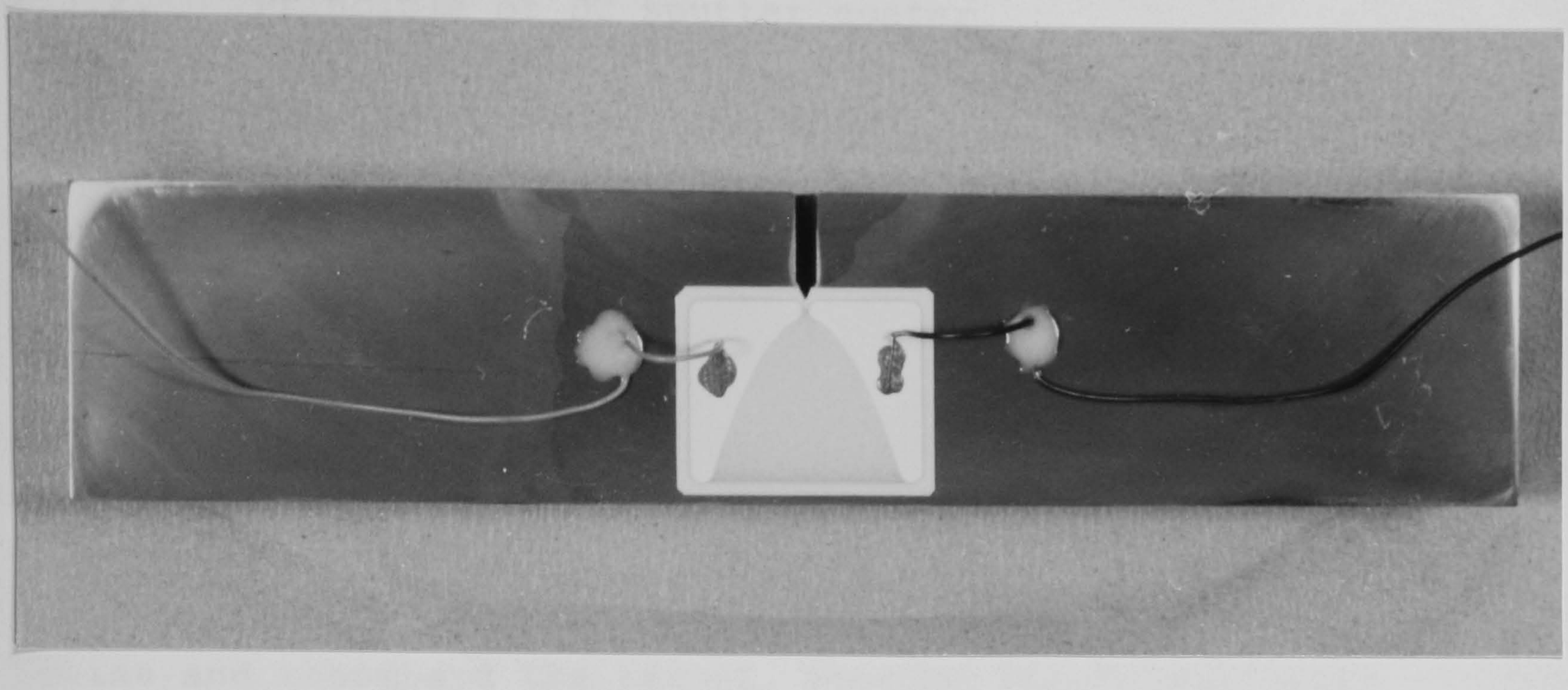

Figure 39 Variable resistance crack propagation gauge mounted on a fatigue sample.

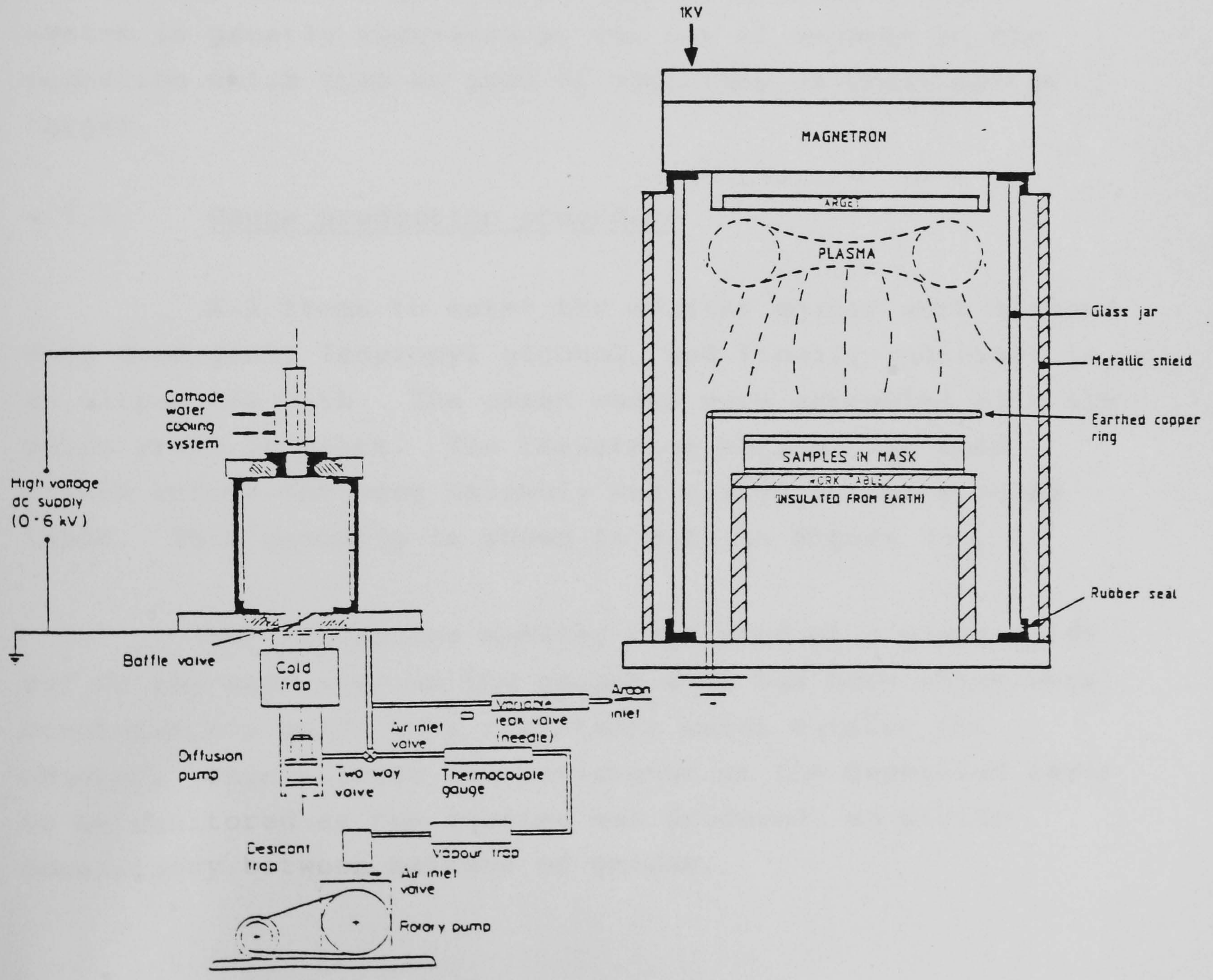

Figure 40 DC sputter coater with expanded diagram of the coating chamber.

4.5.2. Principle of DC sputter coater

The DC sputter coater used for gauge production is shown in Figure 40 with an expanded diagram of the coating chamber.

At low pressure the argon is ionised by the high potential between the magnetron and the earthed copper ring. The negative potential of the target attracts the argon ions resulting in bombardment. Target material is knocked into the chamber volume. Some of these atoms will ionise and rebombard the target, however others will fall onto other surfaces including the sample surfaces. The short mean free path of these atoms ensures even coating without any shadowing effects. The efficiency of the system is greatly increased by the use of magnets in the magnetron which trap an area of electrons in front of the target.

4.5.3. Gauge production procedure

All items to enter the sputter coater were cleaned with detergent, Isopropyl alcohol, and finally inhibisol in an ultrasonic bath. The clean masks were assembled with the polystyrene in place. The resistance monitor was then fitted before the mask assembly was placed on the working table. This assembly is shown in plan in Figure 41.

The resistance monitor consisted of a glass slide cut to the same size as the gauges with bus bars which were connected via leads to a resistance meter outside the chamber. This allowed the resistance of the deposited layer to be monitored as the coating was produced, so giving consistancy between batches of gauges.

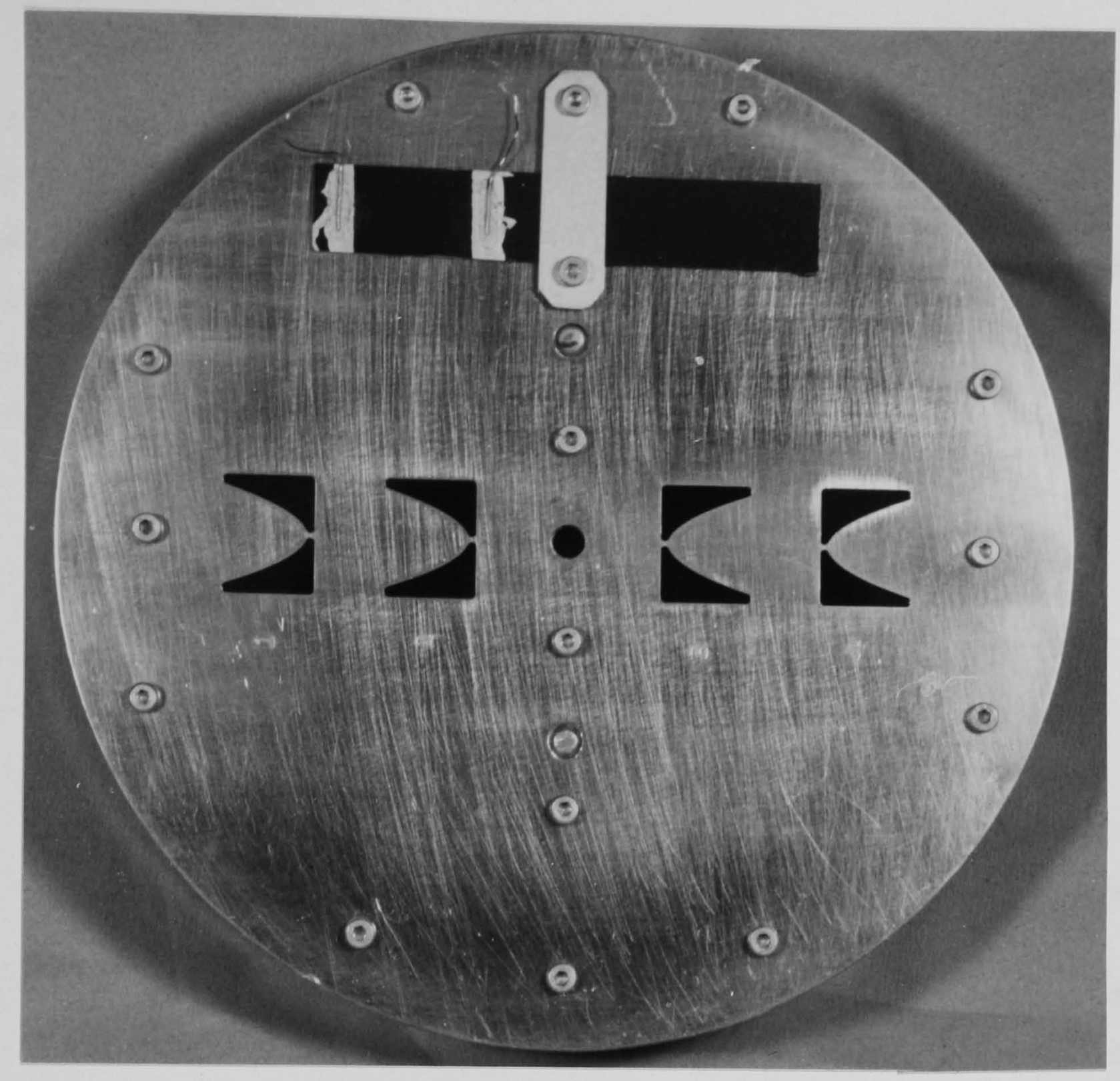

Figure 41. Resistance monitor and mask assembly.

As shown in Figure 40, the copper earth ring was positioned 15mm above the mask assembly and the magnetron a further 45mm above the copper ring. The system was then evacuated to a pressure of 1×10^{-7} torr. Having allowed the system to settle at this pressure, a slow trickle of cleaned argon gas was introduced via a needle valve. The butterfly valve between the chamber and diffusion pump was closed slightly to produce a pressure gradient and improve the flow of argon. A high negative potential was then introduced to the magnetron and a plasma struck. Coating was continued until the desired resistance was achieved when the potential was removed and the plasma extinguished.

A coating time of 25 seconds at a potential of 780 volts and a current of 0.45 amps was found to give 1K ohm resistance. The system was allowed to cool under vacuum before the chamber was vented to air. The samples

were then removed, the mask and target changed for the copper coating, and the coating procedure repeated. However, two coatings with a 15 minute interval were used to produce the required copper deposit. It should be noted that copper will coat at four times the rate of nickel-chrome under the same conditions.

The system was allowed to cool at vacuum to avoid any undesirable oxidation effects.

4.5.4. Variable resistance gauge accuracy

A gauge mounted using strain gauge adhesive was fatigued to a crack length of 3.18mm measured in the gauge at x400 magnification. The gauge was removed and the crack in the metal was measured at 3.38mm showing a discrepancy of 0.20mm. The fatigue was carried out at the same loads to be used in the constant stress intensity range test. However, a second gauge mounted using cyanoacrylate adhesive was found to reproduce the crack length to the accuracy of the measuring technique used (error < +/- 0.01mm). Comparison of Figures 42 and 43 shows the different nature of the crack in identical gauges loaded to the same procedure.

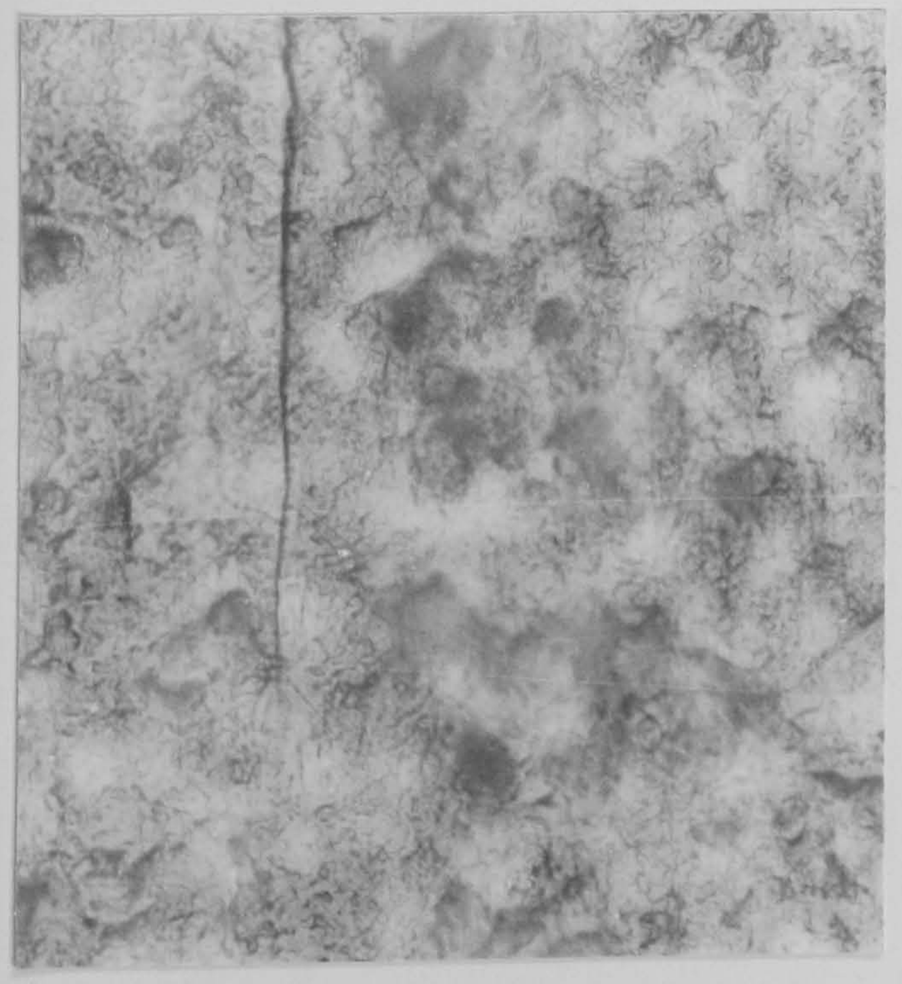

Figure 42
Fatigue crack in gauge mounted [illegible] adhesive.

Figure 43
Fatigue crack in gauge mounted using cyanoacrylate adhesive.

The gauge mounted using strain gauge adhesive shows a very ductile nature with no side cracks. However, the gauge mounted using cyanoacrylate adhesive is behaving in a brittle fashion and has formed cracks in front of the main crack. This is due entirely to plastic deformation in front of the crack. This does not affect the calibration for a constant stress intensity range application as the plastic zone is of consistent size. It was therefore decided to use the cyanoacrylate adhesive for gauge to sample mounting.

4.5.5. Calibration of variable resistance crack propagation gauge

A propagation gauge was mounted on a fatigue sample as shown in Figure 39. The sample was fatigued in a load step-down manner to give an approximately constant stress intensity range $K = 19 +/- 2$ MPa$\sqrt{m}$. The crack length was measured at approximately 0.25mm intervals (at x400 magnification).

The frequency used was 10 Hz and a loading ratio of $R = 0.1$ was maintained throughout the calibration. The resistance of the gauge versus crack length is shown in Figure 44. All the gauges used have been produced to have the same resistance and will therefore fall on the calibration curve prepared. However, minor variations in resistance have been allowed for in the monitoring circuit.

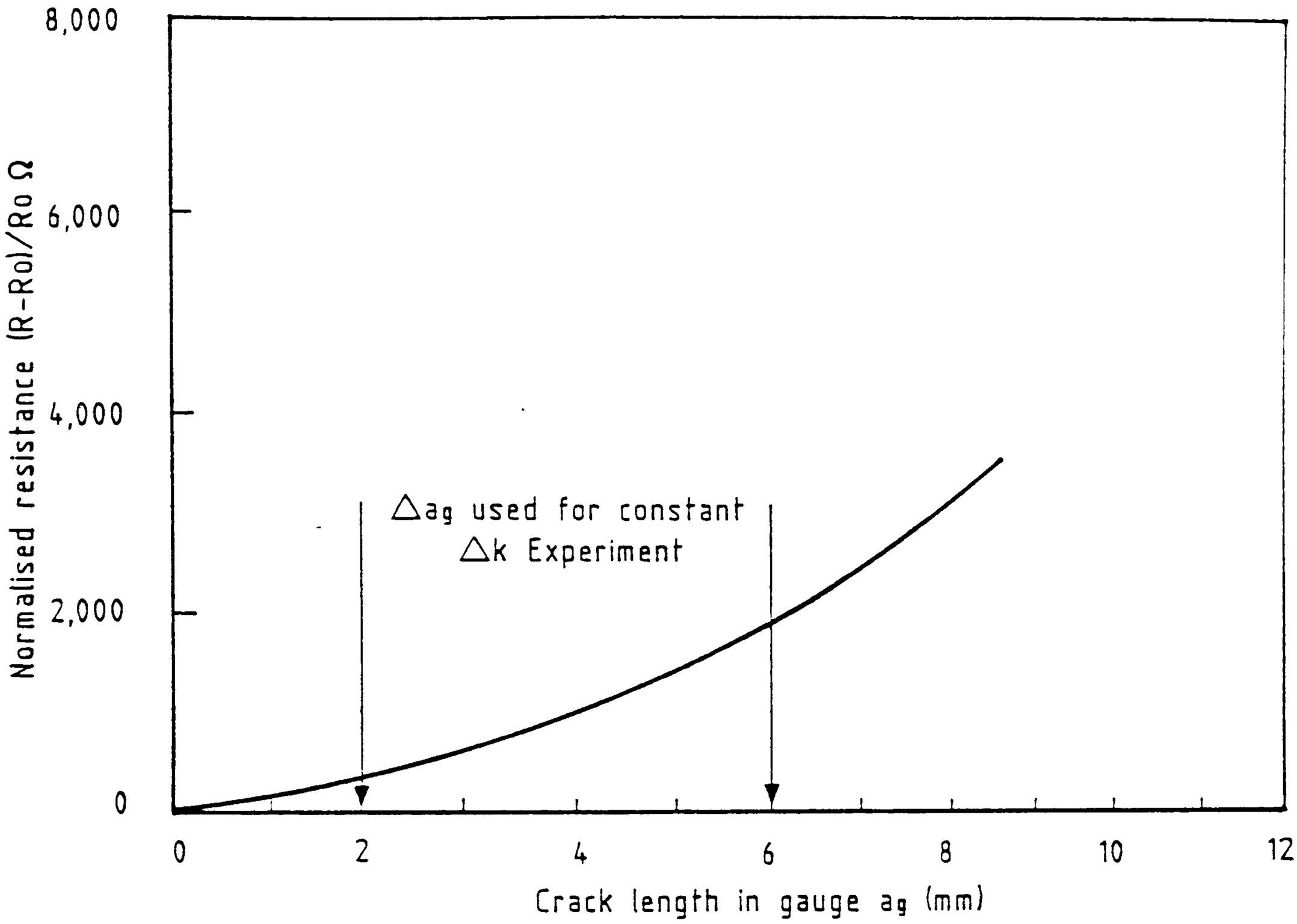

Figure 44. Resistance versus crack length calibration curve for variable resistance gauge.

5.0. RESULTS

It is widely recognised that material, environmental and loading variables are important factors in predicting fatigue life. As a result, considerable effort is expended in identifying and subsequently controlling these variables during fatigue crack growth testing. However, data processing techniques with their associated variables are often neglected. These variables include data processing methods to convert the raw test data (a/N, crack length versus elapsed cycles) to crack growth per cycle data (da/dN versus stress intensity range), and the techniques used to interpret and present fatigue crack propagation curves.

5.1. Fatigue Crack Propagation Data Derivation Interpretation and Presentation

A schematic representation of the analytical aspects associated with the developement of fatigue crack propagation data is presented in Figure 45 and illustrates four of the most popular data processing techniques used to convert raw crack growth data into a da/dN versus ΔK plot. Each technique is considered individually below.

(i) Secant method

Sometimes called "point-to-point" this method involves calculating the slope of the straight line connecting two adjacent points on the 'a ' versus 'N' plot. This may be expressed as:-

$$\frac{da}{dN} = \frac{a(i+1) - ai}{N(i+1) - Ni} \qquad (12)$$

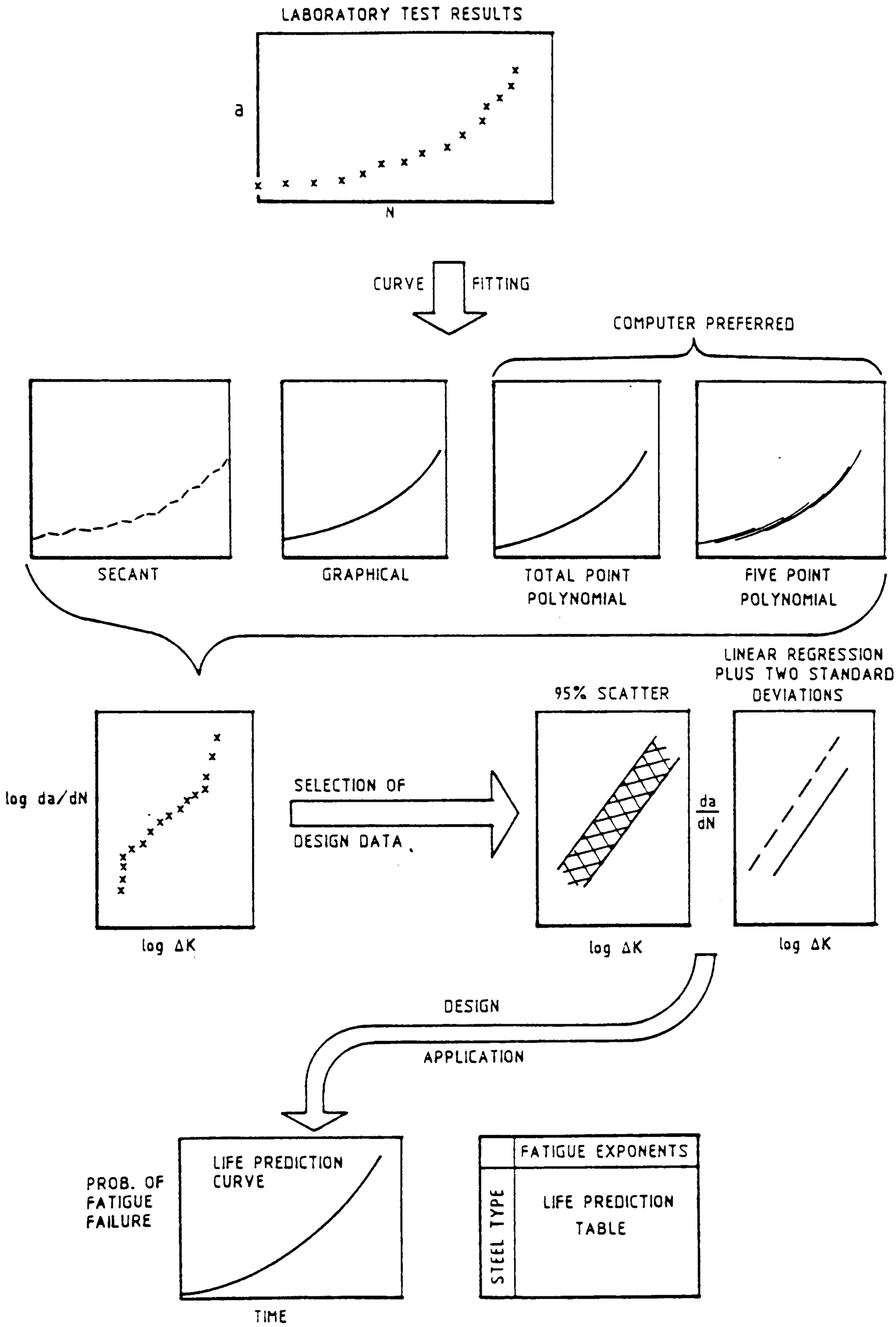

Figure 45 Data processing techniques used to convert raw crack growth data into design curves.

Since the computed da/dN value is an average rate over the a(i + 1) - ai increment, the average crack length (a(i + 1) + ai)/2 is normally used to calculate the corresponding ΔK value.

(ii) Graphical

A smooth curve is fitted by eye to the plotted 'a' versus 'N' data. Tangents to this curve are drawn at regular known values of 'a' (ai). The rate of crack growth, da/dN, at ai is then estimated by measuring the slopes of the tangents to the curve. The corresponding Ki is computed using ai, the crack length at the point of tangency.

(iii) Total data polynomial

A high order polynomial is fitted either to all the data or selected data points covering the entire range of data (84). The curve fitting model is of the general form:-

$$a = \sum_{i+1}^{n} \beta i \; fi \; (N) \qquad (13)$$

The curve fitting functions β to f may be described as follows:-

fi (N) are power functions determined by the min-max criterion to minimize the maximum deviation between the observed and fitted values of crack length.

βi are the regression parameters subsequently determined by the least squares criteria.

The polynomial is integrated with respect to N (elapsed cycles) and the da/dN data derived at each ai, ΔK values corresponding to da/dN data are calculated using ai.

(iv) Incremental sliding polynomial

A polynomial of defined order is fitted to data points ai to a(i + n), where n is typically 5 or 7 and i has values 1 to the total number of data points. The polynomial is integrated with respect to N and the da/dN value derived at a mid point value of 'a' between ai and a(i + n). This process is repeated for data points a(i + 1) to a(i + n + 1) and so on until all the data has been included. From the brief descriptions presented it is obvious that data processing techniques vary greatly in approach and sophistication. Each technique has inherent limitations which may significantly effect the characterisation of fatigue crack propagation behaviour. This may be illustrated by processing hypothetical data and comparing the results. For this purpose an ideal 'a' versus 'N' curve has been derived with its complimentary da/dN versus ΔK plot. A uniform error +/- ξ has been applied to the crack length, and for the purpose of this study an error of +/- 0.04mm was chossen. This curve is shown in Figure 46 together with the data points.

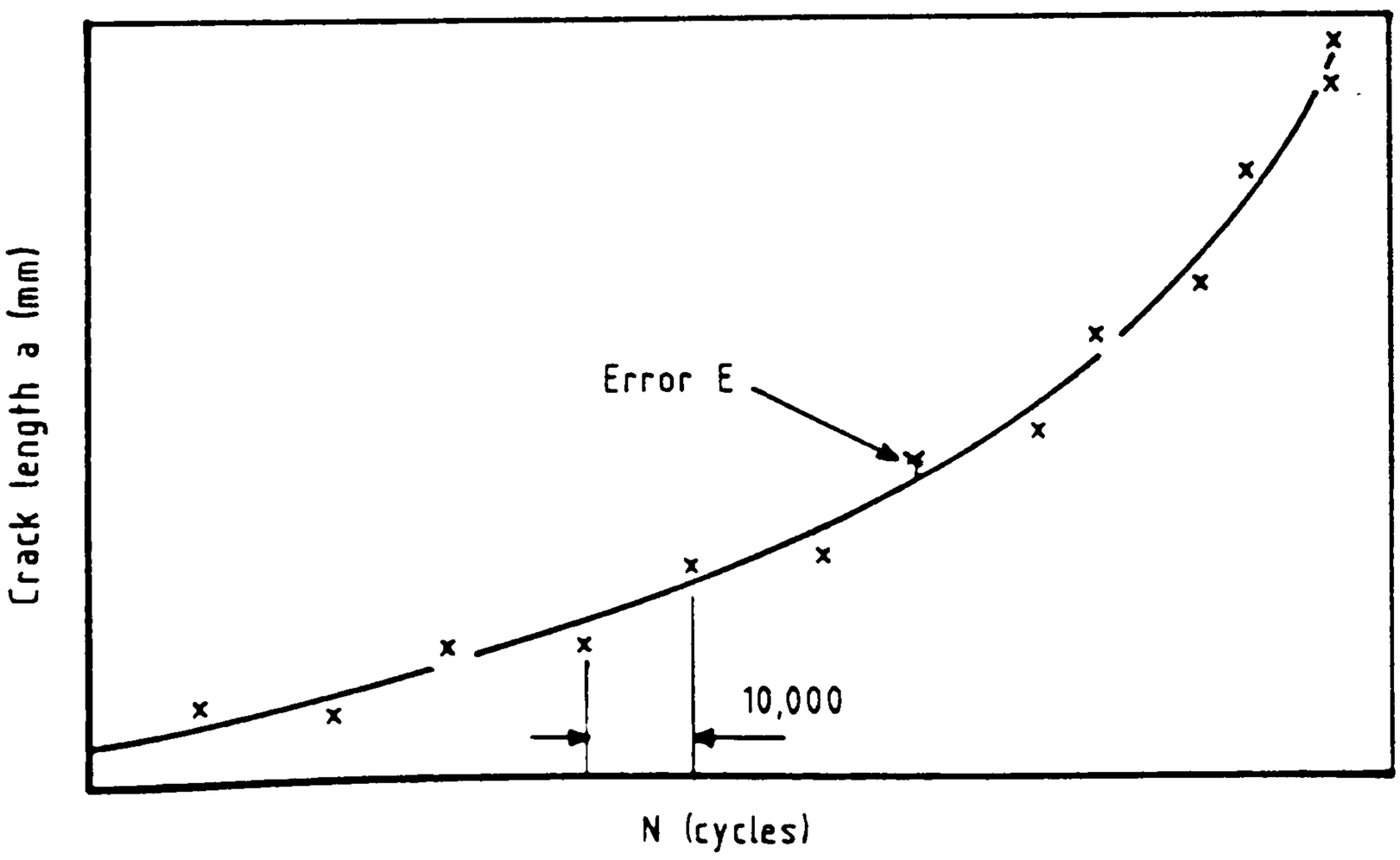

Figure 46 Hypothetical a/N data for processing technique evaluation.

The data points have been processed by the three most popular techniques, namely:-

(i) Secant
(ii) Incremental 5 point polynomial
(iii) Total data polynomial

to derive a da/dN versus ΔK plot. A computer programme was written for techniques (ii) and (iii) which allowed a choice of polynomial order. The results of the processing techniques are shown in Figures 47-49, together with the idealised curve. A linear regression analysis on each technique allows comparisons between the idealised data and the central tendency for each technique.

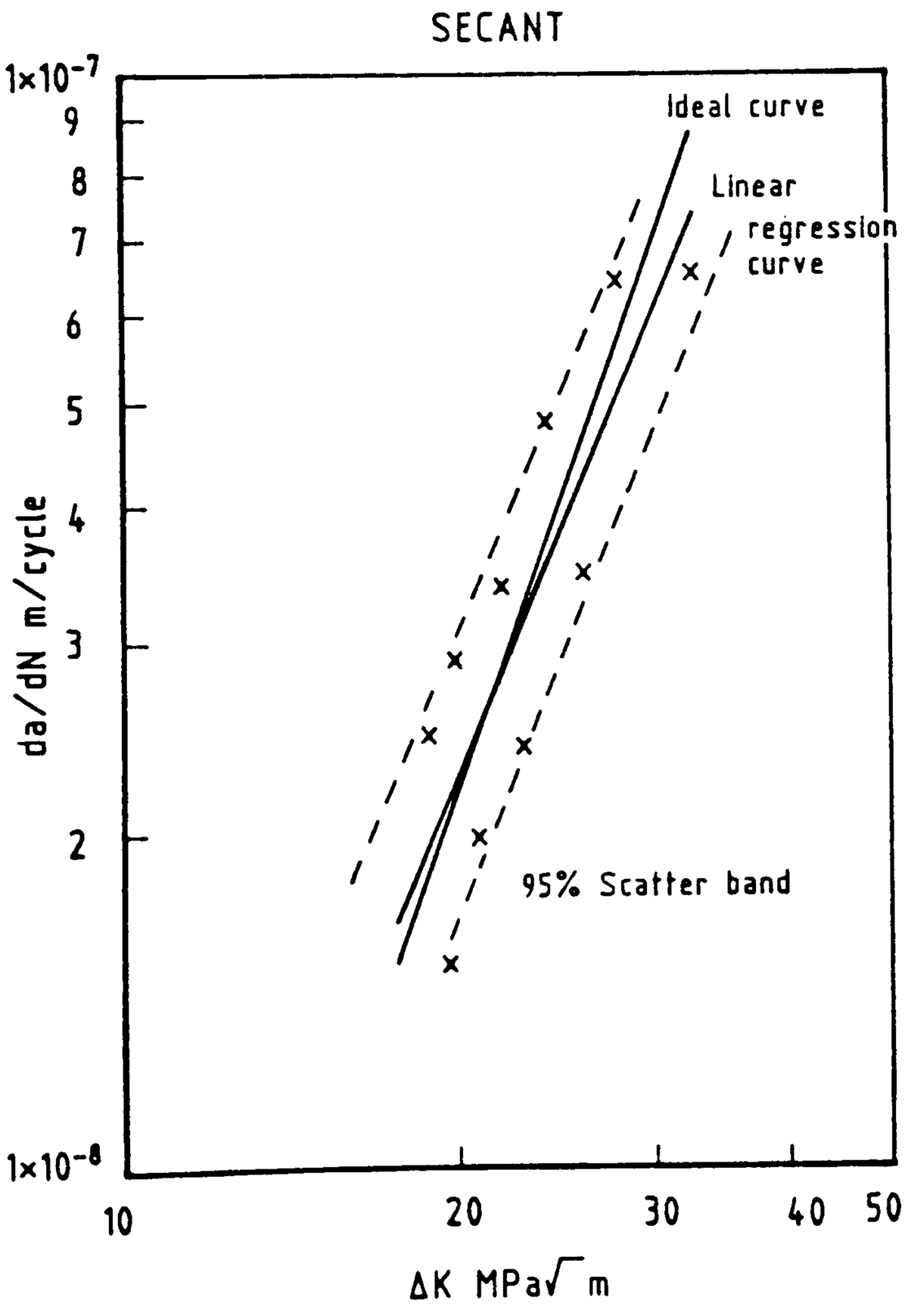

Figure 47 Secant data processing technique.

Figure 47 clearly illustrates that the secant data processing technique has a relatively small but significant effect on the central tendency behaviour as defined by the linear regression line but a very significant effect on the extent of data scatter. The fatigue resistance of a material is characterised by this central tendency line from which the Paris constants may be derived. The correlation coefficient for the secant linear regression analysis was 0.86. In this instance the secant regression line has underestimated the crack growth rate above a ΔK of 20.5 MPa $\sqrt{m}$ and overestimated the crack growth rate below this ΔK value. The amount of scatter may be judged by the width of the scatter band. At a ΔK of 30 MPa$\sqrt{m}$, a maximum crack growth rate of 8.0 and 10^{-8} m/cycle (upper bound) and a minimum growth rate of 5.1×10^{-8} m/cycle (lower bound) may be predicted.

The incremental five point polynomial method has produced a curve very close to the idealised behaviour with a correlation coefficient of 0.998. The technique has underestimated crack growth at higher ΔK but by a negligable amount.

A degree of "smoothing" has occured reducing scatter to a minimum, the overall trend of the hypothetical data has been extremely accurately represented in Figure 48.

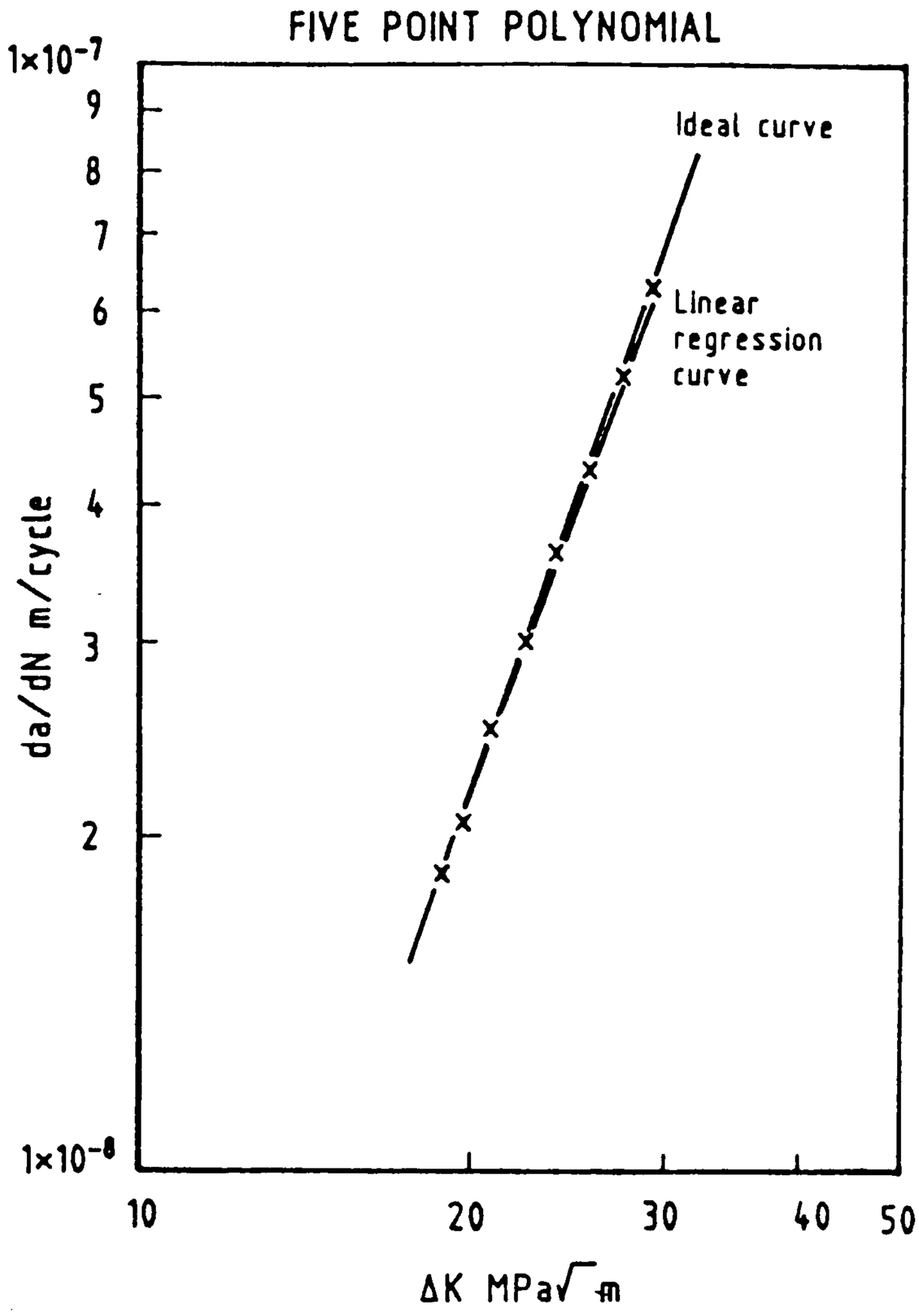

Figure 48 Five point polynomial data processing technique.

The total polynomial curve is greatly affected by the number of terms allowed in the polynomial equation. For this data it was found that a five term polynomial gave the best compromise between accuracy of central tendency and the degree of scatter. As seen in Figure 49 a similar central tendancy to the secant method is produced by this technique with, however, far less scatter. A correlation coefficient for a linear regression analysis on this data was 0.97.

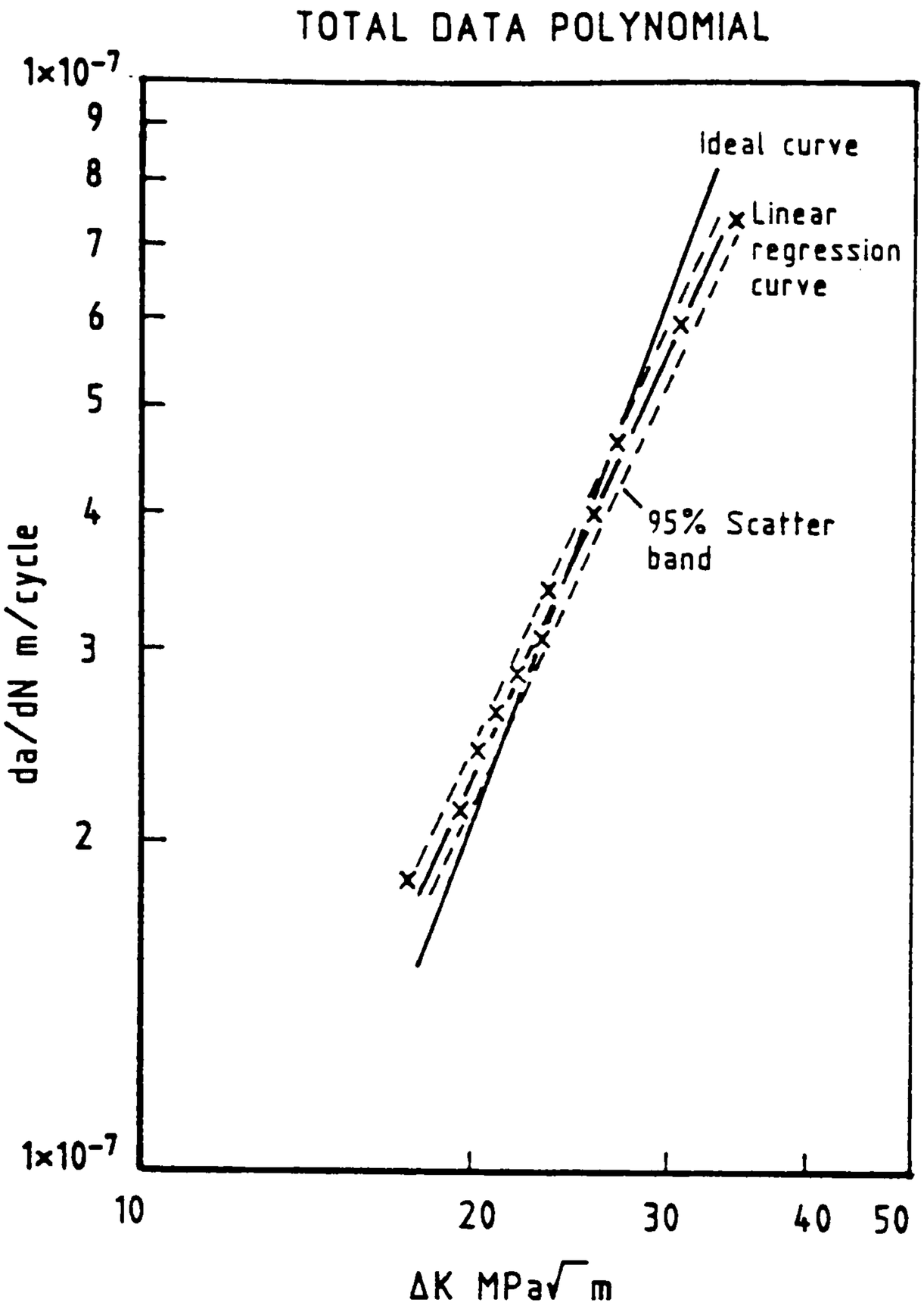

Figure 49 Total data polynomial data processing technique.

The graphical technique is subjective, reducing the possibility of consistent reproducable results. The secant technique tends to accentuate variations from a smooth a/N curve producing a wide scatter in da/dn versus ΔK plots which is sensitive to crack length measurement intervals. Numerical curve fitting techniques generally involve a least squares regression analysis which may induce excessive smoothing of the data possibly disguising real effects due to microstructure or environment. Careful consideration of the advantages and disadvantages presented by each technique would suggest that the incremental five point polynomial method may be the most useful. However, for the purpose of this research it is felt that any automated data processing is not desirable unless a central

tendancy only is required. Although a graphical technique may be described as subjective it does allow closer examination of data at all stages and will not mask any important trends or effects by either smoothing them out or burying them within an unnecessarily wide scatter band.

5.2. In-Air Fatigue Propagation Data

Figure 50 shows the parent plate in-air fatigue properties for N-A-XTRA 70 at a loading ratio of R = 0.6 and a frequency of 0.5 Hertz. Despite the high loading ratio a clear indication of thresholding can be seen at a ΔK of 14 $MPa\sqrt{m}$. The largest degree of scatter occured between a ΔK of 21 and 23 $MPa\sqrt{m}$ when the crack propagation rate varied between 2.8 and 4.2 x 10^{-8} m/cycle. A linear regression analysis has been applied to data points falling above 15 $MPa\sqrt{m}$ for comparison with other data.

The data generated by Kontroll 50 ESM tested to the same experimental procedures is presented in Figure 51. Less scatter resulted from the testing of this material and no indication of thresholding above the starting ΔK of 13 $MPa\sqrt{m}$. Linear regression analysis on this data indicates greater stress intensity range sensitivity to that shown by N-A-XTRA 70 and generally slightly higher growth rates for a given stress intensity range.

The results for RQT 501 are presented in Figure 52. By far the greatest degree of scatter was encountered whilst studying this steel. The higher sensitivity to ΔK will result in a greater degree of scatter despite constant errors in crack length measurement. This occurs simply because of the greater difference in propagation rates encounted for a small change in ΔK. Again no indication of thresholding was found at stress intensity ranges above 13 $MPa\sqrt{m}$.

The results for X80 linepipe in Figure 53 have shown this steel to have similar fatigue crack propagation properties to Kontroll 50 ESM when tested under the same loading conditions. A similar sensitivity to ΔK is seen but at consistantly higher propagation rates for a fixed ΔK value.

BS 4360 grade 55F, Figure 54, has a similar ΔK sensitivity to that shown by N-A-XTRA 70 but at a significantly higher propagation rate for any given stress intensity range. Again no indication of thresholding could be found at stress intensity ranges above 13 MPa $\sqrt{m}$.

The controlled rolled linepipe steel LP-6 exhibited unusual fatigue properties as indicated by Figure 55. In this figure the change in crack length per cycle for both sides of the sample as a function of ΔK have been plotted. Side 'b' has shown conventional fatigue crack propagation data up to a crack length of 15.9mm and a ΔK of 25 MPa $\sqrt{m}$, at which point the fatigue crack has arrested in the propagation plane. Side 'a' has shown normal propagation behaviour for only a short crack extension before crack arrest occurred. The arrest of the fatigue crack is accompanied by a delamination process in bands of high carbide concentration which run at ninety degrees to the normal crack propagation direction. The crack has continued to propagate on side 'a' of the fatigue sample after an interval of 23,000 cycles, the subsequent rate of propagation being increased due to the greater crack length within the bulk of the sample. During periods of normal uninterupted crack growth this material has shown the highest growth rates and sensitivity to ΔK of all six steels.

For the purpose of comparison the five steels which exhibited conventional Paris type behaviour have been plotted on a single diagram together with two published

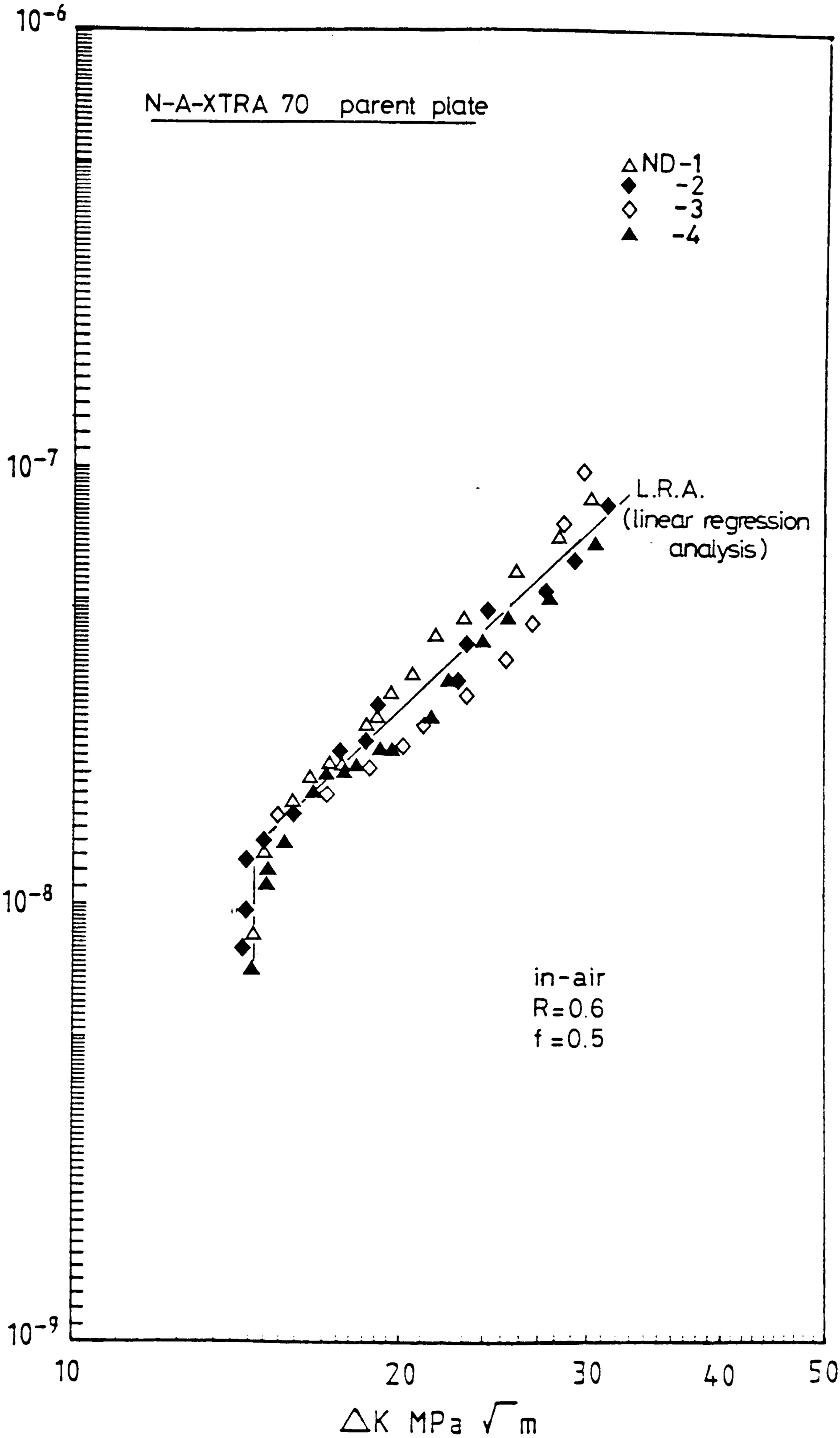

Figure 50. Parent plate in-air fatigue properties for N-A-XTRA 70.

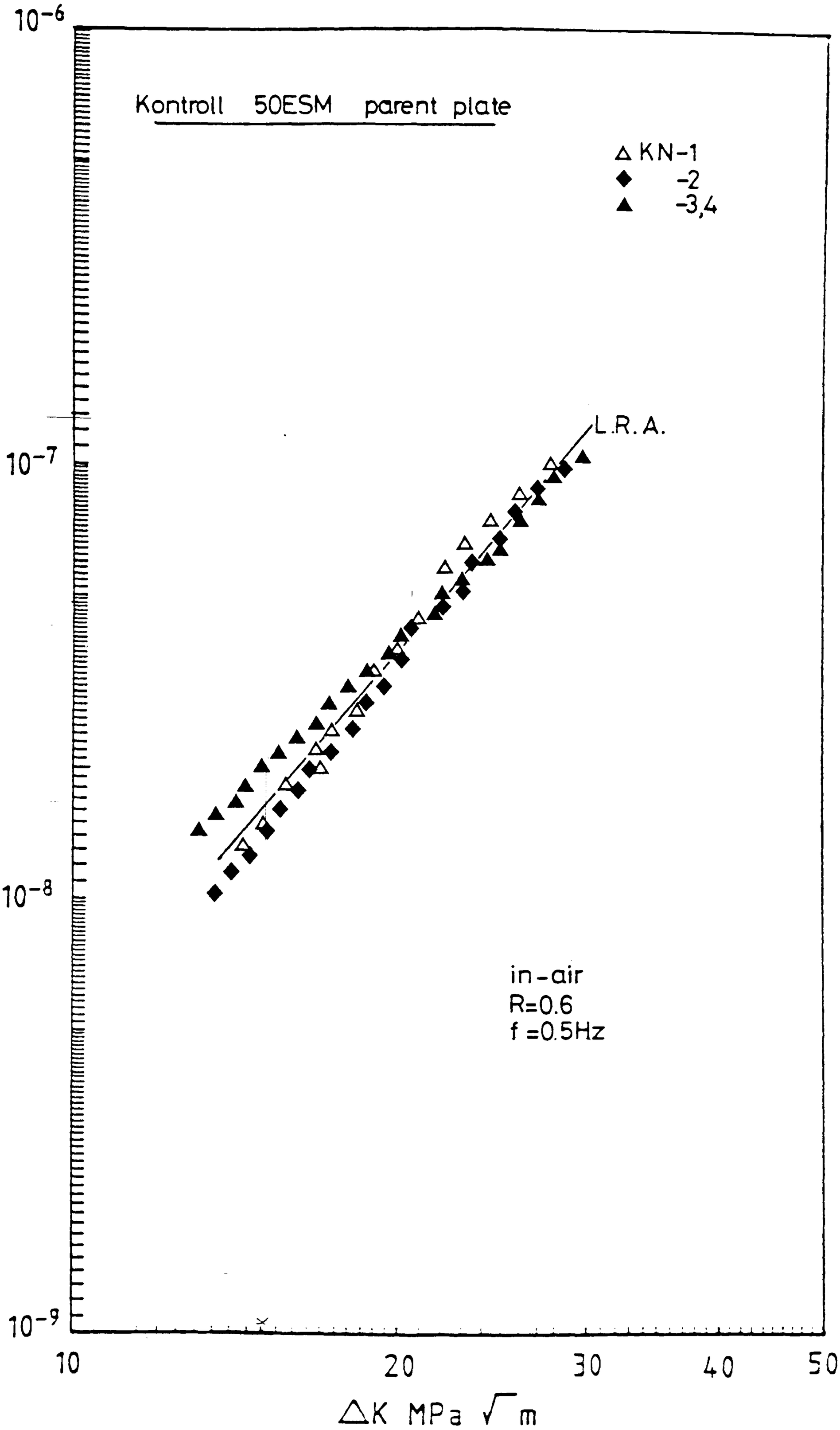

Figure 51. Parent plate in-air fatigue properties for Kontroll 50 ESM.

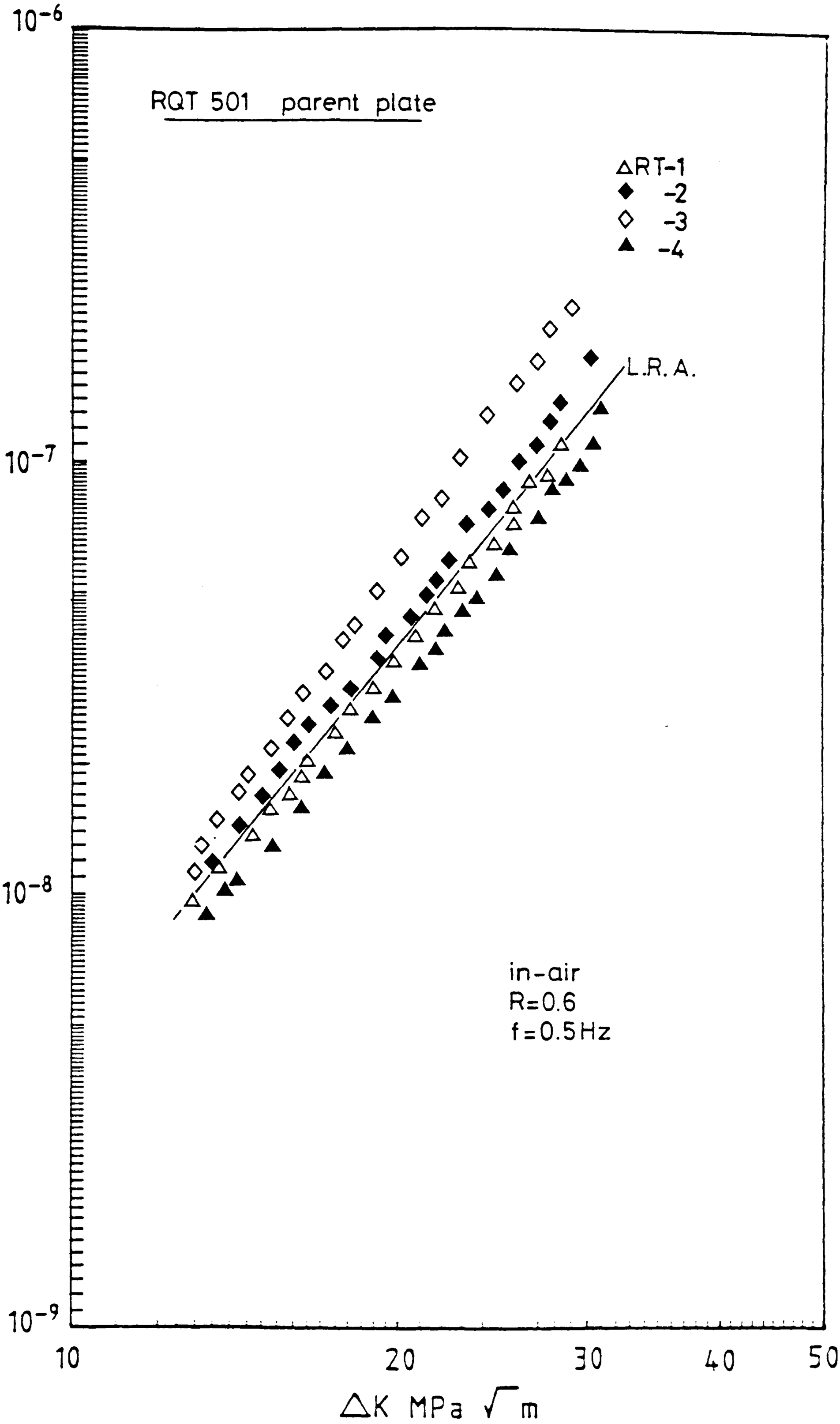

Figure 52. Parent plate in-air fatigue properties for RQT 501.

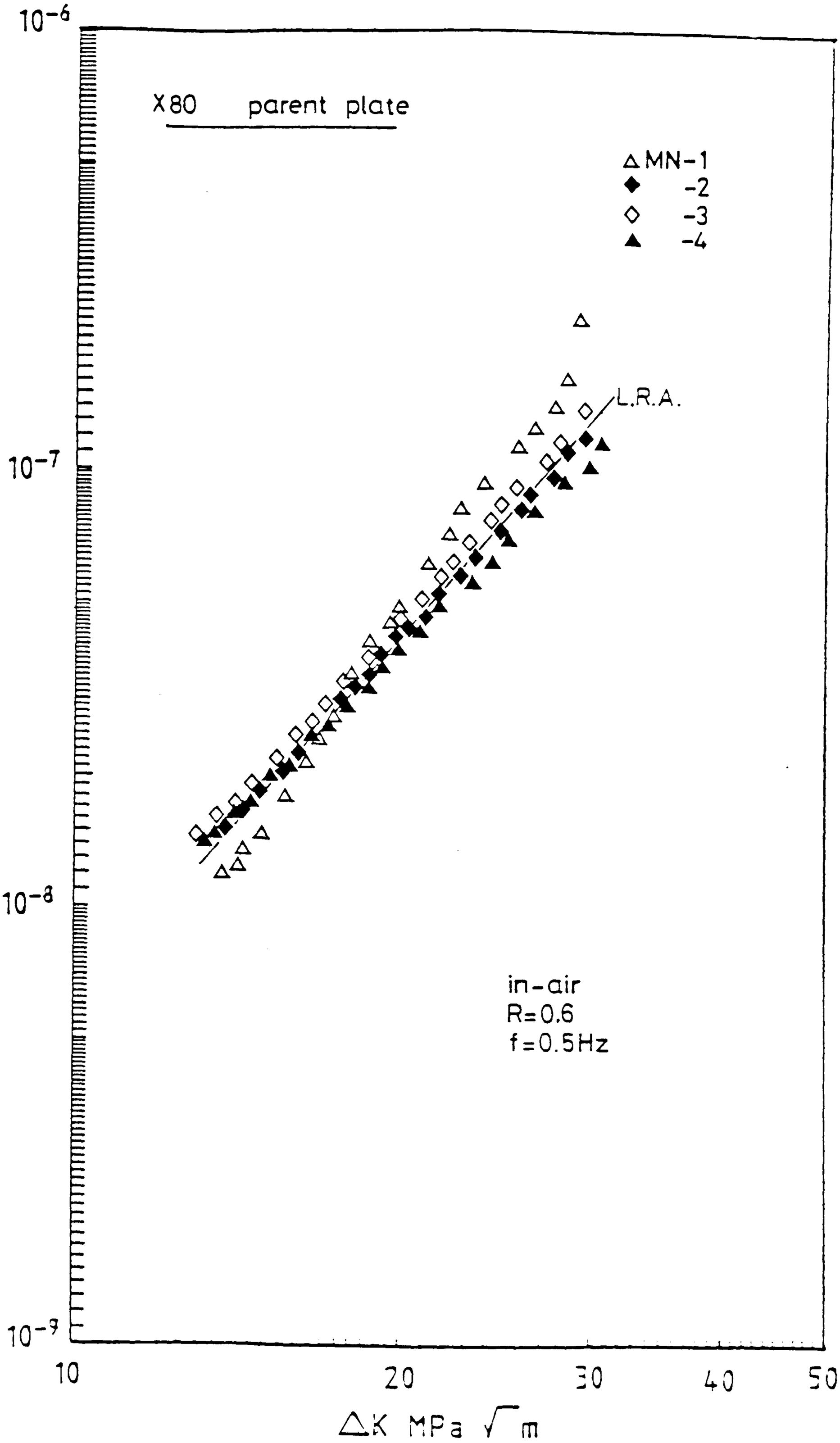

Figure 53. Parent plate in-air fatigue properties for X80 Line-pipe.

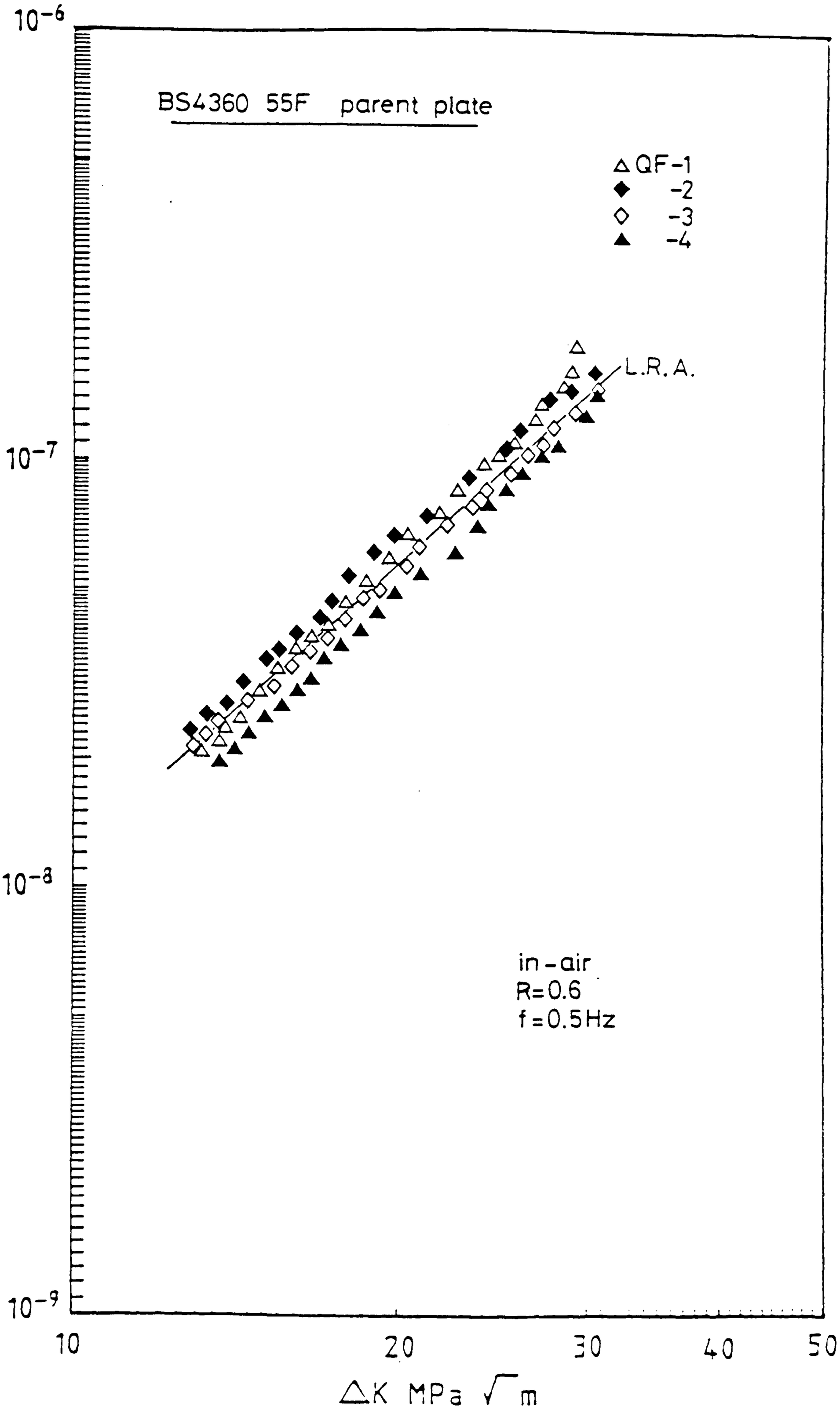

Figure 54, Parent plate in-air fatigue properties for BS 4360 Grade 55F.

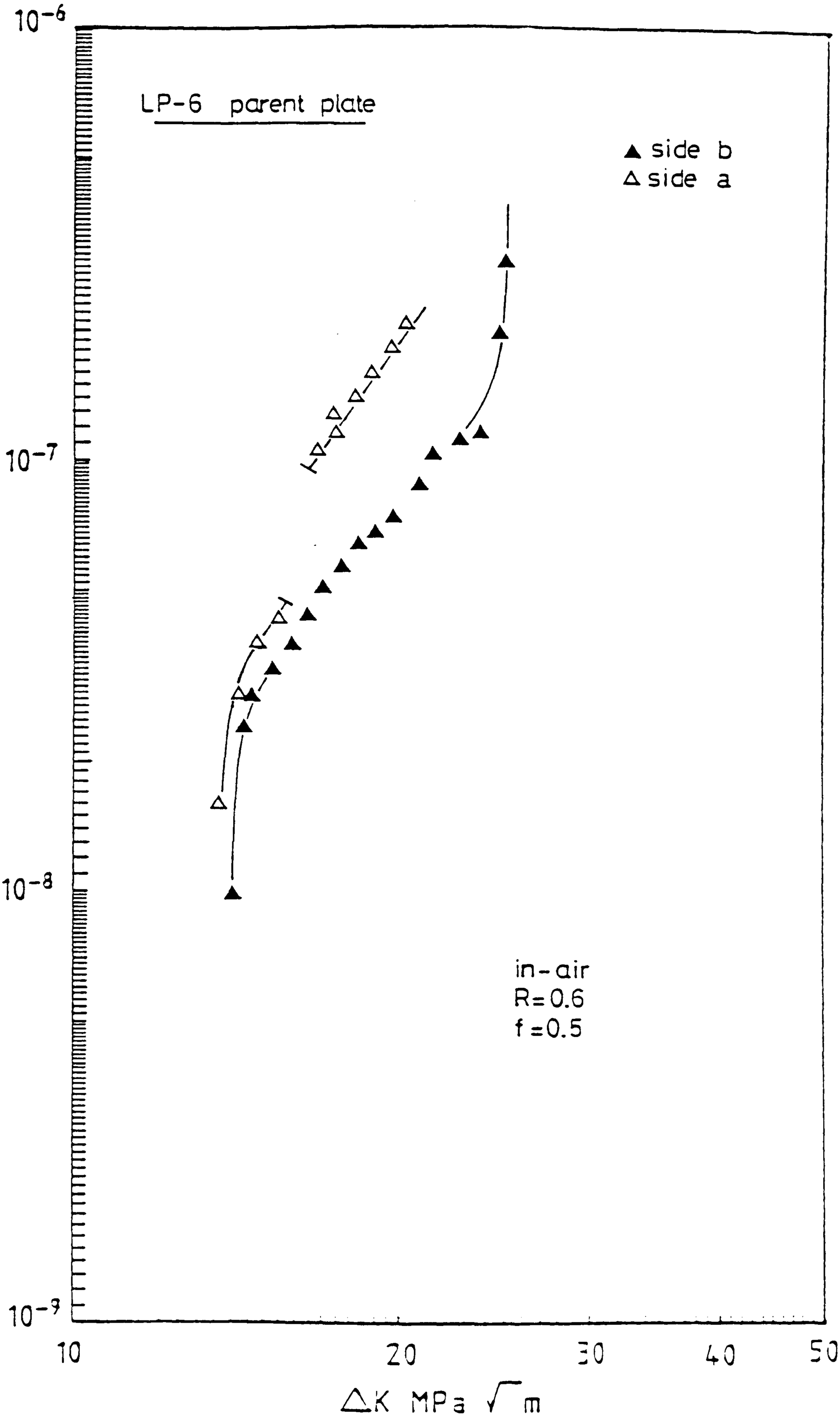

Figure 55. Parent plate in-air fatigue properties for line-pipe steel LP-6.

curves for BS 4360 grade 50D (Figure 56). The two structural steel curves have been extracted from separate sources (85, 87) and demonstrate the effect of loading ratio, R on the characteristic data curve. For a direct comparison it is more reasonable to use curve 'a' as an R value of 0.5 was used to generate this data. Figure 56 indicates that all the steels tested part from the delaminating linepipe steel exhibit superior fatigue properties to those of a structural steel conforming to BS 4360 grade 50D. However, below a ΔK of 14 $MPa\sqrt{m}$ the quenched and tempered steel BS 4360 grade 55F has a higher propagation rate but a lower sensitivity to ΔK. The least ΔK sensitive of all the steels tested was N-A-XTRA 70 which subsequently gave the lowest propagation rates at high ΔK. The steel most sensitive to ΔK was RQT 501. The two controlled rolled steels shown in Figure 56 have similar sensitivities to ΔK and produced growth rates intermediate to the wide range exhibited by the quenched and tempered steels.

As previously stated the results for N-A-XTRA 70 shown in Figure 50 indicated the presence of a fatigue propagation threshold. This was further investigated via a closely controlled stress intensity range step-down experiment the result of which can be seen in Figure 57. The curve is divided into two types of data points to indicate the technique used for crack length measurement. This more sensitive experimental technique indicated a threshold of 11 $MPa\sqrt{m}$ for N-A-XTRA 70 at a loading ratio of 0.6 compared to the value of 14 $MPa\sqrt{m}$ measured in the previous test.

The effect of loading ratio, R, as indicated in Figure 56 on structural steel has been investigated for N-A-ATRA 70. A constant amplitude fatigue test was conducted at a loading ratio R = 0.1 and with a frequency of 0.5 Hertz. N-A-XTRA 70 was chosen for this investigation

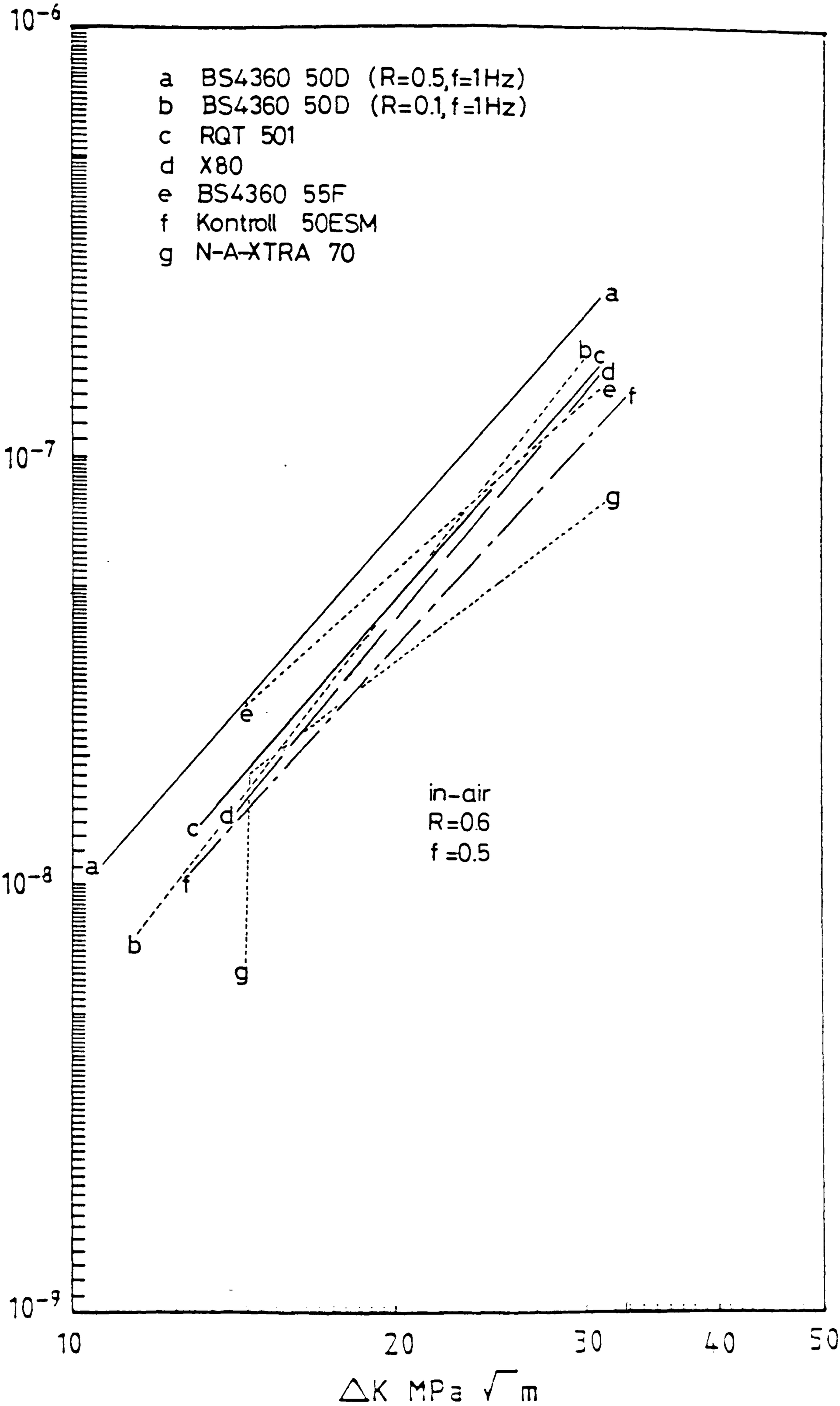

Figure 56 Comparison of HSLA steel fatigue performance with structural steel conforming to BS 4360 grade 50D.

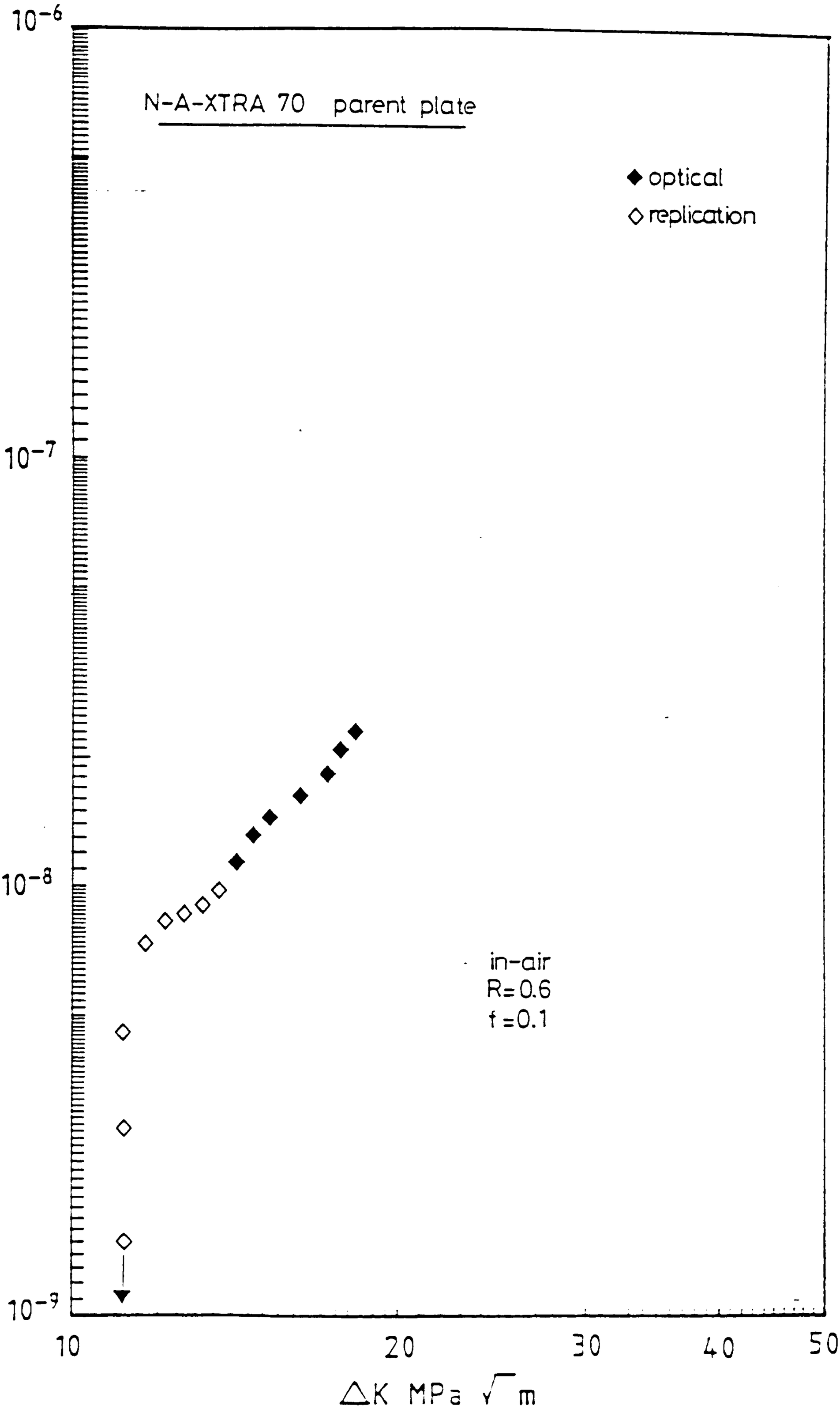

Figure 57. Closely controlled ΔK step-down experiment showing threshold for N-A-XTRA 70.

because of its thresholding characteristics which might have changed under the lower stress ratio loading cycle. The result is shown in Figure 58 and indicates a slight reduction in the threshold ΔK value to 13 MPa $\sqrt{m}$ when compared to the constant amplitude test conducted at R = 0.6. The sensitivity of the steel to ΔK has increased slightly as a result of the lower stress ratio with, however, a reduction in propagation rates at stress intensity ranges below 25 MPa $\sqrt{m}$.

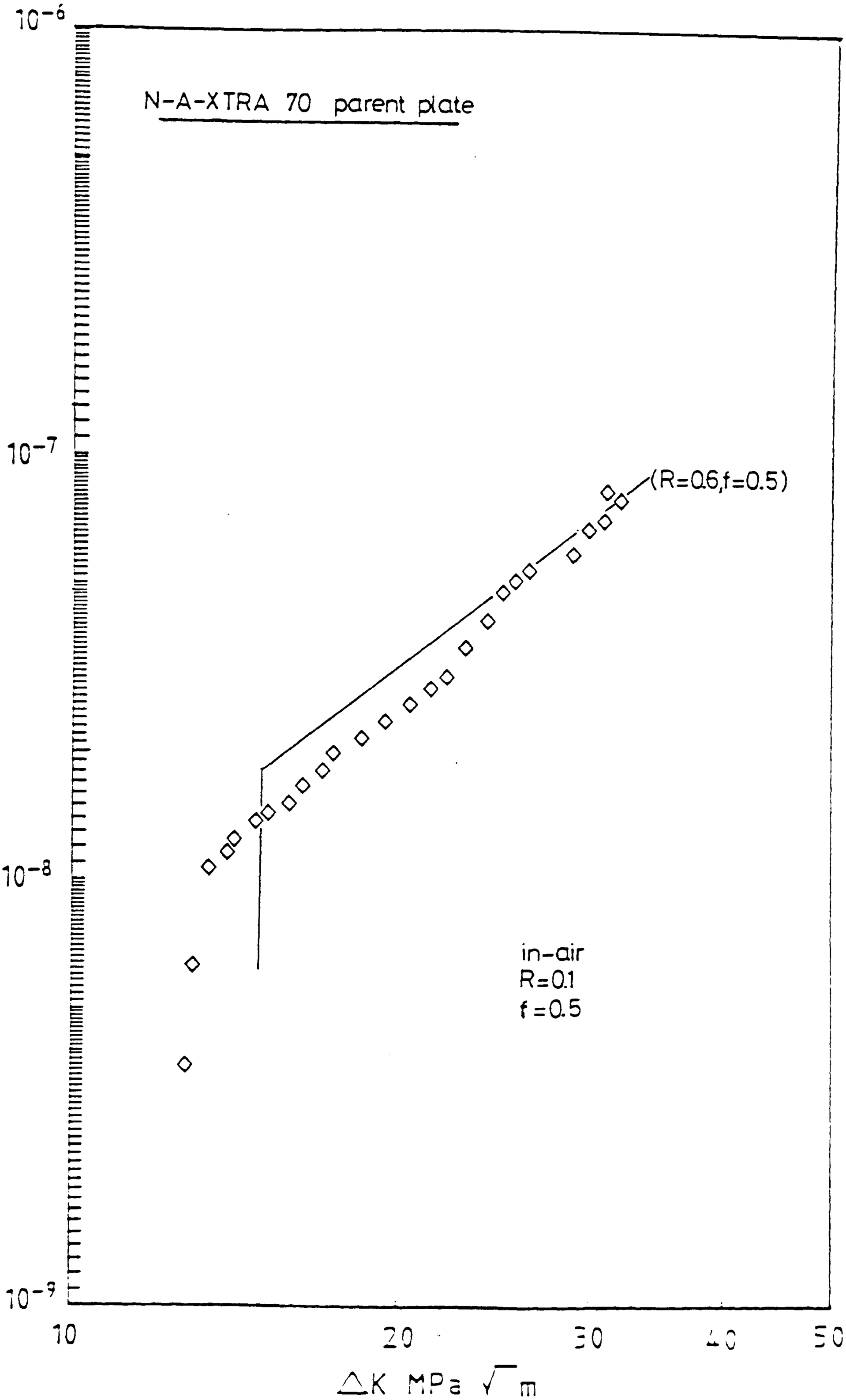

Figure 58. Effect of load ratio on the fatigue properties of N-A-XTRA 70.

5.3. Heat Affected Zone Fatigue Test Data

Initial HAZ fatigue crack propagation tests were carried out on N-A-XTRA 70. The intention was to grow the fatigue crack 0.5mm from the fusion line and within the HAZ. This would ensure that the crack propagated in a microsturcture exhibiting a coarse grain structure. The results shown in Figure 59 indicate a wide variation in sensitivity to stress intensity range and variation in growth rates at constant stress intensity range. Subsequent examination to ascertain the reason for these variations revealed inaccurate notch positioning. The curve labelled number one which exhibited the greatest sensitivity to stress intensity range and highest growth rates represents a sample in which the notch was positioned on the weld metal side of the fusion line. Samples two and three have fallen on a single curve and represent the intended correct notch position. In sample four which showed a lower sensitivity to ΔK the crack had grown in an intermediate HAZ microstructure. This microstructure showing a higher growth rate at lower ΔK values. Sample five had the notch positioned on the edge of the HAZ in a microstructure close to that of the parent plate and has produced a curve which is more characteristic of the parent plate material. These results illustrate problems with this type of test procedure. Clearly consistant notch positioning is crucial if comparison between heat affected zones in different materials are to be made. On subsequent tests only samples with the correct notch position were tested. In the specimens used in the test it is extremely difficult to ensure a straight HAZ after the welding process and therefore although the specimens are etched to identify the correct notch position before machining it is possible for small errors to occur in notch positioning. All samples must be carefully examined following fatigue testing to ensure that the correct microsturctural features have been involved in the fatigue crack propagation process.

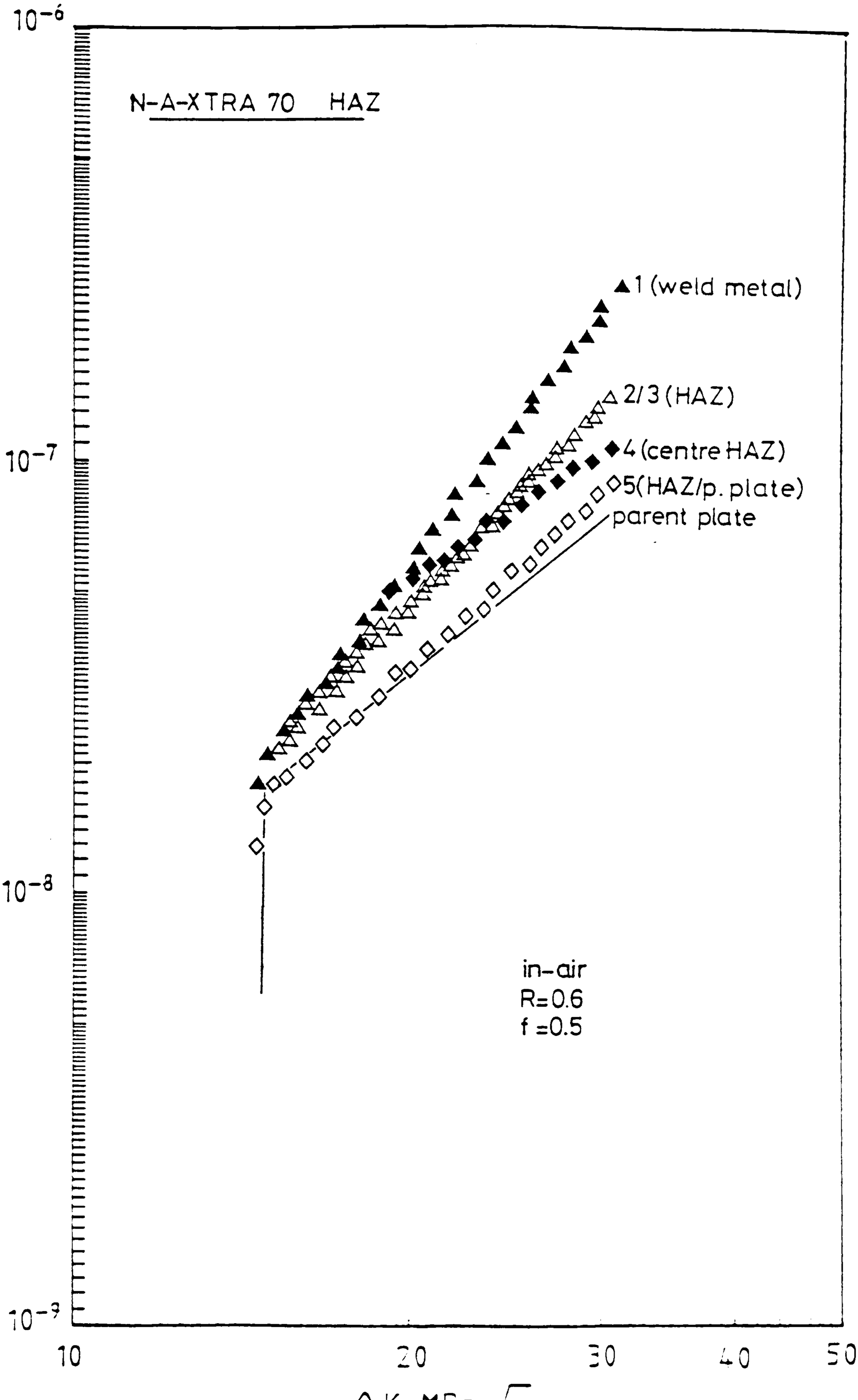

Figure 59 HAZ fatigue data for N-A-XTRA 70 illustrating effect of notch position.

Figure 60 shows the results for two welded samples of Kontroll 50 ESM. Clearly this was an unexpected result which shows a crack propagation mechanism independant of the stress intensity range up to a value of 18 to 20 MPa $\sqrt{m}$. Above this ΔK value the crack propagation rate becomes extremely sensitive to the loading environment. Clearly the microstructure produced in welding is extremely sensitive to the environment. This result is further investigated in the metallography section.

The heat affected zone results for RQT 501, Figure 61, show very little deterioration in terms of fatigue performance over that exhibited by the parent plate. The sensitivity to ΔK has not been affected, however this material did have the highest sensitivity among the parent plates tested.

BS 4360 grade 55F has shown a deterioration in fatigue resistance after welding, Figure 62, with a slight reduction in sensitivity to ΔK.

A similar small reduction in fatigue resistance is exhibited by the controlled rolled steel X80 line-pipe, Figure 63, without however any change in sensitivity to ΔK.

Again for the purpose of comparison a linear regression analysis for each material has been plotted on a single diagram together with published structural steel data, Figure 64. This is a comparison between welded HSLA steels and non-welded structural steel. Three of the HSLA steels compare favourably in these circumstances. the curve for the quenched and tempered BS 4360 grade 55F does show high crack propagation rates at ΔK values below 25 MPa $\sqrt{m}$ but with significantly lower sensitivity to ΔK. Linepipe material LP6 has not been tested in this condition as the previously encountered phenomenom of delamination renders this material unsuitable for offshore structure fabrication.

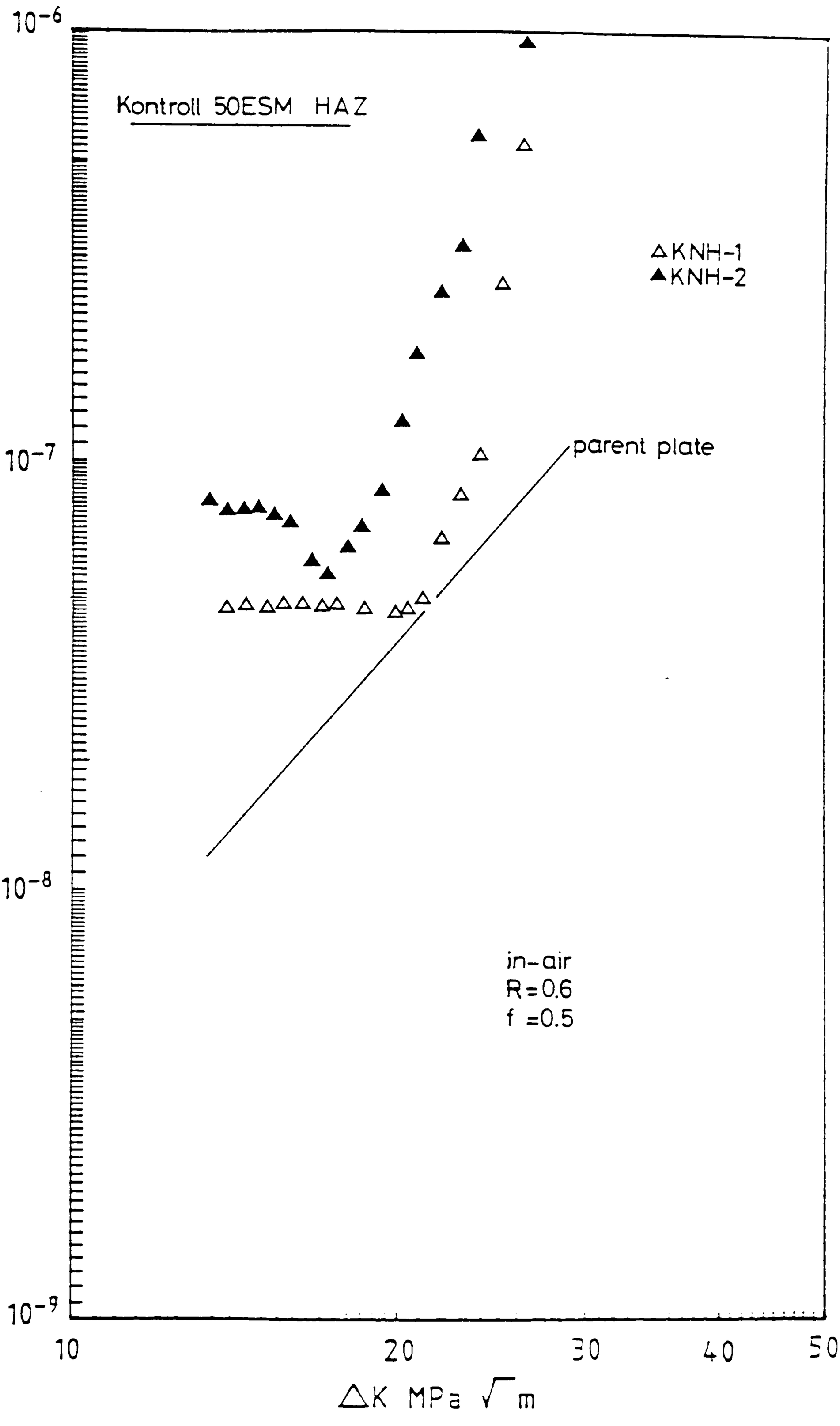

Figure 60, HAZ fatigue data for Kontroll 50 ESM.

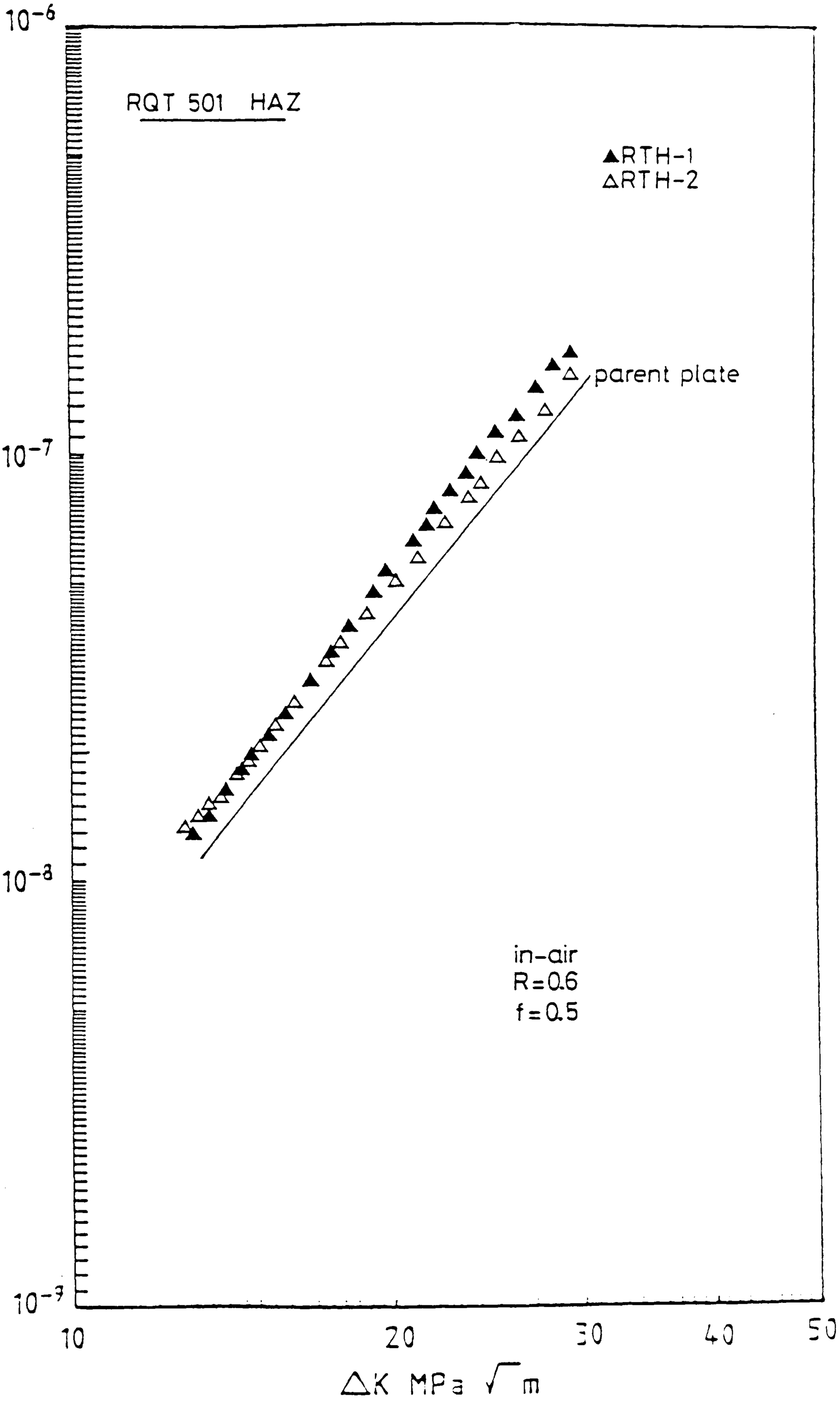

Figure 61, HAZ fatigue data for RQT 501.

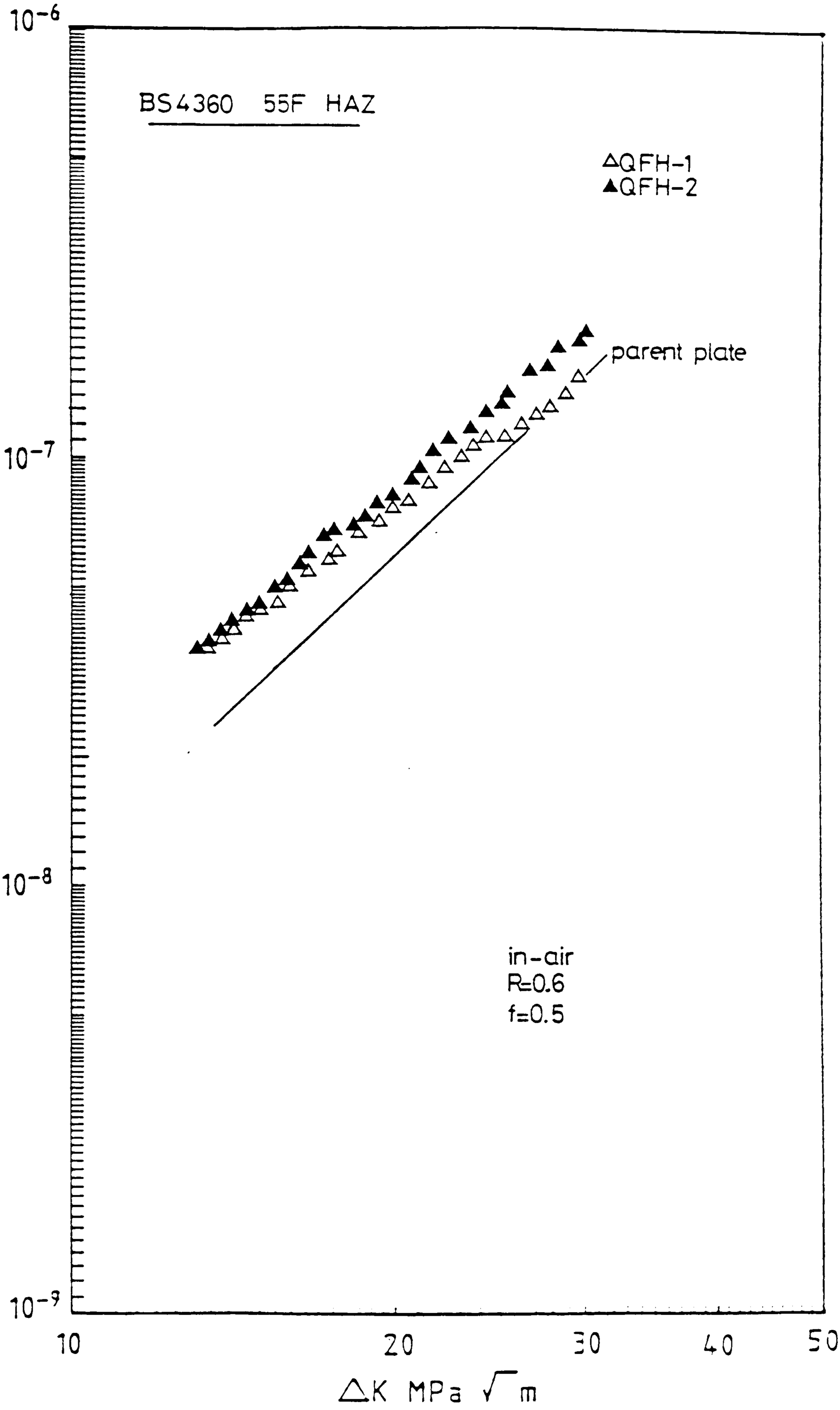

Figure 62, HAZ fatigue data for BS 4360 grade 55F.

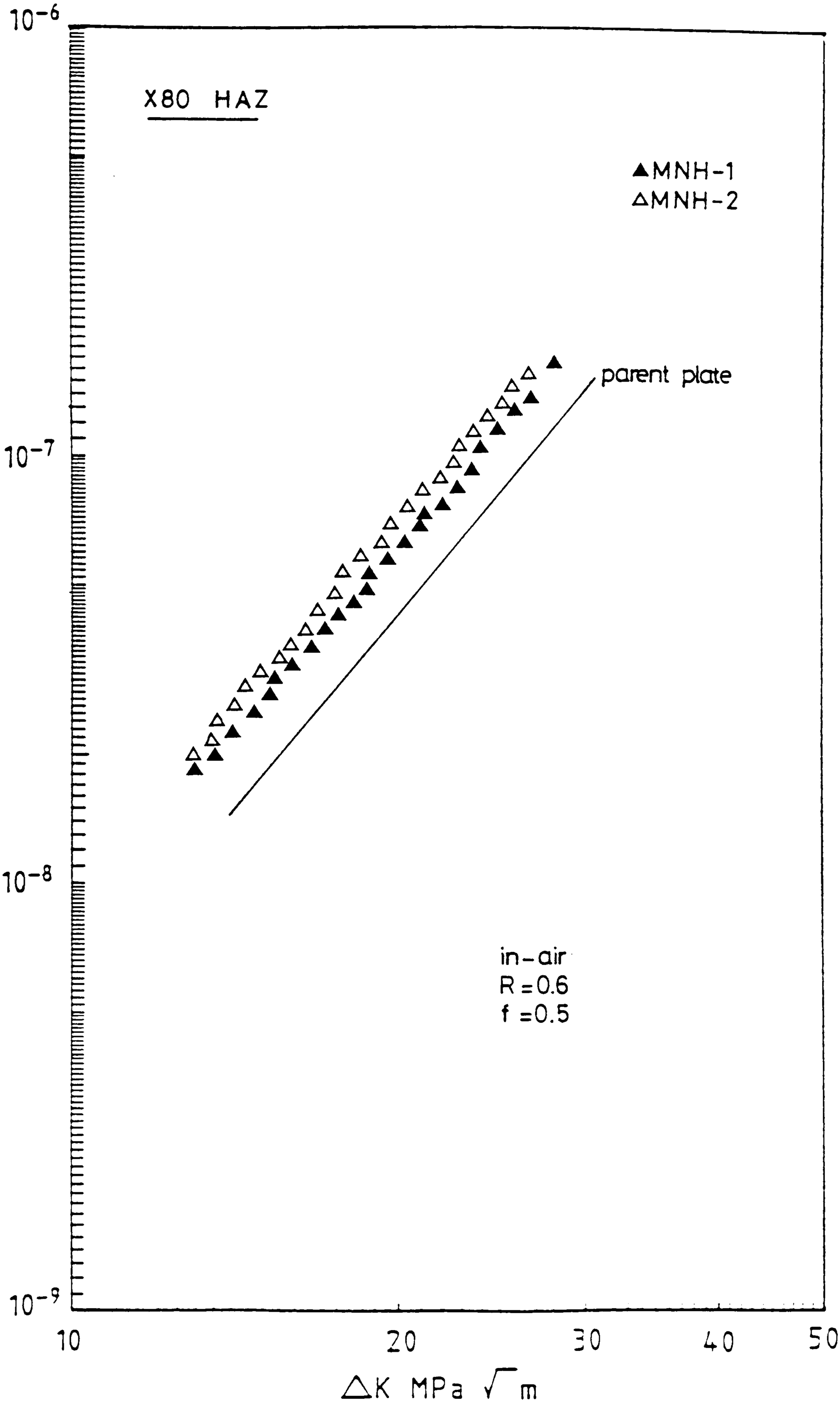

Figure 63. HAZ fatigue data for X80 line-pipe.

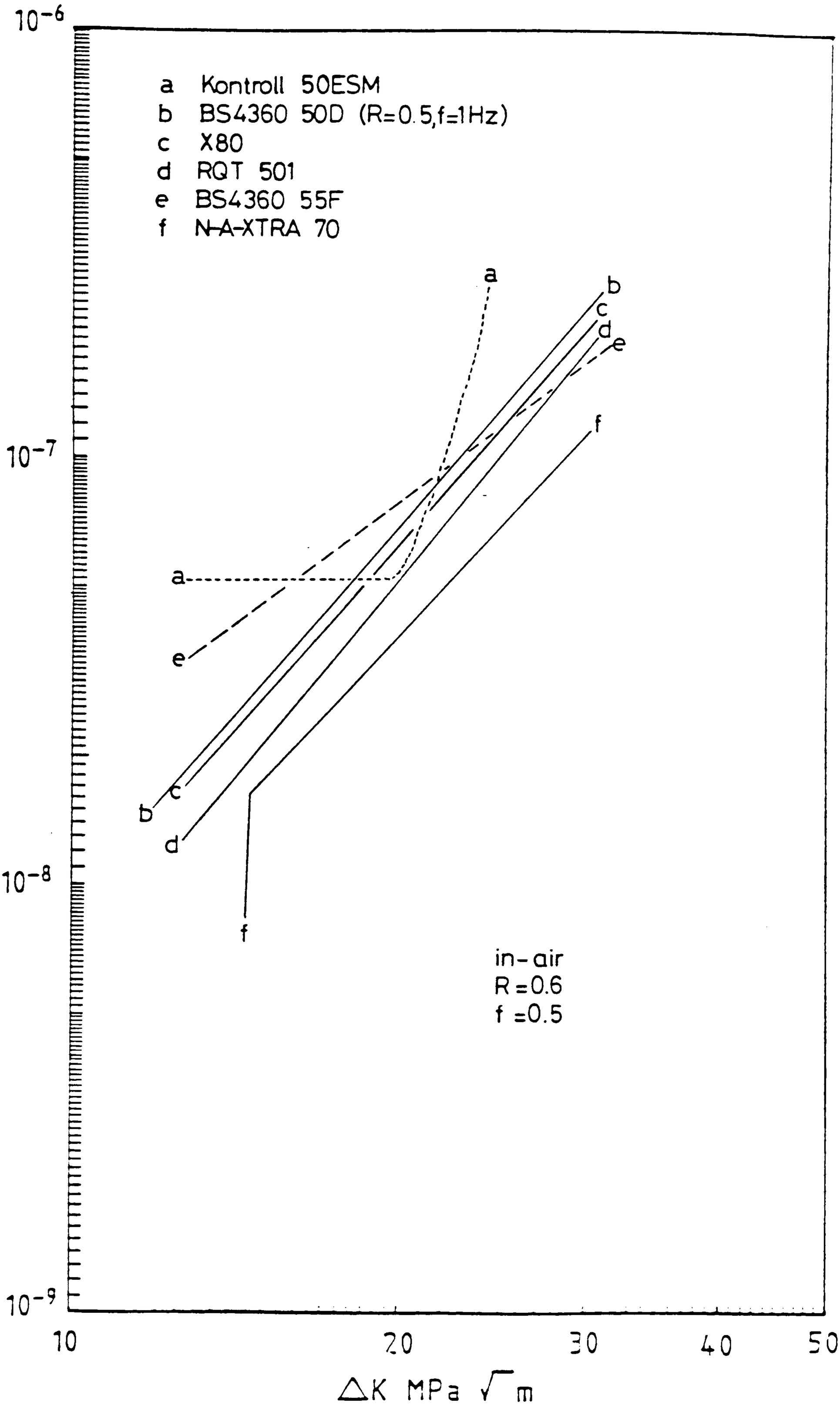

Figure 64 Comparison of HSLA HAZ fatigue performance with parent plate structural steel.

5.4. Corrosion Fatigue Test Data

Corrosion fatigue tests were limited to two steels due to the amount of testing involved. The steels chosen, one reflecting each process technique, were BS 4360 grade 55F (quenched and tempered) and Mannesmann X80 linepipe (controlled rolled). Each steel was tested in three conditions, freely corroding, correctly cathodically protected (-810mV) and overprotected (-1050mV). The results of these experiments are shown in Figures 65 and 66.

Figure 65 shows the results for BS 4360 grade 55F together with the linear regression analysis curve for the in-air results. The correctly protected samples show only a slight reduction in fatigue properties over the average in-air result indicating an effective cathodic protection system and a favourable response to this by the material. The free corroding samples have exhibited a much greater sensitivity to ΔK. Below a stress intensity range of 23 MPa $\sqrt{m}$ the free corroding sample has a greater fatigue resistance however above this value the fatigue resistance has been reduced. It was observed that an excessive build up of corrosion products occured on the fracture surface and it was felt that this was sufficient to delay the crack growth via a crack closure inhibition mechanism. At high stress intensity however, the crack growth per cycle was sufficient to overcome this phenomenon and crack growth was accelerated by the aggressive environment. The curves produced by samples in the overprotected conditions reflect a mechanism dominated by the environment and in fact largely independent of stress intensity range up to a value of 25 MPa $\sqrt{m}$ above which the crack growth approximately follows the freely Corroding trend.

Mannesmann X80 linepipe corrosion fatigue data is shown in Figure 66. Again the correctly protected sample is only slightly worse than the in-air test with similar

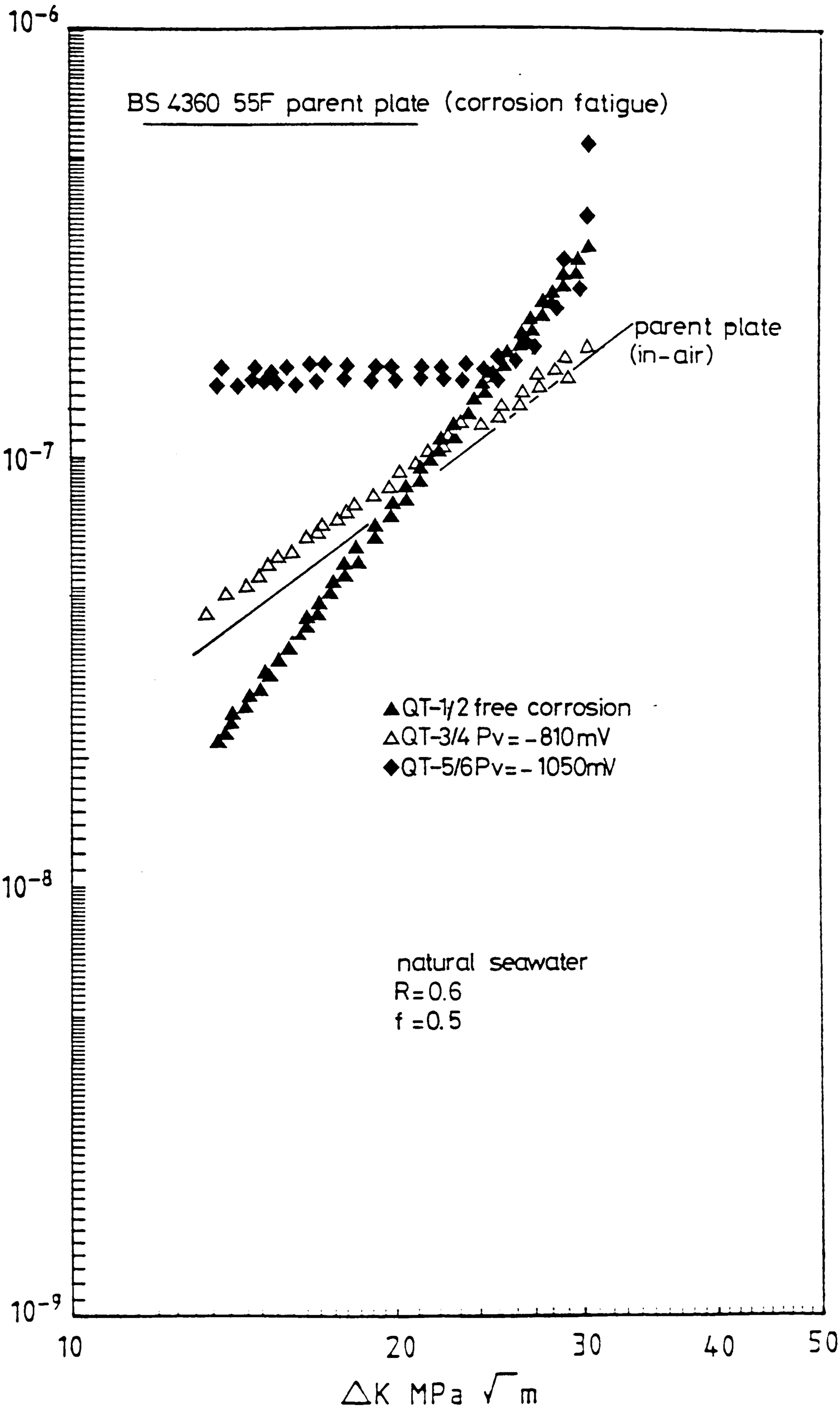

Figure 65. Corrosion fatigue data for the quenched and tempered steel BS 4360 grade 55F.

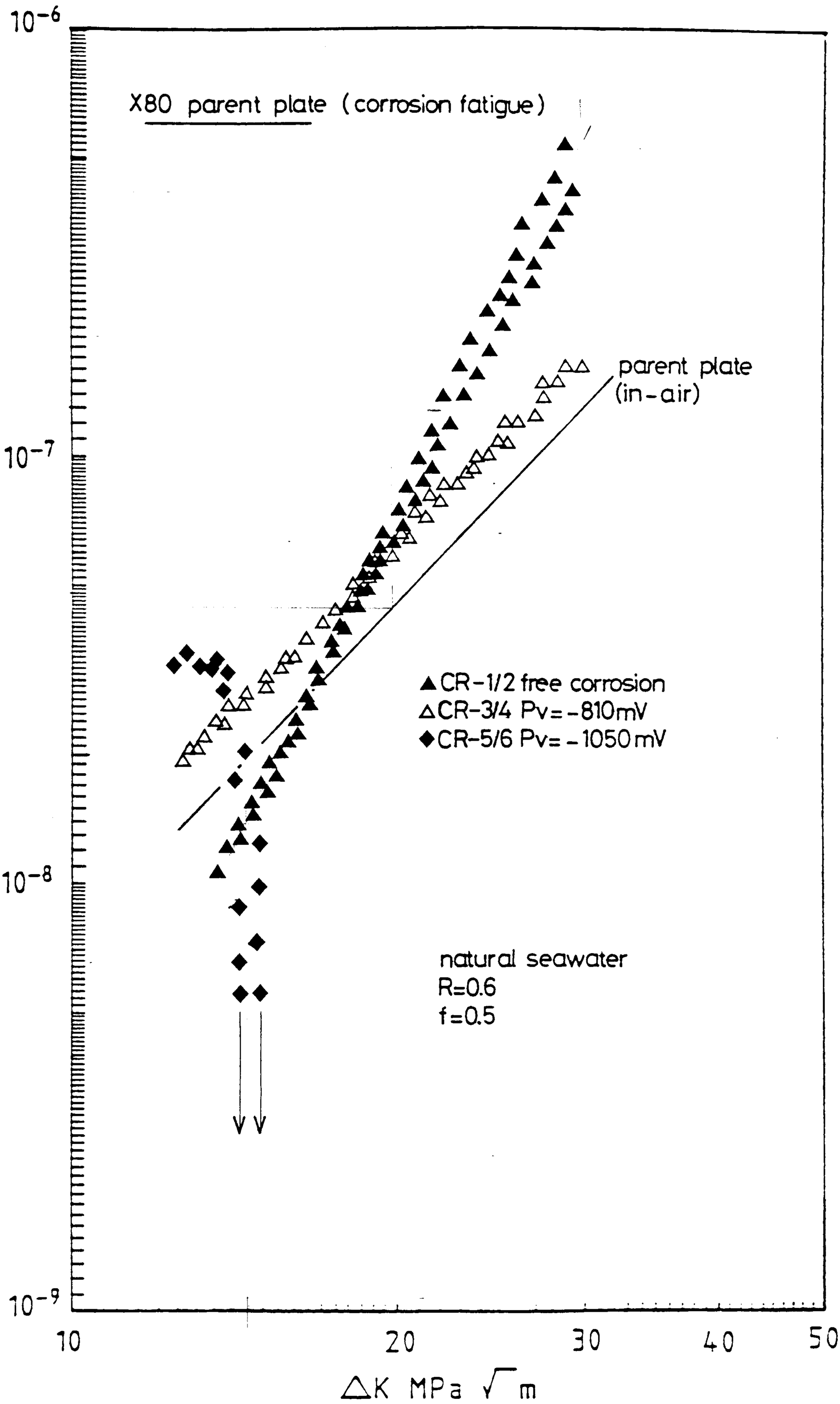

Figures 66 Corrosion fatigue data for the controlled rolled steel X80 line-pipe.

sensitivity to ΔK. the freely corroding sample shows the same trend as seen for BS 4360 grade 55F with the cross over between lower propagation rates at a stress intensity of 21 MPa $\sqrt{m}$. However the results for the overprotected samples were in complete contrast. Initially the propagation rate was higher than that for the correctly protected sample but almost immediatly a thresholding phenomena occured in the form of a complete crack arrest. It was noted that a large amount of calcareous deposit had formed in the crack and this was preventing the crack from closing at minimum load. After arrest had occured the minimum load was reduced to give a stress ratio of 0.1 but this made no difference to the amount of crack closure on unloading. This result is further investigated and explained in the metallography section.

In Figure 67 a comparison between BS 4360 grade 50D (86) tested in a similar manner and environment to the linear regression analysis curves for the correctly protected HSLA steels is made. Correctly protected X80 has a similar ΔK sensitivety to that shown by the structure steel but at much lower propagation rates for any given ΔK value. BS 4360 grade 55F displays a lower sensitivity to ΔK but crack growth rates intermediate to the two steels. It should be noted that the structural steel has shown very limited benefit in terms of fatigue crack propagation from cathodic protection and a similar detrimental effect of overprotection to that shown by the quenched and tempered steel BS 4360 grade 55F.

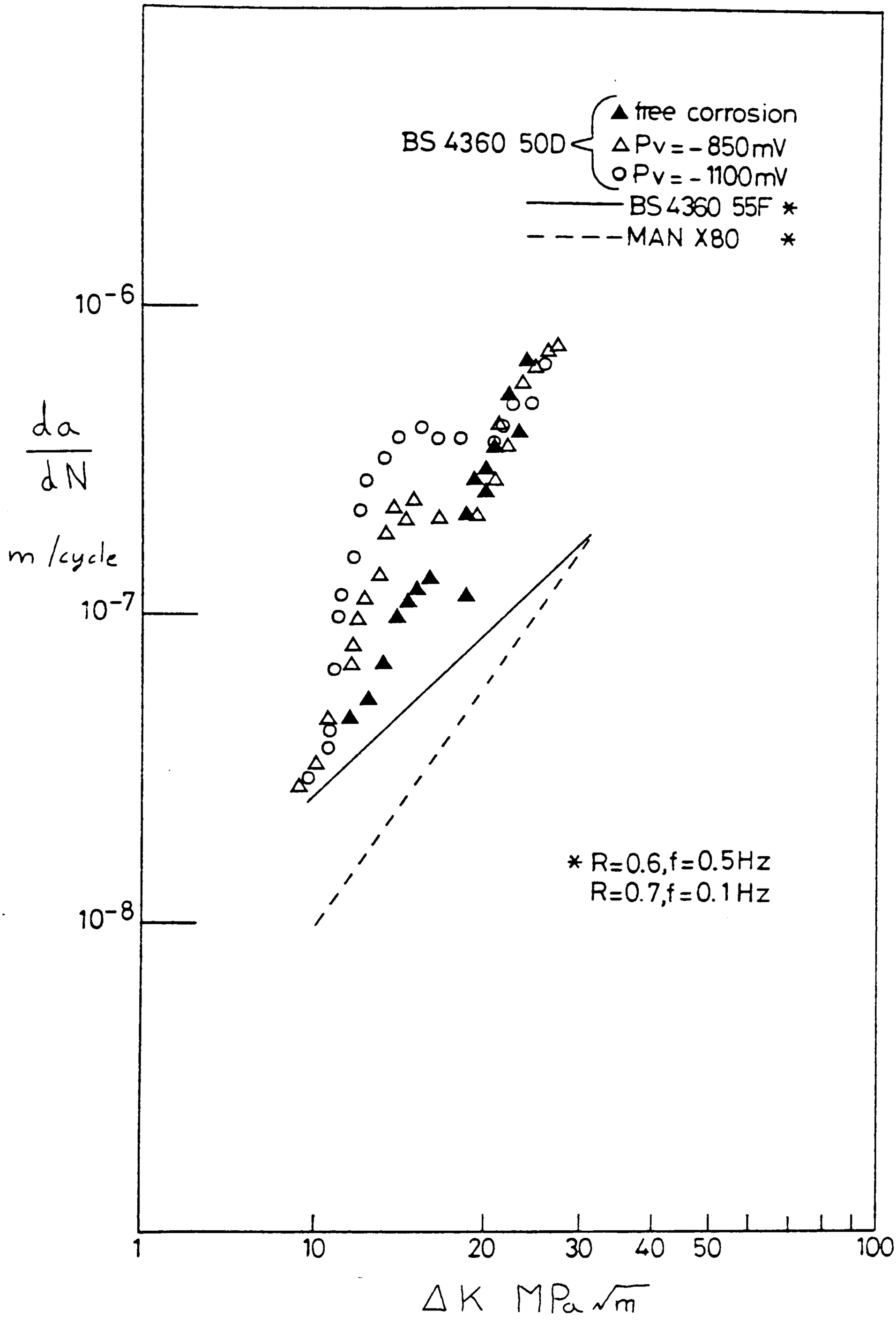

Figure 67. A comparison between correctly protected HSLA steels and three levels of protection for a structural steel.

5.5. Constant Stress Intensity Range Fatigue Test Data

The fatigue crack has been grown through a range of microsturctures which were produced by a single pass bead on plate weld. The relative position of subsequent diagrams to the microstructural gradient is shown schematically in Figure 68. Due to the large amount of data generated by this continuous test the results have been presented in five Figures, numbered 69 to 73.

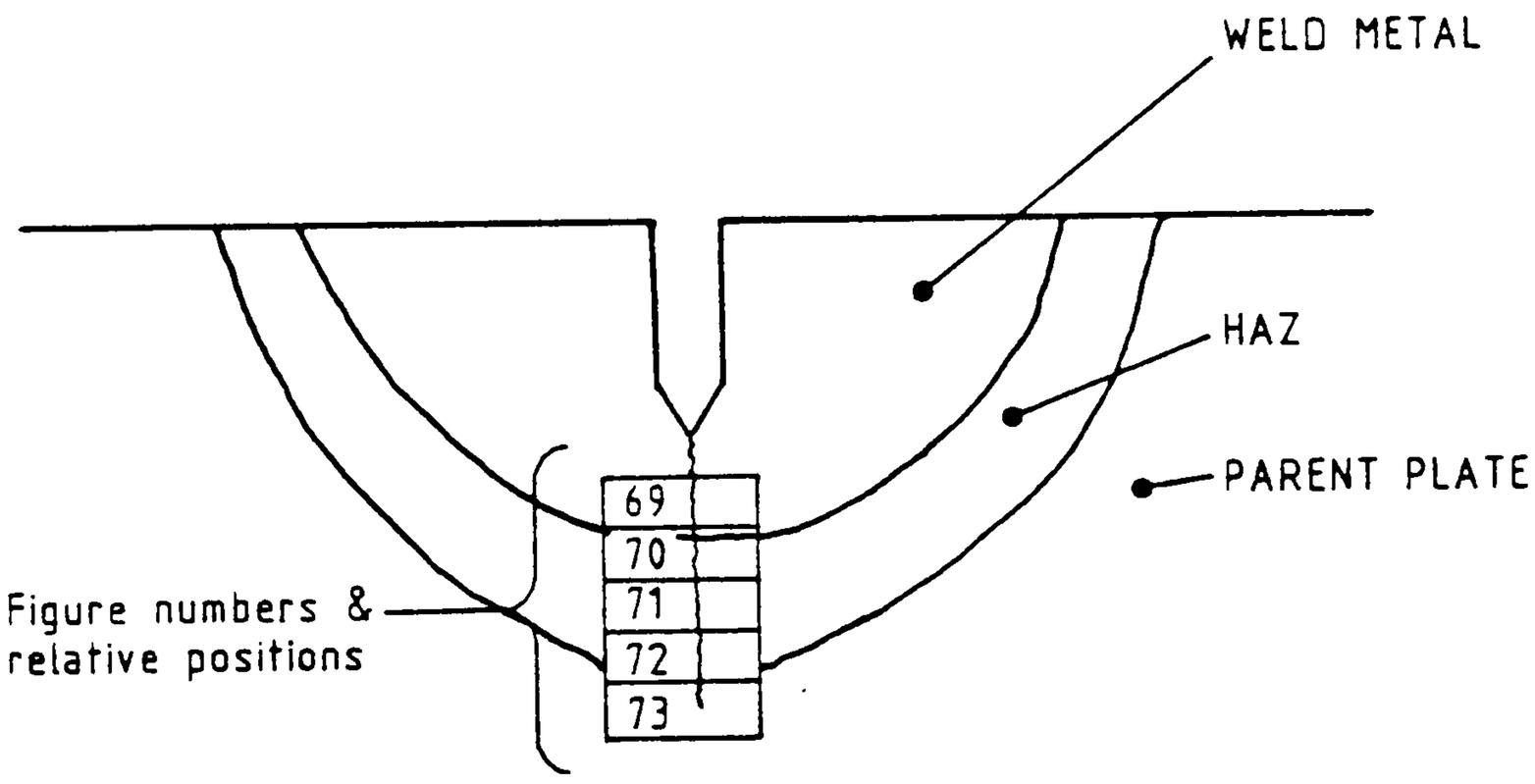

Figure 68 Relative position of Figures 69-73 to the microstructural gradient

The Figures are labelled as follows:-

Figure 69 Weld metal
Figure 70 Fusion boundary/coarse HAZ
Figure 71 Mid HAZ region
Figure 72 Fine HAZ region
Figure 73 Parent plate.

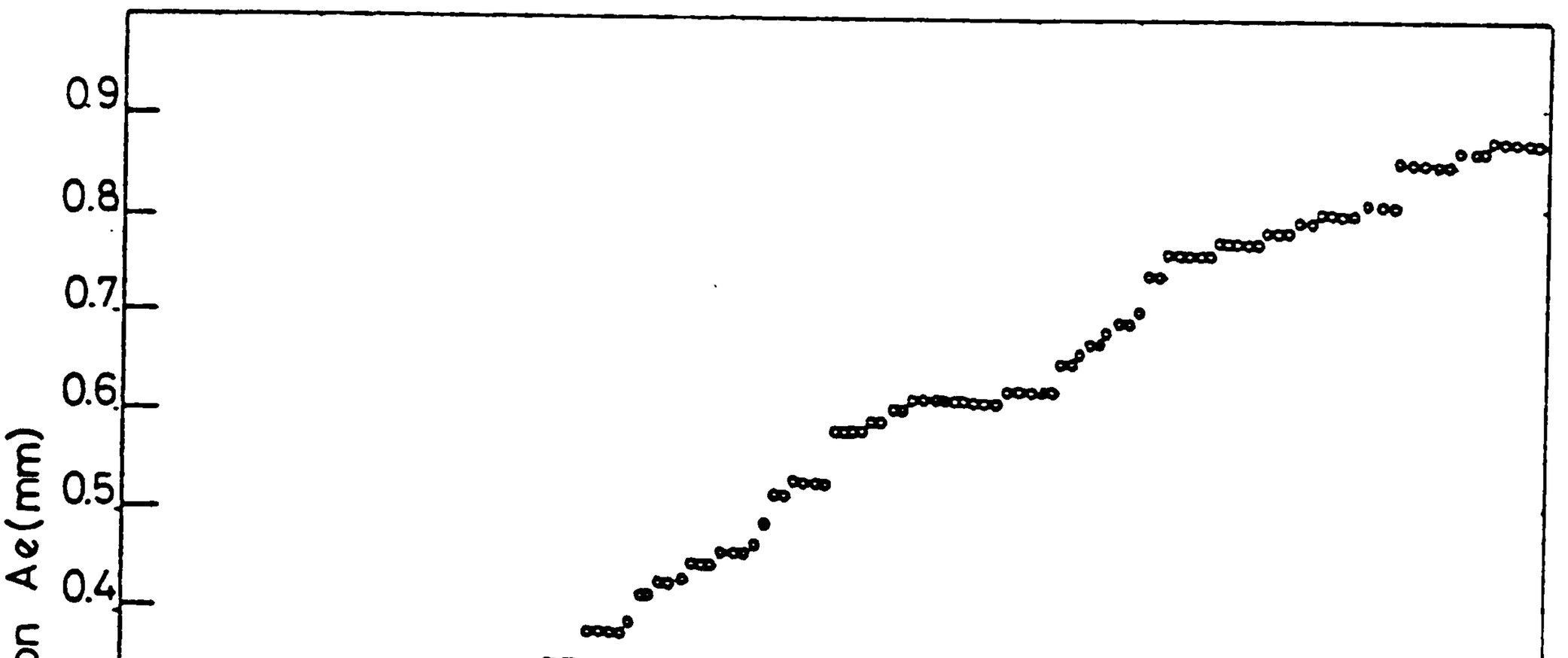

Figure 69 Constant ΔK, weld metal.

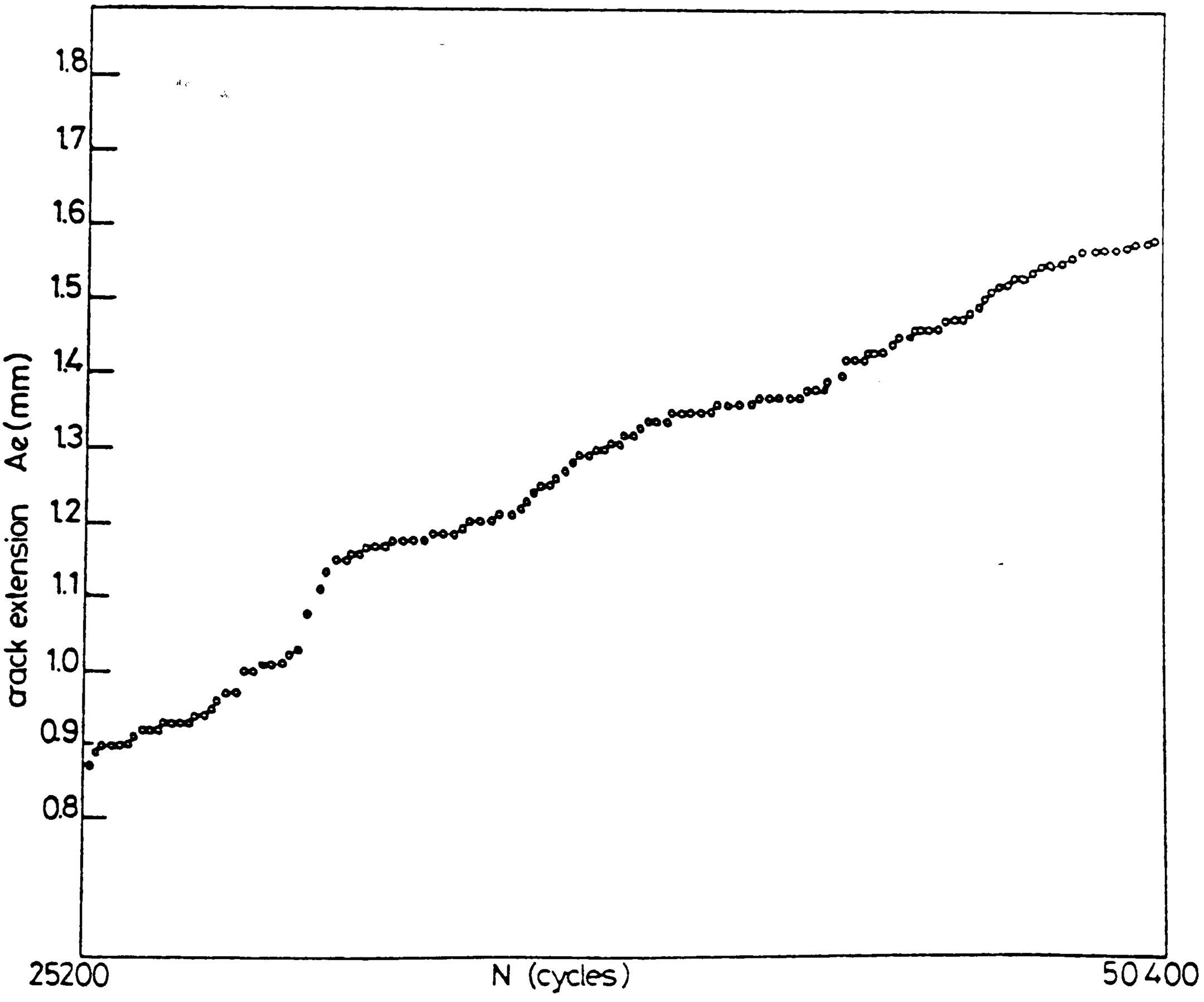

Figure 70 Constant ΔK, fusion boundary/coarse HAZ.

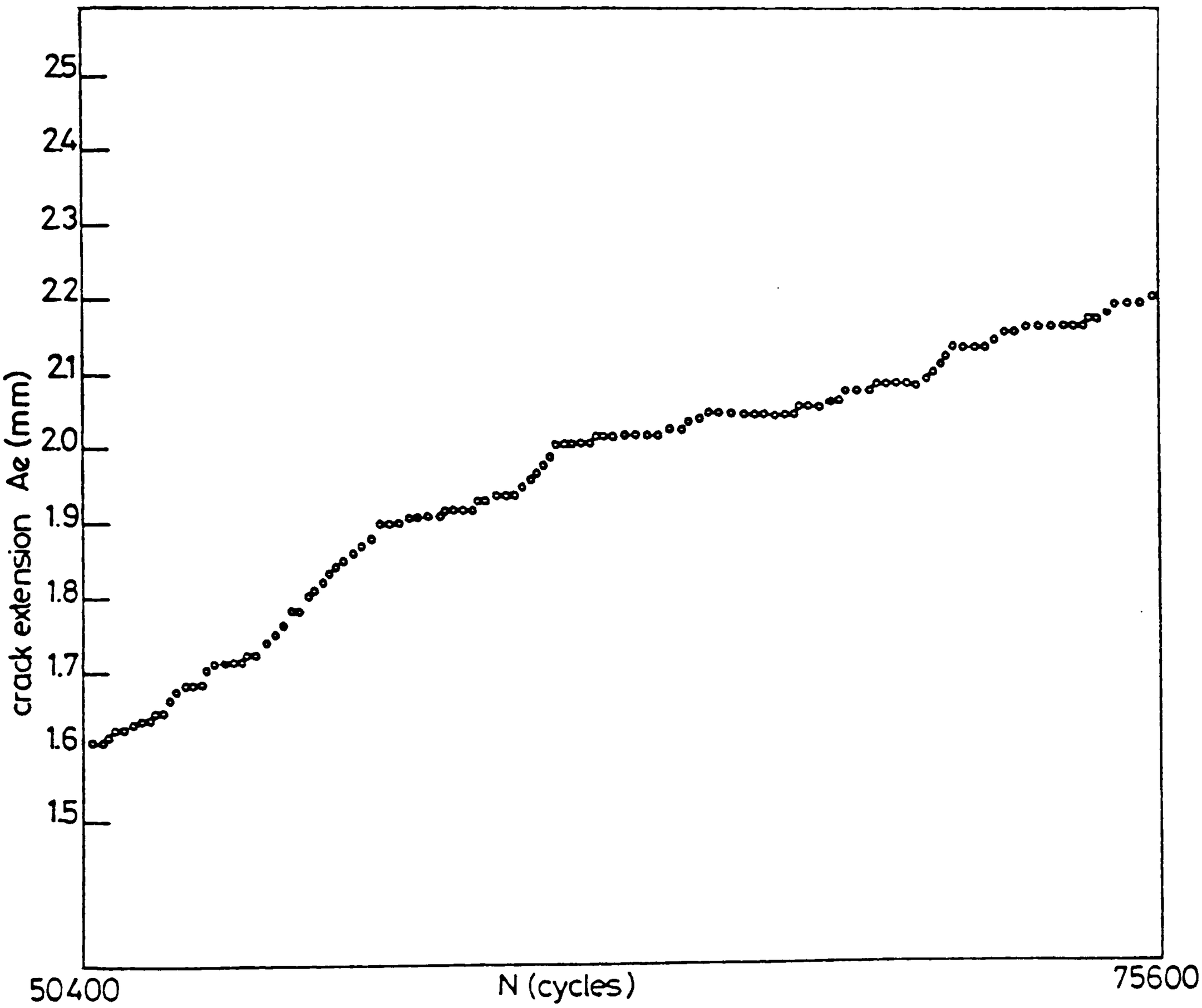

Figure 71 Constant ΔK, mid HAZ region.

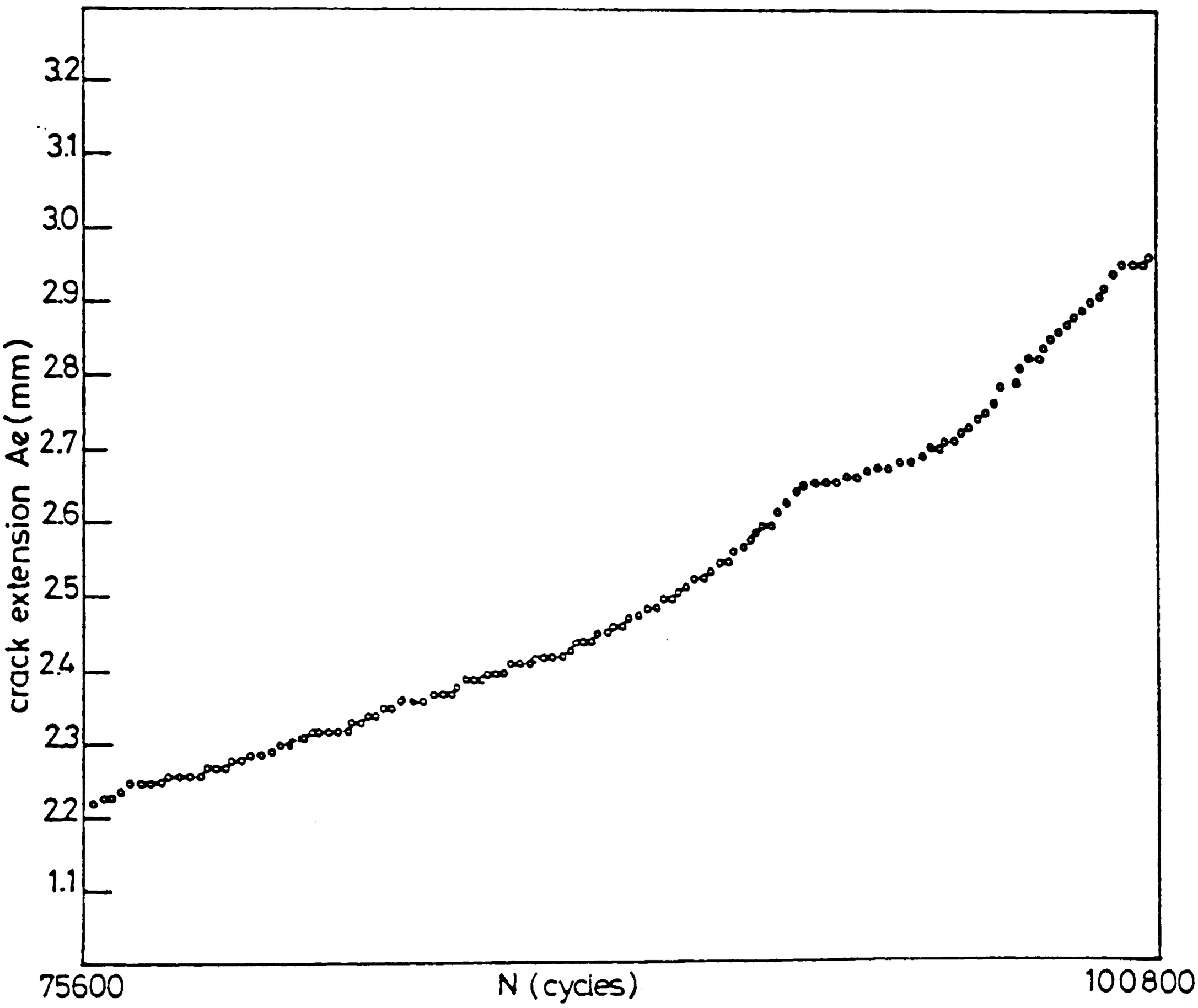

Figure 72 Constant ΔK, fine HAZ region.

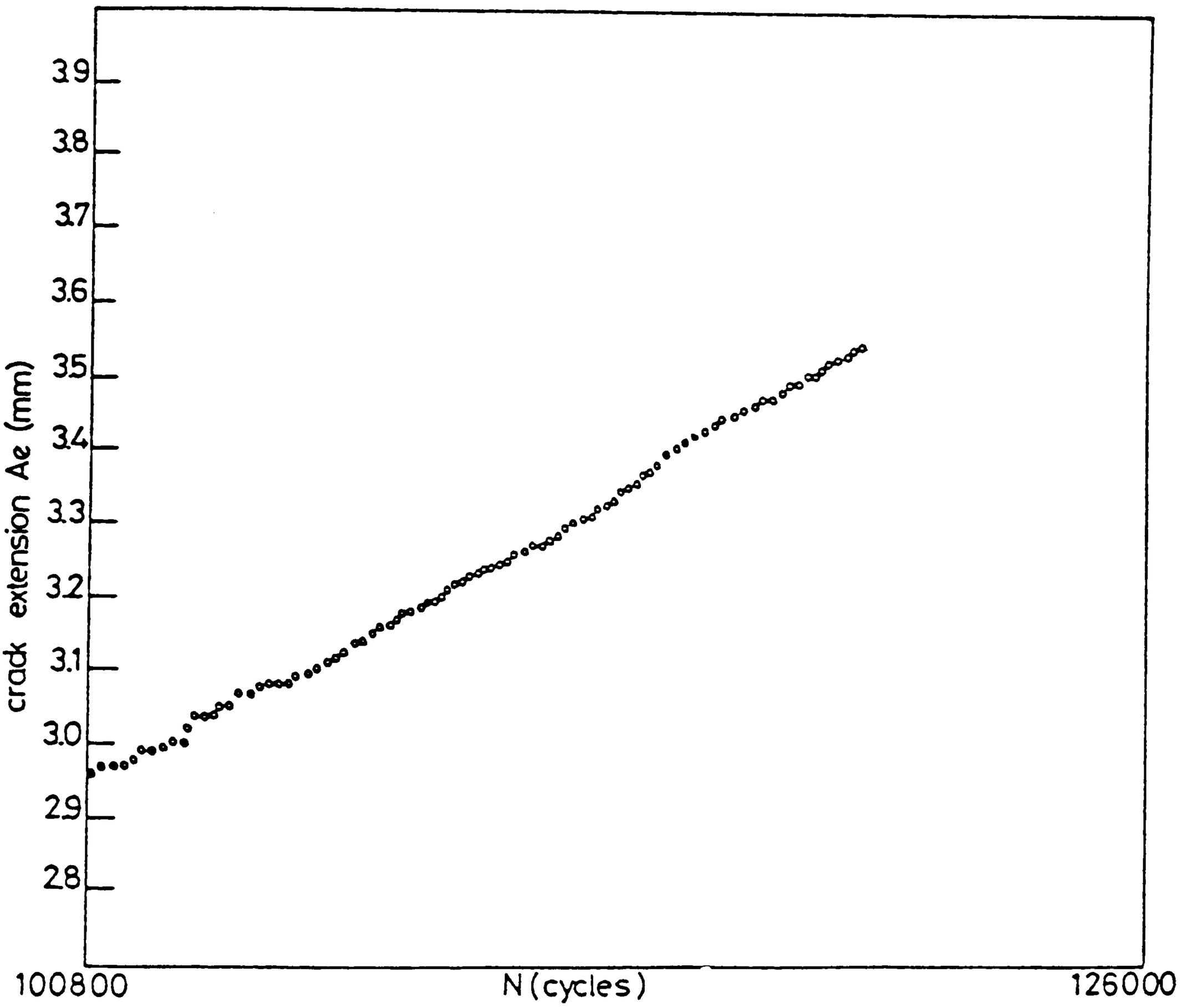

Figure 73 Constant ΔK, parent plate.

The average fatigue crack propagation rate observed in the weld metal was 3.6×10^{-8} m/cycle. However, it can be seen in Figure 69 that the crack propagation is of a discontinuous nature with areas of propagation rates as low as 1.1×10^{-8} and areas of accelerated growth exceeding 2.7×10^{-7} m/cycle. The fusion boundary is clearly marked by an increase in fatigue crack propagation rate over a 0.1mm length of microstructure. The accelerated growth was of the order of 2.4×10^{-7} m/cycle and occured over a two hour period (720 cycles). The accelerated growth was followed by more continuous growth in the relatively coarse HAZ with propagation rates alternating between 5.6×10^{-8} and 1.4×10^{-8} with an average for this region of 2.5×10^{-8} m/cycle. Figure 71 representing the mid HAZ region shows a similar alternating pattern of crack propagation rates. As the crack propagates into the fine HAZ region the fatigue crack propagation becomes more continuous with less variation in crack growth rate. The parent plate represented by Figure 73 shows a continuous nature with a growth rate of 3.2×10^{-8} m/cycle. Metallographic examination has shown changes in fatigue crack propagation mode which may explain the changes in fatigue crack propagation rate and characteristics with the microstructural gradient.

6.0. METALLOGRAPHY

The basis for a metallographic study into fatigue crack propagation is to determine the contributing factors within a microstructure which influence the nature and rate of fatigue crack propagation. Optical microscopy, electron microscopy and surface replication techniques have been applied to all the materials tested to examine the importance of microstructural features on fatigue crack propagation.

6.1. Fatigue in Parent Plate Microstructures

The six steels tested are considered individually in terms of fatigue crack profiles and fracture surface features.

6.1.1. Quenched and tempered steels

6.1.1.1. N-A-XTRA 70

A surface replication technique, as described in section 4.4.3., was developed for very accurate in situ crack length measurement. Replication was found to be a useful technique for studying microstructural influences on fatigue as an etched microstructure was also replicated by the cellulose acetate. For the purpose of studying a fatigue crack path in the quenched and tempered N-A-XTRA 70 microstructure a series of replicas were taken at fixed cyclic intervals. The time period for this study was four hours which corresponds to 7200 cycles at a frequency of 0.5Hz. Loading parameters included a stress ratio of R = 0.6 and a maximum static stress of 9.0kN. The results of this replication study are shown in Figure 74. The crack length at the time of the first replica was 14.28mm extending to 14.43mm in 7200 cycles. This corresponds to an average stress intensity range of 19MPa$\sqrt{m}$ and an average

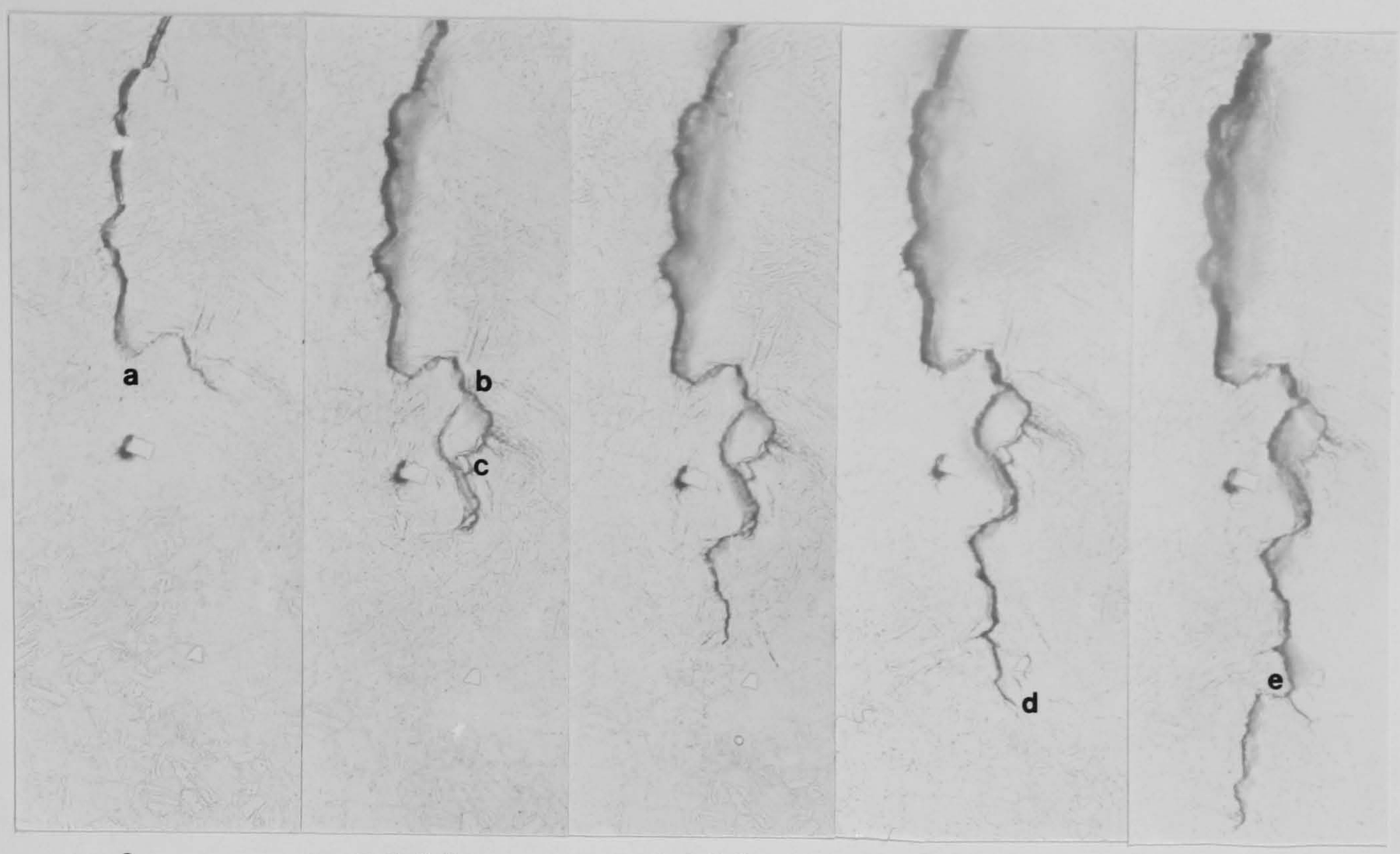

N =	0	1800	3600	5400	7200
	(i)	(ii)	(iii)	(iv)	(v)

Figure 74 Crack profiles as a function of time for N-A-XTRA 70, in-air with R = 0.6 and a frequency of 0.5Hz. (X200)

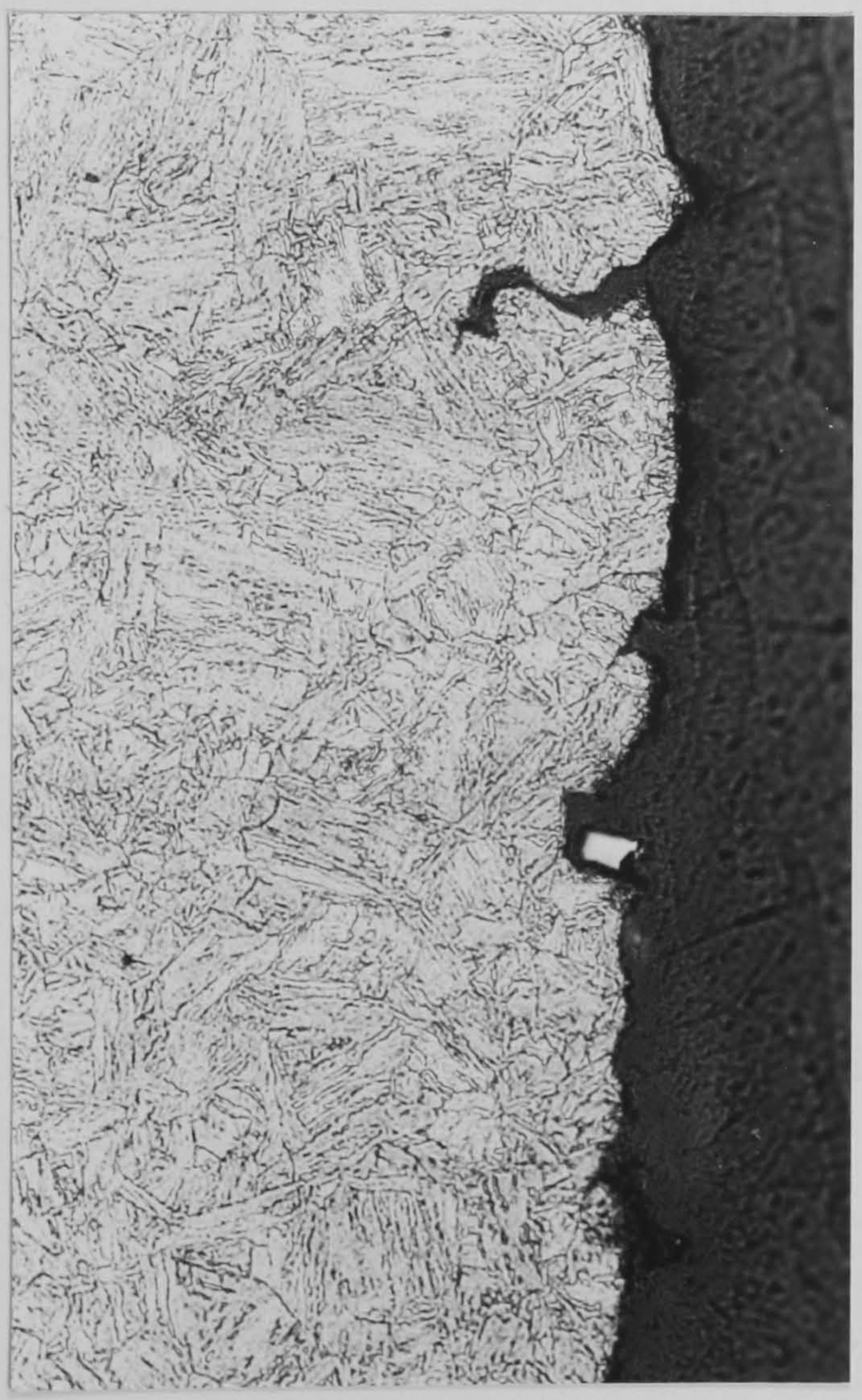

Figure 75

N-A-XTRA 70

Exposed cubic precipitate revealed by the fatigue crack propagation front. Note also the large secondary crack. (X400)

da/dN over the four hour period of 2.1×10^{-8}m/cycle. Thus, this series of photographs represent crack growth within the Paris region of this material occurring at relatively low values of stress intensity range.

From Figure 74 it can be seen that the path followed by the fatigue crack through the microstructure is far from planar. A high degree of crack deviation and secondary cracking is clearly evident and at point 'a' on Figure 74 (i) the crack actually appears to have doubled back upon itself approximately 0.02mm ahead of an inclusion. This phenomenon is certainly not 'real' but an effect caused by the representation of a complex three-dimensional crack in only two dimensions. The apparent 'V' shaped path of the crack resulted from the intersection of two branches of the crackfront in the surface plane of the specimen.

At point 'b' on Figure 74 (ii) the crack appears to have divided and followed two distinct paths to rejoin at point 'c' on the specimen surface. This further demonstrates the complexity of crack front shape and high degree of crack branching exhibited by this microstructure. Examination of the surface of the specimen does not always reveal the major propagating crack front as can be seen by comparing Figures 74 (iv) and 74 (v). Point 'd' on Figure 74 (iv) would appear to be the 'main crack' tip as it breaks the specimen surface at the moment when the replica was taken. However, inspection of Figure 74 (v) reveals this not to be the case. The crack has not propagated any further in the surface plane from point 'd', but instead appears to have propagated from a point further up the crack, labelled 'e' on Figure 74 (v). The complex multiplanar nature of a fatigue crack as it grows within this microstructure is clearly demonstrated by this technique.

The surface replication study has not indicated a favoured propagation route with respect to precipitate distribution for the fatigue crack. However, extensive examination of crack profiles relative to the sample surface and to parallel planes have indicated that this may be the case. Figure 75 clearly shows a second phase particle exposed on the fracture surface by the fatigue crack propagation route. Non dispersive X-ray analysis showed the precipitates to be Zirconium based. Such crack profiles also show evidence of large crack branches which were up to 50μm deep and had surface openings of 8μm.

General observation of the fracture surface revealed cubic second phase particles at all levels of ΔK and across the entire thickness of the fracture surface. As seen in Figure 76, the particles are basically intact on the fracture surface however many are severely cracked. To quantify the frequency of Zirconium precipitate occurance on the fracture surface it was decided to examine three regions of fatigue fracture surface each with an area of approximately $1mm^2$, one in a region of high ΔK, one at medium ΔK and one at low ΔK values. An area of approximately $1mm^2$ was examined at medium ΔK but close to the surface of the specimen. The micrometer adjustment on the SEM was used to measure the areas to be examined. Observations were made at 1K magnification allowing an area of 0.15mm x 0.15mm to be viewed at one time. A square scanning pattern was adopted to cover 49 squares making a total area of $1.1025mm^2$. Having examined the required areas of fatigue fracture surface, the sample was mounted for metallographic examination. The fracture surface was ground off and polished to reveal a plane parallel to the fracture surface; a distance of approximately 1mm further into the material. A precipitate count was carried out in corresponding areas to those examined on the fracture surface. Results indicated a significantly higher occurence of precipitates on the fatigue fracture surface, an increase

between 80% and 100% was observed for all areas (ie up to twice the number of precipitates have been observed on the fracture surface as on an equivalent polished plane parallel to the fracture surface). This result must however be quantified in terms of the actual surface area revealed by the propagation of a non planar fatigue crack. The actual surface area of the fatigue crack fracture face has been estimated at approximately 1.5 times the surface area of the equivalent flat plane. This still gives a significant increase in precipitate count per actual surface area of 20% to 33%. Although some of the exposed particles were cracked most were complete, of consistant size and stood proud of the fracture surface. Flat areas of steel corresponding to the inclusion size were observed on the fracture surface with a similar frequency of occurance to the precipitates. These observations indicate a debonding mechanism between the precipitate and the matrix material for fatigue crack propagation within this microstructure. This survey supports an inclusion favoured fatigue crack propagation route however the extent of the inclusion influence is not certain. Clearly the crack route determining properties of the precipitate are less effective in fatigue as they are in final fracture which is dominated by microvoid coalescence in this microstructure. A significant increase in precipitate count of 90% to 105% was observed on the final failure fracture surface. Figure 77 shows the intact nature of an inclusion seen in a ductile dimple within the region of microvoid coalesence. Despite the large difference in precipitate count between fatigue and final failure fracture surfaces it is felt that the increase in precipitate count of up to 50% per unit of actual surface area is significant and indicates a precipitate preferred propagation route in fatigue.

General observation of the fatigue fracture surface under a scanning electron microscope revealed a multiplanar fracture surface with a high occurance of crack

branching. Figure 78 represents the fatigue fracture surface and shows many large open secondary cracks (up to 2.5μm) together with much smaller and less open cracks. In this Figure the crack has propagated from left to right with an average ΔK of 22Mpa$\sqrt{m}$. The non-planar nature of the crack on a macro scale is clearly illustrated at this lower magnification. Scanning electron microscopy was used to establish whether or not the degree of crack branching varies across the thickness (B dimension, Figure 26) of the fatigue fracture surface and/or the width (W dimension, Figure 26). It was found that the fatigue fracture surface was very irregular and showed a high occurance of crack branching across its entire surface. Figure 76 illustrates the occurance of both wide and narrow crack branches at all values of ΔK. Whilst the occurance of crack branching was consistant at all values of ΔK, a greater number were of the wide open nature at higher ΔK values. It was not possible to detect any variation in crack branch occurrence across the thickness of the sample at constant ΔK. The formation of a crack branch is clearly illustrated in Figure 74 (v). At point 'e' a branch has occured which has failed to propagate beyond a length of 20μm at the sample surface. This branch is extremely narrow at this point in the fatigue test but due to its reasonable size is likely to open up as the main crack becomes longer. Shorter crack branches which can also be seen on Figure 74 (v) are less likely to open up and will form the fine crack branches observed on the fracture surface. Both fine and open branches found on the fatigue fracture surface of this material are of a similar nature and will be termed secondary cracking for the purpose of discussion.

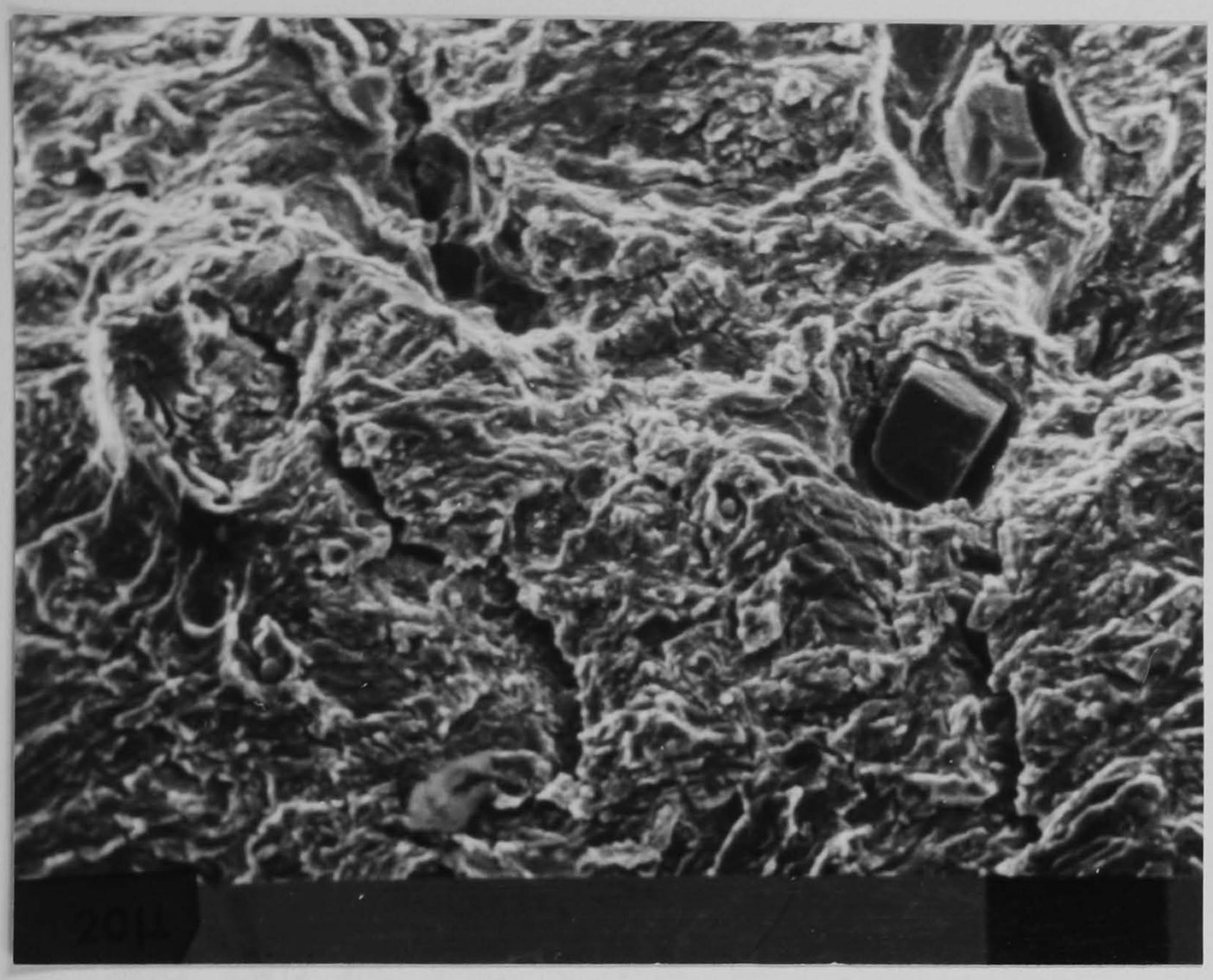

Figure 76

In-tact Zirconium based precipitate on the fracture surface

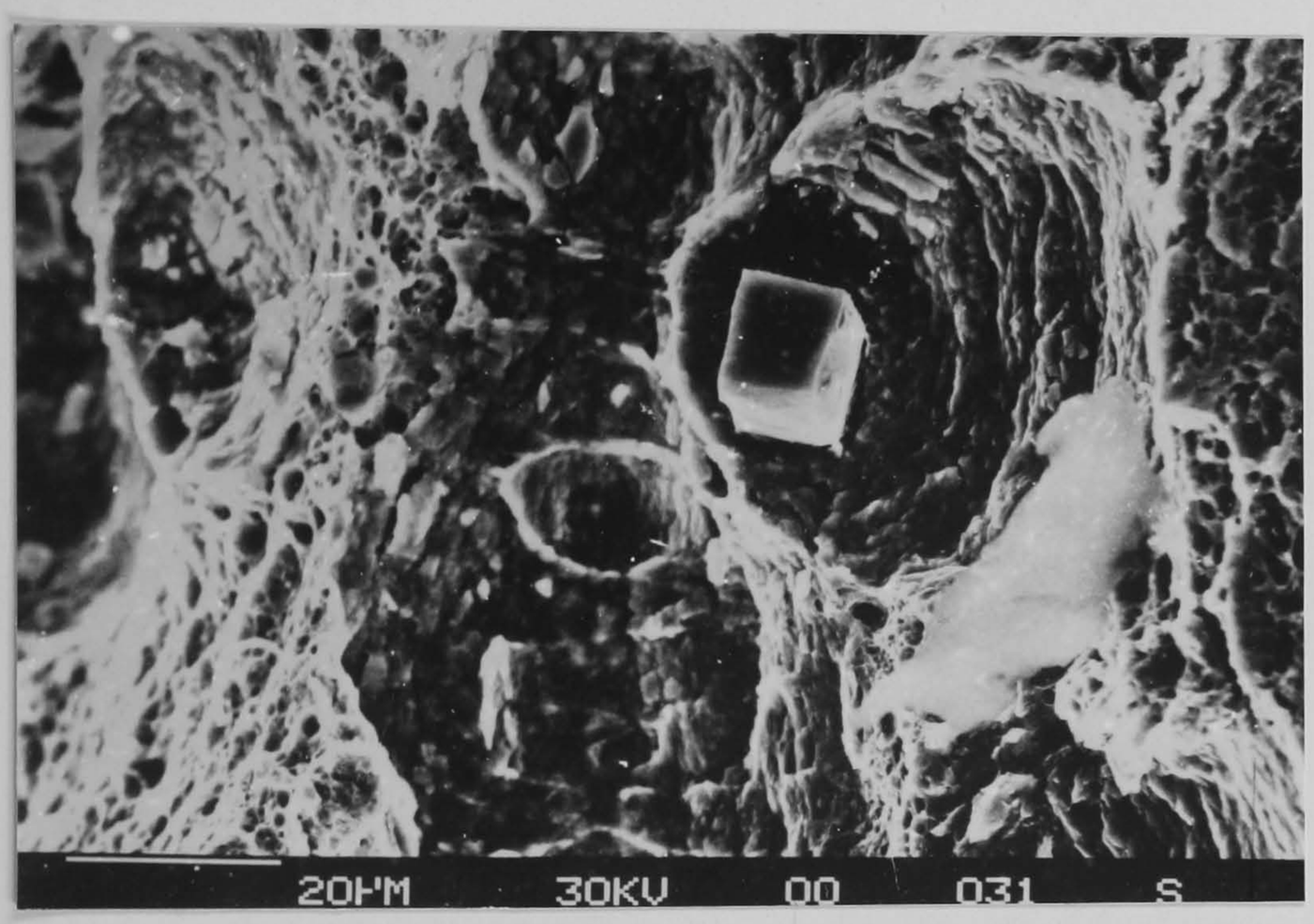

Figure 77

Final failure displaying microvoid coalesence

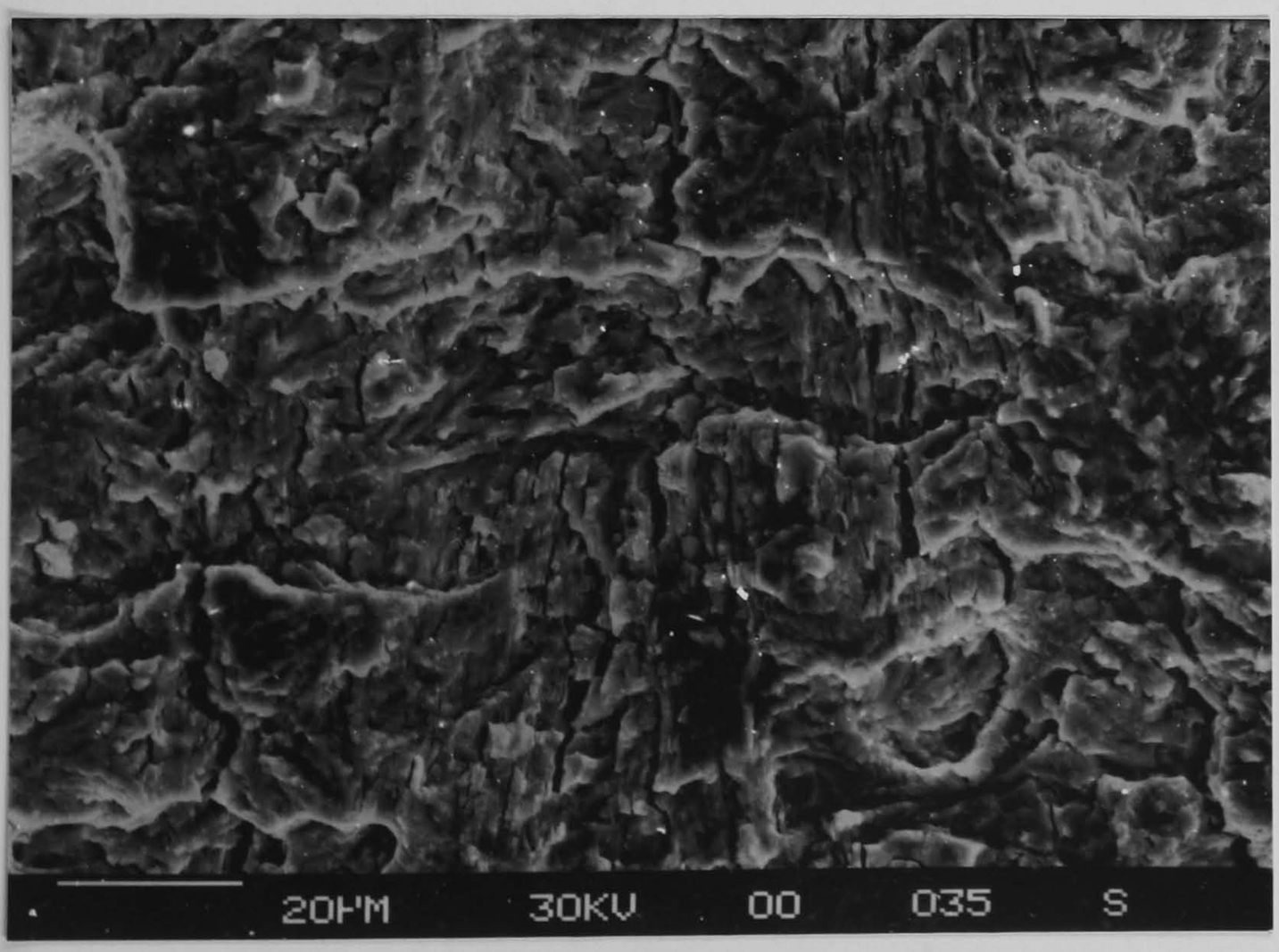

Figure 78

Direction of propagation

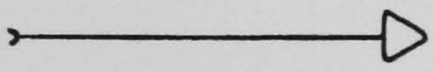

Fatigue crack fracture surface

$\Delta K = 22 MPa\sqrt{m}$.

6.1.1.2. RQT 501

This normally quenched and tempered steel was examined in two conditions namely; quenched only and quenched and tempered. A metallographic study into the effect of tempering on the nature of a fatigue crack propagation within the quenched microstructure was undertaken.

The plate was machined to give six identical fatigue samples. Two were tested in air in the as-quenched condition whilst the other four were tempered, two at 650^{o}C and two at 550^{o}C for one hour. Blanks of the same size were also tempered in order to produce tensile test pieces. Each sample was fatigued at fixed amplitude the results of which are given in Figure 79.

From a comparison of fatigue performance we can see that the as-quenched material has behaved in an environmentally sensitive manner exhibiting stress intensity range insensitive behaviour up to a ΔK of 22MPa$\sqrt{m}$. The tempered samples exhibit the three regions of fatigue normally associated with steel tested in an air environment. The most favourable fatigue crack propagation rates at any given stress intensity range were produced by the steel tempered at 550$^{\circ}C$. The yield strength of the as quenched plate was 585MNm^{-2}, tempering at 550^{o}C reduced this value to 530MNm^{-2} and tempering at 650^{o}C reduced the yield only slightly further to a value of 520MNm^{-2}. Corresponding increases in reduction in area values occured from 50%, through 60% up to 65% for the lowest yield strength.

Metallographic analysis was based on a technique developed to assess crack path deviation and secondary crack formation. The fracture surfaces were mounted in profile and an area of crack extending from 13 to 14mm was photographed. This was then projected onto a screen and an

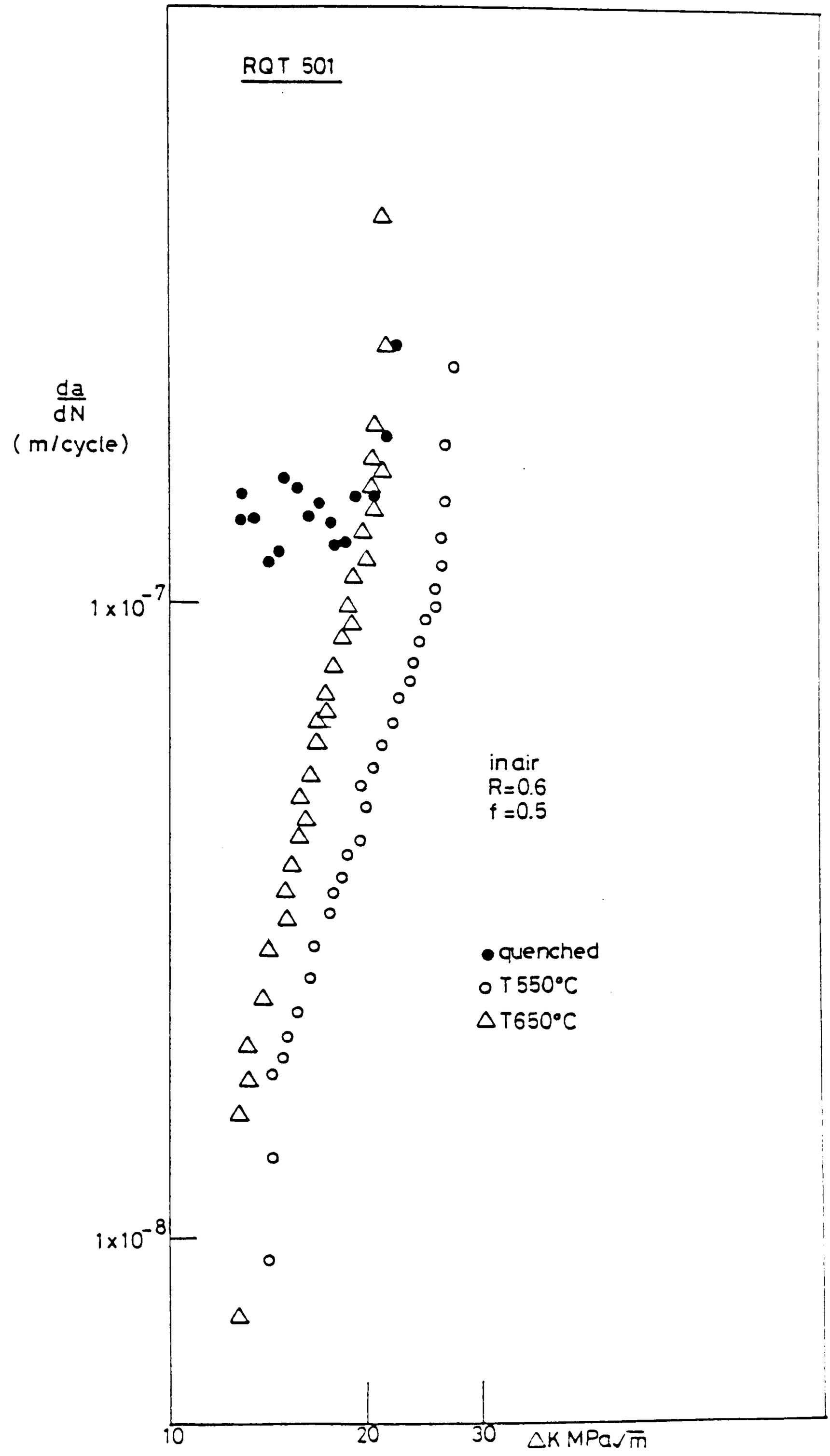

Figure 79. RQT 501 fatigue data for three conditions of tempering.

accurate outline of the fatigue crack profile was drawn. The profile was digitised using a microcomputer and sonic pen giving a very accurate length for the profile. This was converted to a percentage increase in surface area of the fatigue fracture surface over a flat plane. Figure 80 is an actual profile with the digitised profile for comparison. It should be noted that this profile has been drawn by a low resolution printer and therefore containes far less detail than the actual digitised profile.

In addition to the comparision between samples, a comparision betweeen the outer sample surface (region of plane stress) and a parallel plane in the centre of the sample (plane strain) was also made. The results of this survey are summarised in Table III.

Sample					Crack surface area / flat plane area %	
Desig	Ys MPa	UTS MPa	Area Reduct^{n} %	Hv	Sample Surface	Central profile
RQT 501 as quenched	585	795	50	297	135	120
RQT 501 T550	530	690	60	210	156	142
RQT 501 T650	520	695	65	205	160	145

Table III A comparison of the free surface generated by a fatigue crack in RQT 501 after various heat treatments

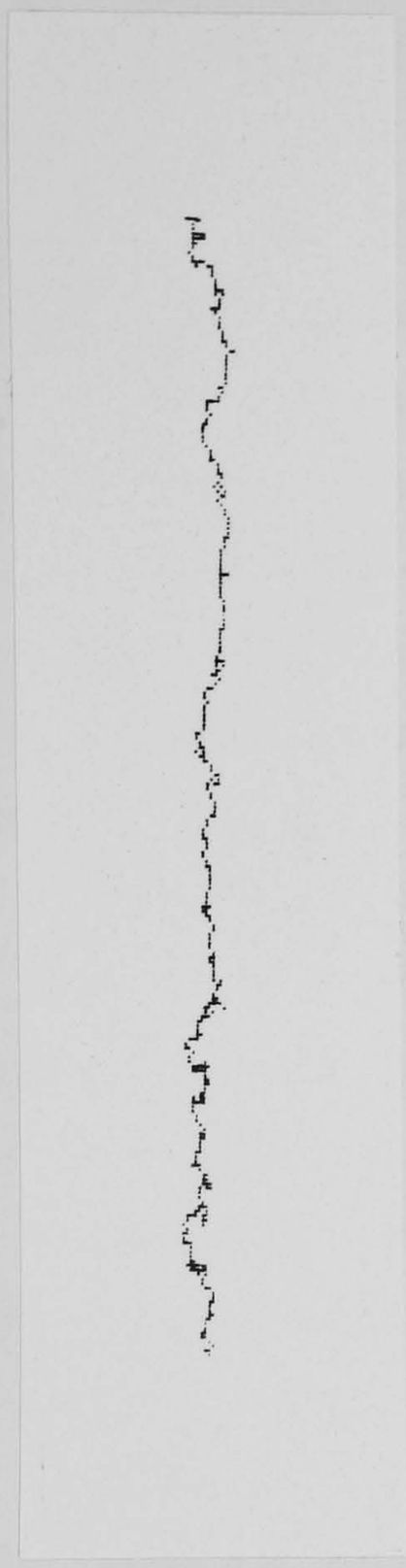

80

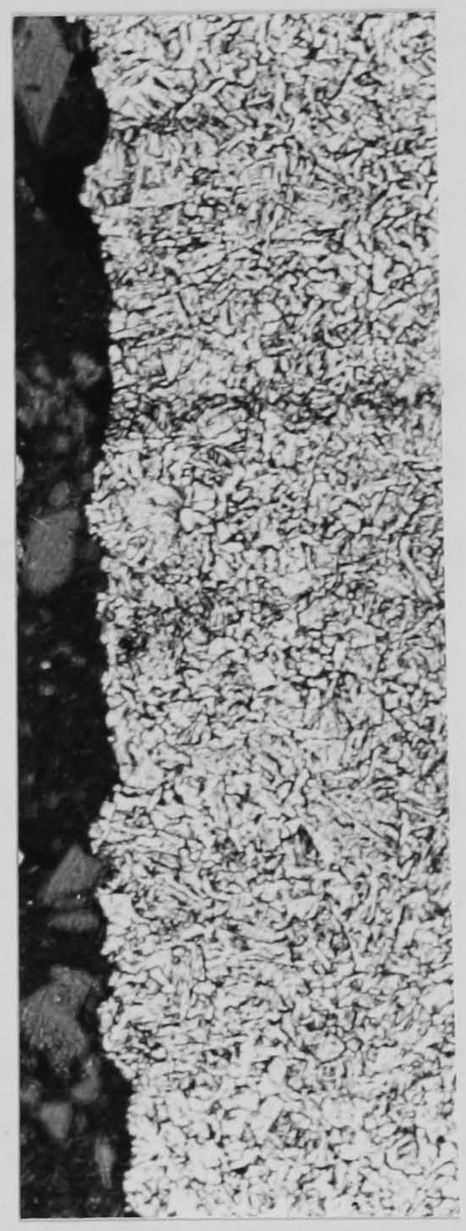

80(a)

Figure 80 Digitised and actual crack profile of RQT 501 (X200)

All conditions of tempering showed a consistant difference of approximately 15% between the surface area generated by the crack on the sample surface and the profile in the centre of the fatigue sample. The difference between the as quenched samples and the tempered samples is in the region of 21% to 25% however the difference between the two conditions of tempering is not significant at 3.5%. The consistent difference between the surface of the sample and a central plane was surprising as this difference was not discernable by subjective scanning electron microscope observation.

The difference between the 'as-quenched' and the tempered samples clearly reflects a change in propagation mechanism from one dependent upon environment to one related to stress intensity range. It was also found that the surface area generated by the fatigue crack consistantly increased with rising ΔK and therefore increasing plastic zone size. This may account for the consistant difference between the sample surface profile and central profiles.

Commercially quenched RQT 501 exhibited a microstructure and fatigue crack profile very similar to that of previous samples tempered at 650^{o}C. Figure 81 shows this profile with a large secondary crack, not typical of the overall profile, but, of a type which consistantly occured when the fatigue crack met a narrow band of manganese sulphide inclusions running through the centre of the commercial plate. This massive, open type of crack branching can also be seen on the fatigue fracture surface in Figure 82. Again the crack branch has occured at a crack length corresponding to the band of manganese sulphide inclusions. This type of branching has not been previously enounted in this study and will be termed macro cracking for the purpose of discussion. Secondary cracks of a similar nature to those observed to form in N-A-XTRA 70 have also been observed on this fracture surface at higher

magnification however their occurance is far less frequent than in N-A-XTRA 70. The nature of the fracture surface is more planar than that of N-A-XTRA 70 reflecting a lower degree of crack path deviation and crack branching.

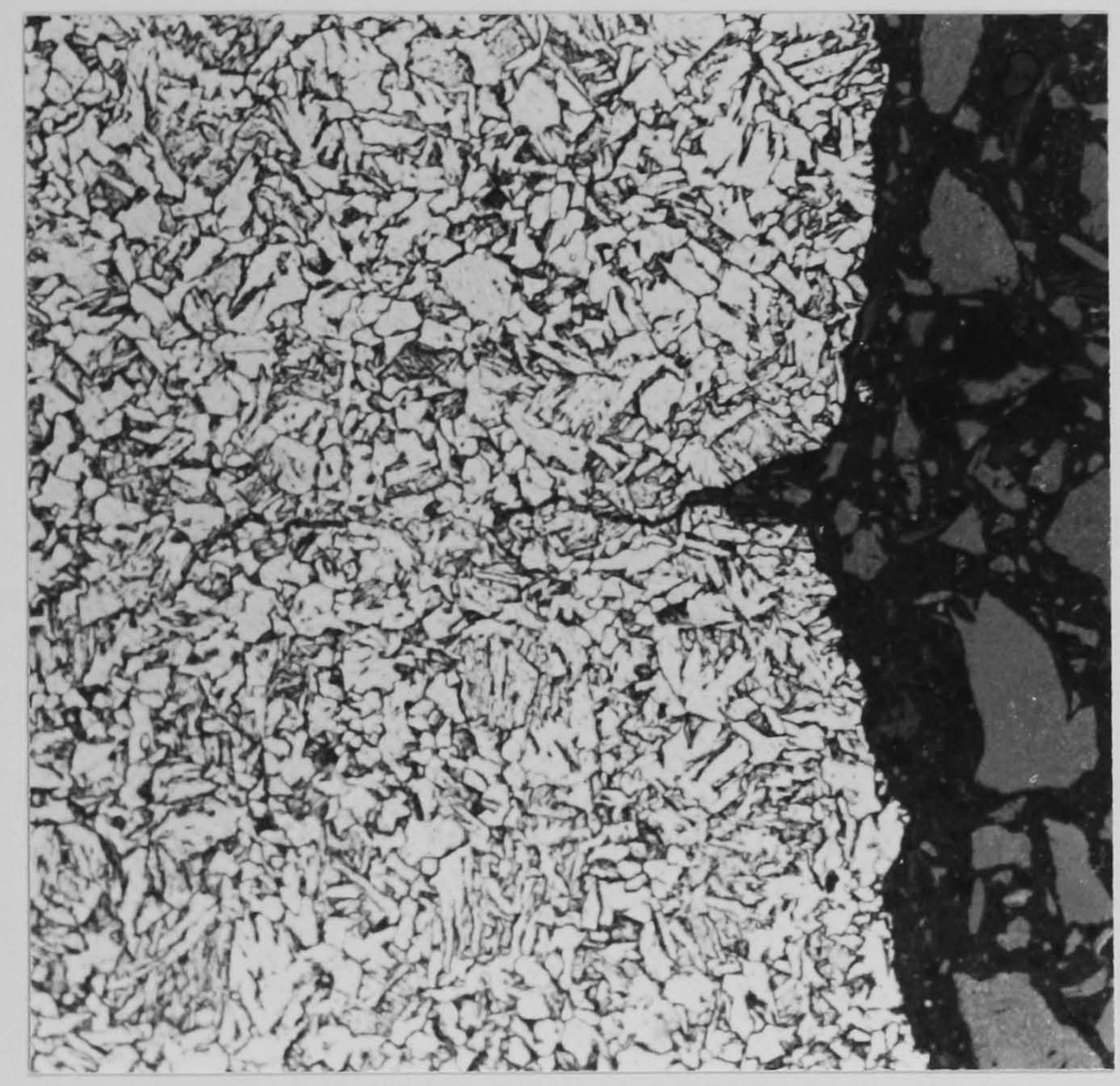

Figure 81

RQT 501 commercial plate fatigue crack profile (X400)

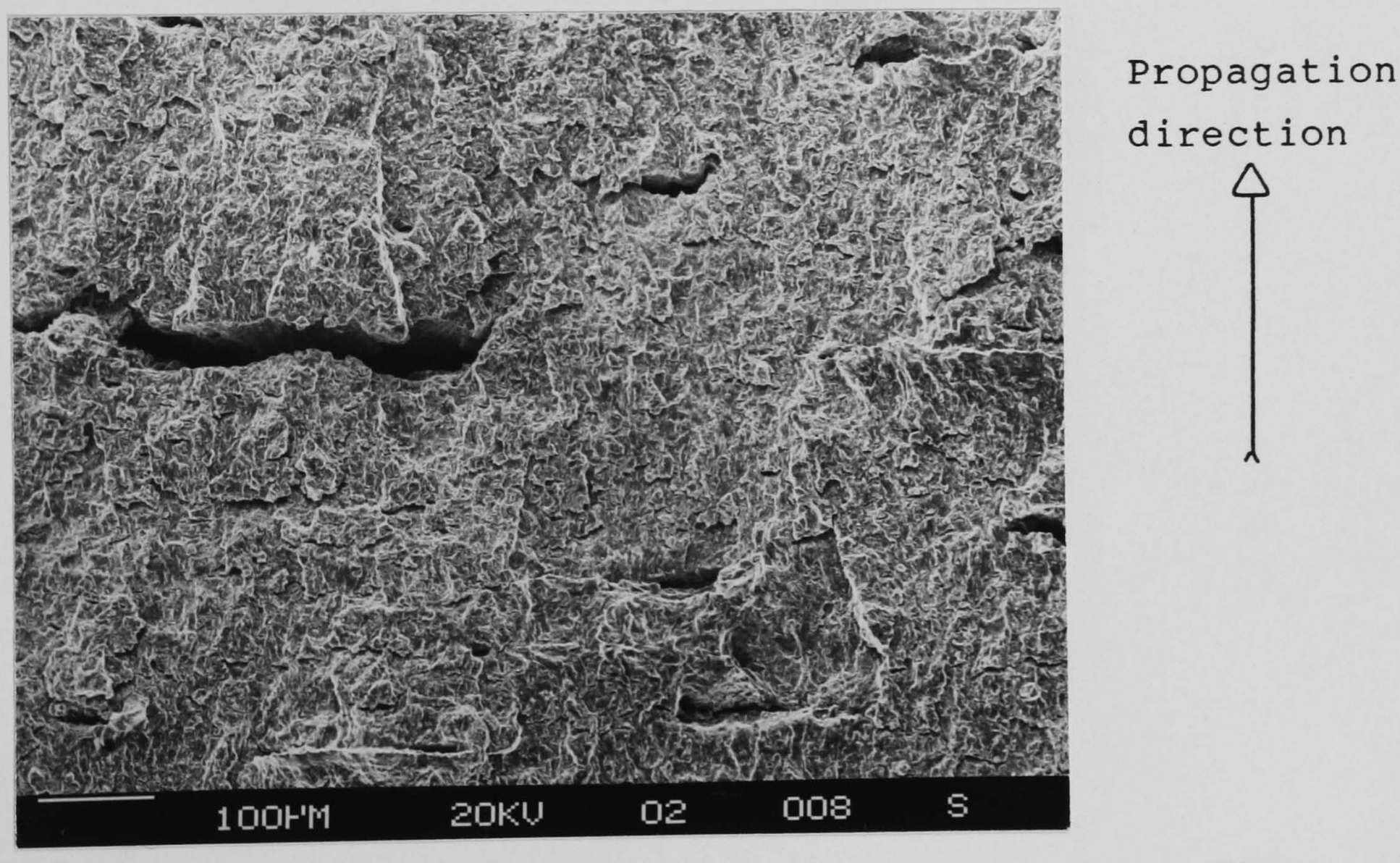

Figure 82 Large open type of crack branching on RQT 501 fracture surface

6.1.1.3. BS 4360 grade 55F

Figure 83 is a profile of a fatigue crack in B54360 grade 55F. This area of fatigue crack propagation corresponds to an average stress intensity range of 16.5MPa$\sqrt{m}$ and was taken from the surface of the sample. Fatigue crack propagation in this material has produced only very short secondary cracks typically only 10 to 15μm long. Examples of such secondary cracks can be seen in Figure 83. Whilst an appreciable degree of secondary cracking and crack path deviation have occured in this quenched and tempered steel, the relatively planar nature of the fatigue crack fracture surface can be seen in Figure 84. The average stress intensity range corresponding to this area of fatigue fracture surface is 20MPa$\sqrt{m}$.

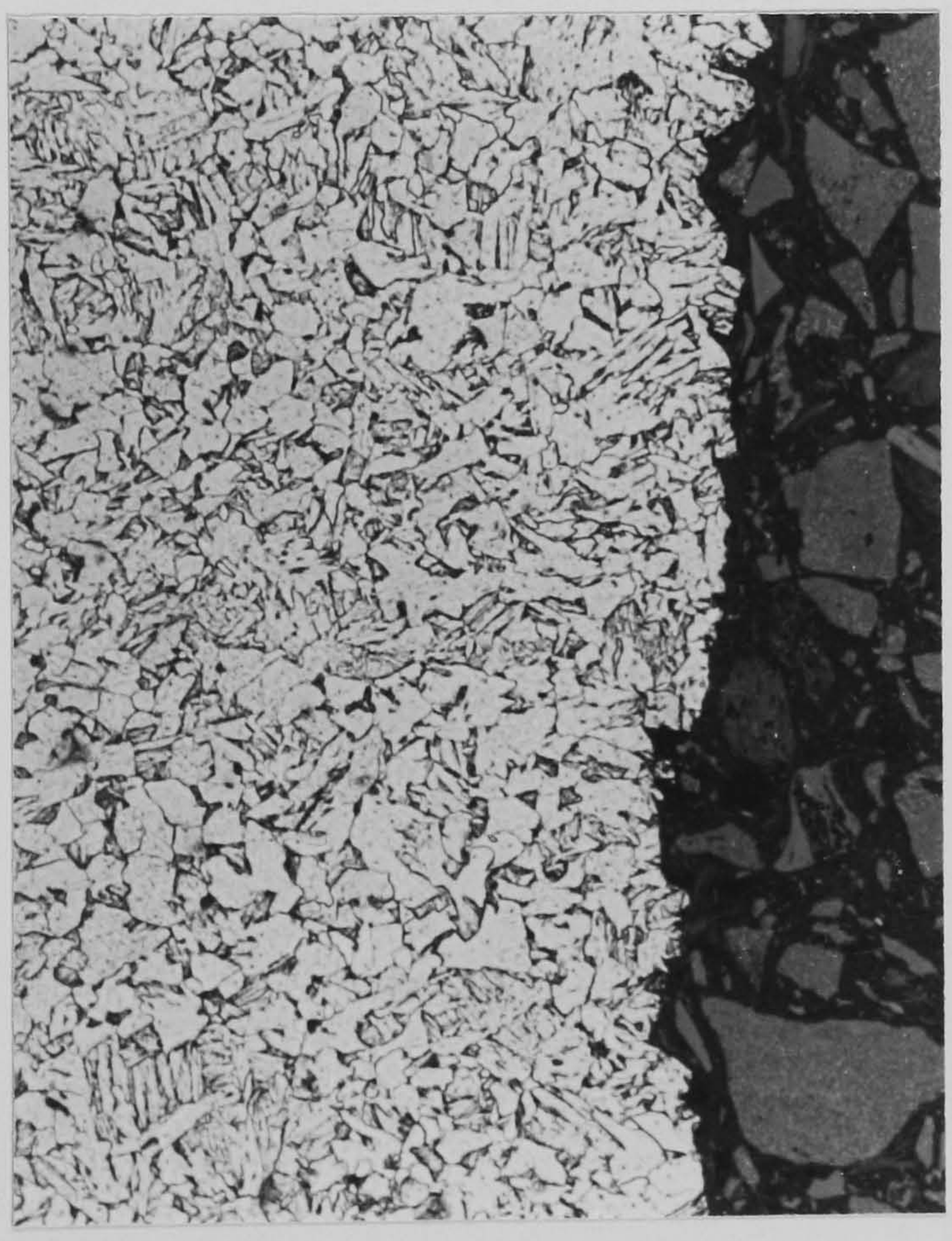

Figure 83 Fatigue crack profile of BS 4360 grade 55F (X400)

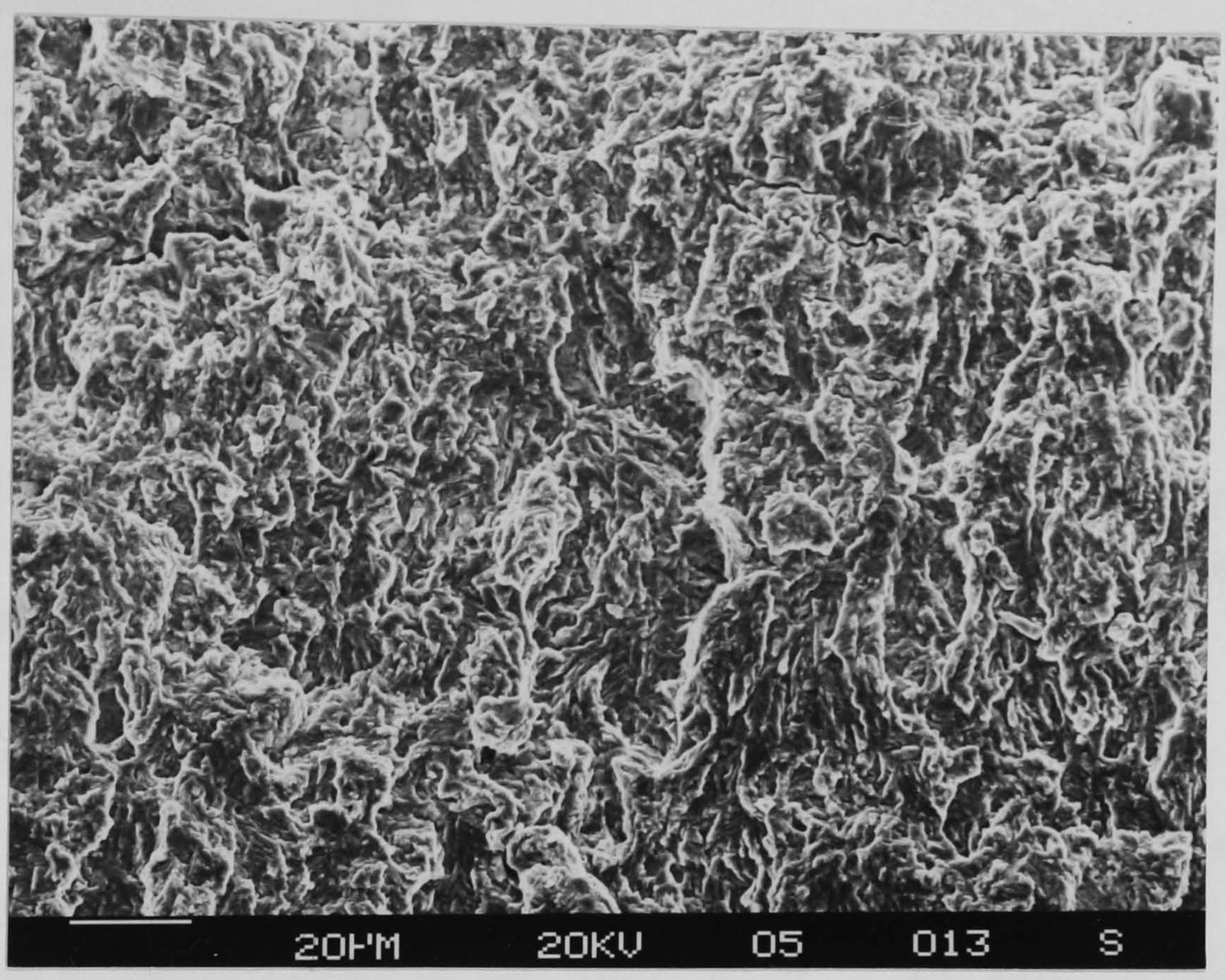

Figure 84 BS 4360 grade 55F fatigue crack fracture surface.

6.1.2. Controlled Rolled Steels

6.1.2.1 LP 6 Line-pipe

This heavily controlled rolled line-pipe steel was observed to delaminate at various crack lengths when exposed to a fatigue loading cycle. The delamination along a plane perpendicular to the macro crack propagation direction was extensive, reaching a length of 5mm in the horizontal plane in one sample. The extent of delamination can be seen on the fracture surface shown in Figure 85. The delamination in this sample has opened upon final failure.

Metallograhpic examination has shown the delamination to occur only along bands of high carbide precipitate concentration. Figure 86 shows the local microstucture associated with just such a delamination. The carbide rich band seen in this Figure is continuous across the entire metallographic sample and has a width of 20 to 25μm. Whilst the largest features of this nature occured at the surface of the sample areas of delamination have been observed accross the entire fatigue fracture surface. Only continuous carbide rich bands with a width of the order of 20μm have caused the fatigue crack to branch in this manner. Closer examination of the fracture surface gives an indication of the sequence of events during the formation of the delamination and the eventual continuation of the fatigue crack beyond this feature. Figure 87 is a diagramatic representation of this sequence of events. The crack has propagated evenly on both sides of the sample until side 'a' reached the carbide rich band through which delamination occured. The crack appeares to arrest on this side as the delamination grows. During this period side 'b' continues to propagate and push the crack front under the delamination. Eventually, the hidden crack front has reached the sample surface and begun to catch up with side 'b'. This process leads to areas of crack arrest followed

by accelerated crack growth. Scanning electron microscopy of the fracture surface reveals areas away from the delamination to be relatively smooth with only slight deviations in propagation route and very infrequent secondary cracks. Although this steel may exhibit a relatively high endurance due to the crack arresting effect of delamination the growth rate when delamination was not a feature was high ie up to 1.0×10^{-7} m/cycle at a stress intensity range of 20MPa$\sqrt{m}$. For these reasons this steel has not been considered to be suitable for further consideration as a candidate HSLA steel for structural application offshore.

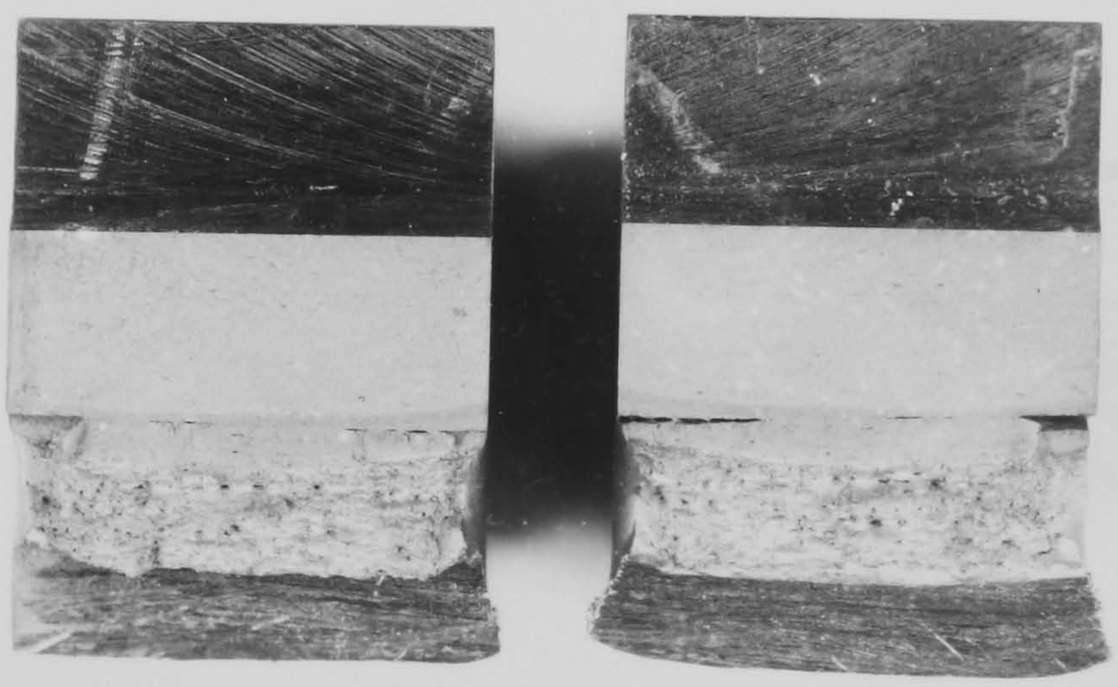

Figure 85 Extensive delamination as seen on the fatigue fracture surface of LP-6 (X3)

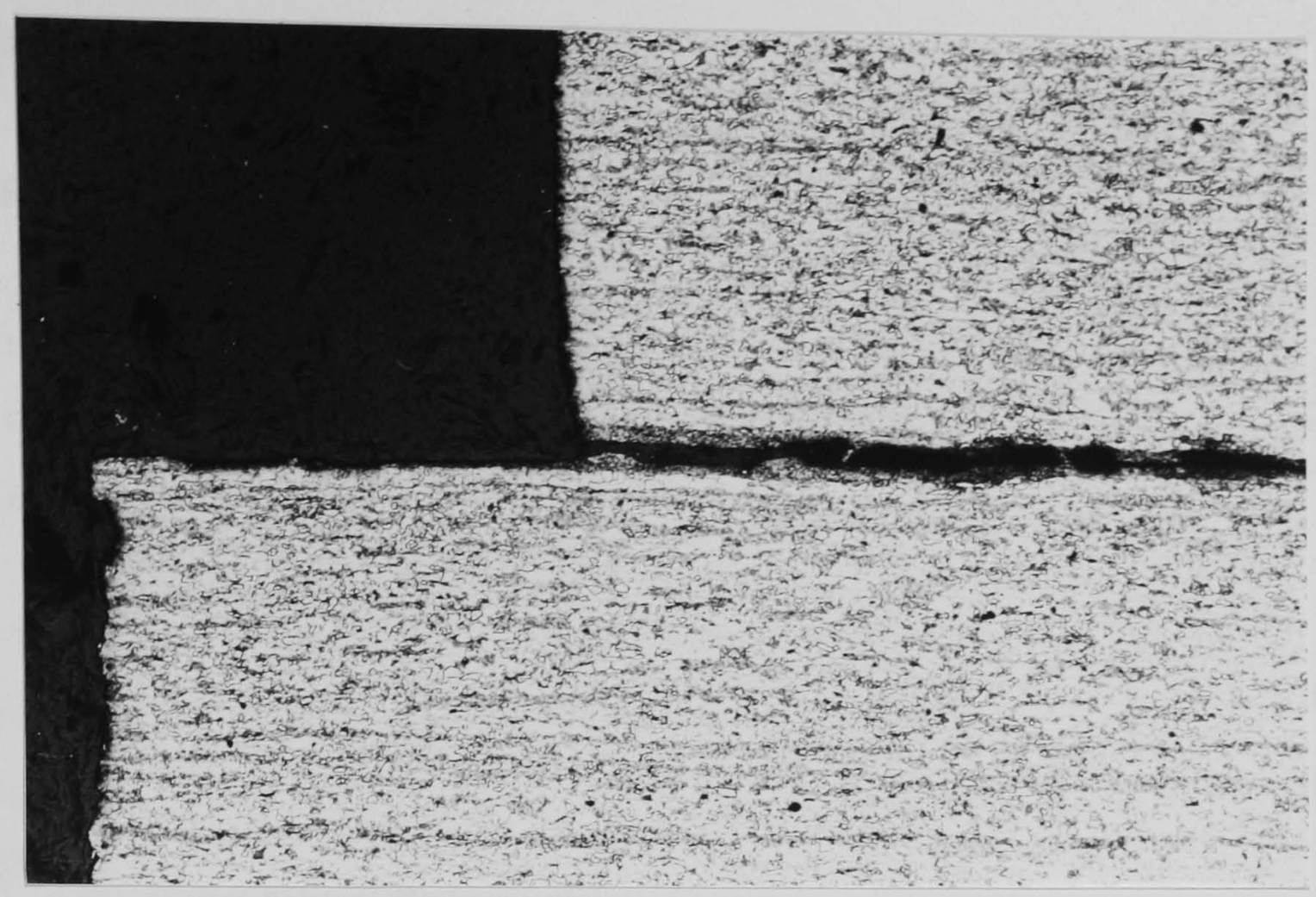

Figure 86 Local microstructure associated with delamination in profile (x200).

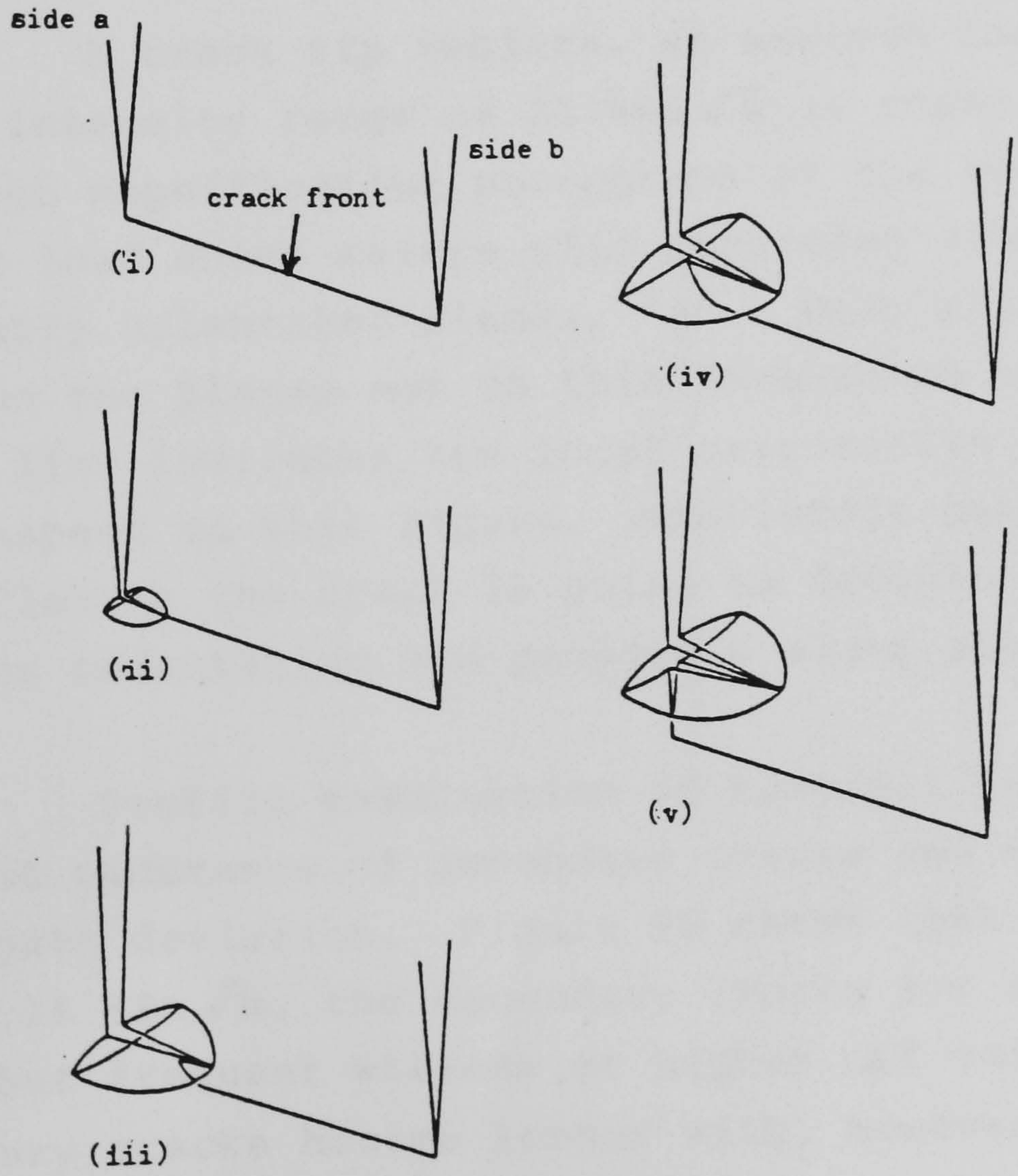

Figure 87 Diagrammatic representation of delamination in LP-6.

6.1.2.2. Kontroll 50 ESM

Replication studies on Kontroll 50 ESM has revealed a complex fatigue crack profile not dissimilar in its complexity of shape to that shown by N-A-XTRA 70. The deviation of fatigue crack propagation route from the planar is marked and can be seen in Figure 88.

The sample has been polished but left in the unetched condition to give an appreciation of the plasticity surrounding the crack. This figure shows areas of slip and plastic deformation both infront of, and in the wake of the propagating crack. Active slip planes appear to be orientated between 40^{o} and 90^{o} to the local crack propagation path and 30^{o} to 45^{o} to the gross propagation direction.

A crack tip replica, at maximum load, with a stress intensity range of 22 MPa$\sqrt{m}$ is shown in Figure 89. This high magnification photograph of the crack tip at maximum load shows severe slip occurring along one set of favourably orientated planes, 'a'. Only mild slip is taking place on the planes not in this favourable orientation. The broken line indicates the local orientation of the crack with respect to this Figure, immediately behind the crack tip. Clearly the crack is going to deviate from its previous orientation and propagate along planes 'a'.

Profile examination of Kontroll 50 ESM has shown a frequent occurance of secondary cracks and a high degree of crack path deviation. Figure 90 shows that at low ΔK values, 18 MPa$\sqrt{m}$, the secondary cracks are short (10 to 15μm) but frequent whereas at higher ΔK values the secondary cracks become longer with, however, the same frequency of occurance.

An interesting feature seen on the fatigue fracture surface of Kontroll 50 ESM, Figure 91, are spherical second phase particles. X-ray analysis showed these precipitates to be manganesse sulphides. Whilst this steel has a very low sulphur content (0.005%) manganesse sulphides will still form. These have clearly been shape modified via a very small addition of a modifying element such as calcium. In this Figure the fatigue crack propagation direction is directly upwards. The degree of crack path deviation is significant in this steel and is accompanied by frequent crack branching.

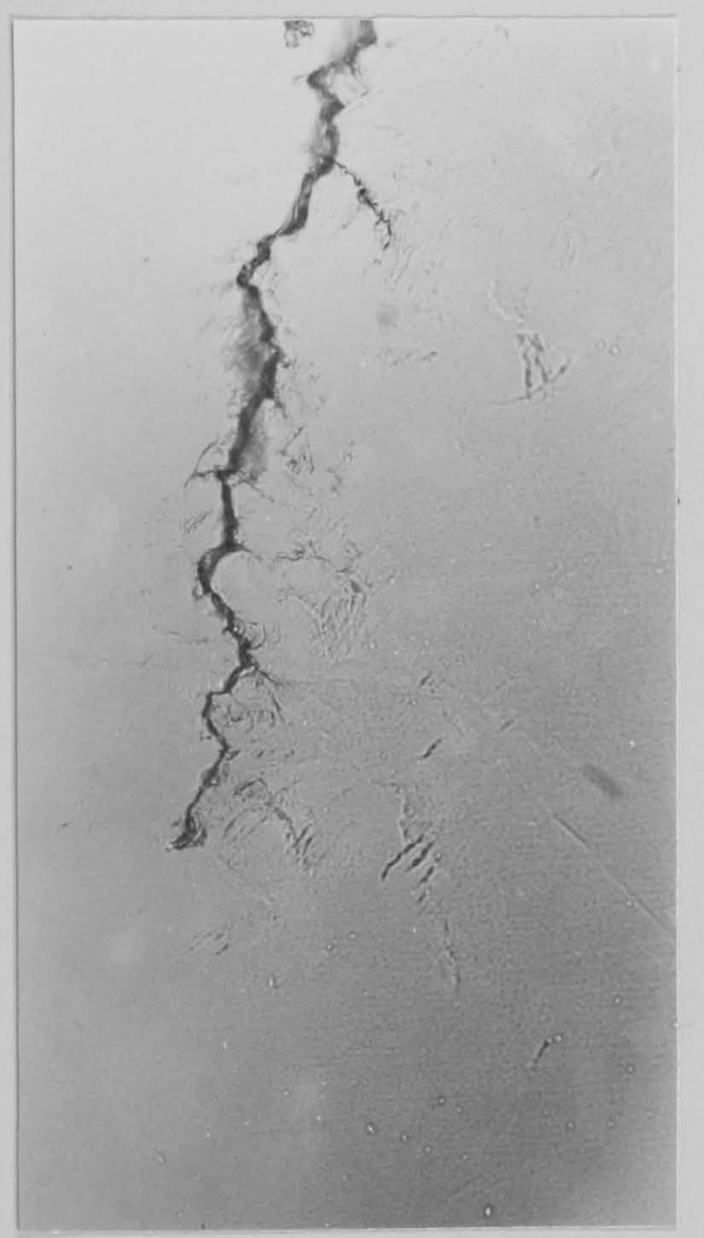

Figure 88

Replica of a fatigue crack in Kontroll 50 ESM

$\Delta K = 18$ MPa $\sqrt{m}$

(X200)

Figure 89

Crack tip replica of Kontroll 50 ESM at maximum

(X800)

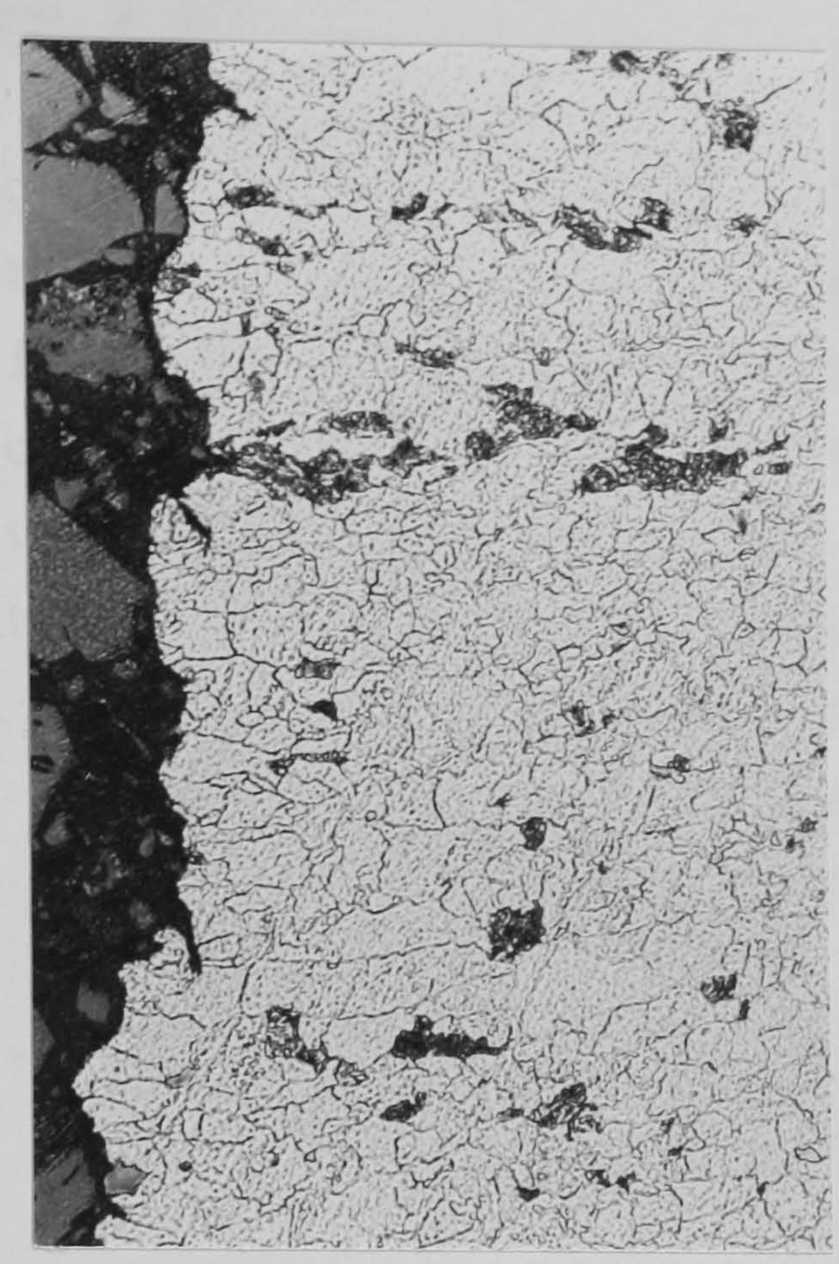

Figure 90 Fatigue crack profile showing secondary crack occurrence in Kontroll 50 ESM (x400).

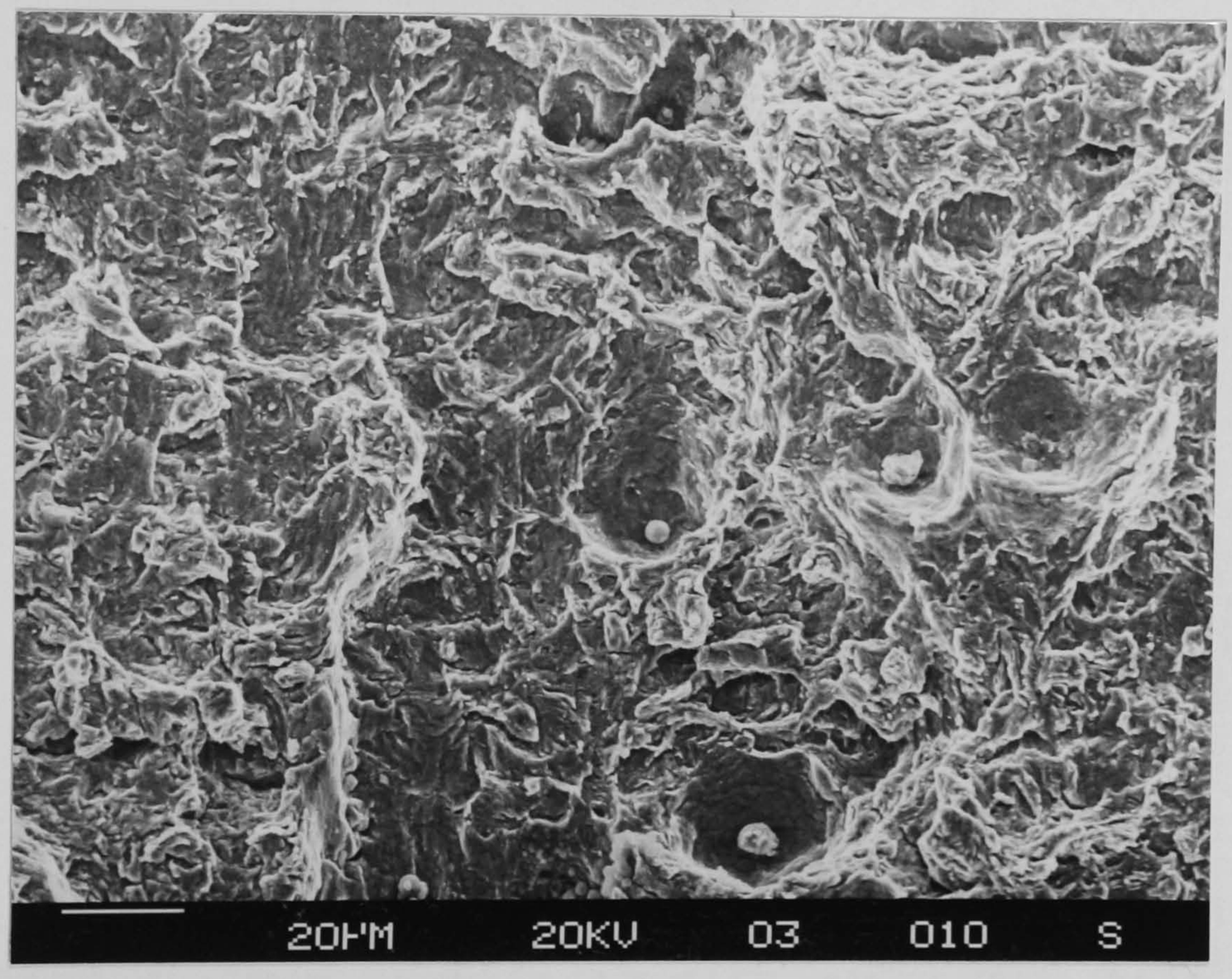

Figure 91, Shape controlled manganese sulphide inclusions exposed on Kontroll 50 ESM fatigue fracture surface.

6.1.2.3. Mannesmann x 80

The fatigue crack profile for this controlled rolled line-pipe steel at medium stress intensity range (ΔK = 21 MPa$\sqrt{m}$) is shown in Figure 92. The high degree of crack path deviation seen in this region of crack growth is typical for all levels of ΔK. A frequent occurrance of secondary cracks, typically 30μm in length, is seen at all ΔK values. Despite the banded controlled rolled microstructure the crack branches appear to grow at the same angle to the gross crack propagation direction whether they are growing in a ferrite or a carbide rich band. The fracture surface is seen in Figure 93 and shows an area of crack growth which occurred at a stress intensity range of 20 MPa$\sqrt{m}$. The multiplanar nature and very high occurrence of secondary cracks is evident from this figure.

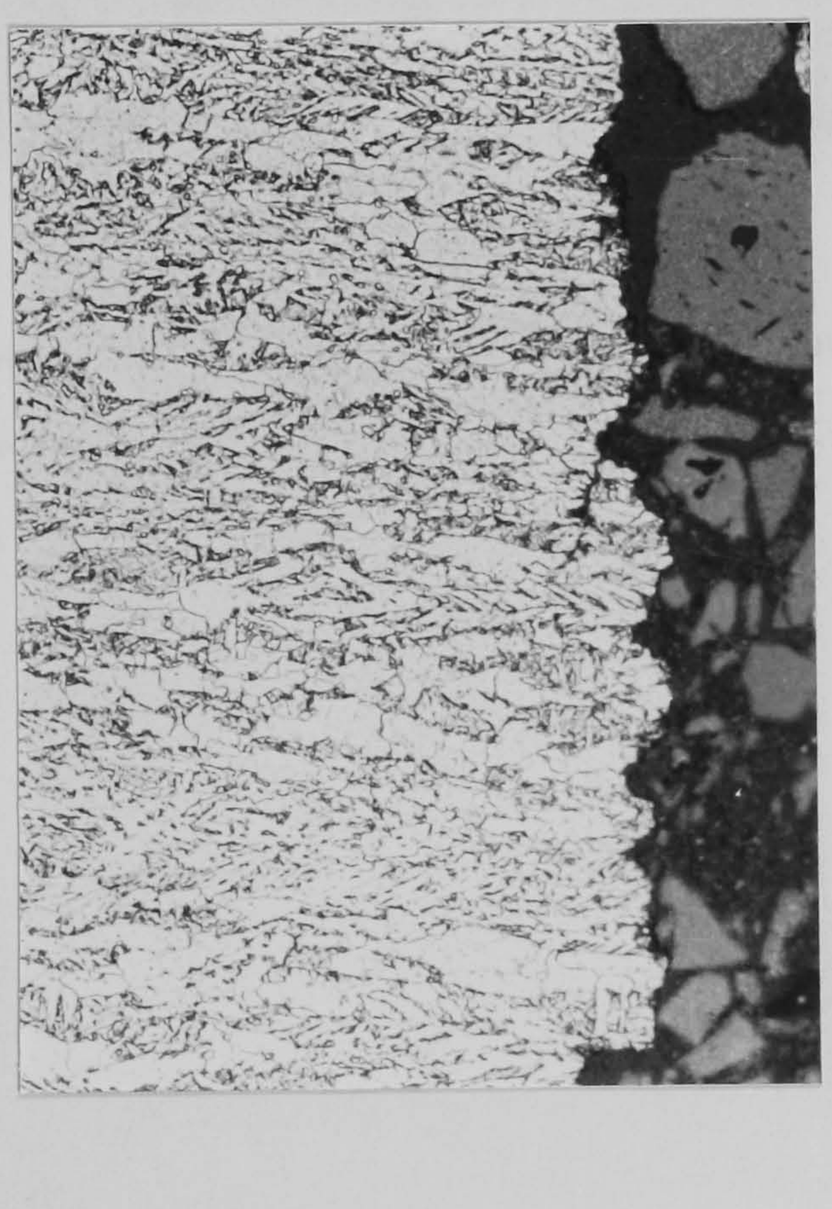

Figure 92 Fatigue crack profile showing secondary cracking and crack path deviation in X80 line-pipe, ΔK = 21MPa$\sqrt{m}$

(x 400)

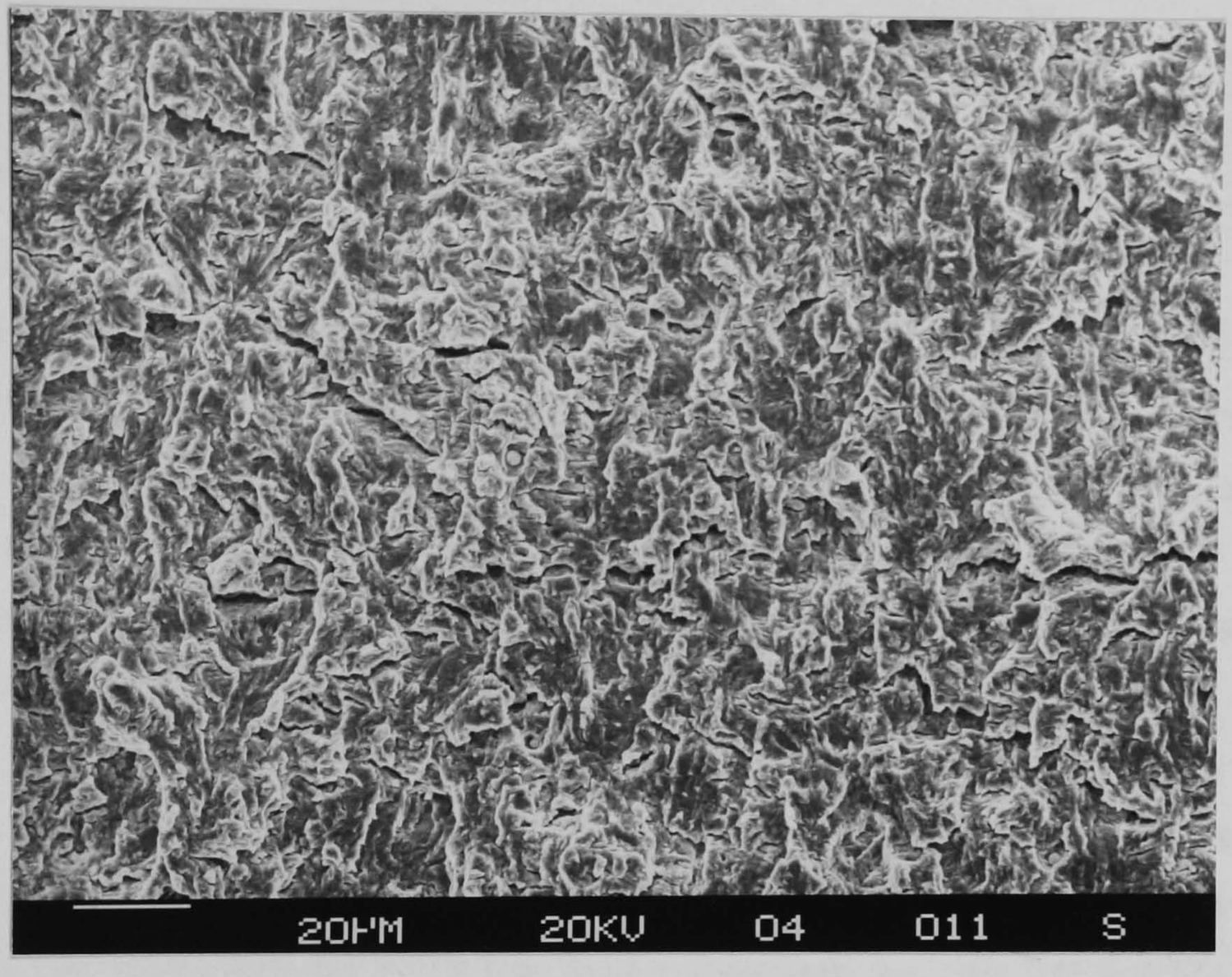

Figure 93 Fatigue fracture surface showing high occurrance of secondary cracks in X80 line-pipe steel

6.1.3. Parent plate metallography summary

metallographic studies of the nature of fatigue cracks propagating in a range of HSLA steels have provided an insight into microstrucutral influences upon the propagation characteristics of fatigue cracks.

The degree of crack path deviation within the parent plate microstructure has been observed to vary greatly from one microstructural type to another. The steels exhibiting the greatest degree of crack path deviation and secondary crack occurance were the controlled rolled steels Kontroll 50 ESM, Mannesmann x 80 and the quenched and tempered steel N-A-XTRA 70. The quenched and tempered steels BS 4360 grade 55F, RQT 501 and the controlled rolled LP6 all produced flatter fracture surfaces with a marked lack of fine secondary cracks.

Two types of crack branching have been observed in HSLA steel, parent plate microstructures. Very large open cracks which can be directly attributed to an obvious microsturctural feature have been termed macro cracking. Finer crack branching not associated with any obvious microstructural feature will be termed secondary cracking for the purpose of discussion. The macro cracks observed in RQT 501, associated with manganese sulphides, and in LP-6 as delamination were observed to run at 90^{o} to the overall propagation direction following a gross microstructural weakness. Secondary cracks, prevalent in N-A-XTRA 70 and Kontroll 50 ESM, tend to run at approximately 45^{o} to the overall propagation direction but may branch at angles up to 90^{o} to the immediately preceeding local propagation direction. The occurance of fine secondary cracks appears to be strongly related to the degree of crack path deviation which is itself dependent upon the microstructure through which the crack is propagating.

Strengthening precipates have been shown to influence the fatigue crack path in N-A-XTRA 70 and the propagation mechanism in Kontroll 50 ESM. In the quenched and tempered steel N-A-XTRA the fatigue crack was shown to favour a route dominated by zirconium based precipitates. Shape controlled precipitates of manganese sulphide have been observed to promote a dimple forming mechanism on a fatigue fracture surface, however due to the very infrequent occurance of this precipitate an effect on the fatigue crack propagation route could not be assessed.

6.2 Multipass Submerged Arc Welded HAZ Microstructures

Five of the original six steels have been welded by a multipass submerged arc welding process for the purpose of studying fatigue crack propagation within the HAZ microstructure. A range of fatigue properties have been observed which generally reflected the properties of the parent plate. This was true for four of the five steels tested the exception to this pattern was Kontroll 50 ESM. This controlled rolled steel exhibited ΔK independent fatigue crack propagation up to a ΔK value of approximately 20 MPa $\sqrt{m}$, above this value of stress intensity range a high sensitivity response was observed.

Fracture surface and profile examination of N-A-XTRA 70, RQT 501, BS 4360 grade 55F and Mannesmann X 80 line-pipe steels revealed the same features for each steel as was observed in the parent plate microstructures. Whilst the same features were observed it was noted that the degree of crack path deviation had reduced and the occurance of secondary cracks was less frequent. Figures 94 and 95 are the fracture profile and fracture surface for BS 4360 grade 55F which, typically of the aforementioned steels, showed only slight deterioration in fatigue properties as a result of welding. Figure 94 is a profile for this steel at a ΔK value of 20 MPa $\sqrt{m}$. The degree of crack path deviation has reduced and secondary cracks are very fine and relatively infrequent. The high magnification photograph of the fracture surface in Figure 95 is very similar to that of the parent plate for this steel with striations and a fine secondary crack clearly visable. However, at lower magnification the slightly smoother nature of the HAZ fracture surface becomes apparent as does the reduction in secondary crack occurance.

Metallographic examination of the Kontroll 50 ESM HAZ samples revealed contrasting features to those observed

in the parent plate samples. The fracture profile, Figure 96, shows a large reduction in crack path deviation and almost no visible secondary cracks. The fracture surface of this sample has shown a type of crack branching not previously encountered. This type of cracking seen in Figure 97 is very fine and has a regular spacing which corresponds to a striation spacing for the rate of propagation recorded during the test. The angular profile and planar nature of areas containing these cracks suggests a mechanism dominated by cleavage. This type of micro cracking appears frequently at all levels of ΔK in relatively small (approximately 10μm) patches which are of the order of the grain size for this microstructure. Areas between those dominated by micro cracking show similar features to the parent plate fracture surface with however a lack of secondary cracks.

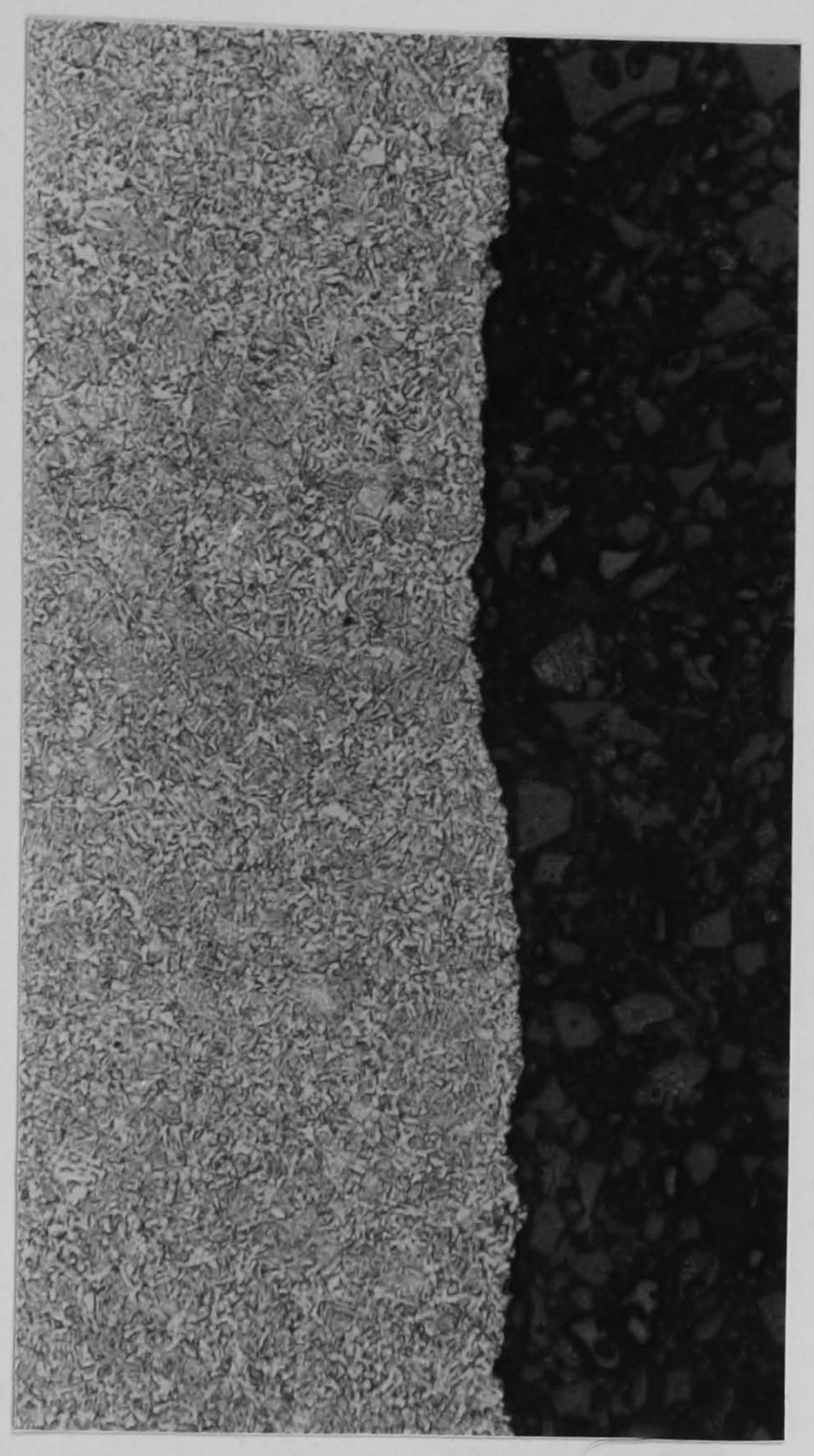

Figure 94

Fatigue crack profile of 55F HAZ showing reduced crack branching and deviation
$\Delta K = 20 MPa\sqrt{m}$

(X200)

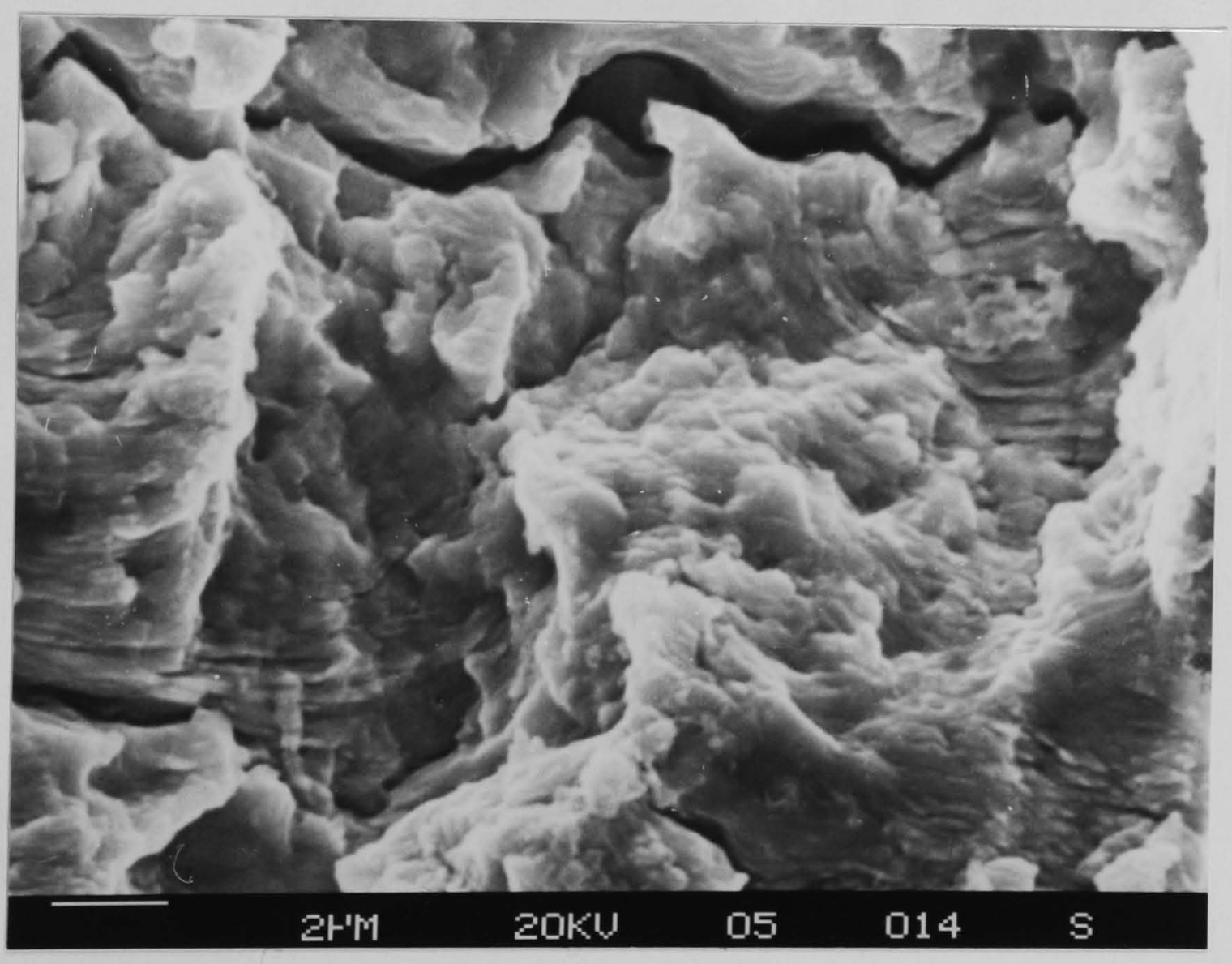

Figure 95 Fatigue striations and secondary cracking seen on 55F HAZ fatigue fracture surface

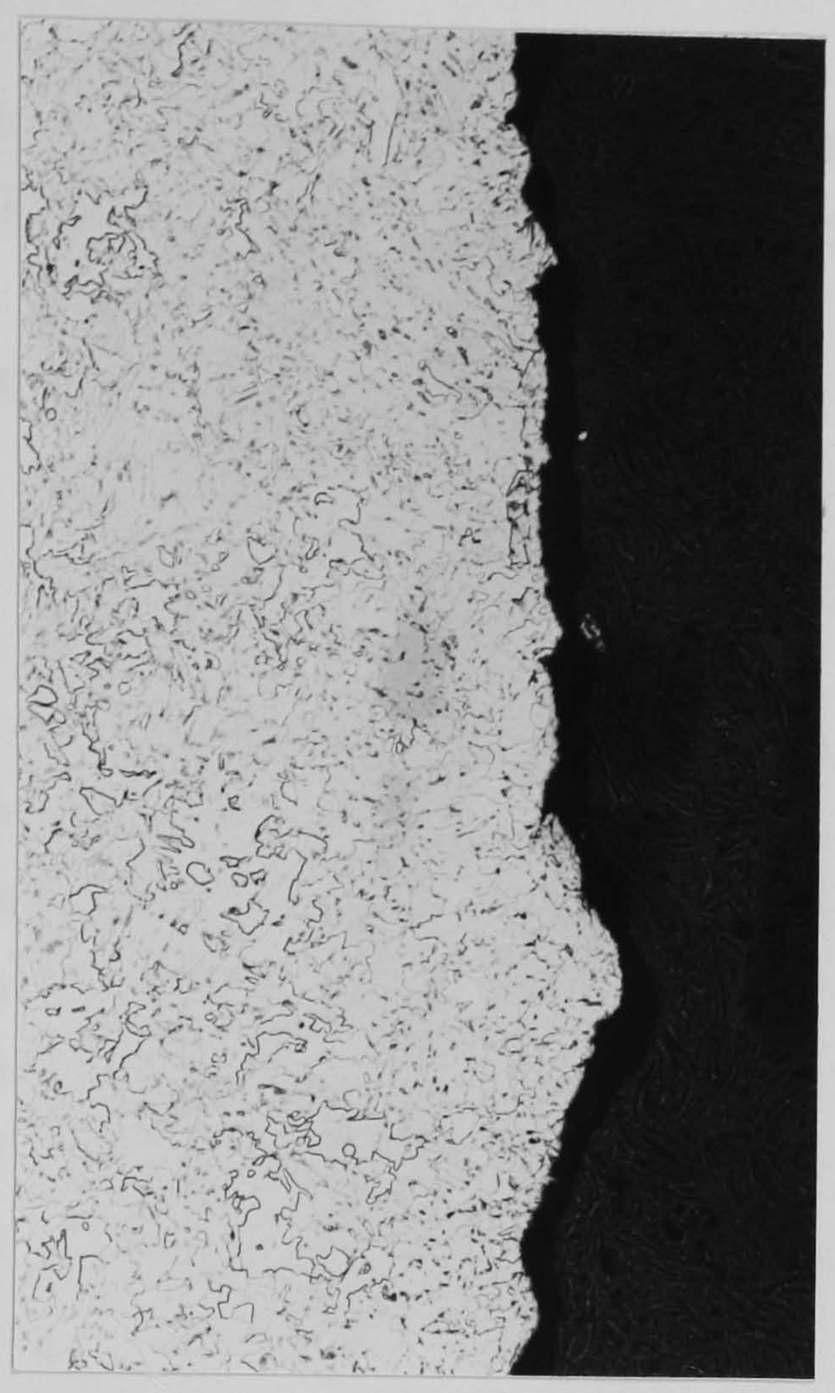

Figure 96

Fatigue crack profile of Kontrol 50 ESM HAZ showing reduced secondary cracking and deviation $\Delta K = 20\ MPa\sqrt{m}$

(X200)

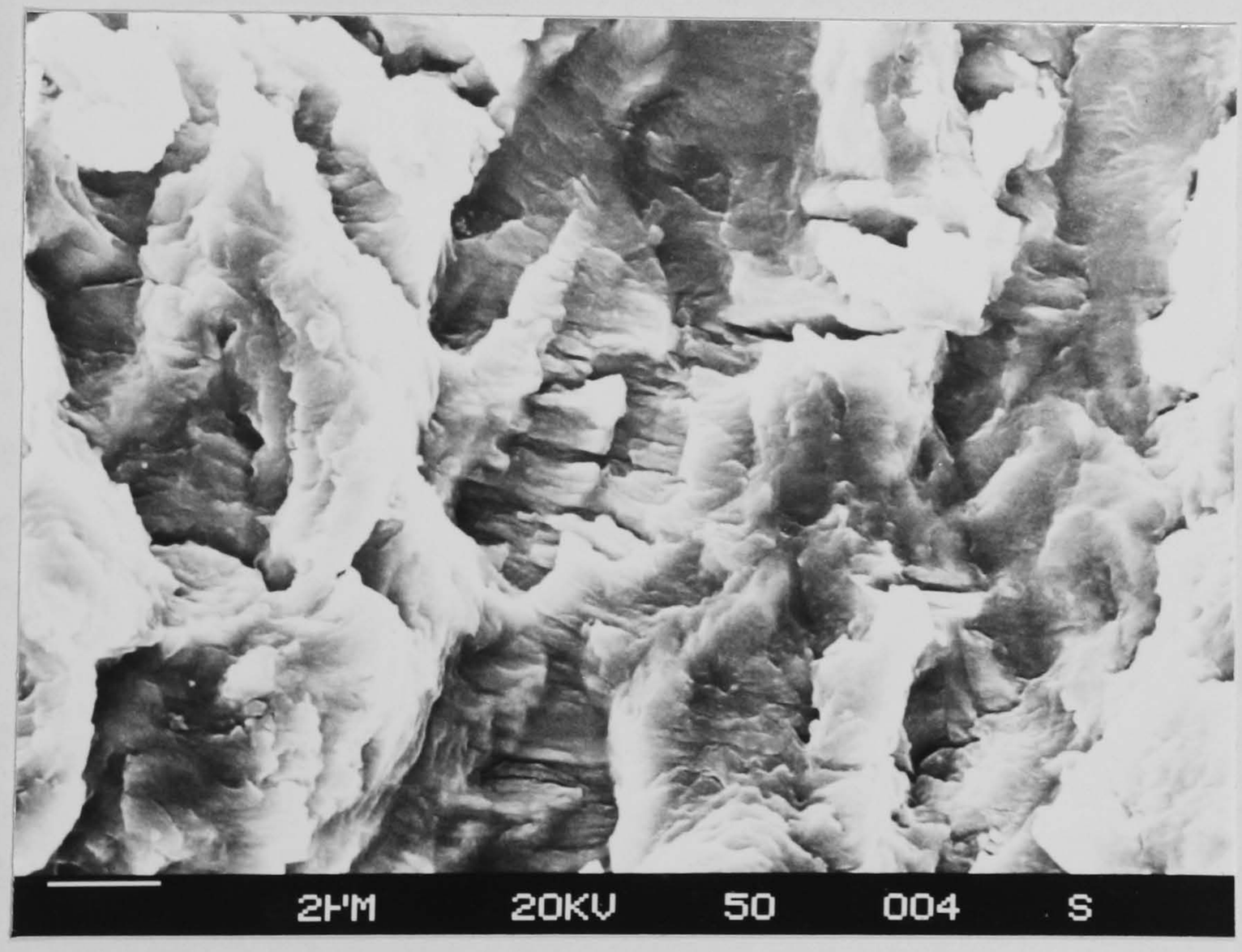

Figure 97 Fine micro cracking observed on Kontroll 50 ESM fatigue fracture surface

6.3. Corrosion Fatigue

Steels produced by the two major current production routes were chosen for a corrosion fatigue study. One steel of each type was tested at three levels of cathodic protection and examined mainly in profile for metallographic features.

6.3.1. Quenched and tempered steel BS 4360 grade 55F

When tested in the freely corroding condition this steel has shown a greater fatigue resistance below a ΔK of 19 MPa $\sqrt{m}$ than in the air environment however above this ΔK value a significant reduction in performance has occurred. Figure 98 is a profile of a free corroding sample showing similar features, in terms of secondary crack formation, to the in-air samples. A certain amount of grain boundary attack as well as enlargement of secondary crack width has occurred as a result of the corrosive environment. An excessive build up of corrosion product occurred on this fracture face the bulk of which was removed via ultrasonic cleaning for profile examination. Scanning electron microscopy was of little benefit due to the corrosion products on the fracture surface. Figure 99 shows the fatigue crack profile for a correctly protected (-810mV) sample. Whilst on a macro scale the fracture surface appeared to be free from corrosion products, in profile we can see that a small amount of corrosion attack has occurred thus indicating that the cathodic protection did not fully extend into the crack tip region itself. Despite this the crack profile shows similar characteristics in terms of crack path deviation and secondary cracking to the in-air samples.

The overprotected condition proved extremely detrimental to the fatigue crack propagation properties of this quenched and tempered steel. At a lower ΔK value

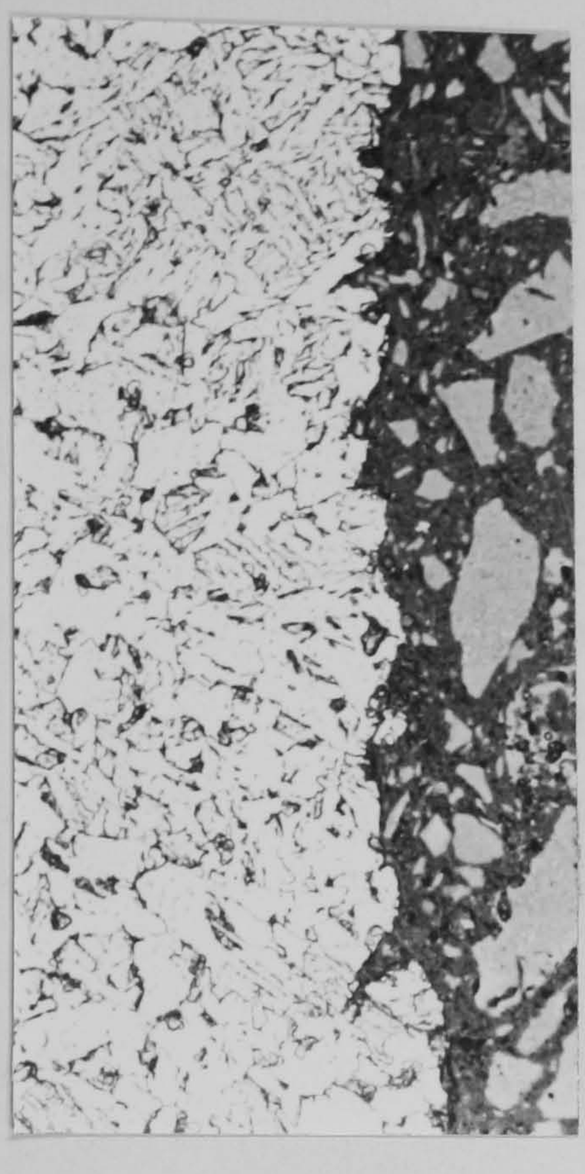

Figure 98

Crack profile of free corroding BS 4360 grade 55F steel
$\Delta K = 19 MPa\sqrt{m}$
(X400)

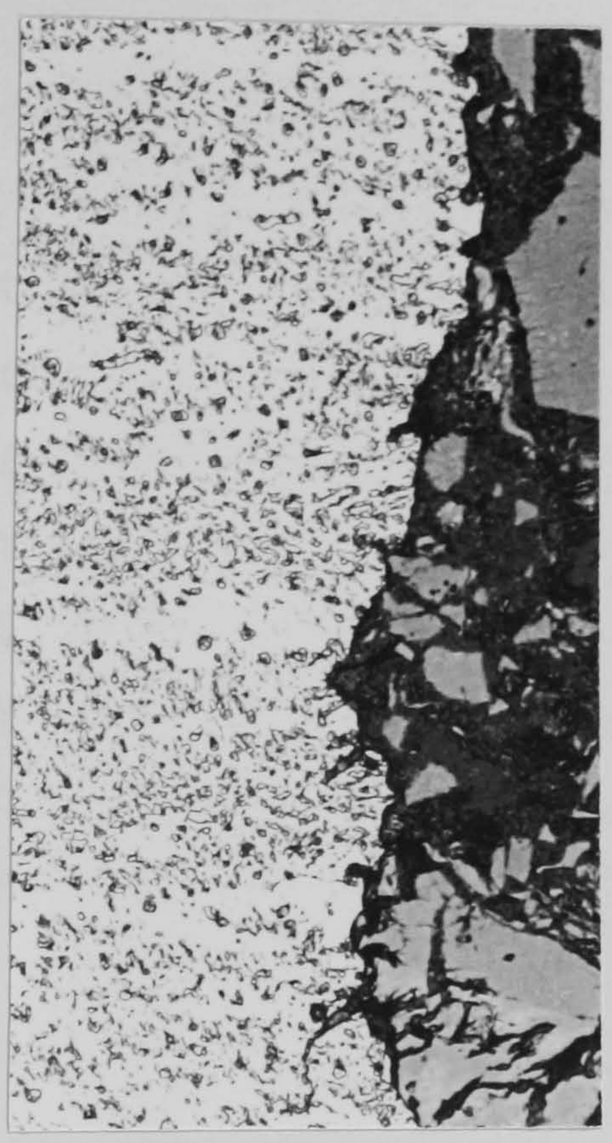

Figure 99

Crack profile of correctly proteected BS 4360 grade 55F steel
$\Delta K = 20\ MPa\sqrt{m}$
(X400)

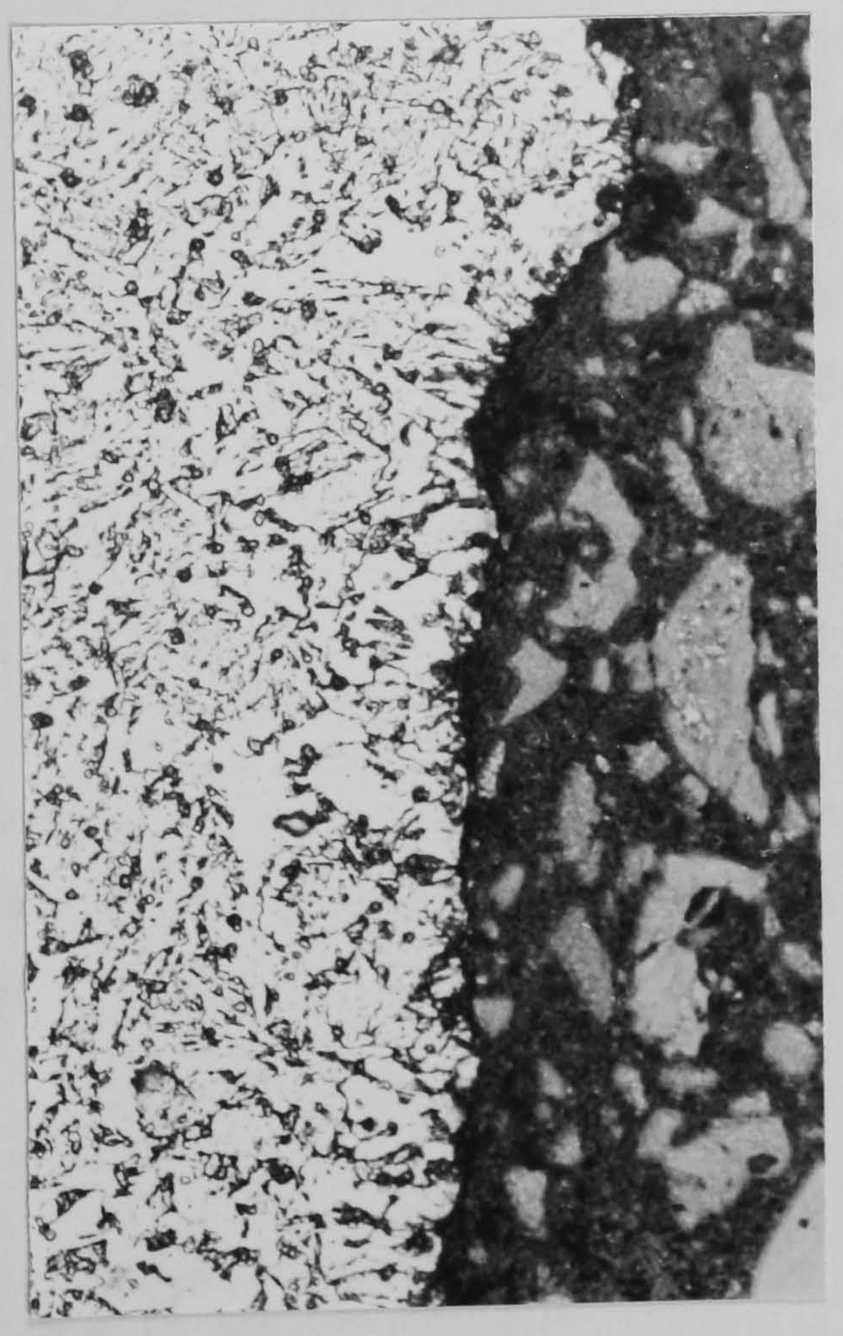

Figure 100

Crack profile of overprotected (-1050mV) BS 4360 grade 55F steel $\Delta K = 20 MPa\sqrt{m}$
(X400)

(below 24 $Pa\sqrt{m}$) a propagation mode which was independant of the stress intensity range was recorded. Above this ΔK value fatigue crack growth rate accelerated rapidly to final failure. Extensive examination of the fracture profile revealed an extremely flat fracture surface with very little crack path deviation and no evidence of crack branching. A typical region from a ΔK of 20 $MPa\sqrt{m}$ is shown in Figure 100. Despite the apparent change in crack propagation mode at a ΔK of 24 $MPa\sqrt{m}$ the crack profile characteristics remained constant.

6.3.2. Controlled rolled steel, X80 Mannesmann line-pipe

Under freely corroding conditions this controlled rolled steel has shown the same trend of reduced fatigue crack propagation rates at low ΔK values (below 19 $MPa\sqrt{m}$) and accelerated growth above this ΔK value.

Excessive corrosion was observed on the fatigue surfaces and examination in profile showed a high degree of corrosion attack.

Figure 101 is typical for this steel in the free corroding environment at a ΔK value of 18 $MPa\sqrt{m}$. Excessive pitting can be seen and a secondary crack at point 'a' has been enlarged in width by corrosion. When correctly protected (Pv = -810mV) the fatigue properties of this steel have been restored, in terms of sensitivity to ΔK, to that of the in-air results. Examination of the fracture profiles for this condition has revealed almost complete protection with only slight evidence of secondary crack enlargement. A reduction in crack path deviation has occurred and a more angular profile than the in-air result has been produced. A typical profile for this test condition is shown in Figure 102.

Testing in the overprotected condition has consistantly resulted in crack growth arrest at a stress intensity range of approximately 18 MPa $\sqrt{m}$. A metallographic section of the fatigue crack in its arrested condition is shown in Figure 103. Despite the appearance of a wide open crack this fatigue sample which has been sectioned for metallography has no external load applied. The crack has been firmly wedged open by an excessive build up of deposits from the seawater. The reduction in crack closure at minimum load was first observed optically whilst making crack length measurements, this observation was confirmed by installation of a clip gauge to a second sample. X-ray analysis of the deposit showed it to be calcareous. Clearly the formation and subsequent packing of calcareous deposits between the newly generated fracture surfaces was reducing the stress intensity range experienced by the crack tip despite the constant remotely applied load. Initial crack propagation was at a slightly accelerated rate compared to the correctly protected result however no identifiable differences exist between the two fracture profiles. However, as the effective stress intensity has been reduced the fatigue crack appears to have entered a multibranching initiation type mechanism before final arrest has occured.

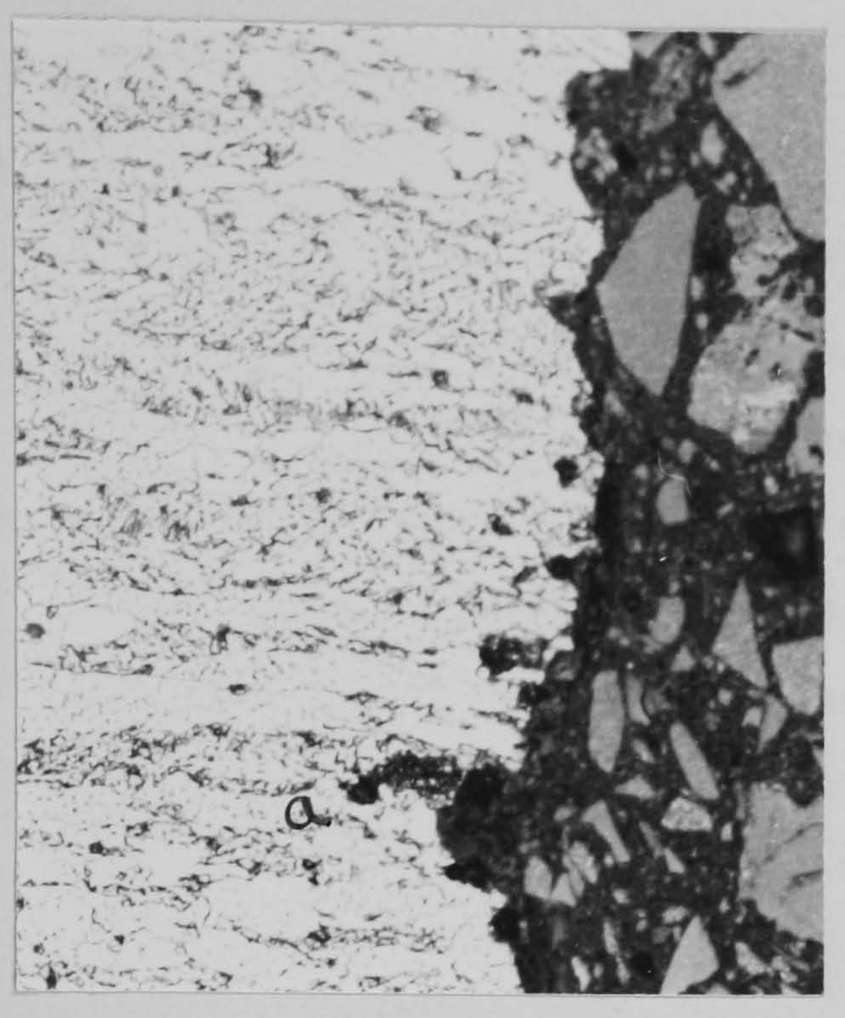

Figure 101

Crack Profile of freely corroding X80 line-pipe steel
$\Delta K = 19 MPa\sqrt{m}$
(X400)

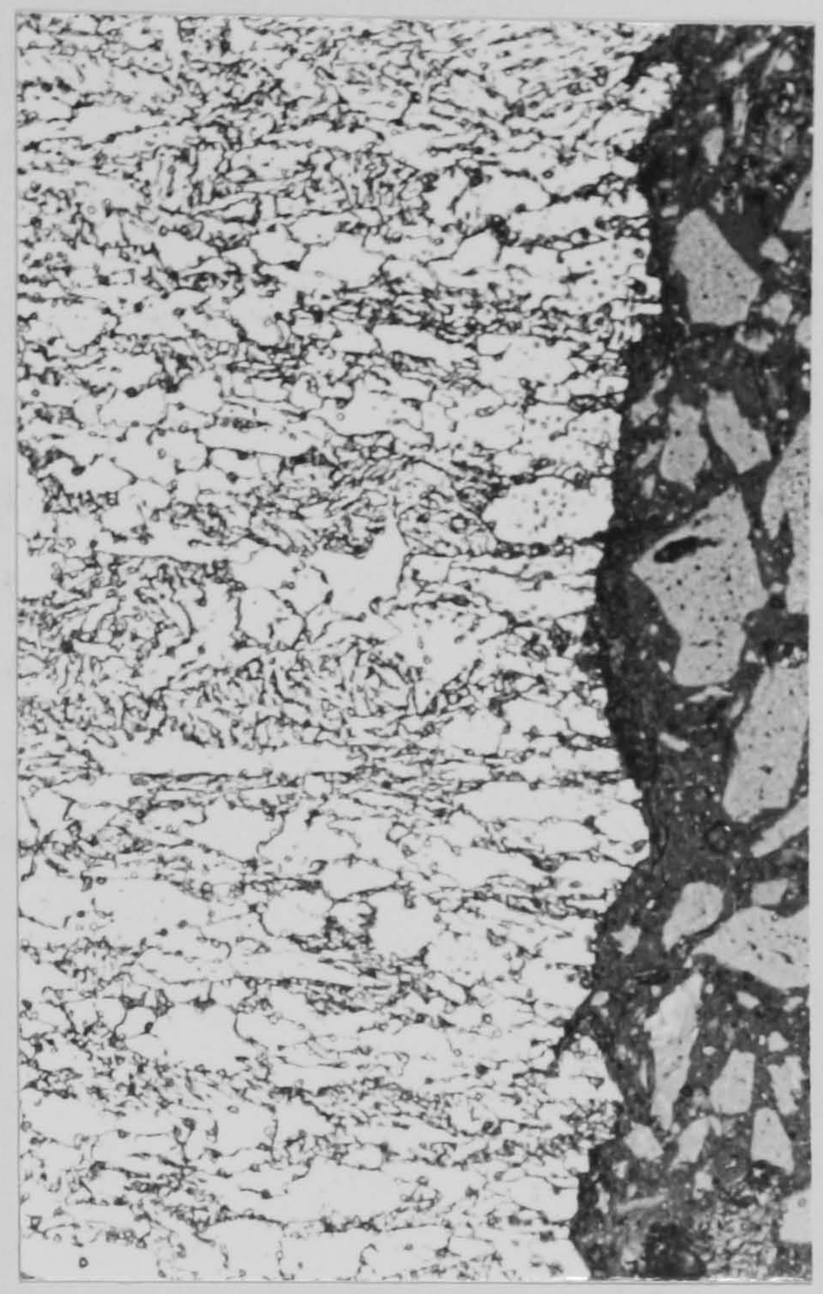

Figure 102

Crack profile of correctly protected X80 line-pipe
$\Delta K = 19 mPa\sqrt{m}$
(X400)

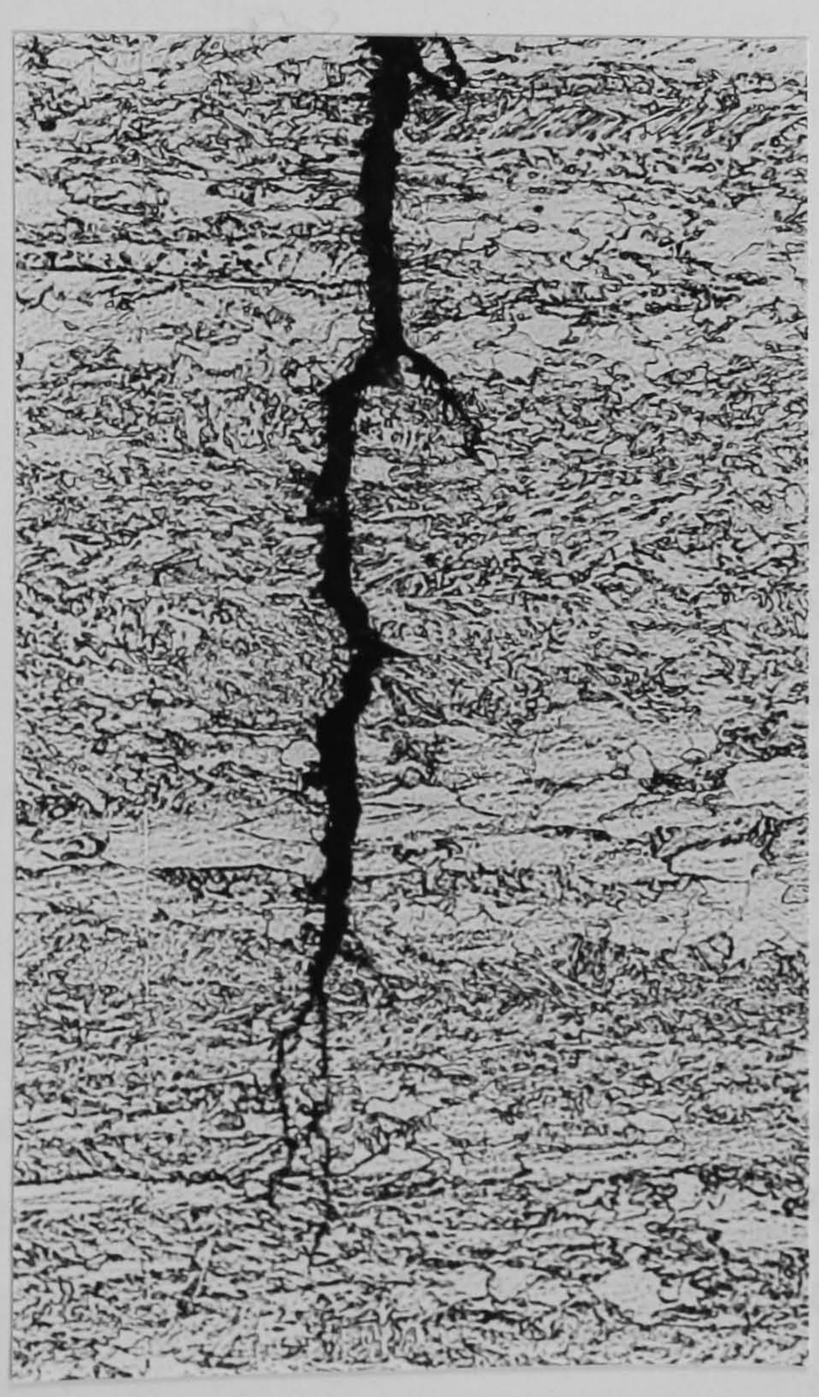

Figure 103

Crack profile of overprotected (-1050mV) X80 line-pipe after crack arrest has occured
(X350)

6.3.3. Summary of corrosion fatigue data

Both the controlled rolled and the quenched and tempered steel produced a similar response to the freely corroding test condition. The reduction in crack growth rates observed at low ΔK values is attributed to a build up of corrosion products between the newly formed fracture faces. The wedging effect of these corrosion products prevents crack closure at minimum load so reducing the ΔK values effective despite the constant remotely applied loads. At low ΔK this load range reduction outweighs the detrimental effects of the seawater environment but does not produce crack arrest. As the crack extends and the stress intensity rises so the crack growth begins to accelerate. Accelerated crack growth reduces the time available for corrosion products to build up behind the crack front and therefore their influence becomes deminished. However, the detrimental effects of a seawater environment do not deminish and so crack growth is accelerated.

Correct impressed current cathodic protection produced a similar response in both the quenched and tempered and the controlled rolled steels. A slight increase in overall growth rate was observed and a similar sensitivity to ΔK.

Over protection (Pv = -1050mV) on the other hand produced two contrasting responses. Clearly the quenched and tempered microstructure is extemely sensitive to a condition in which hydrogen is being generated. Hydrogen embrittlement has generally been associated with high strength steels, additions of substitutional alloying components like chromium and nickel cause an increase in the hydrogen solubility and martensitic microstructures such as those associated with welding have increased hydrogen suceptibility. Examination of Table II shows the main compositional differences between these two steels are

the higher molybdenum and carbon contents in the quenched and tempered steel. The form of the carbide is particularly important and with the quenched and tempered steel having a relatively high carbon content of 0.12% any adverse effect of carbide form will be accentuated. A fatigue crack growth mechanism dominated by the sensitivity of a microstructure to hydrogen has led to a ΔK insensitive response. At greater crack lengths the increased stress intensity (above 24 MPa $\sqrt{m}$) becomes a contributing factor to accelerated crack growth.

The initially accelerated fatigue crack growth occuring in the Controlled rolled X80 line pipe steel was not very significant indicating a microstructure which is tolerant to a hydrogen producing environment. This is despite its similar yield strength to the quenched and tempered steel. Any steel which is not sensitive to hydrogen is likely to benefit from the effects of calcareous deposit build-up on fatigue fracture surfaces even at a high stress ratio as used in this study (R = 0.6).

6.4. Constant ΔK Fatigue Crack Propagation Through a Microstructural Gradient

The results for a continuously monitored and closely controlled fatigue crack propagation experiment under constant ΔK conditions have shown unique growth characteristics for different microstructures. In addition they have identified a very wide range in local fatigue crack growth rates which would not have been observed by any previous crack monitoring system. The duration of this test was 13 days or 110,000 cycles during which time over 660 crack length measurements were recorded. The total crack extension was 3.54mm giving an average propagation rate of 2.97×10^{-8}m/cycle. The stress intensity range was monitored at 19.5 MPa $\sqrt{m}$ throughout this test. The crack length was digitally recorded every 30 minutes (180 cycles)

to an accuracy of 0.01mm (resolution 0.005mm) thus giving a very detailed record of fatigue crack propagation. The detailed a/N data recorded by this procedure is found in section 5.5. Figures 69 to 73.

After a carefully controlled pre-fatigue the continuously monitored test was started with the crack front within the weld metal microstructure. The initial 1.05mm of crack extension within the weld-metal microstructure occured over a 30060 cycle period giving an average crack propagation rate of 3.49×10^{-8}m/cycle. Closer examination of the data reveals a discontinuous nature to fatigue crack growth within this microstructural region. Periods of low crack propagation rate down to 1.06×10^{-8}m/cycle for periods up to 3800 cycles have occured followed by periods of extremely rapid growth exceeding 2.75×10^{-7}m/cycle for a 180 cycle period. Metallographic examination of the weld metal region of fatigue fracture surface and profile has shown crack path deviation to be relatively minor. Figure 104 shows that the fracture surface for the weld metal region is relatively planar and has no significant secondary cracking. The area shown in Figure 104 is one which exhibited faint striations the spacing of which correspond approximately to the area of accelerated fatigue crack growth for this region. Striation spacing corresponding to the lower propagation rate could not be resolved.

At a crack extension of 1.05mm the fatigue crack front entered a period of sustained accelerated growth. A crack extension of 0.11mm over a cyclic period of 720 cycles occured giving a growth rate of 1.53×10^{-7}m/cycle. The fatigue crack profile for this region of sustained accelerated growth is shown in Figure 105. The fatigue crack appears to follow a crystallographic plane for a distance of 100μm before normal crack orientation is restored. Examination of the fracture surface within the 100μm accelerated growth region revealed a major departure

from a striation forming mechanism. This can be seen in Figure 106 which clearly shows the formation of micro cracks as a result of fatigue crack propagation within this microstructural region. The spacing of the micro cracks corresponds very closely to the observed fatigue crack propagation rate. The crack propagation mechanism which promotes the formation of micro cracks clearly leads to accelerated fatigue crack growth. This extremely narrow band of accelerated fatigue crack growth would not have been identified using any previously encounted experimental technique.

Fatigue crack propagation through the microstructural gradient of the mid to fine HAZ is more continuous in nature. In this microstructural region the fatigue crack propagation alternates between periods of relatively low but sustained growth, approximately 1.50 x 10^{-8} and areas of higher propagation rates, approximately 7.20 x 10^{-8}m/cycle. These regions of sustained growth typically vary between 0.05 and 0.15mm. A typical region from the mid to fine HAZ is shown in Figure 107. This photograph clearly shows an increased occurance in secondary cracks and a marked increase in crack path deviation. Striations are only faintly visable on this fracture surface. Close to the finest grain size region of the HAZ, fatigue crack growth has become more and more continuous with any change in growth rate occuring over a longer cycle period. On entering the parent plate the nature of the a/N curve has become very smooth and continuous with a growth rate of 2.78 x 10^{-8}m/cycle which is only 2 x 10^{-9}m/cycle slower than the average rate for the entire experiment but is however a factor of ten slower than the measured growth rate in the 100μm wide course gained HAZ. The fracture surface for the parent plate can be seen in Figure 108. Fine striations are clearly visable on this multiplanar fracture face. A similar frequency of occurance of secondary cracks was observed to the fine HAZ. From the

recorded crack growth data and the metallographic study of the fatigue crack characteristics it is clear that the mechanism by which crack extension is occuring is in fact changing with the microstructural gradient. A micro hardness survey across the microstructural gradient, Figure 109, gives an indication of the changing hardness and therefore yield strength from weld metal, through the HAZ and into the parent plate.

The average hardness in the weld metal is Hv = 290. This falls to Hv = 265, 0.4mm away from the fusion boundary at which point the hardness rises rapidly to a maximum Hv = 435 approximately 0.1mm into the HAZ. The hardness falls from this peak to the average parent plate value in an erratic manner. The average parent plate hardness is Hv = 208. A hardness range of 56 vickers points was encounted within the weld metal whilst the range within the parent plate was only 18 points. Clearly fatigue crack propagation rate cannot be linked to yield strength as indicated by the hardness of a microstructure as despite the wide range of hardness values recorded the average propagation rate within the weld metal, HAZ and parent plate has remained relatively constant. However local propagation rates within each microstructural region have varied extremely dramatically with clear evidence from metallographic study of a change in propagation mechanism. It is interesting to note that the region of highest hardness and therefore yield strength has produced the longest period of sustained rapid crack growth due to a departure from a ductile striation mode of crack extension.

Whilst a steady state propagation would have been observed using conventional crack monitoring techniques, the new technique developed for this study has shown a wide range in local propagation rates due to microstructural influences. The coarse grained region of HAZ microstructure which produced a greatly accelerated fatigue crack

propagation rate was very small (0.1mm) and would not have been identified by other experimental techniques. Although small, this microstructural region is likely to be present in an area of high stress concentration and could therefore offer an easy site for fatigue crack initiation.

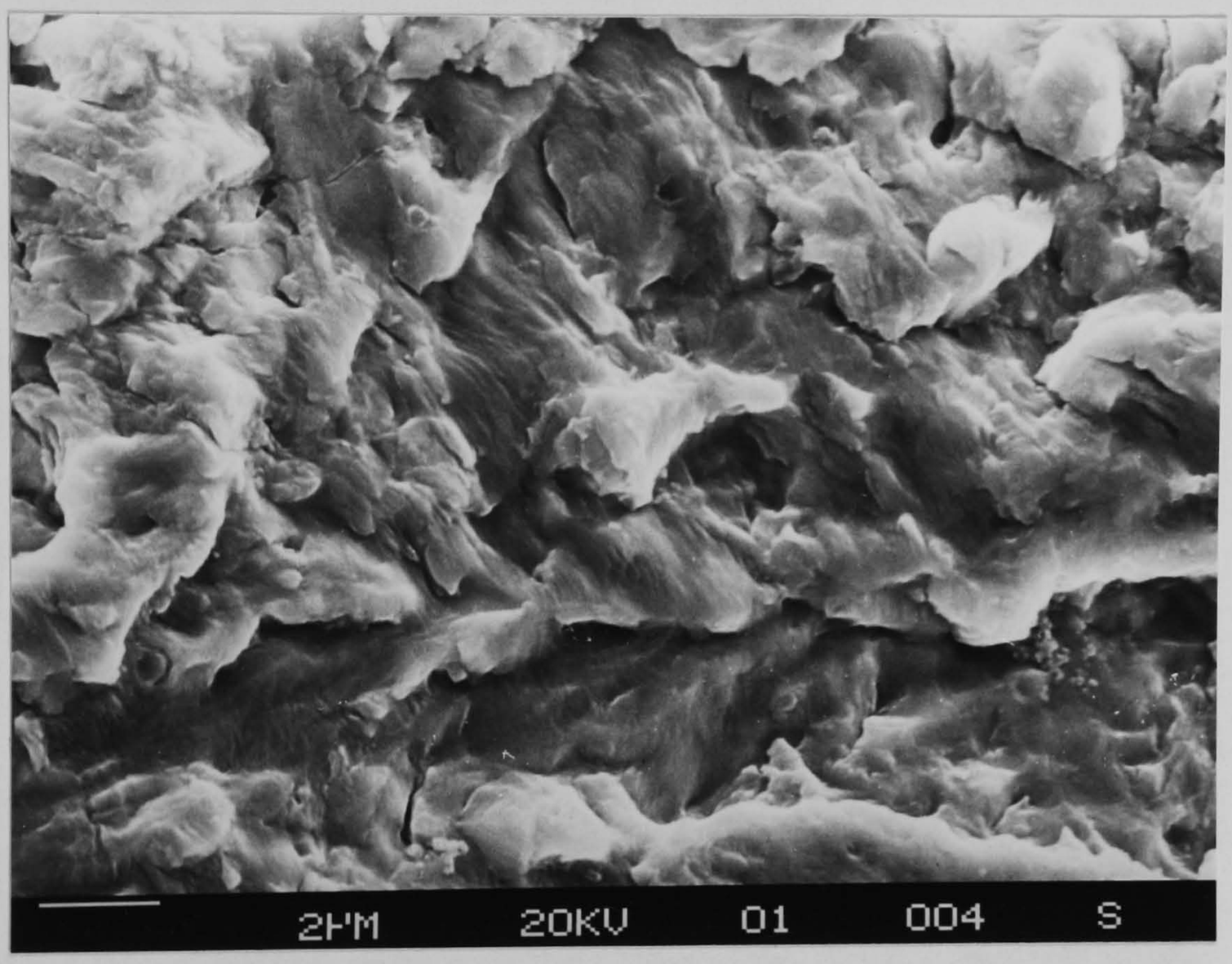

Figure 104

Fatigue fracture surface in weld metal microstructure showing faint striations

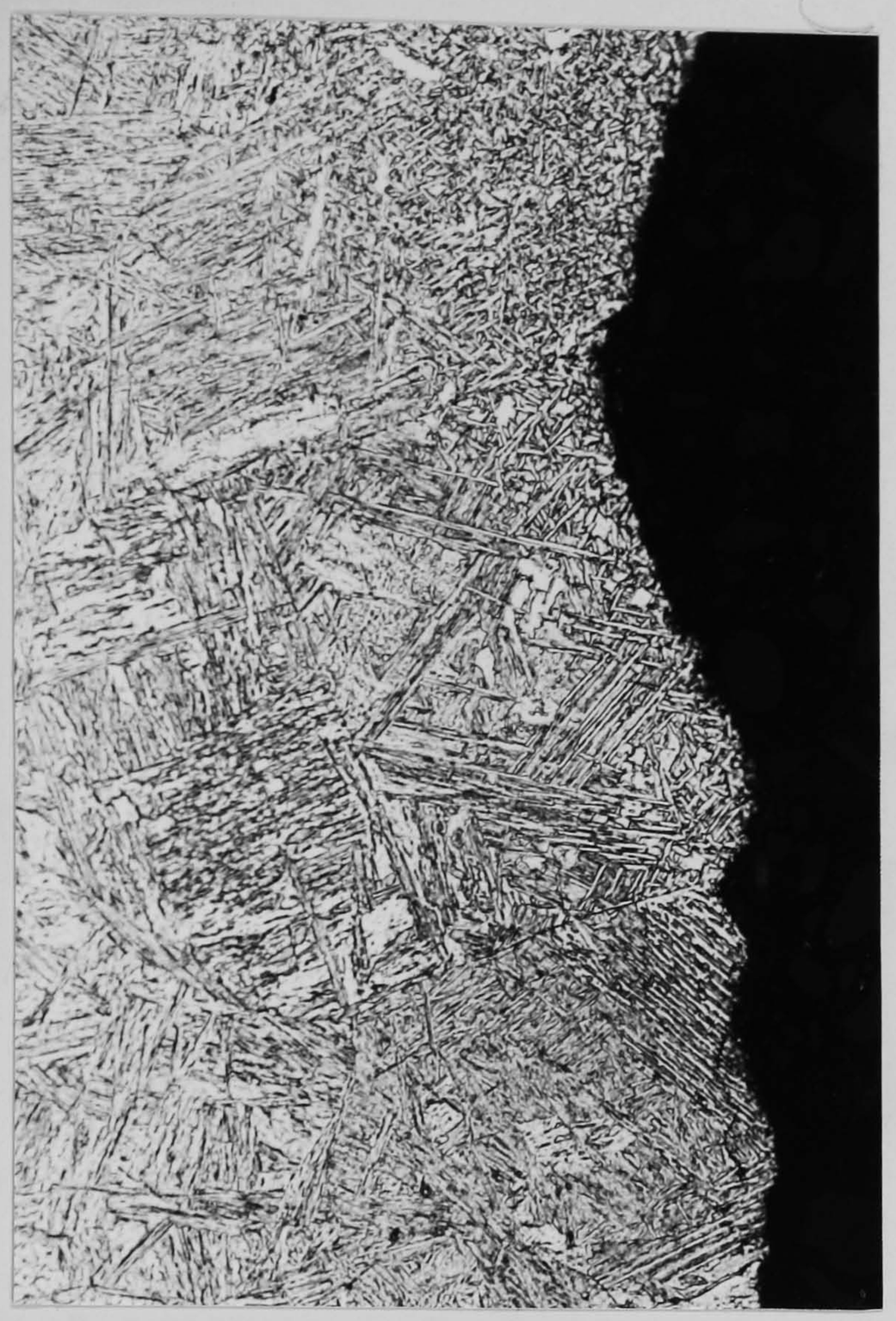

Figure 105

Fatigue crack profile in region of sustained accelerated growth (1.53×10^{-7} m/cycle)

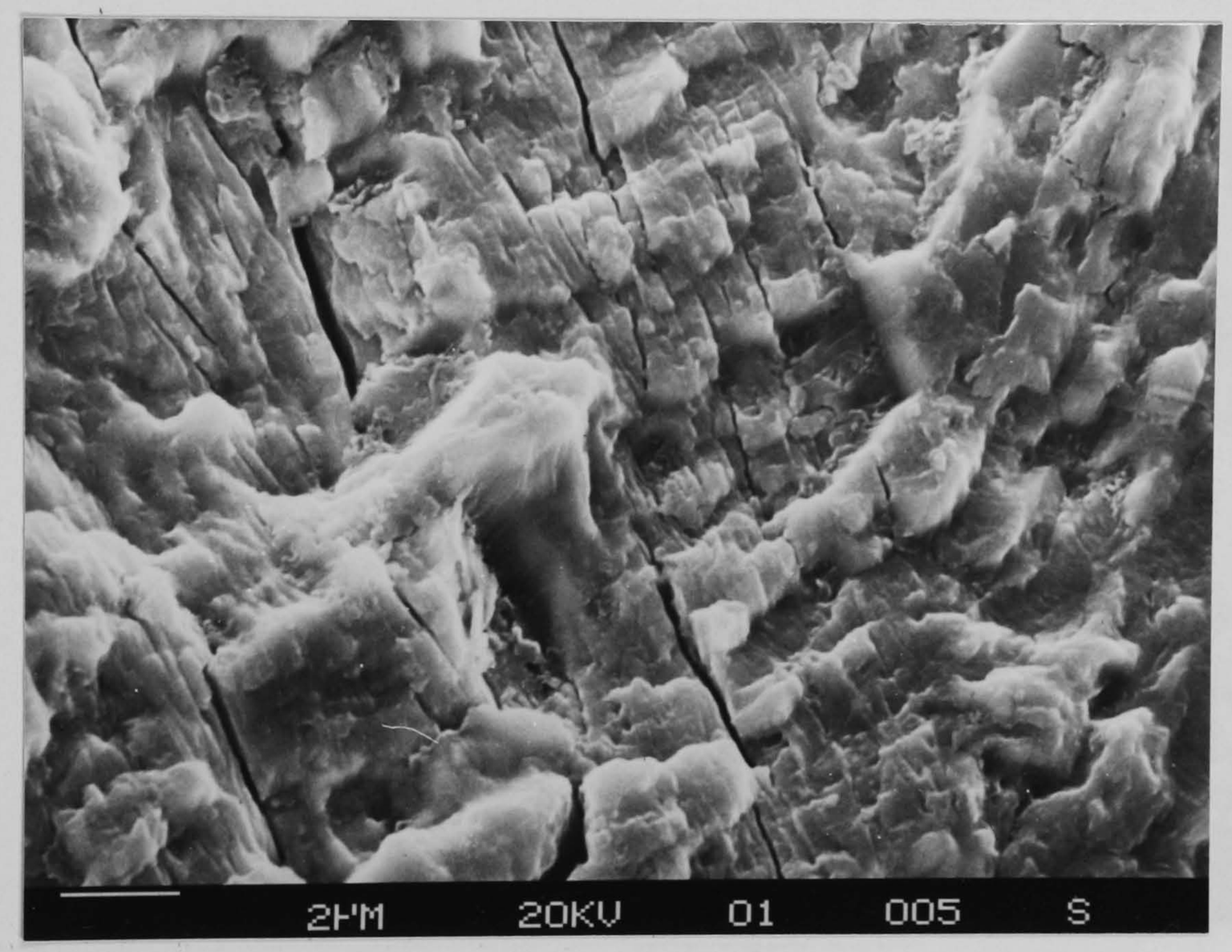

Figure 106

Fatigue fracture surface in region of sustained accelerated growth showing formation of fine micro cracks

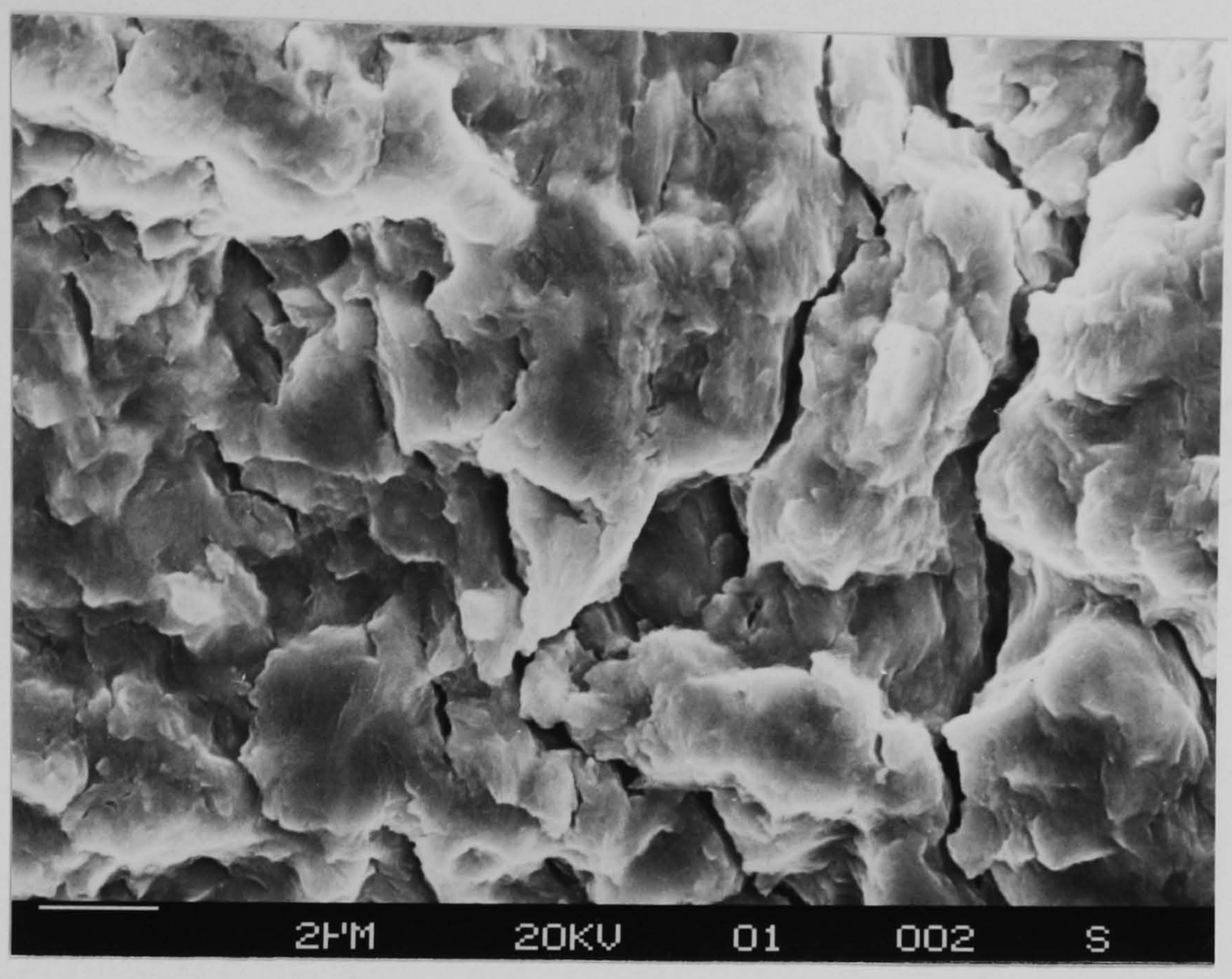

Figure 107

Fatigue fracture surface in mid to fine HAZ, secondary cracks are evident but striations are indistinct

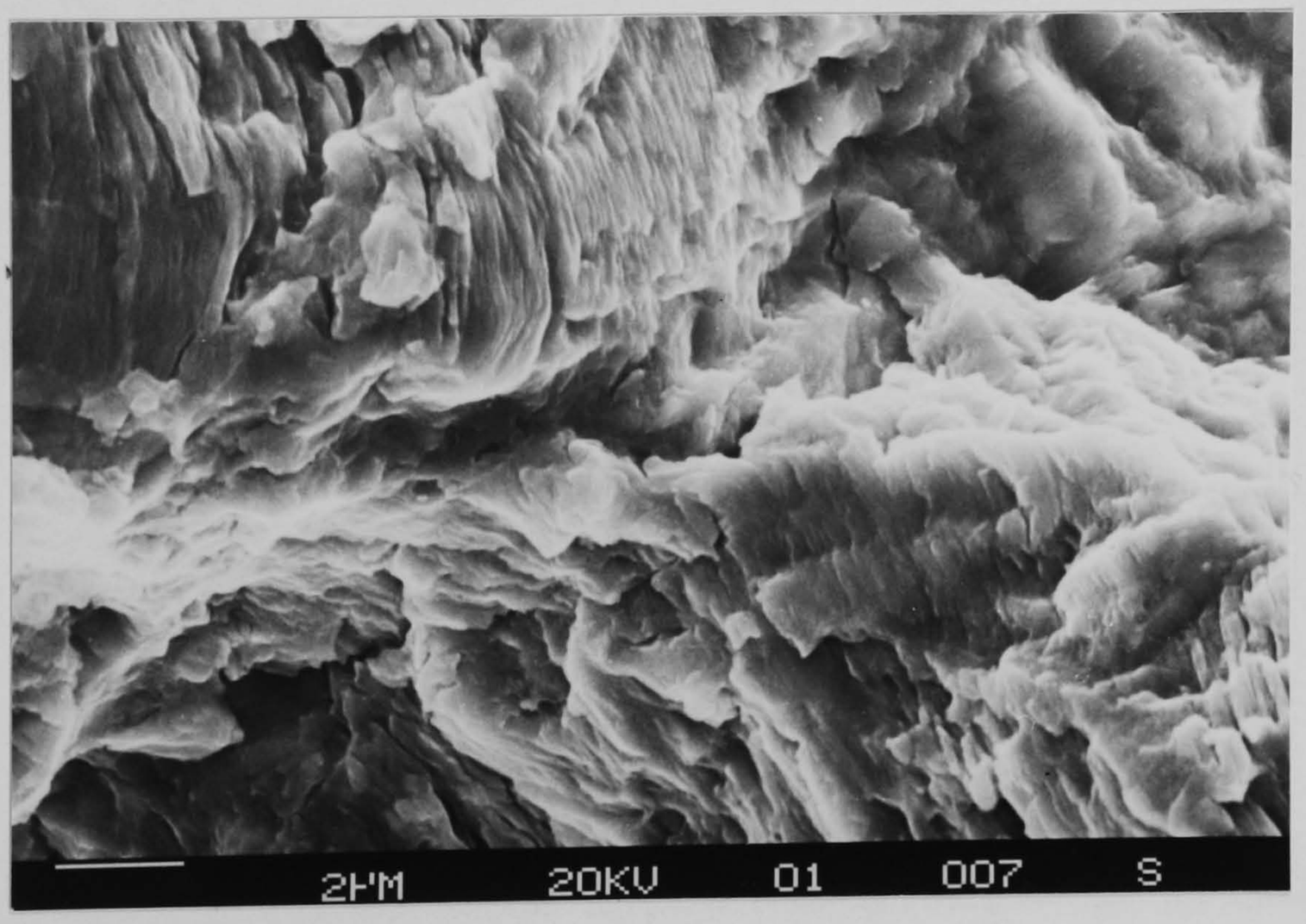

Figure 108

Parent plate region with an abundance of striations on the fracture surface

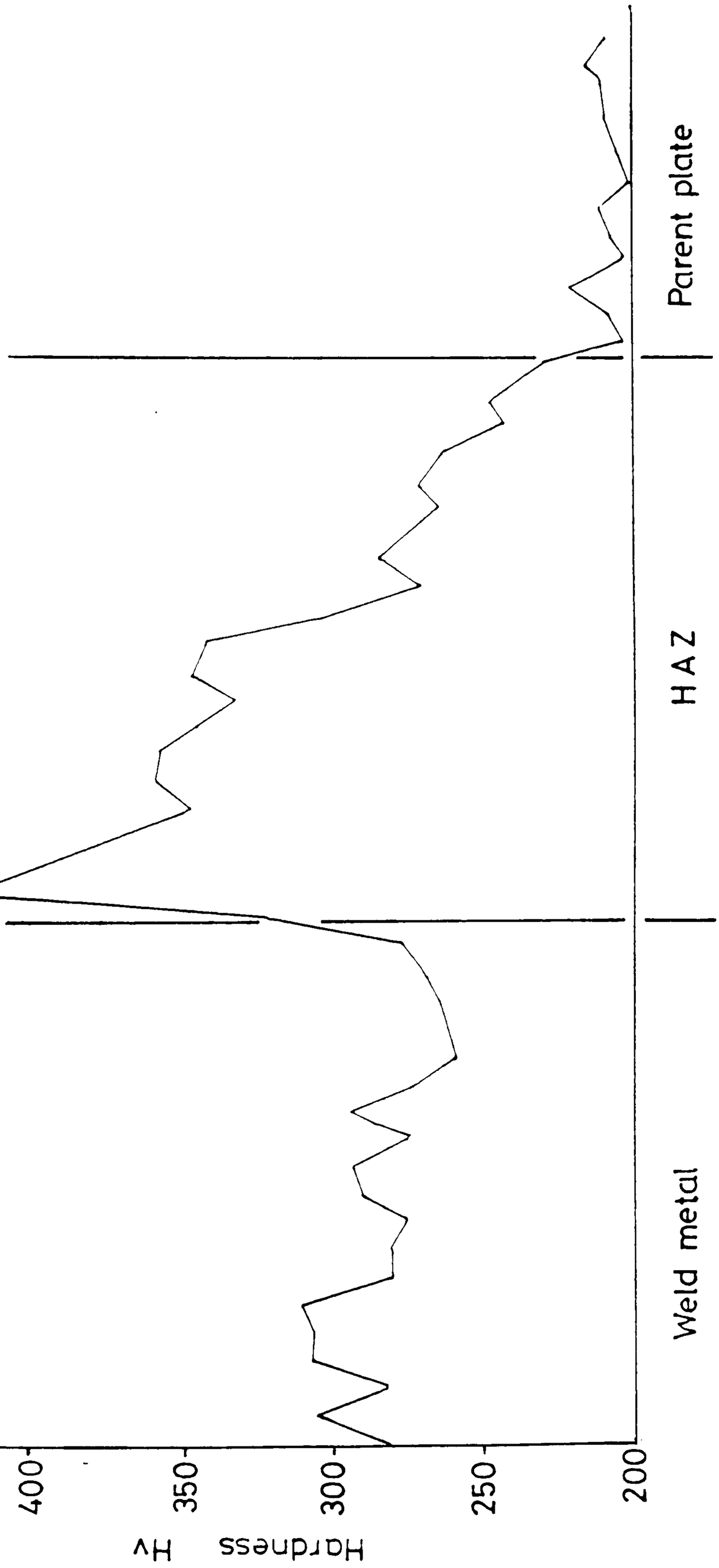

Figure 109 Microhardness survey accross the microstructural gradient through which the constant K crack was grown.

7.0 DISCUSSION

7.1 Fatigue Crack Elastic/Plastic Interactions

If an understanding of fatigue crack propagation mechanisms is to be gained we must first consider a sharp crack in a plate and the effect of a remotely applied load on the crack tip and its surrounding material. As the uniaxial applied load is increased a stress state is generated at the crack tip. If the crack tip was infinitely sharp then the stress concentration generated would instantly exceed the yield stress and the crack would become blunted. Therefore, our so called "sharp" crack can only be sharp on a macro and not atomic level.

We must also consider the stress state in terms of constraint. A crack in a thin plate will be in a state of plane stress. This means a non-hydrostatic stress state and the possibility of shear at the uniaxial yield stress, and therefore no constraint on yielding.

By contrast, in a thick plate the stress state will contain an important hydrostatic component which will reduce the effective shear component. Thus a higher applied stress will be required to produce the local strains needed for shear to occur. Clearly yielding is constrained.

For the purpose of this discussion we will consider the unconstrained plane stress condition and the behaviour of the material directly ahead of the crack tip in terms of elastic and plastic components.

7.1.1. Plastic zones

A plastic zone is a region of material ahead of the crack tip which has both an elastic and a plastic strain component. If we consider what happens at the crack tip

upon loading the nature of a plastic zone will become apparent. The stress developed at the crack tip is dictated by the stress intensity factor and cannot be evaluated by remotely measured loads. As the stress is applied to the crack, low local strains will occur of an elastic nature. Exceeding the yield stress at the crack tip will result in yielding and associated work hardening. Thus a nonrecoverable component will occur in addition to the measureable elastic component. The area over which this plastic component is effective is termed the plastic zone. The relationship between elastic and plastic components within a plastic zone have been described with the stress intensity factor K in the form:

$$\varepsilon_{ij} = \frac{K}{\sqrt{2\pi r E}}\, g_{ij}(\nu, \theta) \qquad (14)$$

$$\sigma_{ij} = \frac{K}{\sqrt{2\pi r}}\, f_{ij}(\theta) \qquad (15)$$

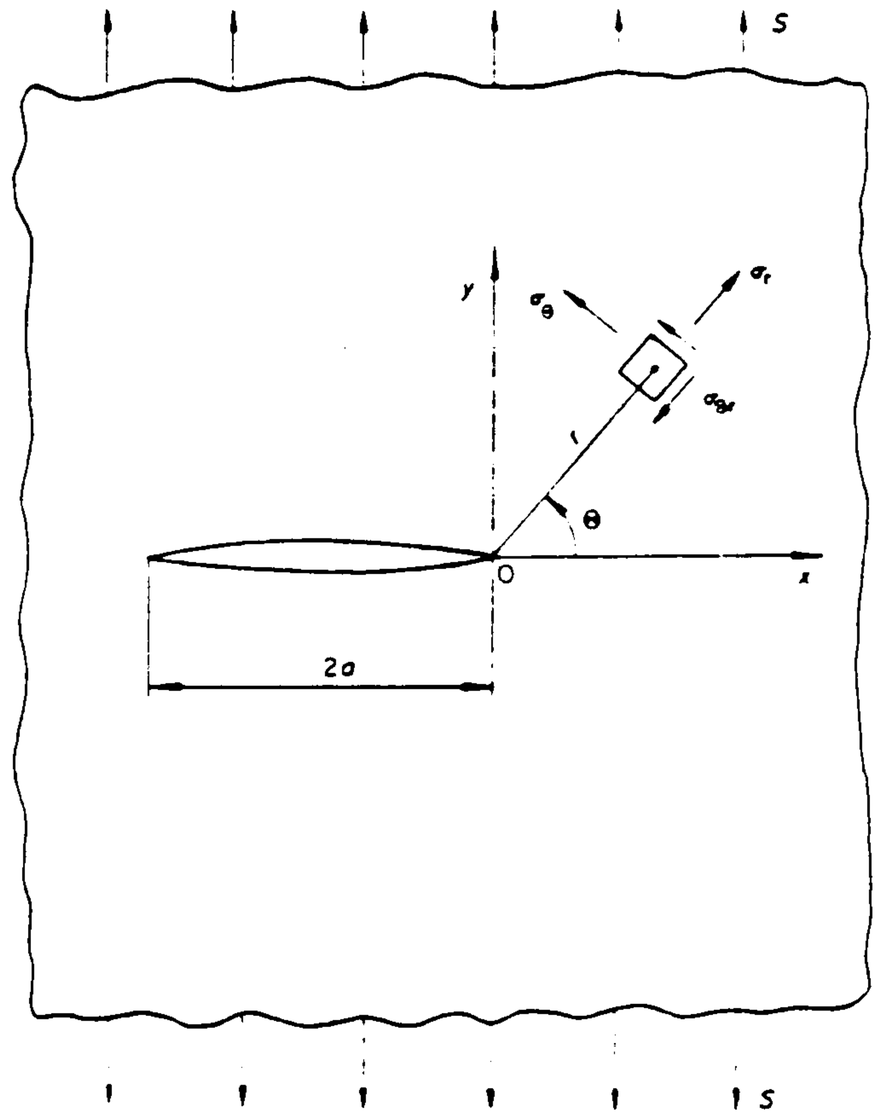

Figure 110 Through crack in an infinite plate

However, in a real material a plastic zone is created at the crack tip so these expressions are only valid outside the plastic zone.

Hutchinson (87) used the well known Ramburg-Osgood stress/strain relation:-

$$\tilde{\varepsilon} = \tilde{\sigma} + \alpha(\tilde{\sigma})^{N'} \qquad (16)$$

to solve the problem of elastic/plastic strains and stresses at the crack tip. He demonstrated that the stress/strain relationship can be discribed according to the following equations:-

$$\tilde{\varepsilon}_{ij} = \tilde{g}_{ij}(\nu, \theta, N') \left(\frac{S^2 a}{\sigma_y{}^2 r} \right)^{1/(N'+1)}$$

$$+ h_{ij}(\theta, N') \left(\frac{S^2 a}{\sigma_y{}^2 r} \right)^{N/(N'+1)} \qquad (17)$$

$$\tilde{\sigma}_{ij} = \tilde{f}_{ij}(\theta, N') \left(\frac{S^2 a}{\sigma_y{}^2 r} \right)^{1/(N'+1)} \qquad (18)$$

Irwins solution is shown together with the Hutchinson model and suggested modifications by Glinka (89) in Figure 111.

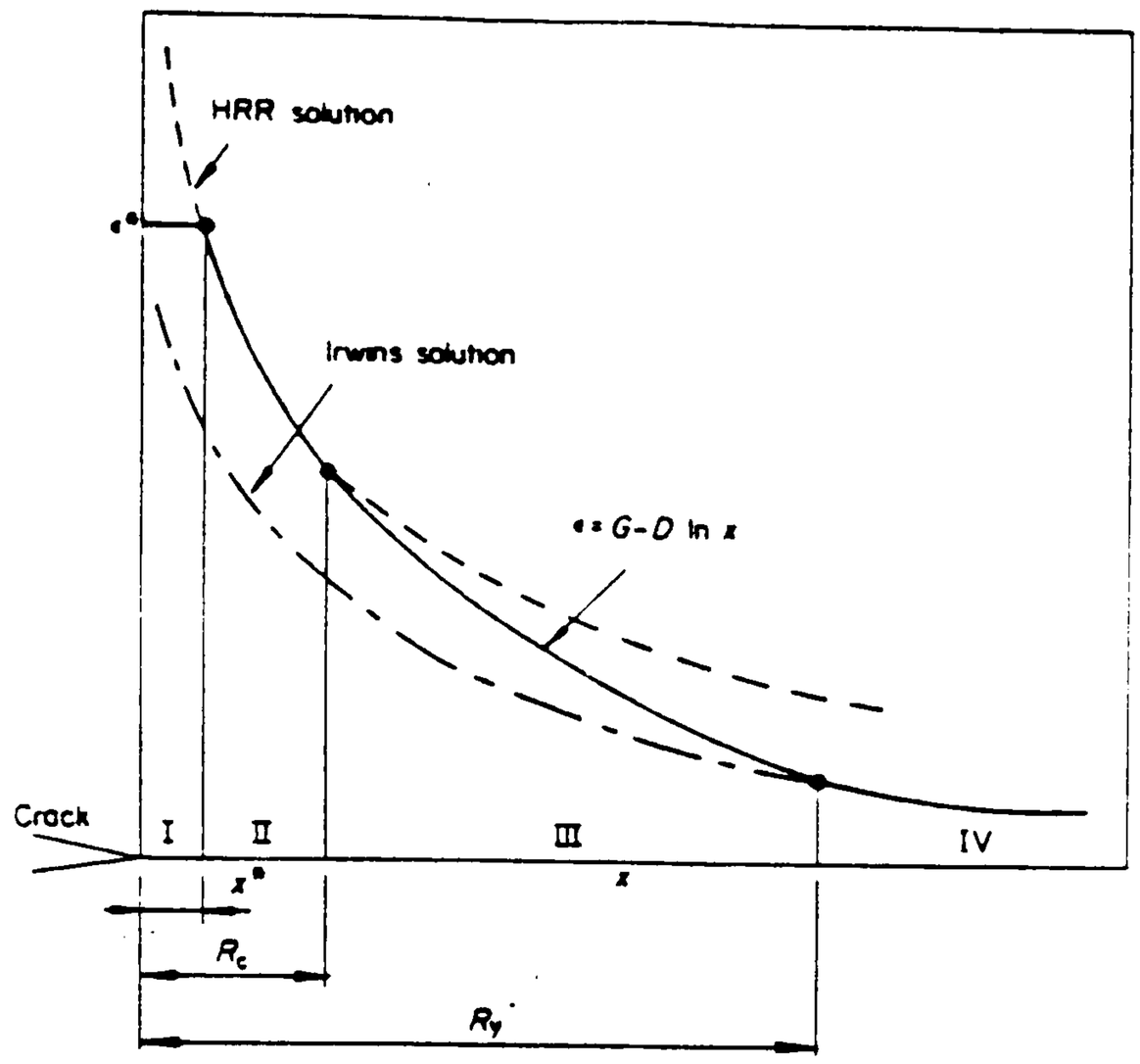

Figure 111 Theoretical strain distribution ahead of the crack tip

The strain distribution ahead of the crack tip has been divided into four regions. Glinka (89) has suggested that the region adjacent to the crack tip cannot be discribed by either solution and is a region of very high finite strain with a low strain gradient. Region II exhibits a high strain gradient which will be higher than that predicted by the Irwin solution. It is suggested that this region is approximately as wide as the reversed plastic zone at the crack tip and is best described by the Hutchinson Solution. In Region III the plastic strain component is reducing with distance from the crack tip until Region IV is reached. Again Glinka suggests neither the Irwin solution nor the Hutchinson model correctly describes this region and has proposed an expression of the form:

$$\varepsilon = G - D.\ln X \qquad (19)$$

based on experimental (90) and theoretical results. Region IV is outside the plastic zone and therefore the domain of elastic behaviour where Irwins model is valid.

The maximum size of the plastic zone is related to the yield strength and the highest stress intensity, Kmax, produced at the crack tip. A description of the monatonic plastic zone size is given by:-

$$Z = \frac{1}{2\pi}\left(\frac{Kmax}{\sigma_y}\right)^2$$

$$\text{where } Kmax = \frac{\Delta K}{(1 - R)} \qquad (20)$$

where Z is a distance in front of the crack tip below which plasticity is encounted at maximum load.

7.1.2. Reverse plastic flow

As a remotely applied load, on a crack within a polycrystalline material, is increased so the stress at the crack tip will quickly rise until the yield strength is exceeded. Crack tip blunting will then occur and a plastic zone will be created. The plasticity within this zone is a result of dislocation movement along favourable slip planes in suitably orientated grains giving an anelastic strain component and also reinitiation of dislocations accross grain boundaries to give a nonrecoverable plastic strain component. Clearly the extent of plasticity will depend upon the load and will be at its greatest at peak load. As

the applied load is removed the elastic strain within the plastic zone and in the bulk elastic material will be recovered. The plastic zone has undergone a volume increase the vast majority of this volume change being attributed to plastic deformation and only a very small proportion to an elastic strain. The recovery of elastic strain in the bulk elastic material will therefore put the plastic zone into a compressive stress state. It is possible that this compressive stress may be great enough to promote reverse plastic flow as well as an elastic strain recovery. This gives rise to the reverse plastic zone which is a measure of plastic recovery during a fatigue cycle. This phenomenon has been reported by Glinka (89) and is depicted as Region II in Figure 111.

If a ductile specimen is plastically strained first in tension and then in compression, the strain hardening is found to have operated in both directions. However, there is some initial discrepancy between the two yield values in the forward and reverse direction. This is known as the Bauschinger effect and is illustrated in Figure 112.

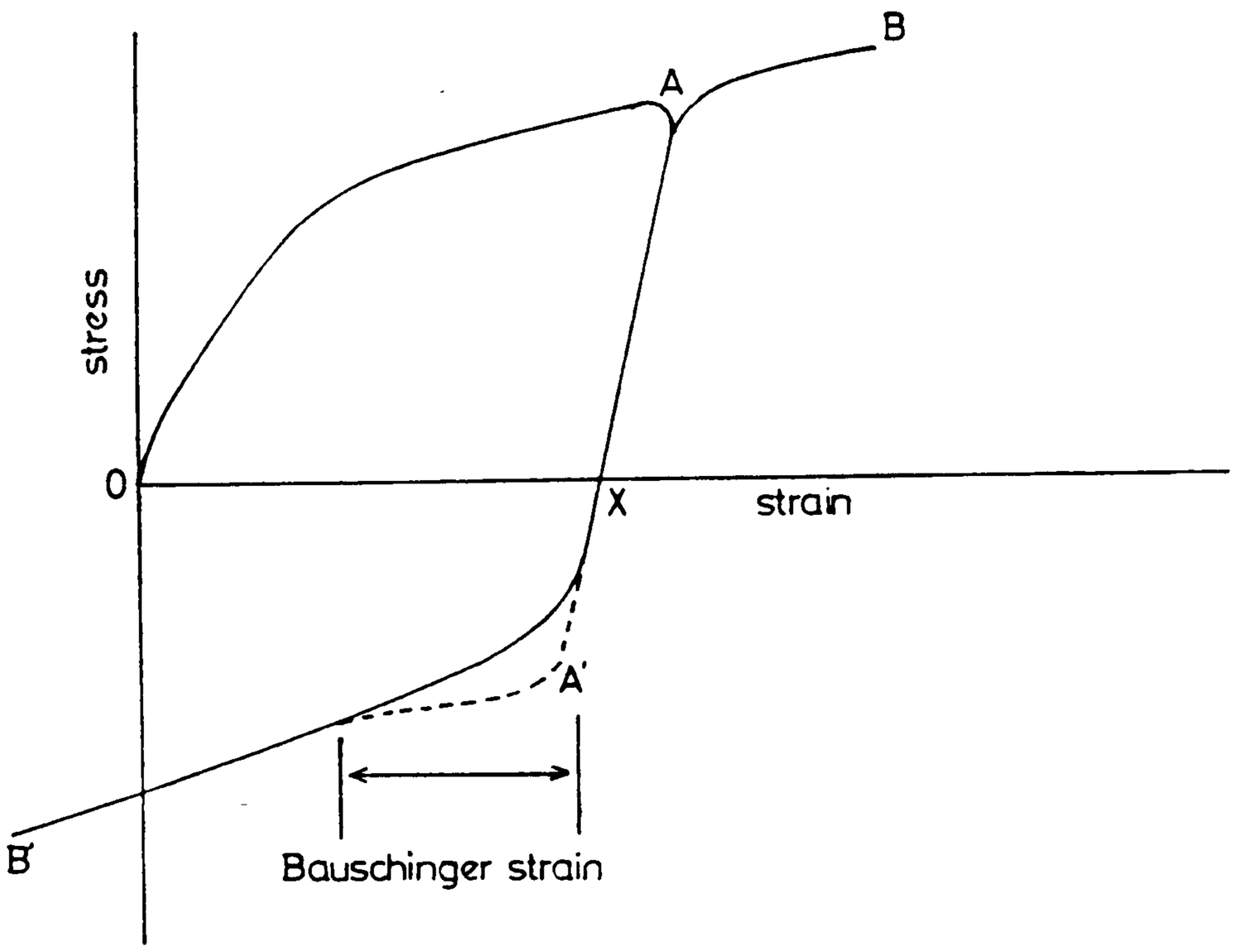

Figure 112 The Bauschinger strain effect.

Although the yield stress is initially rather lower in the reverse direction of straining it soon rises to the former value as if no change in the direction of straining had occurred. Whilst this effect will favour reverse yielding, there is no stress intensity factor for compression and so yielding will not be enhanced. As reverse plastic flow occurs in response to the compressive stress applied by the elastic strain recovery, so the residual stress is not great enough to cause yielding. Thus the strain gradient in front of the crack tip created by the plastic zone will be modified by any reverse plastic flow. The effect of reverse plastic flow will be a further increase in yield as compressive work hardining occurs.

The importance of reversed plastic flow is not well established nor indeed is whether it actually occurs under different loading conditions. Clearly this type of mechanism would have a delaying effect on crack growth as a measure of plastic recovery will have occurred.

7.1.3. Effect of an overload on fatigue crack propagation

Overload is taken to mean an applied cycle in which the Pmax is much higher for one cycle than on previous cycles. This type of loading sequence is shown in Figure 113.

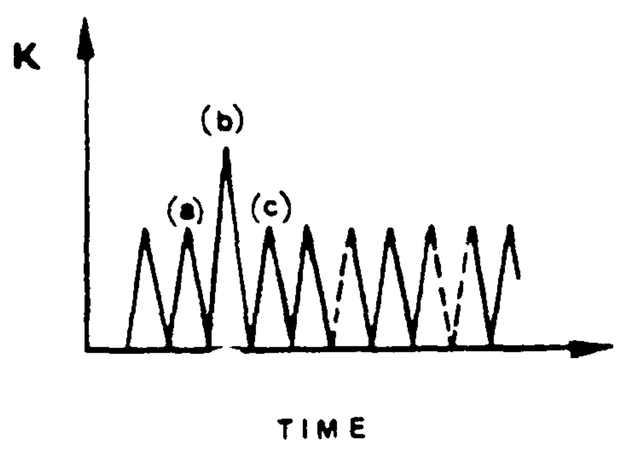

Figure 113 Normal loading sequence with peak overload (b)

As Pmax (overload) is applied we must consider what happens to the crack tip plastic zone and the crack tip shape.

The plastic zone in an overloaded sample has a greater volume so creating a higher residual compressive stress state than is present after normal loading. Clearly the compressive stress state will have a delaying effect on crack propagation over subsequent normal loading cycles by reducing the effective stress intensity at the crack tip. This stress intensity reduction may result in crack arrest.

Work by Robin et al (92) has attempted to relate the influence of residual stress on overload retardation. Materials of differing yield strength and consequently different plastic zone sizes were investigated. The evaluation of crack growth rate and of the crack opening ratio obtained at an overload ratio of 2.5 are plotted below.

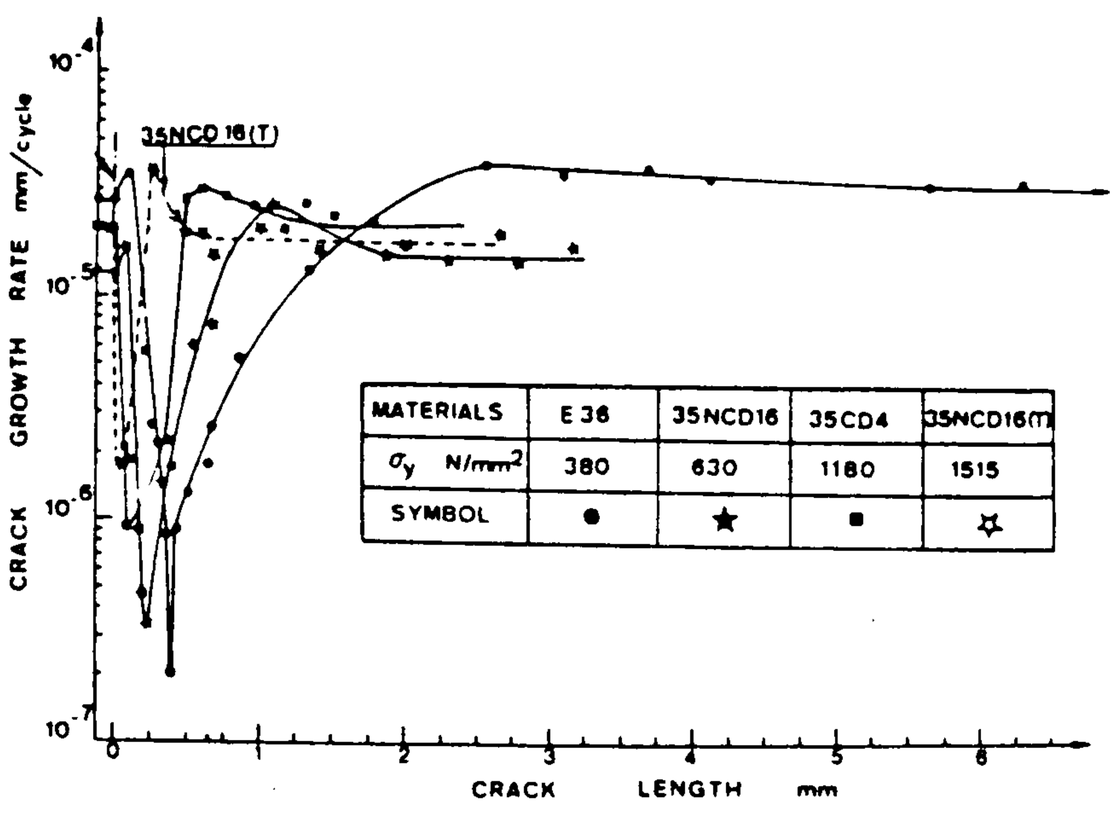

Figure 114 Effect of the yield stress on the crack propagation rate after overload, Rpeak = 2.5

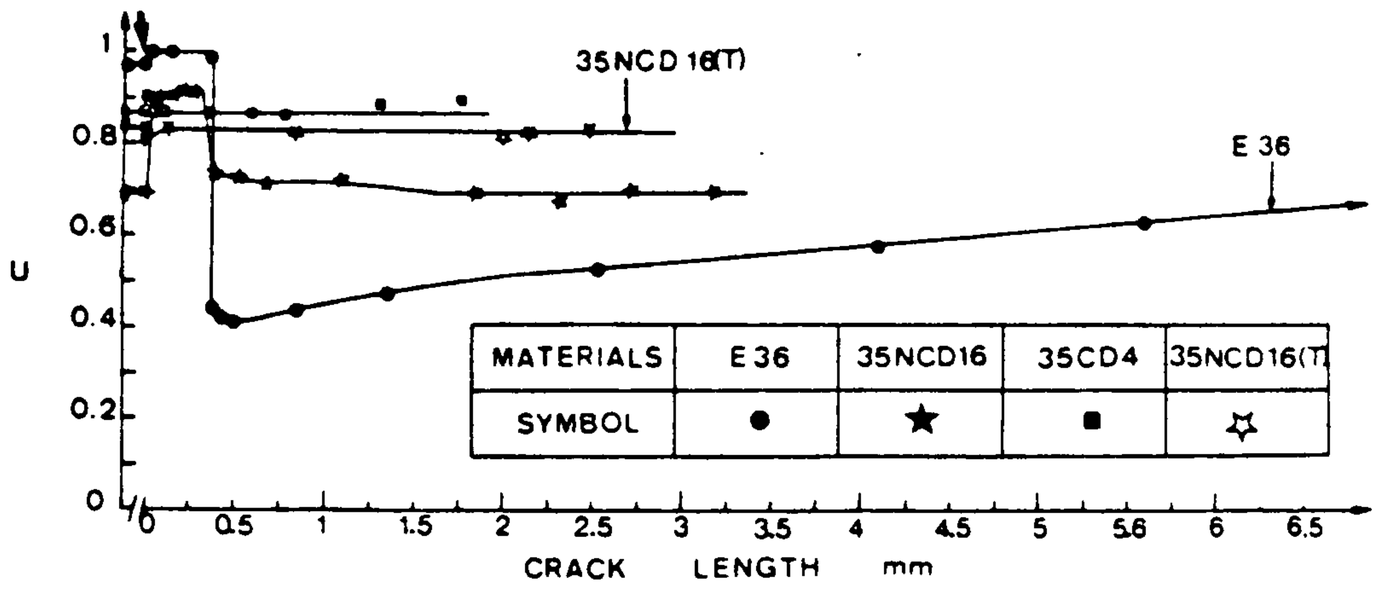

Figure 115 Effect of the yield stress on the U ratio after an overload, Rpeak = 2.5

From these results it would appear that crack retardation is strongly affected by the yield strength and consequently the plastic zone size. The crack opening ratio also shows dependance on the yield strength; the lower the yield strength of the material, the greater is the variation of the crack closure load.

Models have been developed, based on plastic zone theory, by Fuhring et al (93) and Matsuoka et al (94) in an attempt to predict crack retardation for a specimen subjected to the loading sequence as shown in Figure 113. After the overload, a new tensile plastic zone is created, four times smaller than the original one. This is because of a compressive stress state resulting from the overload plastic zone. Fuhring shows that the new tensile plastic zone decreases until a crack length a_F has been reached at which the tensile plastic zone size after is at its smallest. Matsuoka disagrees and suggests that the tensile plastic zone size remains constant until the crack reaches a length a_M. The tensile plastic zone size subsequently increases by both models. For plastic zone size calculations both models assume an ideal stationary crack and that the magnitude of the residual stresses are not affected by the crack growth.

McCartney (95) has suggested a further effect influencing a delay after overload. The superposition method for residual stresses following overloads leads to predictions of crack closure and hense retardation during the propagation of a crack through its overload plastic zone. However, this effect is unlikely to be important at high stress ratios (above R = 0.4).

Work by Robin et al, (92) on the influence of a single peak overload on the propagation of fatigue cracks in E36 steel has shown that the Elber crack closure concept cannot explain the retardation phenomenon since changes in the crack growth rate and the crack opening ratio were not found to be similar.

At the beginning of this discussion we assumed that the crack tip does not change shape on appliances of an overload and clearly this is not true. Upon application of a single peak overload in E36 steel, Mille (96) has

observed an immediate broadening of the load/crack mouth opening diagram which is assumed to be an indication of crack tip blunting. However, as this effect is only seen for a few cycles in which retardation occurs, it seems that crack tip blunting is unable to explain the effects of overloads.

7.1.4. Crack closure

A fatigue crack subjected to a cyclic load with a stress ratio of one would fully close at minimum load. However the wake of plastic deformation formed on previous loading cycles may prevent this from occuring. Clearly this will have an important effect on the stress/strain relationship around the plastic zone preceeding the crack tip. If the crack is not allowed to fully close the elastic strain within the material immediately surrounding the plastic zone will not be relieved, leading to high residual compressive stresses being applied to the plastic zone region. This situation is illustrated in Figure 116.

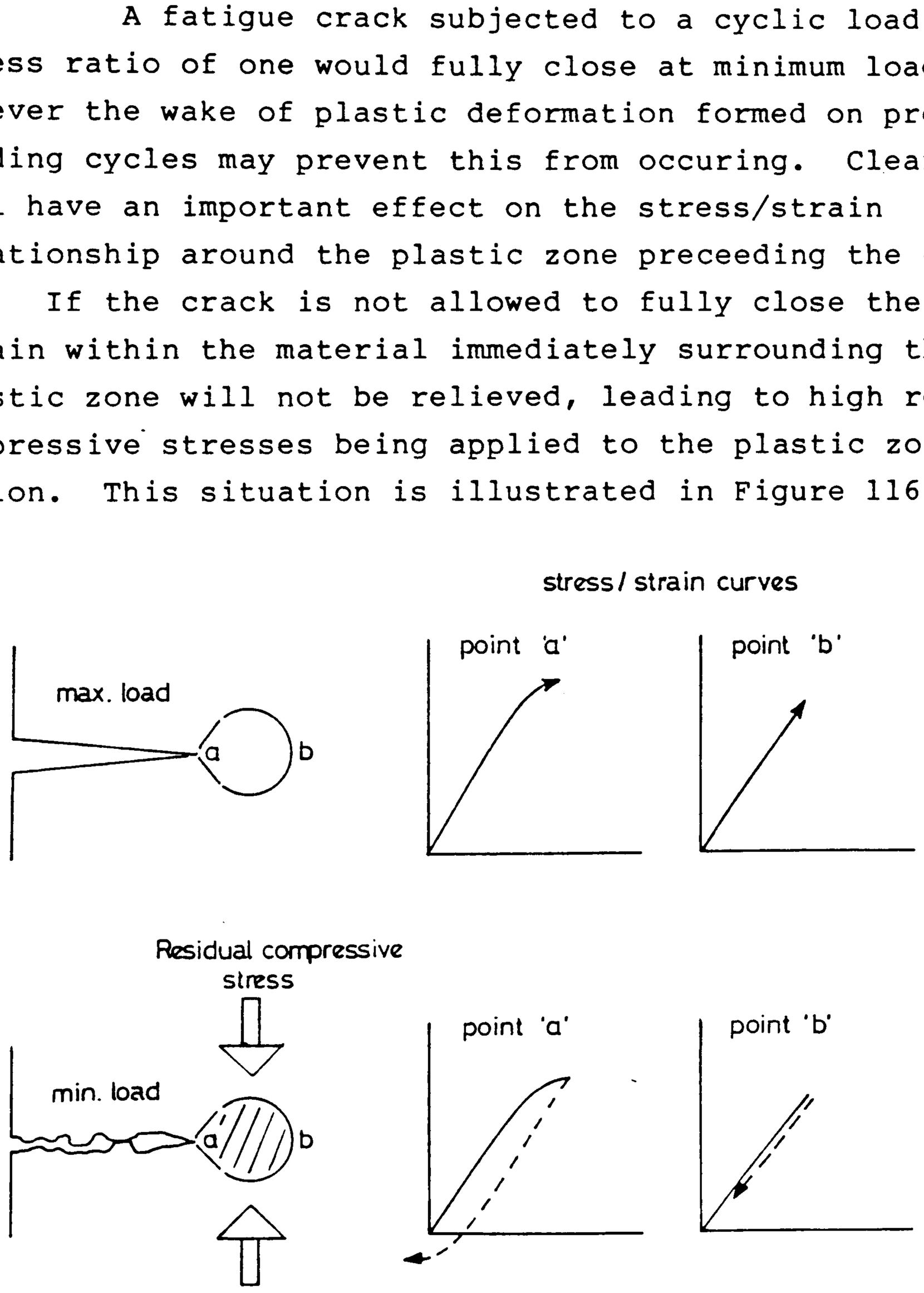

Figure 116 Effect of crack closure on the plastic zone stress state.

A residual compressive stress applied to the plastic zone may have one of two effects:-

1) Local residual compressive stresses must be overcome before the crack tip experiences a tensile stress intensity so reducing the effective stress range on subsequent cycles,

2) higher compressive stresses acting on the plastic zone may be sufficient to activate a reverse plastic flow mechanims and hence provide a form of plastic recovery. Both effects will have a delaying effect on subsequent fatigue crack propagation.

7.2. Fatigue in HSLA Steel Microstructures

A description of fatigue crack propagation based on the formation of a plastic zone ahead of the crack tip does not consider the influence of microstructure. This approach would predict yield strength to be the only major consideration for predicting fatigue crack propagation rates. Indeed we might expect materials of high yield to produce the most favourable crack growth resistance. However, this is not the case in fatigue crack propagation as seen for a range of materials in Figure 56 the inferior crack growth resistance of some higher strength steels is frequently attributed to a departure from a striation forming mechanism. Other departures from the simple model include deviation of the crack from a single propagation plane, formation of several types of crack branching, the influence of precipitates and inclusions and a departure from a stress intensity range dependant mechanism due to the environment. All the above departures from the simple model of fatigue have been observed in one or more of the HSLA steels studied in this thesis together with a wide range in fatigue performance. This has confirmed the view that yield strength is only one of many parameters dictating the fatigue performance of HSLA steels.

7.2.1. Non-planar fatigue crack propagation

Metallographic examination has shown the degree of crack path deviation to vary greatly between the six steels studied. The steels which displayed this characteristic most strongly were N-A-XTRA 70, Mannesmann X80 and Kontroll 50 ESM, one of which is a quenched and tempered steel with a very high yield strength ($\bar{\sigma}y = 690 Nmm^{-2}$) the other two being controlled rolled with relatively low yield strengths of $550 Nmm^{-2}$ and $470 Nmm^{-2}$ respectively. The extensive crack path deviation encounted in these widely different steel types may be due to high precipitate levels in the quenched

and tempered steel and a fine polygonal grain structure in the controlled rolled steels.

In body centred cubic iron, slip occurs on several planes {110}, {112}, {123}, but always in the same close packed <111> direction which is common to each of these planes. Thus a wide range of slip systems are available within this structure. A fatigue crack propagating within a fine grained microstructure will have a crack front which crosses many more grains each with a different crystallographic orientation with respect to the crack front. Although each grain has a large number of available slip systems those upon which slip can most easily occur and are most favourably orientated to maximum shear stress are likely to dictate the direction of crack advancement. The finer the grain size the more multiplanar the crack will become although on a macro scale it may appear to be smooth. Clearly the fine grained microstructure produced by the controlled rolling production route is likely to exhibit greater crack path deviation which will in turn produce greater fatigue resistance.

The activation of slip systems within a grain is also greatly influenced by the presence of interstitial atoms. Contrell (97) first observed that interstitial atoms such as carbon and nitrogen would interact strongly with the strain fields of dislocations. A locking mechanism produced by strings of carbon atoms thus substantially raising the stress for dislocation movement. Substitutional solute atoms also have a strengthening effect, this is in general proportional to the difference in atomic size of the solute from that of iron.

Both substitutional and interstitial solute atoms increase the yield strength of the iron crystal by restricting the movement of dislocations which will in turn reduce the number of slip systems available for which the

required stresses to cause slip will be generated. This will promote crack path deviation, and an uneven crack front. The high level of precipitates found in the quenched and tempered steel N-A-XTRA 70 will therefore promote crack path deviation and hence produce a beneficial effect in terms of fatigue crack growth resistance.

7.2.2. Effect of large microstructural features

It has been observed that precipitates of zirconium carbo-nitrides in N-A-XTRA 70 can influence the path of a fatigue crack to an extent where a large number of these precipitates appear on the fracture surface. Their intact nature indicates a debonding mechanism. The zirconium carbo-nitrides are harder than the surrounding material and therefore will not plasticly deform in the stressed region ahead of the crack tip. Activated slip planes ahead of the crack extending to a precipitate may therefore promote a debonding mechanism. The precipitate to matrix interface will subsequently behave as a void and promote a micro-void coalescense mode of fatigue crack propagation. Thus the presence of hard precipitates will promote crack path deviation but a large volume fraction will be required for a significant effect on the propagation mode and hence on the crack propagation rate.

Shape modified, approximately spherical, precipitates of manganese sulphide have also been found to promote a microvoid coalesence mechanism in Kontroll 50 ESM. Ductile dimples of a similar nature to those encounted on the N-A-XTRA final failure surface have been seen on Kontroll 50 ESM, however due to the relatively rare occurance of such precipitates in this low sulphur steel it is not possible to ascertain whether the crack path has been influenced by their presence.

Clearly the deviation of a fatigue crack from an orientation of 90^{o} to the maximum tensile stress will result in a lower stress intensity at the crack tip on subsequent cycles and therefore it could be argued that greater resistance to fatigue would result. However, for the fatigue crack to deviate in such a way an easier path for crack propagation must have been found. The route taken by the fatigue crack following precipitates is likely to be a factor of 1.5 times the distance of a non-deviating crack as measured in N-A-XTRA 70 and will therefore promote fatigue endurance. From this work it would appear that an increase in fatigue endurance could be gained via precipitate induced crack path deviation however further work is required in this field as previous researchers have reported accelerated crack growth rates associated with dimple formation (51).

7.2.3. Fatigue crack branching

In the six parent plate HSLA steel microsturctures studied the occurance and nature of fatigue crack branching has varied greatly. Two types of crack branching have been identified in the parent plate and a further type in HAZ microstructures. Both types associated with the parent plate are believed to reduce fatigue crack propagation rates whereas the type observed only in the HAZ has been associated with higher propagation rates.

7.2.3.1. Macro fatigue crack branching

Found only in parent plate microstructures this type of cracking has been termed macro because of its association with clearly identifiable microstructural features significantly larger than the grain size. LP-6 linepipe steel exhibited macrocracking in the form of a delamination mechanism associated with bands of high carbide precipitate concentration. The delamination ran for up to 5mm in a plane of carbides running at 90^{o} to the propagating

crack direction. Figure 86 shows this in profile. Whilst the carbide band clearly offered an easy route for crack propagation, and indeed crack propagation along this band was in excess of 1 x 10^{-6}m/cycle, the net effect was a delay to crack propagation at the surface of the sample and an increased fatigue endurance.

Crack branching of a similar nature was observed along bands of microstructure containing large numbers of elongated manganese sulphide inclusions. Clearly a similar weak resistance to cracking has promoted an extreme form of branching, as shown in Figure 81, however no noticeable delay in fatigue crack propagation occured as a result of this feature.

Whilst severe crack branching or delamination may promote fatigue endurance in these tests the fractrue toughness properties associated with the features promoting this behaviour are not desirable. Also it is likely that an improvement in fatigue endurance in one propagation direction will lead to accelerated crack growth rates in a crack growing in the same plane as the microstructural weakness. It is therefore impractical to promote this type of crack behaviour as a means of increasing fatigue endurance.

7.2.3.2. Secondary cracking

This fine crack branching has been found to be associated with microstructures which promote crack path deviation. Secondary cracks are typically up to 100μm long with narrow openings which may widen on final failure. In particular N-A-XTRA 70, Kontroll 50 ESM and Mannesmann X80 all show a high occurrance of this type of crack branching. Although the propagation path of a fine

secondary crack does not follow any identified microstructural features, the actual occurence of this type of branching is clearly favoured by certain microstructural types. It is interesting that the highest yield strength quenched and tempered steel should produce an abundance of secondary cracks and yet the two lower yield quenched and tempered steels have not. The higher yield N-A-XTRA 70 has by far the highest carbon equivalent value 0.33, a full 0.1 higher than RQT 501, with a large proportion of this being due to the increased carbon content. The high concentration of carbides is likely to promote crack branching of this nature. Unfortunately it is also likely to lead to a loss of fracture toughness.

The controlled rolled steels have much lower carbon equivalent values and lower yield strengths than N-A-XTRA 70. The high occurence of secondary cracking in these steels is clearly a result of some other property. The fine polygonal grain structure of this type of material has been seen to promote crack deviation and it is believed that this also promotes secondary crack formation.

The multiplanar nature of a fatigue crack which frequently branches will certainly lead to increased fatigue endurance over a straight non-branching crack. The stress intensity range will be reduced by the uneven crack front so promoting fatigue endurance. A greater area of fracture surface exposed by a deviating branching crack whilst maintaining a ductile mode of crack propagation again leads to increased endurance.

7.2.3.3. Microcracking

Fine cracks with a spacing corresponding to the expected striation spacing ie 1×10^{-7}m, were first observed in the heat affected zone microstructure of Kontroll 50 ESM. They were identified again whilst investigating a small

region (100μm) of rapid crack growth (>1 x 10^{-7}m/cycle) observed in a closely controlled and monitored, constant stress intensity range experiment. A typical example of this is shown for BS4360 grade 55F in Figure 106.

In both steels this feature was associated with increased fatigue crack propagation rates. The planar nature of the fracture surface in this region suggests a mechanism dominated by cleavage with little plastic deformation. Clearly a departure from a ductile striation forming mechanism has occured to one which forms micro-cracks. Despite the higher yield strength of the areas of microstructure in which this mechanism dominates the process of cleavage requires far less energy than plastic deformation resulting in more rapid crack growth.

7.2.4. Environmental effects

Strong environmental effects have been observed in several steels and it has been shown that these effects are highly dependent upon microstructure.

Both the quenched and tempered steel BS4360 grade 55F and the controlled rolled X80 linepipe have shown a change in fatigue performance characteristics when exposed to a corrosive environment. The sensitivity of both steels to stress intensity range was increased. At low stress intensity range the crack was observed to propagate more slowly, this reduction in growth rate being a direct result of the corrosive environment either by the build up of corrosion products between the fracture surfaces reducing the effective stress intensity range or by corrosion blunting of the crack tip. Corrosion is a time dependant process and as the crack begins to increase its growth rate with rising stress intensity range so the beneficial effects of corrosion are diminished. Above a stress intensity range of approximately 21MPa$\sqrt{m}$ the detrimental effects of the

environment are stronger than the diminishing crack delaying effects, ie ΔK effective is increasing towards ΔK applied, and increased crack propagation rates are observed. Both steel microstructural types have shown the same response to the seawater environment with enhanced fatigue endurance in the low stress intensity range, thus indication the suitability of use of both steels in the free corroding condition.

An impressed current cathodic protection potential of -810mV has restored the sensitivity of both steels to that of the in-air result. However, complete protection has not extended to the crack tip and an overall slight increase in fatigue crack propagation at all stress intensity range values has resulted. Whilst the fracture surfaces appeared corrosion free after testing subsequent metallographic examination revealed slight corrosion attack as seen in Figure 99 in profile for BS4360 grade 55F. It is significant that no reduction in crack growth rates occurred at low stress intensity range values despite crack tip corrosion. It is therefore clear that a large build-up of corrosion products between the fracture surfaces is the most important mechanism promoting fatigue endurance at low stress intensity range in a corrosive environment.

High cathodic overprotection potentials, greater than -950mV, promote the formation of monatomic hydrogen at the metal to liquid interface. Some atoms will combine to form molecular hydrogen and ultimately gas bubbles, however, a proportion will diffuse into the fatigue sample. The effect of high hydrogen levels within the sample on the fatigue crack propagation mechanism is therefore likely to dictate the fatigue performance of the steel in an overprotected condition. From the contrasting results for the two steel types we can deduce that the quenched and tempered microstructure is extremely sensitive to hydrogen generated in the overprotected environment whilst the

controlled rolled steel is not. Examination of the fracture profile of BS4360 grade 55F revealed a flat straight crack with no secondary cracking. By contrast the short crack extension which occurred in the controlled rolled steel before crack arrest had all the features of the parent plate, including crack path deviation and secondary cracks, Figure 103. Calcareous scale deposition is favoured by a high cathodic sample potential and a deposit soon forms on the sample fracture surfaces. For the quenched and tempered steel this has little effect because crack propagation is generating almost ten times more fracture surface than the controlled rolled steel every cycle. The scale forming on the controlled rolled fracture surface soon fills the crack opening enough to prevent crack closure at minimum load. This results in a lower ΔK effective and hence reduced propagation rates. As the crack slows, more scale is formed and compressed until the loading cycle has been reduced sufficiently to cause complete crack arrest.

Whilst both microstructural types have shown a favourable response to cathodic protection up to -810mV the sensitivity of the quenched and tempered steel to overprotection makes it far less attractive for offshore applications than the controlled rolled steel.

7.3. Design Against Fatigue

A range of fatigue endurance properties have been observed together with changing crack propagation mechanisms in the HSLA steel microstructures studied. A direct comparison with structural steel conforming to BS4360 grade 50D suggests that benefits in terms of lower fatigue crack propagation rates could be obtained from utilisation of these steels.

The most favourable result from each production route type of steel is shown in Figure 117 with a geometric upper boundary line which encompasses all the data scatter for comparison with the structural steel. From this Figure it is clear that the reduction in crack propagation rates is significant at all levels of stress intensity range encounted in this work. At low stress intensity range a reduction in growth rate of the order of one half is observed.

Clearly such an improvement in fatigue endurance could be of great value to the offshore industry. An offshore structure built from this high yield strength material to the same dimensions as used for the structural steel could offer enhanced structural integrity. This would be achieved because the structure would be operating at a lower applied stress to yield stress ratio with a material which has superior fatigue resistance. Alternatively a lower section thickness could be used for construciton so increasing the applied stress but only to the same applied stress to yield stress rato as used for the structural steel. This approach would reduce structure weight, and therefore cost, whilst maintaining the same level of integrity as long as the higher strength material shows an equivalent increase in fatigue endurance. A material which showed a higher increase in fatigue endurance than would be expected as a result of the increased yield strength of that

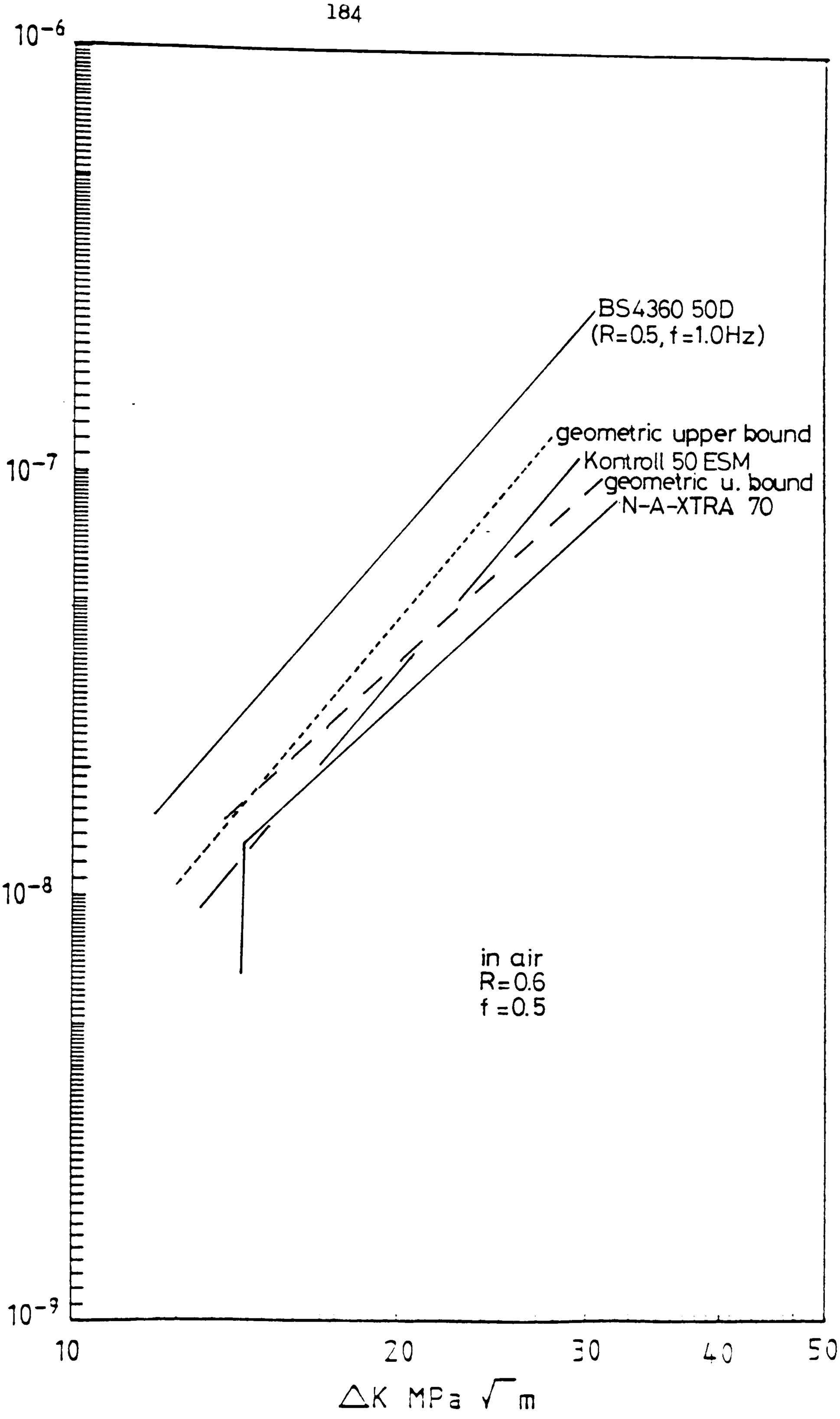

Figure 117 Geometric upper bound data for HSLA steels for comparison with structural steel data.

material, could be used at a higher applied stress to yield stress ratio and hence produce a major weight and cost reduction. This possibility would be highly dependent on ensuring adequate resistance to fracture and all possible applications would require proven weldability.

In order to calculate the magnitude of the weight reduction which might be achievable via the use of a higher strength steel we must first consider the design life and failure criterion for an offshore structure. A suitable failure criterion might be the propagation of a crack from a pre-existing flaw to a depth equal to the wall thickness of the structure. This thickness may be 50mm. The expected working life of an offshore structure is 20 years which at a cycling frequency of four cycles per minute gives a minimum life of 4.2×10^{7} cycles. This would suggest that the maximum tolerable growth rate would be 1.2×10^{-9}m/cycles. This is however a mean growth rate and is not applicable to actual growth rates measured on real structures. During the life of an offshore instalation a fatigue crack will spend most of its life in a state of threshold due to the relatively low loads developed at the crack tip. Under more demanding conditions the crack will propagate, typically at rates of 1×10^{-8} to 5×10^{-8}m/cycles (98). For the purpose of this comparison we will assume a crack extension of 50cm in 20 years which corresponds to a growth rate of 1.2×10^{-8}m/cycle. For a structural steel this would typically be achieved by a constant stress intensity range of 11 MPa $\sqrt{m}$ however both Kontroll 50 ESM and X80 linepipe steels could achieve the same performance at a constant stress intensity range of 13.5 MPa $\sqrt{m}$. A corresponding thickness reduction to give this higher stress intensity range would result in a weight saving of approximately 23%. It should be noted that the chosen value of crack growth rate for this analysis is below the threshold for N-A-XTRA 70. However this figure would be reduced by the addition of stiffeners requried to avoid buckling if thinner plate sections were used.

Clearly a significant weight reduction could be achieved via a wider utilisation of HSLA steel in applications subjected to a cyclic fatigue load. It is however important to assess whether the increases in fatigue endurance is greater or less than that expected for the increase in yield strength. For this purpose a diagram has been produced, Figure 118, which represents the fatigue performance of the HSLA steels tested and BS4360 grade 50D normalised for yield strength. From this Figure it is clear that the improvement in fatigue endurance is not generally equivalent to the increased yield strength for HSLA steels. However, Kontroll 50 ESM actually shows a greater resistance to fatigue as a function of yield strength than BS4360 grade 50D. This HSLA steel has the lowest yield strength, $470Nmm^{-2}$ and by far the lowest carbon equivalent (PCM Ceq = 0.19) and the highest fracture toughness, (260J at $-40^{o}C$).

The normalised performance of RQT 501 and X80 linepipe steel are very similar X80 linepipe which has performed better has a slightly lower yield strength and carbon equavalent to RQT 501 but a fracture toughness, of 232J at $-40^{o}C$. The fracture toughness of RQT 501 is 200J at $-40^{o}C$.

Although N-A-XTRA 70 performed better than all the other steels tested it has by far the highest yield strength and has therefore not shown any advantage after normalising for yield. This steel also has the highest carbon equivalent (PCM Ceq = 0.33) and the lowest fracture toughness (31J at $-40^{o}C$), of all the HSLA steels tested and it is perhaps these factors which have led to a reduced normalised fatigue performance. BS4360 grade 55F has the lowest fatigue performance to yield stress ratio of all the steels tested. This steel has the second highest yield of $580Nmm^{-2}$, an intermediate carbon equivalent but a relatively low fracture toughness of 164J at $-40^{o}C$. From Figure 118 it is clear that the quenched and tempered steels have fallen

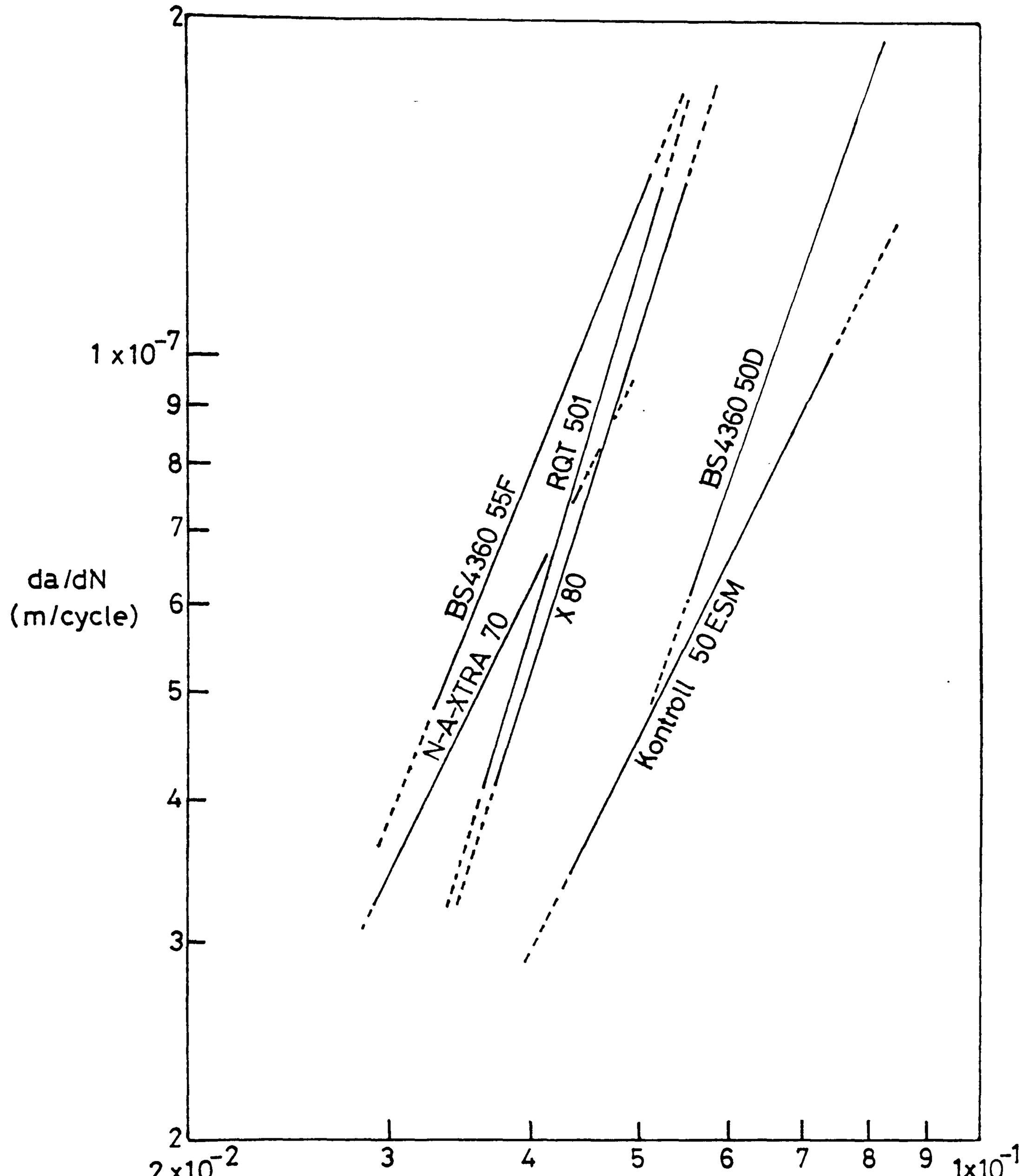

Figure 118 Fatigue performance of HSLA steels and a structural steel normalised for yield strength.

in a group which suggests that this production route mechanism for increasing yield strength does not increase fatigue resistance by a corresponding amount. The curve representing Kontroll 50 ESM on the other hand does suggest that a controlled rolling route may lend to steels which could match higher yield strengths with corresponding improved fatigue performance. This theory is not supported by the result for X80 linepipe however which has shown a similar fatigue endurance to yield strength ratio to the quenched and tempered steels. This is despite a high fracture toughness of 232J at $-40^{o}C$. The carbon equivalent level for this steel, PCM Ceq = 0.23, is however closer to that of the quenched and tempered steels and probably contributes considerably to its higher yield strength of $550Nmm^{-2}$.

Despite this failure to match higher yield strength with improved fatigue resistance in the majority of HSLA steels it should be remembered that all these steels show a significant improvement over structural steels and that this improvement could be utilised whilst maintaining the same degree of safety to give a 20% reduction in weight. For this weight reduction advantage to be used we must fully understand the fatigue properties of the HAZ produced by the welding of HSLA steels. The HAZ produced by a multipass submerged arc welding process at a heat input of 3.0 kJ has shown fatigue properties which reflect those of the parent plate with a slight reduction in fatigue resistance for all but one of the steels tested.

Unfortunately equivalent data for BS4360 grade 50D was not available for comparison. The results for the HSLA steels welded at this relatively high heat input were considered encouraging with the exception of Kontroll 50 ESM. The exceptional sensitivity of this HAZ to the environment and the excessive fatigue crack propagation rates recorded were thought to be the result of non

adherence to the welding procedure and in particular to the flux pre-bake which was specified as two hours at 300°C. Unfortunately this material was supplied as a small test plate from Japan and there was insufficient material to repeat the welding procedure. This result indicates that further work is required in this area of study before some HSLA steels could be used with total confidence in welded structures subjected to a fatigue loading environment.

Whilst corrosion fatigue testing has been limited to two steels, one from each prodution route, the results have shown some very interesting trends. In general the correctly protected samples have reflected the parent plate results well with only a slight but constant reduction in fatigue endurance at all levels of stress intensity range.

Full restoration of fatigue resistance is probably not achieved because of the difficulty in achieveing the correct potential at the crack tip. Freely corroding samples produced the same trend in both production route types showing reduced crack growth rates at lower values of stress intensity range and accelerated growth at higher values. Clearly the corrosive environment is having a detrimental effect on fatigue properties. However corrosion products forming between the fracture surface are thought to have reduced the effective load range and hence inhibited fatigue crack propagation.

Contrasting results were recorded for the two steel types tested in an overprotected condition. The susceptability of the quenched and tempered steel to hydrogen produced by overprotection was clearly demonstrated. The horizontal section of this plot, Figure 65, suggesting a propagation process independent of the stressing environment. P Millars investigation into the effects of impressed current cathodic protection on the quenched and tempered steel N-A-XTRA 70 (99) have confirmed

the susceptability of this quenched and tempered microstructure to overprotection. Crack propagation rates in excess of 10^{-7}m/cycle were recorded at stress intensity ranges above 20MPa $\sqrt{m}$ at protection potentials in excess of -1100mV Ag/AgCl. The X80 linepipe steel showed an initial increase in crack propagation rate at low stress intensity range followed by complete crack arrest. The initial increase in crack growth rate demonstrated a slight susceptability to a hydrogen rich environment but the detrimental effects were rapidly diminished by a build up of calcareous deposits between the cracks fracture surfaces reducing the effective load range at the crack tip.

Corrosion fatigue data produced by Scott and Silvester (85) working on BS4360 grade 50D in a seawater environment reported fatigue crack propagation rates at ΔK values below approximately 18MPa $\sqrt{m}$ to be usually less than those obtained in air. At cathodic potentials between -800mV and -1000mV there was clear evidence from the record of crack opening displacements that the minimum opening displacements tended to increase with time more rapidly than the maximum values. This phenomenon was found to be due to the precipitation of near stoichiometric calcium carbonate (>80% $CaCO_3$ as aragonite) down the sides of the crack which impeded crack closure when the load on the specimen was reduced. In several experiments, Scott & Silvester reported that between -800 and -1000mV, the growth rate declined during the experiment when the starting value of ΔK was below 15MPa $\sqrt{m}$; this was attributed to an effective reduction in the cyclic stress intensity at the crack tip due to the prevention of complete crack closure by calcium carbonate. The results of Scott & Silvester are shown in Figure 119. It should be noted that a direct comparison with the data produced by this study is not possible since the loading parameters used (frequency - 0.1Hz, stress ratio, $R < 0.1$) and the environment (temperature = $20^{o}C$) are not the same. The effect of temperature has been reported

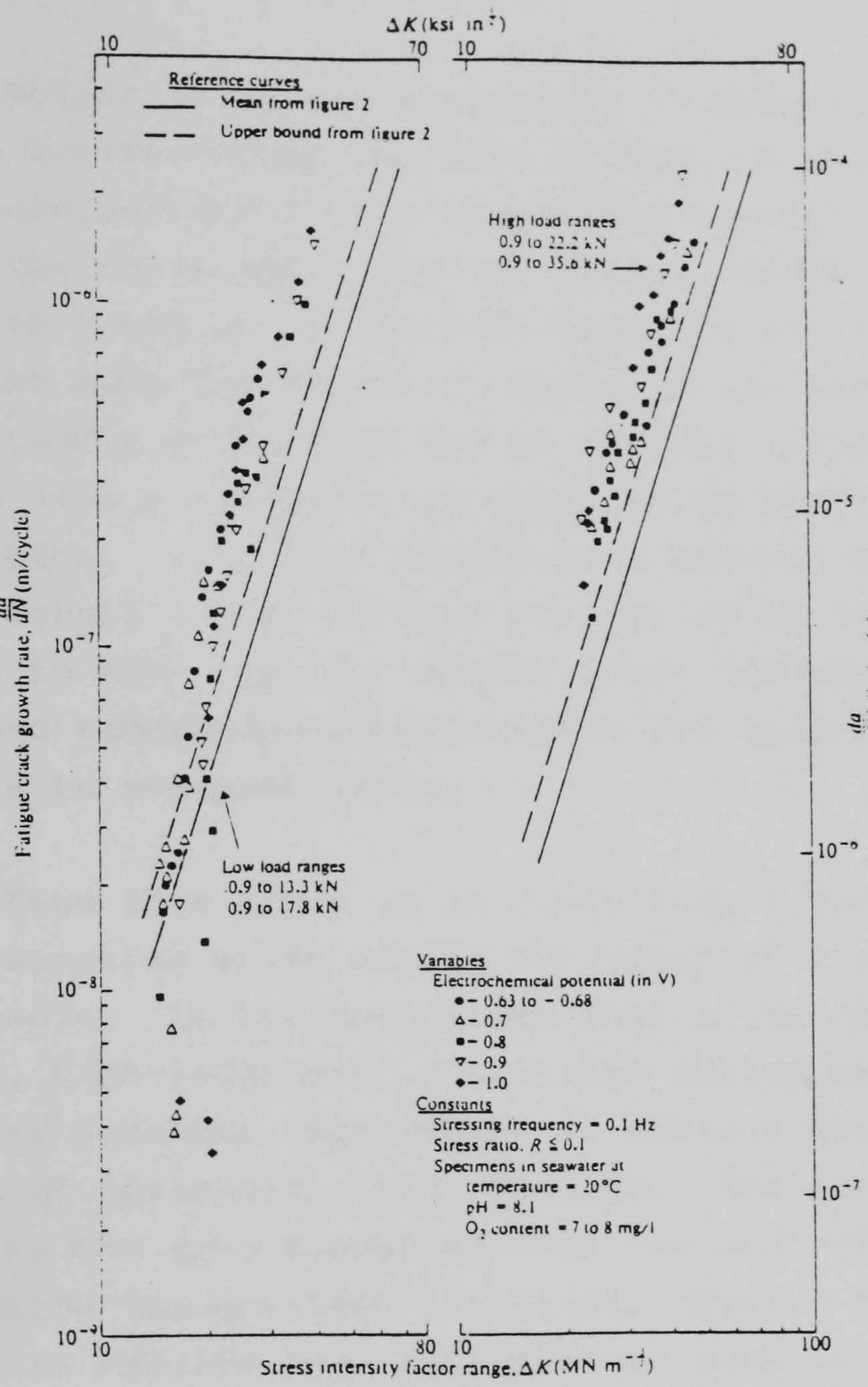

Figure.119 Fatigue crack propagation data as a function of electrochemical potential in seawater (BS 4360 50D).

by Scott & Silvester as a significant variable. Above ΔK = 18MPa$\sqrt{m}$ lowering the temperature from 20°C to 5°C reduced the crack growth rate by about a factor of two at all three electrochemical potentials tested.

Whilst it is not acceptable to make a direct comparison between these two sets of data we can draw some important conclusions from a comparison between the relative effect of the environment and the in-air result for each steel. This leads us to conclude that the X80 linepipe steel is the most favourable in terms of its response to correct cathodic protection and no serious susceptability to a hydrogen rich environment as produced by severe cathodic overprotection. Both HSLA steels have demonstrated a superior restoration of fatigue properties by correct protection to that seen for BS4360 grade 50D however the quenched and tempered microstructures are clearly the most susceptible to overprotection.

From this study it is clear that a wide range of fatigue properties exist within the group of steels termed as HSLA steels. It has been shown that a low carbon equivalent, high toughness, controlled rolled microstructure produces the greatest improvement in fatigue performance as a function of increased yield strength. The corrosion fatigue data has also suggested that the controlled rolled microstructure has greatest potential, however the heat affected zone results have indicated an area in which more work would be of benefit if a high level of confidence in the wider use of these steels is to be achieved.

8.0. CONCLUSIONS

1) A range of microalloyed HSLA steels with yield strengths ranging from 470 to 690 Nmm^{-2} have exhibited a significant improvement in fatigue crack propagation resistance compared to conventional lower strength (350 NMM^{-2}) carbon manganese structural steels. The fatigue crack growth rate in the Paris region being typically reduced by a factor of two.

2) The improvement in fatigue crack propagation rate is not directly related to either an increase in yield strength or an increase in the Charpy Vee fracture toughness (as defined by Cv impact energy) but is microstructure dependent.

3) High heat input welding (3kJ/mm) does not significantly increase the fatigue crack propagation rates in the HAZ's of such steels. The slopes of the related Paris curves were largely unchanged although the curves were displaced slightly to faster crack propagation rates. The fastest crack propagation rates were found in the coarse grained HAZ region.

4) A newly developed crack monitoring gauge has been used for the first time in an experiment devised and implemented to accurately measure the crack propagation behaviour of very small regions of alloy microstructure. Very rapid crack growth rates were measured in an extremely small region (100μm) corresponding to the coarse inner HAZ. The fatigue crack growth in the weld metal was more irregular than in the parent plate or fine HAZ material. The crack propagation rate in such regions increased by a factor of 10 compared to the adjacent microstructures both in the weld metal and in the outer HAZ. The newly developed technique has great potential for studying the effect of localised microstructural regions in fatigue crack propagation studies.

5) Alloy microstructure influences fatigue crack propagation primarily by changing the mode of crack propagation. For example, departures from the ductile striation mode to one dominated by cleavage increased crack propagation rates in the coarse HAZ regions. Also controlled rolled microstructures promote the ductile striation mode of fatigue with a resulting improvement in performance compared to quenched and tempered steels.

6) In general microstructures which gave good performance in fatigue have shown pronounced secondary cracking both in terms of an increased number and an increased depth of the cracks observed. Such microstructures also show greater crack path deviation. In one such alloy which exhibited secondary cracking an increased volume fraction of precipitates was measured on the fracture surface indicating that the precipitates were playing a role in influencing the path followed by a fatigue crack.

7) In a steel alloy with a highly banded microstructure the fatigue crack arrested in the through thickness direction and propagated at an accelerated rate along the carbide rich bands causing delamination of the specimen.

8) When correctly cathodically protected such steels show comparable fatigue behaviour in sea water to in-air tested materials but with slightly increased crack propagation rates. Under freely corroding conditions accelerated crack growth rates occur at values of ΔK above 20 MPa $\sqrt{m}$ but reduced crack growth rates occur at lower ΔK values associated with a build up of corrosion products causing a reduction in the applied stress. Cathodic overprotection caused a very severe reduction in fatigue performance in a quenched and tempered steel whereas with a controlled rolled steel the effect was much less pronounced.

9. REFERENCES

1) Booth, G. S. and Wylde, J. G. "Fatigue considerations in offshore steel structures in the North Sea", Welding Institute research bulletin, March 1978, R148/3/78, Vol 19 pp6, 9.

2) Warwick, P. C., Hart, N., Taylor, D. S. and Satta, A., "The Hutton TLP mateing joint weld out" Metal construction" July 1985, pp423.

3) Easterling, K. "Introduction to the Physical Metallurgy of Welding" Butterworth and Co (Publishers) Ltd 1983

4) Bohle, S. D. and Billingham, J. "Effect of Heat Input on HAZ Toughness in HSLA Steels" Metals Technology, September 1983, 10, pp363.

5) Pite, A. N. G. "Fatigue Crack Propagation in HSLA Steels" MSc thesis, Cranfield Institute of Technology, 1981

6) Wiess, G. "Effect of stress relief and microstucture on fatigue crack propagation in a welded HSLA steel" MSc thesis, Cranfield Institute of Technology, 1983.

7) BS 5400 mark 10

8) Pickering, F. B., "High Strength Low Alloy Steels - A Decade of Progress", Micro alloying 1975 pp9.

9) Hall, E. O., Proceedings Physics Society series B 1951, Vol.64, pp747.

10) Petch, N. J., Journal of Iron and Steel Institute 1953, Vol 174, pp25.

11) Wiester, H. J. and Ulmer, H., "Stahl und Eisen" 1959, Vol.79, pp1120.

12) Korchynski, M. and Stuart, H. "Low alloy High strength steels" London/Scandinavian conference Nuremberg 1970, pp17.

13) Pearson, T. F. and Delippa, M. Journal of Iron and Steel Institute 1967 Vol. 205, pp257.

14) Gaurne, D. T. and Lewis, G. M. H. "Strengthening Mechanisms in High Strength Microalloyed Steels" Material Science and Technology, March 1985, Vol.1, pp183.

15) Gladman et al in: Micro alloying 75 Union Carbide Corporation 1975.

16) Decca, R. F. Metal Trans. Vol.4, 1973, pp2495

17) Martin, J. W. "Precipitation Hardening" Pergammon Press New York 1966

18) Gladman, T. Dulieu, D. and McIvor, I. D. in "Micro Alloying '75" 32, 1977 New York, Union Carbide Corporation

19) Hall, H. O. Proceedings Physics Soc. 1951 Vol.64B pp747

20) Petch, "In Fracture" ed. Averbach et al, John Wiley 1959

21) Paris, P. and Erdouan, F. "Journal Basic Eng. Trans. ASME Ser. D 1963, 85, 528

22) Watson, D. and Ellison E. G. ASTM Spec. Tech. Publ. 415, 1967 "Fatigue Crack Propagation" Int. Metall. Rev., Vol. 17 pp 100 1972

23) Roberts, R. and Endogan, F. "The effect of mean stress on fatigue crack propagation in plates under extension and bending" Trans. Am. Soc. Mech. Engrs., J. BAS. Eng. 1967, 89, 885.

24) Forman, R. G. Kearney, V. E. and Engle, R. M. "Numerical annalysis of crack propagation in cyclic loaded sturctures" ibid 459.

25) Elber, W. "The significance of Fatigue crack closure" Damage tolerance in aircraft structures ASTM, STP 486, 1971 pp230

26) Elber, W. "Fatigue Crack Closure under Cyclic Tension" ibid 1970 2, 37

27) Mussura, J. K. and Radon, J. C. "Effect of Stress Ratio and Frequency on Fatigue Crack Growth" Fat. Engng. Mats. and Struct. Vol.1, pp457 to 470.

28) Lindly, T. C. and Richards, C. E. "The relevance of crack closure to fatigue crack propagation" Mats. Sci. and Engng., 14 (1974) 281 to 293.

29) Esaklul, K. A. et al Scripta Met. Vol. 17 (1983) pp1079.

30) Benoon, J. P. and Edmonds, D. V., Met. Sci., Vol. 12 (1978) pp223.

31) Ritchie, R. O., J. Eng. Materials and Tech., Vol 99 (1977), pp195

32) Masounave, J. and Bailon, J. P., Scripta Met. Vol. 10 (1976), pp165.

33) Richards, C. E. CEGB report RD/L/R 1679, (1970)

34) Broek, D., Dutch National Aerospace Lab. Report NLR-MP-6900 1 U (1969)

35) Gerberich, W. W. and Moody, N. R., Met. Sci., Vol. 14 (1980), pp95.

36) Ritchie, R. O., Met. Trans. Vol. 8A (1977), p1131.

37) Rice, J. R., Fatigue Crack Propagation ASTM STP 415 pp247 (1967).

38) Forsyth, P. J. E. and Ryder, D. A., Aircraft Eng. 32 pp46 (1960).

39) Taylor, D., Engineering Advisory Services Ltd (1985) ISBN 947817 050.

40) Cadman, A. J. Brook, R. and Nicholson, C. E. "Factors effecting the measurement of the fatigue threshold (K_{th})" vol.17 no.9 pp1053.

41) Pook, L. P. and Greenan, A. F. report No.571 National Engineering Laboratory, 1974.

42) Chappus, P. Massounave, J. and Bailsplodge, J. P. "Advances in fracture" ICFS Vol.3, pp1343, 1981 Pergamon Press.

43) Scott, P. M., "Corrosion fatigue and offshore structures" dept. of Energy, OTP 2.

44) Cooke, R. J. and Beevers, C. J. Eng. Fract. Mech. 5, 106.

44b Jaske, C. E., Broek, D., Slater, J. E., Utah, D. A. and Martin, C. J. "Corrosion fatigue of cathodically protected welded carbon steel in cold sea water" Report API Committee on Offshore Safety and Antipolution Research, Dallas, Texas, Feb. 1977.

45) Endo, K. and Miyas, Y. "Effects of cyclic frequency on the corrosion fatigue strength" Bull. JSME, 1, 374 to 380, 1958.

46) Zappfe, C. A. and Worden, C. D. Trans. Am. Soc. Metals. 41 pp396 1949

47) Ryder, D. A. Royal Aircraft Establishment Technical Note Met. pp288 1958

48) McMillan, J. C. and Pelloux, R. M. N. ASTM STP 415 pp505 (1967)

49) Laird, C. ASTM STP 415 pp139 (1967)

50) Richard, C. E. and Lindley, T. C. "The influence of Stress intensity and microstructure on fatigue crack propagation" Eng. Fract. Mech. 1972 Vol.4, No.4 pp951 to 978.

51) Beevers, C. J., "Micromechanisms of fatigue crack growth at low stress intensities" Met. Sci. Aug-Sep 198 pp418.

52) Richard, C. E. acta met 19, 583 1971.

53) Wright, R. N. and Argon, A. S. Trans. Am. Inst. Mech. Engng. 1, 3065 (1970)

54) Pearson, S. Royal Aircraft Establishment Tech. Report. 68232 1968

55) Wei, R. P. Trans. Am. Soc. Metals 60, 279 (1967)

56) Pelloux, R. M. N. Trans. Am. Soc. Metals. 57, 511 (1964)

57) Broek, D. Conf. on Fracture, Brighton P754 (1969)

58) McMahon, C. J. ASTM STP 407, 127 (1968)

59) Evans, P. R. V. Owen, N. B. and Hopkins, B. E. Engng. Fracture. Mech. 3, 109 (1971)

60) Spitzig, W. A. and Wei, R. P. Trans. Am. Soc. Metals. 60 279 (1967)

61) Dahlberg, E. P. Trans. Am. Soc. Metals 58, 46 (1965)

62) Evans, P. R. V. Madhara, N. M. and Chart, T. G., Czech. J. Phys. 1319 381 (1969)

63) Lindley, T. C. and Richards, C. E. Engng. Fract. Mech. (1972), Vol. 4, pp951.

64) Plumbridge, W. J. and Ryder, D. A. Metals and Materials 3, 119 (1969)

65) Griffiths, J. R., Mogford, I. L. and Richards, C. E. Metal Sci. J. 5 150, (1971)

66) Crooker, T. W., Cooley, L. A., Lange, E. A. and Freed, C. N. Trans, Am. Soc. Metals 61, 568 (1968)

67) Jack, A. R. and Price, A. T. Acta. Met. to be published (ditto no 63)

68) Clark, W. G. Engng. Fracture Met. 1 385 (1968)

69) Gerberich, W. W. and Hartblower, C. E. Trans. Am. Soc. Metals 61 184 (1968)

70) Forsyth, T. J. E. and Ryder, D. A. Metallurgia 63 117 (1961)

71) Hertzberg, R. W. ASTM STP 415, 305 (1967)

72) Raydon, T. C. and Woodtli, T. "Influence of Microstructure on a Cyclic Crack Growth in a Low Alloy Steel" Int. J. Fatigue 6 No. 4 (1984) pp221-228

73) Lancaster, J. F. "Metallurgy of Welding" 1980 ISBN 004 6690093

74) Thomas, M. et al, "Quantifying the Effect of Micro Alloying Elements on Structures during Processing" Micro Alloying 75. October 1-3 (1975) Washington D. C.

75) Pircher, H. and Klapdor, "Controlling Inclusions in Steel by Injecting Calcium into the Ladle" Micro Alloying 75, October 1-3, 1975

76) Ito, Y. and Bessyo, K. Weldability formula of high strength steels related to HAZ cracking J. Japanese Welding Soc. (1968) 37 9 983

77) Walkinson, F. and Kitada, T., "Safe welding procedures for C-Mn and low alloy steels comparison of welding institute and Japanese approaches. Welding Institute Research Bulletin 1974 15 (9) 271.

78) Suzuki, H. 'Comparison of Carbon equalents for steel weldability' IIW lX-B Document 1983 October.

79) Cottrell, CLM, "Hardness equivalent may lead to a more critical measure of weldability Metal Construction, Dec 1984 pp 740

80) Yurioko, N. Oshita, S. and Tamelina, H "Study on Carbon equavalents to assess cold cracking tendancy and hardness in steel welding in connection with the development of low carbon burnitic linepipe steels" Australian Welding Research Association, Melbourne, March 18 1981.

81) Short, R., "The Effect of Microstructure on Fatigue Crack Propagation", MSc thesis Cranfield Institute of Technology, (1984)

82) Thornton, C. E. "Investigation of the Mechanical Properties of Joints in RQT 501" Technical Report No CET 28R (Oerlikon).

83) Tidswell, R., "Crack Growth Monitoring using Thin Film Technology" MSc thesis, Cranfield Institute of Technology (1985).

84) Clark, W. G. and Hudak, S. J. "Variability in Fatigue Crack Growth Rate Testing" J. Test. Eval., 3 (1975) pp454-476

85) Scott, P. M. and Silvester, D. R. V., "The Influence of Mean Tensile Stress on Corrosion Fatigue Crack Growth in Structural Steel Immersed in Seawater", Dept. of Energy, UK Offshore Steels Research Project, Interim Technical Report UKOSRP 3/02 (May 25, 1977)

86) Johnson, R., Bretherton, B. Tomkins, B, Scott, P. M. and Silvester, D. R. V., "The effect of Seawater Corrosion on Fatigue Crack Propagation in Structural Steel" UKOSRP 3/03 1975.

87) Hutchinson, J. W. "Singular Behaviour at the end of a tensile crack in a hardening material" J. Mech. and Phys. of Solids 16 No1, (1968) pp13-31.

88) Irwin, G. R. "Fracture Mechanics" Structural Mechanics - Proceedings of the 1st symposium on Naval Structural Mechanics (Pergumon Press, New York, 1958) pp557-592.

89) Glinka, G. "A cumulative model of fatigue crack growth", Int. J. Fatigue April 1982, pp59

90) Davidson, D. L. and Lankdord, J. Plastic strain distribution at the tips of propagating fatigue cracks' J. Engng. and Tech. Trans. ASME 98 No2 (1976) pp146-151.

91) Wnuk, M. P. "Extension of a stable crack at a variable growth step' Symposium on Crack Fromation and Propagation (CISM, IUTAM, PAS, Tuczno, Poland, March pp23-27, 1981.

92) Robin et al "Influence of an overload on the fatigue crack growth in Steels" Fat. Engng Mats. Structs Vol.6 No.1 pp 1-13, 1983.

93) Fuhring, H. and Seeger, T. 'Structural Memory of cracked components under irregular loading' ASTM STP 677, 1979, pp144-167

94) Matsuoka, S., Tonaka, K. and Kawahara, M., 'The retardation phenomenon of fatigue crack growth in HT 80 steel. Engng. Fract. Mech. 8, 1976, pp507-523

95) McCartney, L.N. 'A theoretical explanation of the delaying effects of overloads on fatigue crack propagation'. Int. J. Fract. Vol 14, No.2 1978 pp213 232

96) Mille, P. 'Closure phenomena at crack tips in steels', PhD thesis, Univ. of Tech. of Compiegne (1979)

97) Cottrell, A.H. 'An Introduction to Metallurgy', pp266-269, Edward Arnold (Publishers) Ltd, London (1967)

98) Bristol, P., 'A review of the fracture mechanics approach to the problems of design, quality assurance, maintenance, and repair of offshore structures.' Proceedings of E.O.S.R.S. Welding Institute Abington Nov. (1978) Cambridge.

99) Private Communication P. Miller, Cranfield Institute of Technology, 1987